NASA Technical Memorandum 83199
Part 2

Aircraft Noise Prediction Program Theoretical Manual

William E. Zorumski
Langley Research Center
Hampton, Virginia

National Aeronautics
and Space Administration

Scientific and Technical Information Branch

1982

CONTENTS

Part 1*

*Chapters 1 to 7 are published under separate cover.

Part 2

8. NOISE SOURCES

8.1 FAN NOISE MODULE

INTRODUCTION

The Fan Noise Module predicts the broadband noise and pure tones for an axial flow compressor or fan. The method is based on the method developed by M. F. Heidman (ref. 1). The method employs empirical functions to predict the sound spectra as a function of frequency and polar directivity angle.

The total fan noise is predicted by summing the noise from six separate components. The six component sources selected are inlet broadband noise, inlet rotor-stator interaction tones, inlet flow distortion tones, combination tone noise, discharge broadband noise, and discharge rotor-stator interaction tones. All noise sources are combined into a single 1/3-octave-band spectrum for each directivity angle.

The method requires input of several parameters. The fan entrance and exit flow parameters can be provided by the Fan Noise Parameters Module or directly by the user. Additional user-provided parameters are required. The module is executed once for each set of values of the input parameters. The output is a table of the mean-square acoustic pressure as a function of frequency, polar directivity angle, and azimuthal directivity angle. Although fan noise is assumed not to vary with azimuthal directivity angle, it is introduced so that the output table is compatible with other noise tables.

SYMBOLS

A	fan inlet cross-sectional area, m^2 (ft^2)
A_e	engine reference area, m^2 (ft^2)
a,b	exponents
B	number of rotor blades
C	mean rotor blade chord, m (ft)
c_∞	ambient speed of sound, m/s (ft/s)
D	directivity function
d	fan rotor diameter, m (ft)
F	power function
f	frequency, Hz

f_b	blade passing frequency, Hz
G	constant matrix
i	inlet guide vane index
K	constant
k,ℓ	inlet flow distortion indices (eqs. (10) and (11))
M_d	fan rotor relative tip Mach number at design point
M_m	design point Mach number index, max $(1,M_d)$
M_r	fan rotor relative tip Mach number
M_t	fan rotor tip Mach number
M_x	flow Mach number
M_∞	aircraft Mach number
$\dot{m}$	mass flow rate, kg/s (slugs/s)
N	rotational speed, Hz
N_e	number of engines
n	tone harmonic number
$\langle p^2 \rangle^*$	mean-square acoustic pressure, re $\rho_\infty^2 c_\infty^4$
p_{ref}	reference pressure, 2×10^{-5} Pa (4.177×10^{-7} lb/ft^2)
r_s	distance from source to observer, m (ft)
r_s^*	dimensionless distance from source to observer, re $\sqrt{A_e}$
S	tone spectrum function
s	rotor-stator spacing, m (ft)
ΔT	total temperature rise across fan, K ($^\circ$R)
T_∞	ambient temperature, K ($^\circ$R)
V	number of stator vanes
ζ	cut-off factor
η	frequency parameter
θ	polar directivity angle, deg

Π^* acoustic power, re $\rho_\infty c_\infty^3 A$

Π_{ref} reference power, 1×10^{-12} W (7.376×10^{-13} ft-lb/s)

ρ_∞ ambient density, kg/m^3 (lb/ft^3)

ϕ azimuthal directivity angle, deg

Superscript:

* dimensionless quantity

INPUT

The fan parameters are required from either the output of the Fan Noise Parameters Module or the user. Ambient conditions are required for computation of sound pressure levels. The frequency, polar directivity angle, and azimuthal directivity arrays establish the independent variable values for the output table. The fan inlet cross-sectional area, number of rotor blades, number of stator vanes, inlet guide vane index, inlet flow distortion index, fan rotor diameter, fan rotor tip relative Mach number at design point, and rotor-stator spacing are required for the geometric description of the fan. Finally, the engine reference area, number of engines, and distance to the observer are required. The range and default values of the input parameters are given in table I.

A_e engine reference area, m^2 (ft^2)

N_e number of engines

r_s distance from source to observer, m (ft)

Fan Geometry

A^* fan inlet cross-sectional area, re A_e

B number of rotor blades

d^* fan rotor diameter, re $\sqrt{A_e}$

I inlet guide vane index

M_d fan rotor relative tip Mach number at design point

D inlet flow distortion index

s^* rotor-stator spacing, re C

V number of stator vanes

Fan Noise Parameters

$\dot{m}^*$ mass flow rate, re $\rho_\infty c_\infty A_e$

N^* rotational speed, re c_∞/d

ΔT^* total temperature rise across fan, re T_∞

Ambient Conditions

c_∞ ambient speed of sound, m/s (ft/s)

M_∞ aircraft Mach number

ρ_∞ ambient density, kg/m^3 (slugs/ft^3)

Independent Variable Arrays

f frequency, Hz

θ polar directivity angle, deg

ϕ azimuthal directivity angle, deg

OUTPUT

The output of this module is a table of the mean-square acoustic pressure as a function of frequency, polar directivity angle, and azimuthal directivity angle. In addition, the pseudo-observer distance r_s is provided for the Propagation Module.

r_s distance from nozzle exit to pseudo-observer, m (ft)

Fan Noise Table

f frequency, Hz

θ polar directivity angle, deg

ϕ azimuthal directivity angle, deg

$\langle p^2(f,\theta,\phi)\rangle^*$ mean-square acoustic pressure, re $\rho_\infty^2 c_\infty^4$

METHOD

The prediction methodology presented in reference 1 is used to compute the far-field noise. A schematic of a typical fan is shown in figure 1. The coordinate system and directivity angles are also shown. The general approach for the prediction method is presented. Then, the detailed prediction for each fan noise component is discussed.

The equation for the far-field mean-square acoustic pressure for a fan is

$$\langle p^2 \rangle^* = \frac{A^* \Pi^*}{4\pi (r_s^*)^2} \frac{D(\theta)\ S(\eta)}{(1 - M_\infty \cos\theta)^4} \tag{1}$$

In equation (1), Π^* is the overall power, D is the directivity function, and S is the spectrum function. The source to observer distance r_s is expressed in dimensionless form as

$$r_s^* = r_s / \sqrt{A_e} \tag{2}$$

The forward velocity effect is accounted for by the Doppler factor, $(1 - M_\infty \cos\theta)^4$. The frequency parameter η is defined as

$$\eta = (1 - M_\infty \cos\theta) \frac{f}{f_b} \tag{3}$$

where the blade passing frequency f_b is

$$f_b = \frac{N^* B c_\infty}{d^* \sqrt{A_e}} \tag{4}$$

The acoustic power Π^* for the fan is expressed as

$$\Pi^* = K\, G(i,j)\, (s^*)^{-a(k,\ell)} M_m^b (\dot{m}^*/A^*) (\Delta T^*)^2\, F(M_r, M_m) \tag{5}$$

Equation (5) contains several empirical constants and the empirical power function F. The constant K is different for each noise component. The constant G depends on the noise component and the indices i and j defined as

$$i = \begin{cases} 1 & \text{(Fan with no inlet guide vanes)} \\ 2 & \text{(Fan with inlet guide vanes)} \end{cases} \tag{6}$$

and

$$j = \begin{cases} 1 & (\delta > 1.05) \\ 2 & (\delta \leq 1.05) \end{cases} \tag{7}$$

The fundamental tone cut-off factor δ is defined as

$$\delta = \frac{M_t}{\left|1 - \frac{V}{B}\right|} \tag{8}$$

where the fan rotor tip Mach number M_t is

$$M_t = \pi N^* \tag{9}$$

If $M_t > 1.05$, then $\delta = M_t$. The fundamental tone cut-off occurs when the value of δ is less than 1.05. The cut-off factor determines the range of the tip Mach number where the fundamental blade passing frequency dominates.

The rotor-stator spacing exponent $a(k,\ell)$ depends on the noise component and the indices k and ℓ defined as

$$k = \begin{cases} 1 & (s^* \leq 1) \\ 2 & (s^* > 1) \end{cases} \tag{10}$$

and

$$\ell = \begin{cases} 1 & \text{(No inlet flow distortion)} \\ 2 & \text{(Inlet flow distortion)} \end{cases} \tag{11}$$

Inlet flow distortion tends to reduce rotor-stator spacing effects. Inlet flow distortion is assumed to occur during static and ground roll operations.

The design point Mach number index M_m is defined as

$$M_m = \max\,(1, M_d) \tag{12}$$

where M_d is the design value of the relative tip Mach number. The exponent b in equation (5) gives the effect of M_m on each fan noise component.

The final empirical quantity in equation (5) is the power function F. The power function depends on the fan noise source and is, in general, a function of the relative tip Mach number M_r and the design point Mach number index. The relative tip Mach number is defined as

$$M_r = \left(M_x^2 + \quad^2\right)^{1/2} \tag{13}$$

where the tip Mach number M_t is defined by equation (9) and the axial flow Mach number M_x is equal to $\dot{m}^*/A^*$ since the inlet static density and speed of sound can be assumed equal to the ambient values.

As indicated by equation (1), each fan noise source has its own directivity function D and spectrum function S. Using these functions and the acoustic power, the mean-square acoustic pressure is computed as a function of frequency and polar directivity angle for a given set of input parameters. The broadband noise is expressed as 1/3-octave-band data. The pure tones are values at discrete frequencies. The pure tones must be added to the appropriate 1/3-octave band so that a total 1/3-octave-band fan noise spectrum is determined. For a given value of the 1/3-octave-band center frequency parameter η the lowest harmonic number that falls within that band is

$$n_\ell = [10^{-1/20}\ \eta] + 1 \tag{14}$$

and the highest harmonic number is

$$n_u = [10^{1/20}\ \eta] \tag{15}$$

where [ ] indicates the integer part of the enclosed real number. If $n_\ell > n_u$, then there is no tone within the band. If $n_\ell \leq n_u$, then there are $n_u - n_\ell + 1$ tones within the band. The pure tone mean-square pressures for each harmonic number n are then added to the appropriate band. The tones are propagated to the observer as 1/3-octave-band data.

The empirical constants and functions used to compute the acoustic power for the six fan noise components are summarized in table II. The directivity and spectrum functions are summarized in tables III and IV, respectively. Each fan noise component is discussed in detail as follows.

Inlet Broadband Noise

Inlet broadband noise is associated with random unsteadiness or turbulence in the flow passing the blading. Some of the sources of this random unsteady flow are turbulence in boundary layers, blade wakes and vortices, and the inlet flow. Although predictions of the individual sources of broadband noise are beyond the scope of this module, the total broadband noise radiated from the inlet is predicted.

The acoustic power due to broadband noise from the inlet is

$$W^* = (1.552 \times 10^{-4})(s^*)^{-a(k,2)} M_m^2 (\dot{m}^*/A^*)(\Delta T^*)^2\, F(M_r) \tag{16}$$

where the constant $a(k,\ell)$ is

$$a(k,\ell) = \begin{bmatrix} 0.5 & 0.5 \\ 0.5 & 0 \end{bmatrix} \tag{17}$$

The exponent a defined by equation (17) accounts for the fact that the acoustic power varies inversely with the rotor-stator spacing except where inlet flow distortion effects dominate rotor-stator spacing effects at $s^* > 1$. The power function F is

$$F = \begin{cases} 1 & (M_r \leq 0.9) \\ 0.81 M_r^{-2} & (M_r > 0.9) \end{cases} \tag{18}$$

which is plotted in figure 2.

The mean-square acoustic pressure due to inlet broadband noise is computed from equation (1). The directivity function D is given in table III and plotted in figure 3. The spectral function S is given by

$$S = 0.116 \exp\left\{-0.5\left[\frac{\ln (n/2.5)}{\ln \sigma}\right]^2\right\} \tag{19}$$

where σ is the geometric mean deviation and is equal to 2.2. Equation (19) is plotted in figure 4.

Inlet Rotor-Stator Interaction Tones

Discrete tone generation is associated with lift fluctuations on rotor or stator blades. Interaction tones are generated by rotor blades intersecting the wakes from preceding stator vanes or inlet guide vanes or by rotating wakes from a rotor impinging on stator vanes. The tones are propagated from the blades as spinning duct modes. No attempt is made to determine the specific characteristics of each propagated mode, only the average far-field characteristics are predicted.

The acoustic power due to inlet rotor-stator interaction tones is

$$W^* = (2.683 \times 10^{-4})\, G(i,j)\, (s^*)^{-a(k,\ell)} M_m^{4.31} (\dot{m}^*/A^*)\, (\Delta T^*)^2\, F(M_r, M_m) \tag{20}$$

where the constants are

$$G(i,j) = \begin{bmatrix} 1 & 0.580 \\ 0.625 & 0.205 \end{bmatrix} \tag{21}$$

and

$$a(k,\ell) = \begin{bmatrix} 1 & 1 \\ 1 & 0 \end{bmatrix} \tag{22}$$

The constants in the matrix G account for the effect of inlet guide vanes and fundamental tone cut-off. The exponent on the rotor-stator spacing accounts for the inverse variation of the acoustic power except when inlet flow distortion effects dominate at $s^* > 1$. The power function F is

$$F = \begin{cases} 0.397M_m^{-2.31} & (M_r \le 0.72) \\ 2.053M_m^{-2.31}M_r^5 & \left(0.72 < M_r \le 0.866M_m^{0.462}\right) \\ 0.315M_m^{3.69}M_r^{-8} & \left(0.866M_m^{0.462} < M_r\right) \end{cases} \tag{23}$$

which is plotted in figure 5.

The mean-square acoustic pressure due to inlet rotor-stator interaction tones is computed from equation (1). The directivity function D is given in table III and plotted in figure 6. The spectral function S is a discrete function given by

$$S(\eta) = \sum_{n=n_\ell}^{n_u} S(n,i,j) \tag{24}$$

where n_ℓ and n_u are the lower and upper values of the harmonic number associated with the 1/3-octave band with a center frequency parameter value of η. For $n = 1$,

$$S(1,i,j) = \begin{bmatrix} 0.499 & 0.136 \\ 0.799 & 0.387 \end{bmatrix} \tag{25}$$

and for $n > 1$,

$$S(n,i,j) = \begin{bmatrix} 0.250 & 0.432 \\ 0.101 & 0.307 \end{bmatrix} \times 10^{-0.3(n-2)} \qquad (26)$$

where i and j are defined by equations (6) and (7), respectively. The function $S(n)$ is plotted in figures 7 to 10 prior to being converted to 1/3-octave-band data.

Inlet Flow Distortion Tones

Inlet flow distortion has an effect on broadband noise and rotor-stator interaction tones. In addition, inlet flow distortion can generate unsteady lift on the blades which produces additional pure tone noise. The average properties of the far-field noise are predicted.

The acoustic power due to inlet flow distortion tones is

$$\Pi^* = (1.488 \times 10^{-4})(s^*)^{-a(k,\ell)} M_m^{4.31} (\dot{m}^*/A^*)(\Delta T^*)^2 F(M_r, M_m) \qquad (27)$$

where $a(k,\ell)$ and $F(M_r,M_m)$ are defined by equations (22) and (23), respectively, and the power function F is plotted in figure 5.

The mean-square acoustic pressure due to inlet flow distortion tones is computed from equation (1). The directivity function D is the same as for the inlet rotor-stator interaction tones as given in table III and plotted in figure 6. The spectral function S is given by

$$S(\eta) = 9 \sum_{n=n_\ell}^{n_u} 10^{-\eta} \qquad (28)$$

which is plotted in figure 11 prior to being converted to 1/3-octave-band data.

Combination Tone Noise

When the relative speed of the rotor blade tips exceeds a Mach number value of 1, shock waves are formed at the leading edge of each rotor blade. These shock waves propagate through the engine inlet as a series of Mach waves. The resulting spectrum contains harmonics of the shaft speed instead of the blade passing frequency. The resultant noise is not purely tonal but extends in a frequency interval on either side of the harmonic frequency. This combination tone noise is often referred to as "buzz-saw" noise.

The acoustic power due to combination tone noise is

$$\Pi^* = K\, G(i,j)\, (\dot{m}^*/A^*)\, (\Delta T^*)^2\, F(M_r) \tag{29}$$

The acoustic power for three harmonics of the shaft rotational speed are computed. They are expressed as fractions of the fundamental tone of the blade passing frequency. The constants K for each harmonic are 6.225×10^{-4} for the 1/8 fundamental combination tone, 2.030×10^{-3} for the 1/4 fundamental combination tone, and 2.525×10^{-3} for the 1/2 fundamental combination tone. The constant $G(i,j)$ is given by

$$G(i,j) = \begin{bmatrix} 1 & 1 \\ 0.316 & 0.316 \end{bmatrix} \tag{30}$$

This accounts for the fact that inlet guide vanes inhibit the propagation of combination tones through the inlet. The power function F is given by

$$F(M_r) = \begin{cases} 0 & (M_r < 1) \\ 10^{-6.75(1.61-M_r)} & (1 \le M_r \le 1.61) \\ 10^{-1.21(M_r-1.61)} & (1.61 < M_r) \end{cases} \tag{31}$$

for the 1/8 fundamental combination tone,

$$F(M_r) = \begin{cases} 0 & (M_r < 1) \\ 10^{-14.75(1.322-M_r)} & (1 \le M_r \le 1.322) \\ 10^{-1.33(M_r-1.322)} & (1.322 < M_r) \end{cases} \tag{32}$$

for the 1/4 fundamental combination tone, and

$$F(M_r) = \begin{cases} 0 & (M_r < 1) \\ 10^{-31.85(1.146-M_r)} & (1 \le M_r \le 1.146) \\ 10^{-1.41(M_r-1.146)} & (1.146 < M_r) \end{cases} \tag{33}$$

for the 1/2 fundamental combination tone. The power function is plotted in figure 12.

The mean-square acoustic pressure is computed separately for each combination tone by equation (1). Then, the three harmonics are summed to yield the 1/3-octave-band spectrum due to combination tone noise. The directivity function D is the same for all three harmonics and is given in table III and plotted in figure 13. The spectrum function S is given by

$$S(\eta) = \begin{cases} 0.405(8\eta)^5 & (\eta \leq 0.125) \\ 0.405(8\eta)^{-3} & (\eta > 0.125) \end{cases} \tag{34}$$

for the 1/8 fundamental combination tone,

$$S(\eta) = \begin{cases} 0.520(4\eta)^5 & (\eta \leq 0.25) \\ 0.520(4\eta)^{-5} & (\eta > 0.25) \end{cases} \tag{35}$$

for the 1/4 fundamental combination tone, and

$$S(\eta) = \begin{cases} 0.332(2\eta)^3 & (\eta \leq 0.5) \\ 0.332(2\eta)^{-3} & (\eta > 0.5) \end{cases} \tag{36}$$

for the 1/2 fundamental combination tone. The spectrum functions for combination tone noise are plotted in figure 14.

Discharge Broadband Noise

The discharge broadband noise is created by the same mechanisms as the inlet broadband noise. The acoustic power of the discharge broadband noise is

$$\Pi^* = (3.206 \times 10^{-4})\, G(i,j)\, (s^*)^{-a(k,\ell)} M_m^2 (\dot{m}^*/A^*)(\Delta T^*)^2\, F(M_r) \tag{37}$$

where $a(k,\ell)$ is the same as for inlet broadband noise given by equation (17) and $G(i,j)$ is

$$G(i,j) = \begin{bmatrix} 1 & 1 \\ 2 & 2 \end{bmatrix} \tag{38}$$

The factor G shows that the presence of inlet guide vanes doubles the acoustic power of the discharge broadband noise. The power function F is given by

$$F(M_r) = \begin{cases} 1 & (M_r \leq 1.0) \\ M_r^{-2} & (M_r > 1.0) \end{cases} \tag{39}$$

and is plotted in figure 15.

The mean-square acoustic pressure due to discharge broadband noise is computed from equation (1). The directivity function D is given in table III and is plotted in figure 16. The spectrum function S is the same as the inlet broadband noise spectrum as given in equation (19) and plotted in figure 4.

Discharge Rotor-Stator Interaction Tones

The discharge rotor-stator interaction tones are created by the same mechanisms as the inlet rotor-stator interaction tones. The acoustic power of the discharge rotor-stator interaction tones is

$$\Pi^* = (2.643 \times 10^{-4})\, G(i,j)\,(s^*)^{-a(k,\ell)} M_m^2 (\dot{m}^*/A^*)(\Delta T^*)^2\, F(M_r) \tag{40}$$

The matrix $a(k,\ell)$ is the same as for inlet rotor-stator tones given by equation (21) and the matrix $G(i,j)$ is

$$G(i,j) = \begin{bmatrix} 1 & 0.580 \\ 2.50 & 0.820 \end{bmatrix} \tag{41}$$

which gives the effect of inlet guide vanes and fundamental tone cut-off. The power function F is the same as the discharge broadband noise as given in equation (39) and plotted in figure 15.

The mean-square acoustic pressure due to discharge rotor-stator interaction tones is computed from equation (1). The directivity function D is given in table III and plotted in figure 17. The spectrum function S is the same as the inlet rotor-stator interaction tones as given in equations (24) to (26) and plotted in figures 7 to 10.

Output Computation

The 1/3-octave-band mean-square acoustic pressure for a fan is the sum of the mean-square pressures from the six fan noise components. The user has the option of deleting one or more of the noise source components if desired.

The mean-square acoustic pressure is computed for each desired value of the frequency, polar directivity angle, and azimuthal directivity angle. The total noise is the mean-square acoustic pressure multiplied by the number of engines N_e for the output table. In addition, printed output is available of the sound pressure level SPL defined as

$$SPL = 10 \log_{10} \langle p^2 \rangle^* + 20 \log_{10} \frac{\rho_\infty c_\infty^2}{p_{ref}} \tag{42}$$

and the power level PWL defined as

$$PWL = 10 \log_{10} \Pi^* + 10 \log_{10} \frac{\rho_\infty c_\infty^3 A^* A_e}{\Pi_{ref}} \tag{43}$$

REFERENCE

1. Heidmann, M. F.: Interim Prediction Method for Fan and Compressor Source Noise. NASA TM X-71763, 1975.

TABLE I.- RANGE AND DEFAULT VALUES OF INPUT PARAMETERS

Input parameter	Minimum	Default	Maximum
A_e, m^2	0.01	$\pi/4$	10
N_e	1	1	4
r_s, m	0.01	$\sqrt{A_e}$	100
A^*	0.1	1	10
B	2	20	100
d^*	0.3	1.128	4
i	1	1	2
M_d	0.5	1.0	2.0
j	1	1	2
s^*	0.2	1	10
V	10	50	200
m^*	0	0.2	10
M_∞	0	0	0.9
N^*	0	0.3	0.5
ΔT^*	0	0.2	1.3
c_∞, m/s	200	340.294	400
ρ_∞, kg/m^3	0.2	1.225	1.5

TABLE II.- CONSTANTS AND FUNCTIONS FOR FAN ACOUSTIC POWER

Source	K	$\begin{bmatrix} G(1,1) & G(1,2) \\ G(2,1) & G(2,2) \end{bmatrix}$	$\begin{bmatrix} a(1,1) & a(1,2) \\ a(2,1) & a(2,2) \end{bmatrix}$	b	$F(M_r, M_m)$
Inlet broadband noise	1.552×10^{-4}	$\begin{bmatrix} 1 & 1 \\ 1 & 1 \end{bmatrix}$	$\begin{bmatrix} 0.5 & 0.5 \\ 0.5 & 0 \end{bmatrix}$	2	$\begin{cases} 1 & (M_r \le 0.9) \\ 0.81M_r^{-2} & (M_r > 0.9) \end{cases}$
Inlet rotor-stator interaction tones	2.683×10^{-4}	$\begin{bmatrix} 1 & 0.580 \\ 0.625 & 0.205 \end{bmatrix}$	$\begin{bmatrix} 1 & 1 \\ 1 & 0 \end{bmatrix}$	4.31	$\begin{cases} 0.397M_m^{-2.31} & (M_r \le 0.72) \\ 2.053M_m^{-2.31}M_r^{5} & \left(0.72 < M_r \le 0.866M_m^{0.462}\right) \\ 0.315M_m^{3.69}M_r^{-8} & \left(M_r > 0.866M_m^{0.462}\right) \end{cases}$
Inlet flow distortion tones	1.488×10^{-4}	$\begin{bmatrix} 1 & 1 \\ 1 & 1 \end{bmatrix}$	$\begin{bmatrix} 1 & 1 \\ 1 & 0 \end{bmatrix}$	4.31	$\begin{cases} 0.397M_m^{-2.31} & (M_r \le 0.72) \\ 2.053M_m^{-2.31}M_r^{5} & \left(0.72 < M_r \le 0.866M_m^{0.462}\right) \\ 0.315M_m^{3.69}M_r^{-8} & \left(M_r > 0.866M_m^{0.462}\right) \end{cases}$
1/8 fundamental combination tone noise	6.109×10^{-4}	$\begin{bmatrix} 1 & 1 \\ 0.316 & 0.316 \end{bmatrix}$	$\begin{bmatrix} 0 & 0 \\ 0 & 0 \end{bmatrix}$	0	$\begin{cases} 0 & (M_r < 1) \\ 10^{-6.75(1.61-M_r)} & (1 \le M_r \le 1.61) \\ 10^{-1.21(M_r-1.61)} & (M_r > 1.61) \end{cases}$

TABLE II.- Concluded

Source	K	$\begin{bmatrix} G(1,1) & G(1,2) \\ G(2,1) & G(2,2) \end{bmatrix}$	$\begin{bmatrix} a(1,1) & a(1,2) \\ a(2,1) & a(2,2) \end{bmatrix}$	b	$F(M_r, M_m)$
1/4 fundamental combination tone noise	2.030×10^{-3}	$\begin{bmatrix} 1 & 1 \\ 0.316 & 0.316 \end{bmatrix}$	$\begin{bmatrix} 0 & 0 \\ 0 & 0 \end{bmatrix}$	0	$\begin{cases} 0 & (M_r < 1) \\ 10^{-14.75(1.322-M_r)} & (1 \le M_r \le 1.322) \\ 10^{-1.33(M_r-1.322)} & (M_r > 1.322) \end{cases}$
1/2 fundamental combination tone noise	2.525×10^{-3}	$\begin{bmatrix} 1 & 1 \\ 0.316 & 0.316 \end{bmatrix}$	$\begin{bmatrix} 0 & 0 \\ 0 & 0 \end{bmatrix}$	0	$\begin{cases} 0 & (M_r < 1) \\ 10^{-31.85(1.146-M_r)} & (1 \le M_r \le 1.146) \\ 10^{-1.41(M_r-1.146)} & (M_r > 1.146) \end{cases}$
Discharge broadband noise	3.206×10^{-4}	$\begin{bmatrix} 1 & 1 \\ 2 & 2 \end{bmatrix}$	$\begin{bmatrix} 0.5 & 0.5 \\ 0.5 & 0 \end{bmatrix}$	2	$\begin{cases} 1 & (M_r \le 1.0) \\ M_r^{-2} & (M_r > 1.0) \end{cases}$
Discharge rotor-stator interaction tones	2.643×10^{-4}	$\begin{bmatrix} 1 & 0.581 \\ 2.50 & 0.820 \end{bmatrix}$	$\begin{bmatrix} 1 & 1 \\ 1 & 0 \end{bmatrix}$	2	$\begin{cases} 1 & (M_r \le 1.0) \\ M_r^{-2} & (M_r > 1.0) \end{cases}$

TABLE III.- DIRECTIVITY LEVELS FOR FAN NOISE

θ, deg	Inlet			Discharge	
	Broadband directivity level, $\log_{10} D$	Discrete tone directivity level, $\log_{10} D$	Combination tone directivity level, $\log_{10} D$	Broadband directivity level, $\log_{10} D$	Discrete tone directivity level, $\log_{10} D$
0.	0.43	0.30	-0.43	-3.70	-3.45
10.	0.53	0.45	-0.33	-3.27	-3.05
20.	0.63	0.60	-0.18	-2.84	-2.65
30.	0.63	0.60	0.02	-2.41	-2.25
40.	0.63	0.60	0.32	-1.98	-1.85
50.	0.43	0.48	0.52	-1.55	-1.45
60.	0.18	0.25	0.52	-1.12	-1.05
70.	-0.12	-0.08	0.17	-0.69	-0.65
80.	-0.47	-0.45	-0.23	-0.34	-0.35
90.	-0.87	-0.85	-0.38	-0.04	-0.05
100.	-1.32	-1.30	-0.43	0.19	0.15
110.	-1.87	-1.85	-0.48	0.34	0.35
120.	-2.42	-2.40	-0.53	0.43	0.45
130.	-2.97	-2.95	-0.58	0.46	0.45
140.	-3.52	-3.50	-0.63	0.26	0.25
150.	-4.07	-4.05	-0.68	-0.14	-0.10
160.	-4.62	-4.60	-0.73	-0.54	-0.45
170.	-5.17	-5.15	-0.78	-1.04	-0.85
180.	-5.72	-5.70	-0.83	-1.54	-1.35

TABLE IV.- SPECTRUM FUNCTIONS FOR FAN NOISE

Source	Spectrum function
Inlet broadband noise	$S(\eta) = 0.116 \exp\left\{-0.5\left[\frac{\ln (\eta/2.5)}{\ln 2.2}\right]^2\right\}$
Inlet rotor-stator interaction tones	$S(\eta) = \sum_{n=n_\ell}^{n_u} S(n,i,j)$ where $S(1,i,j) = \begin{bmatrix} 0.499 & 0.136 \\ 0.799 & 0.387 \end{bmatrix}$ $S(n,i,j) = \begin{bmatrix} 0.250 & 0.432 \\ 0.101 & 0.307 \end{bmatrix} \times 10^{-0.3(n-2)} \quad (n > 1)$
Inlet flow distortion tones	$S(\eta) = 9 \sum_{n=n_\ell}^{n_u} 10^{-n}$
1/8 fundamental combination tone noise	$S(\eta) = \begin{cases} 0.405(8\eta)^5 & (\eta \leq 0.125) \\ 0.405(8\eta)^{-3} & (\eta > 0.125) \end{cases}$

TABLE IV.- Concluded

Source	Spectrum function
1/4 fundamental combination tone noise	$S(\eta) = \begin{cases} 0.520(4\eta)^{5} & (\eta \le 0.25) \\ 0.520(4\eta)^{-5} & (\eta > 0.25) \end{cases}$
1/2 fundamental combination tone noise	$S(\eta) = \begin{cases} 0.332(2\eta)^{3} & (\eta \le 0.5) \\ 0.332(2\eta)^{-3} & (\eta > 0.5) \end{cases}$
Discharge broadband noise	$S(\eta) = 0.116 \exp\left\{-0.5\left[\frac{\ln(\eta/2.5)}{\ln 2.2}\right]^{2}\right\}$
Discharge rotor-stator interaction tones	$S(\eta) = \sum_{n=n_{\ell}}^{n_u} S(n,i,j)$ where $S(1,i,j) = \begin{bmatrix} 0.499 & 0.136 \\ 0.799 & 0.387 \end{bmatrix}$ $S(n,i,j) = \begin{bmatrix} 0.250 & 0.432 \\ 0.101 & 0.307 \end{bmatrix} \times 10^{-0.3(n-2)} \quad (n > 1)$

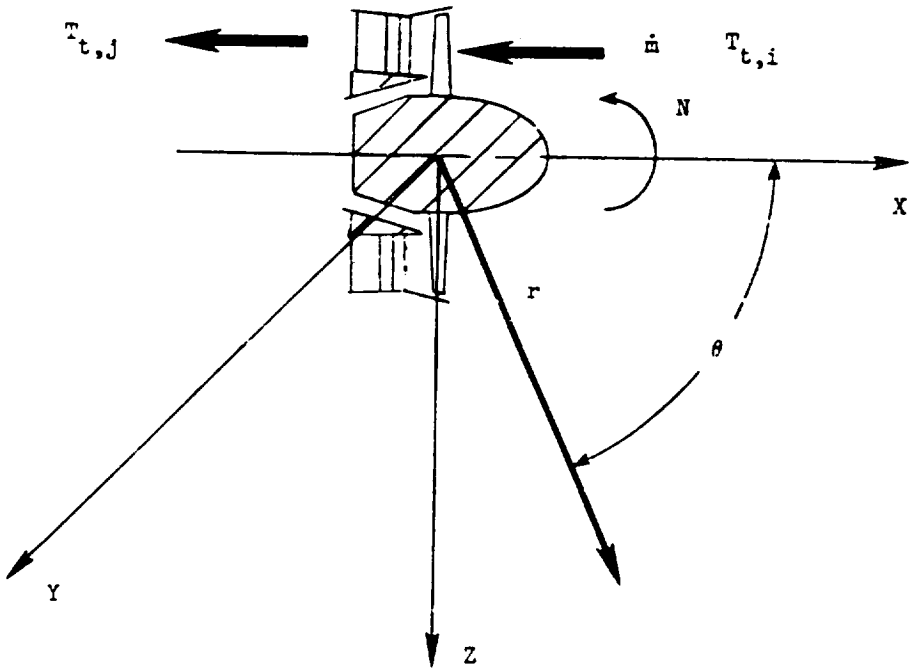

Figure 1.- Schematic diagram of typical axial flow fan.

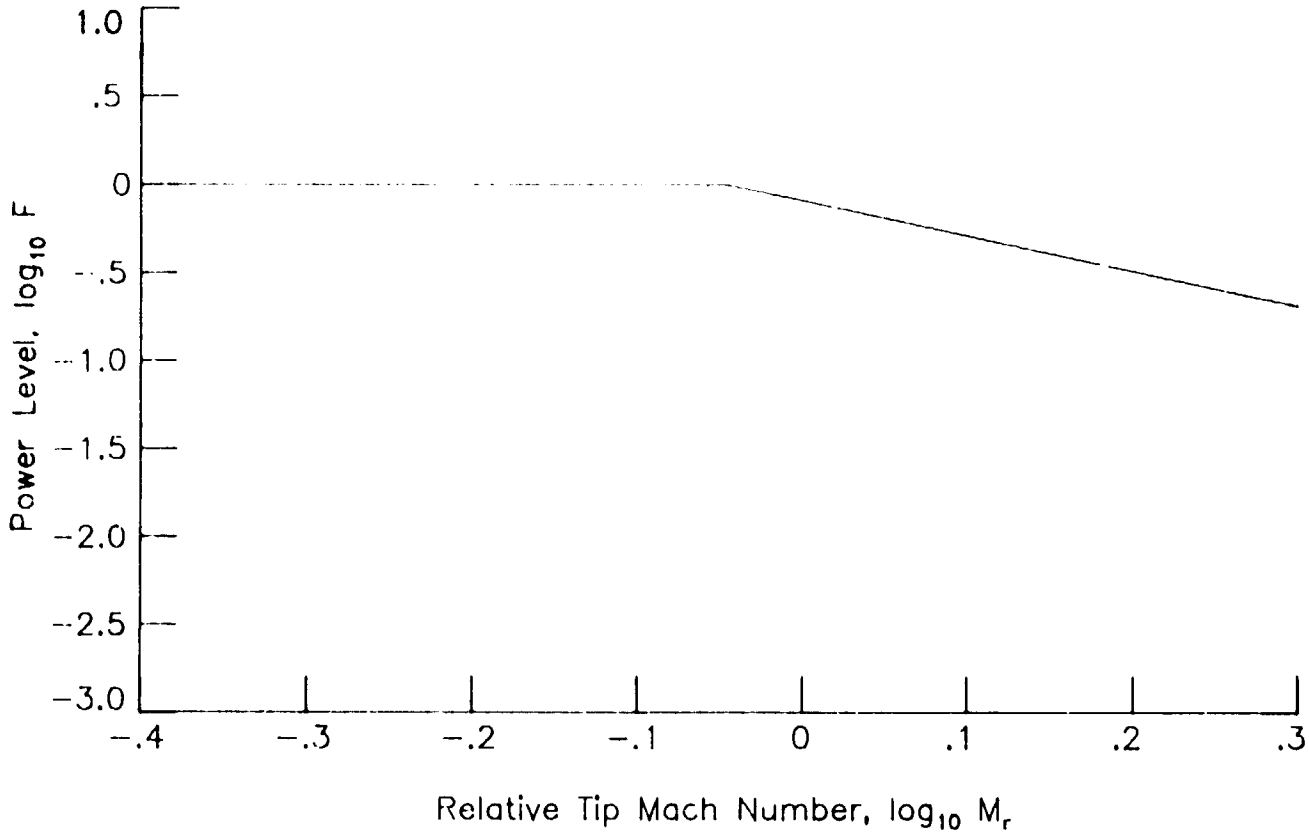

Figure 2.- Power level for inlet broadband noise.

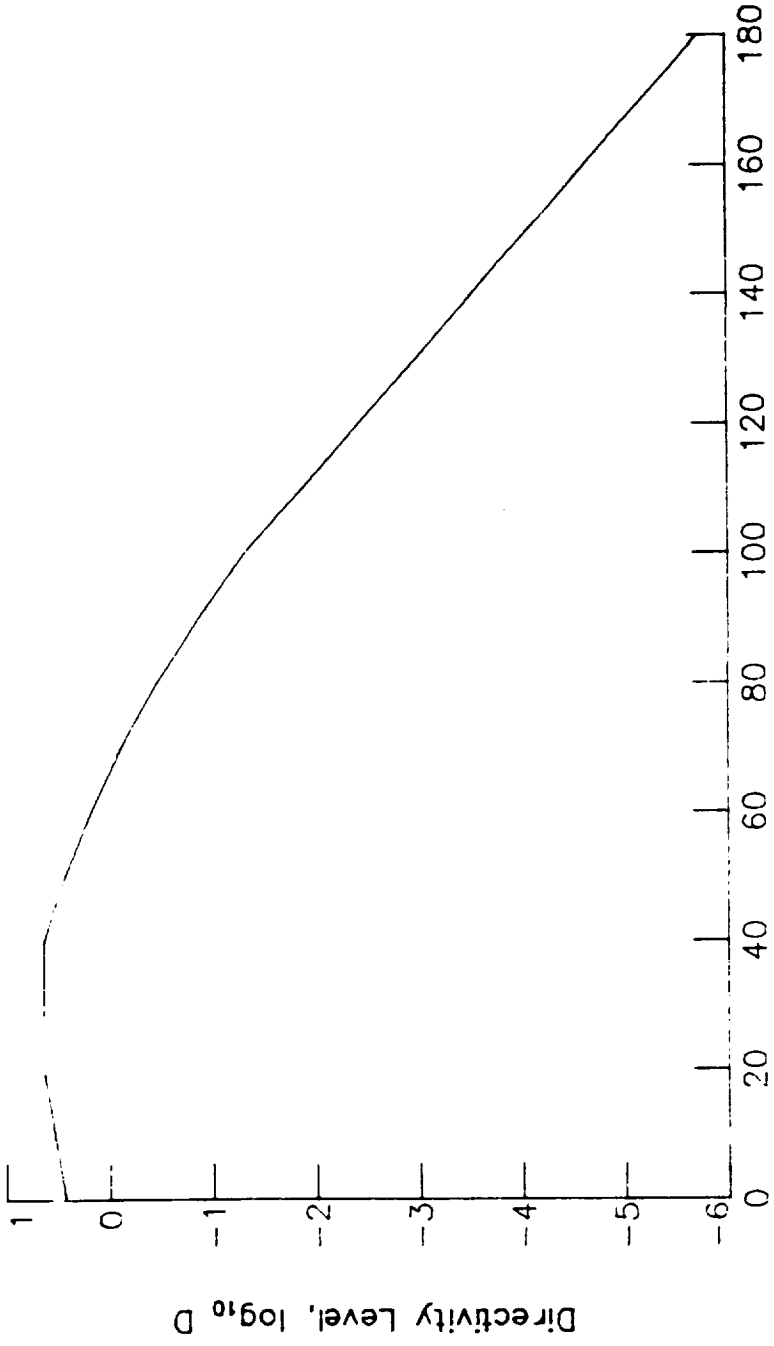

Figure 3.- Directivity level for inlet broadband noise.

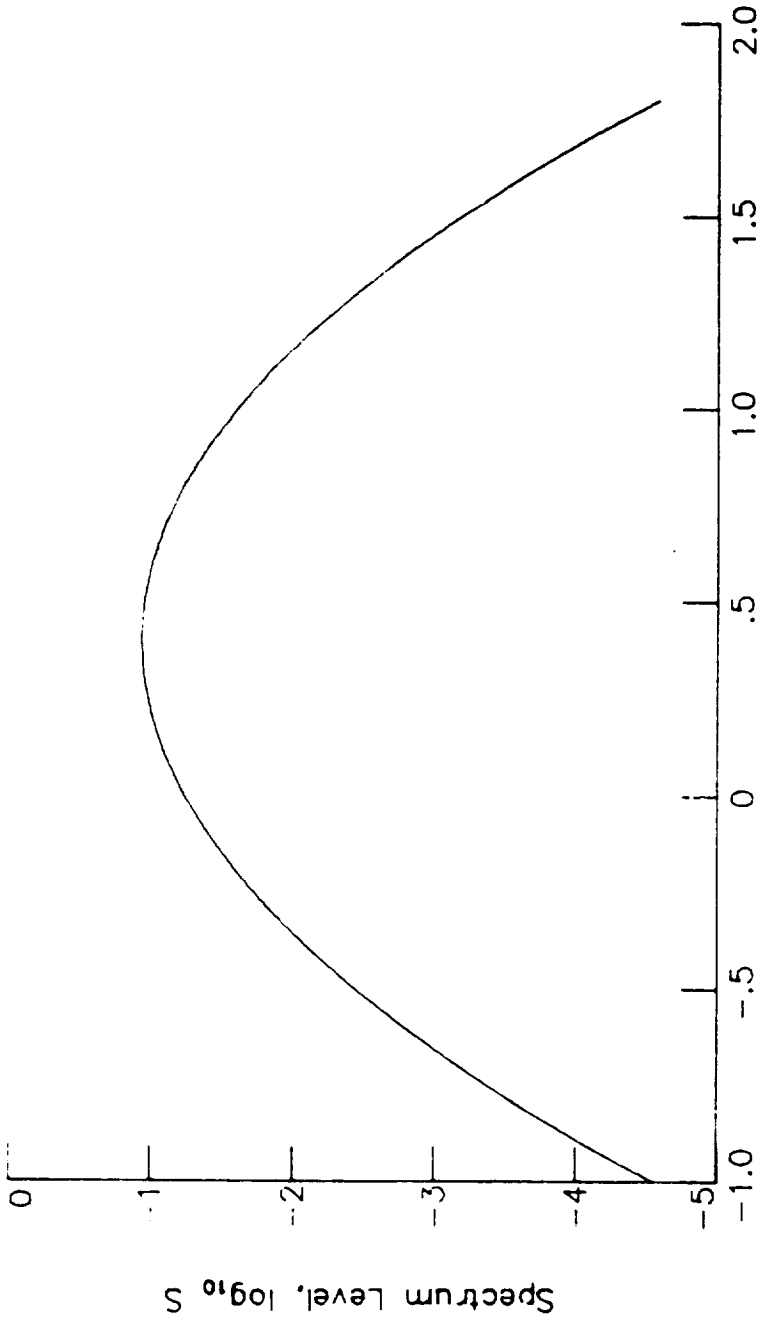

Figure 4.- Spectrum level for inlet and discharge broadband noise.

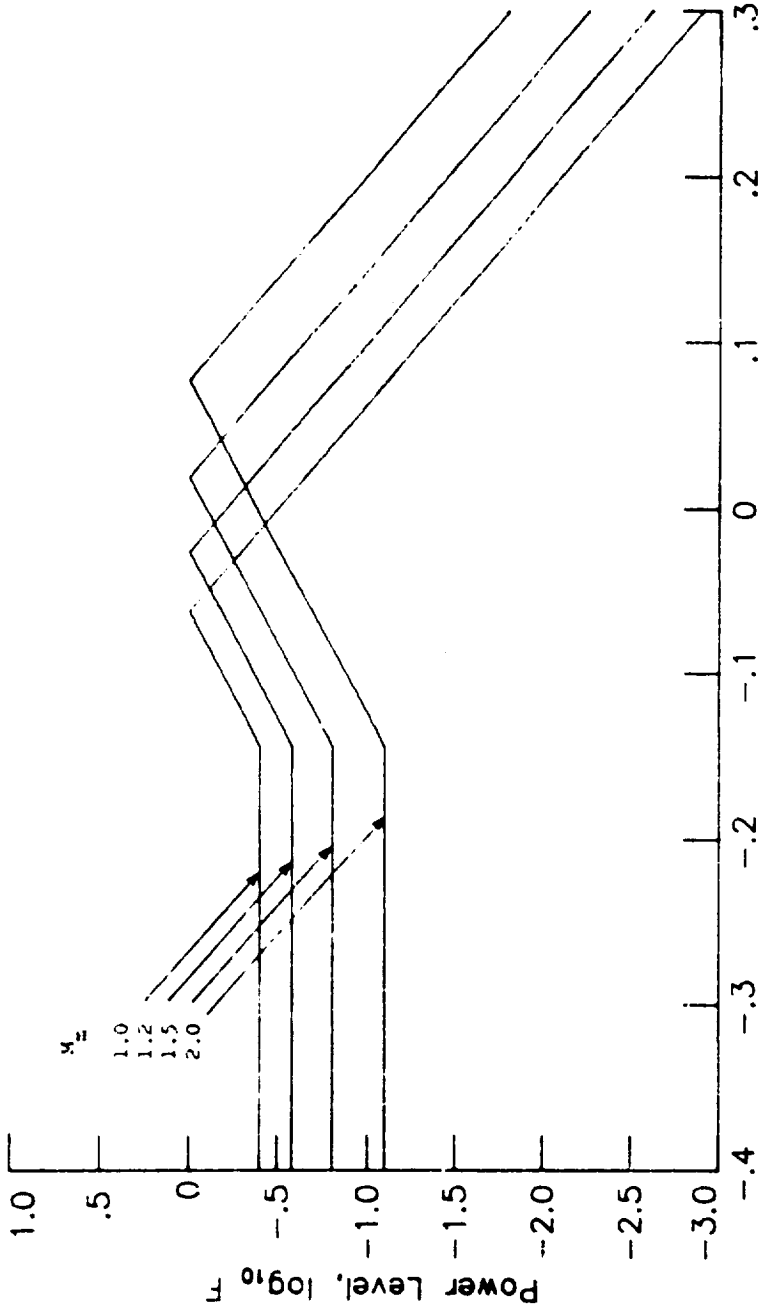

Figure 5.- Power level for inlet rotor-stator interaction tones and inlet flow distortion tones.

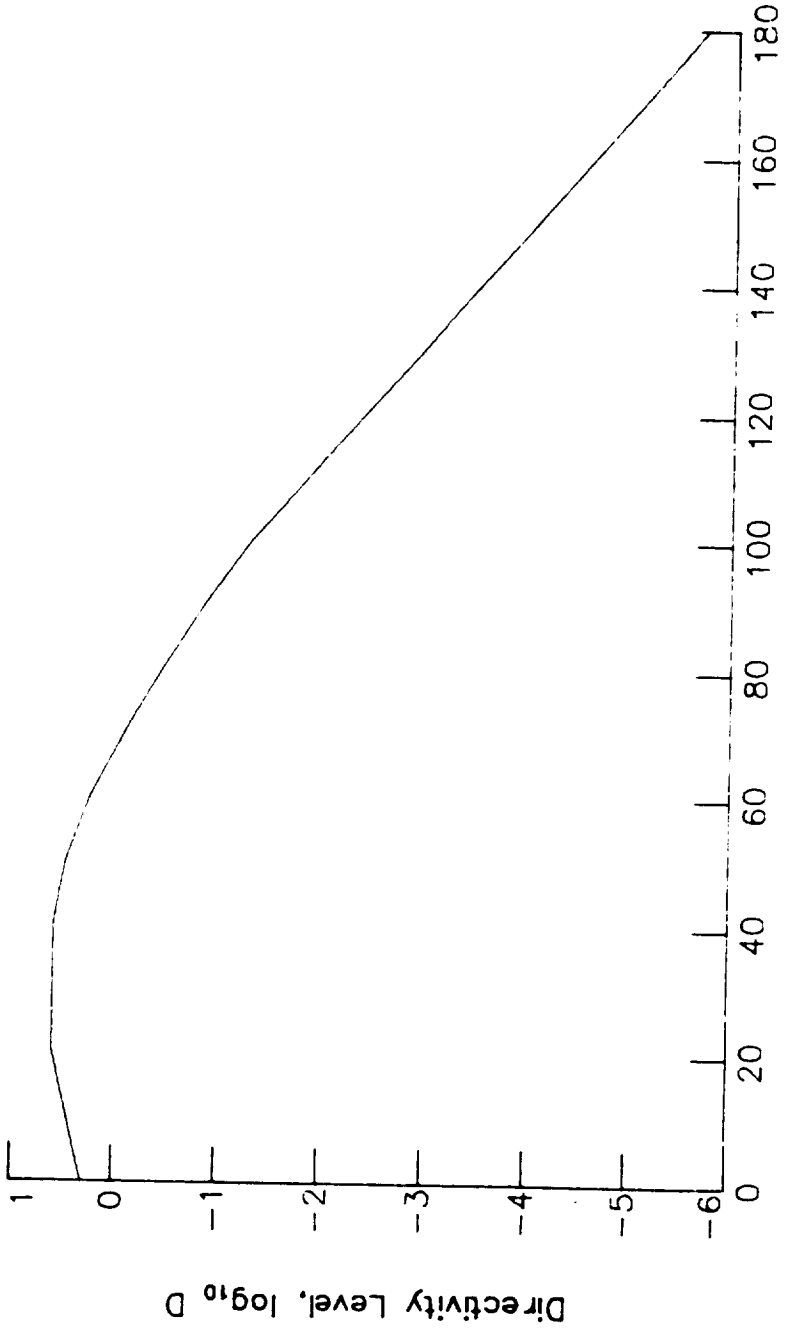

Figure 6.- Directivity level for inlet rotor-stator interaction tones and inlet flow distortion tones.

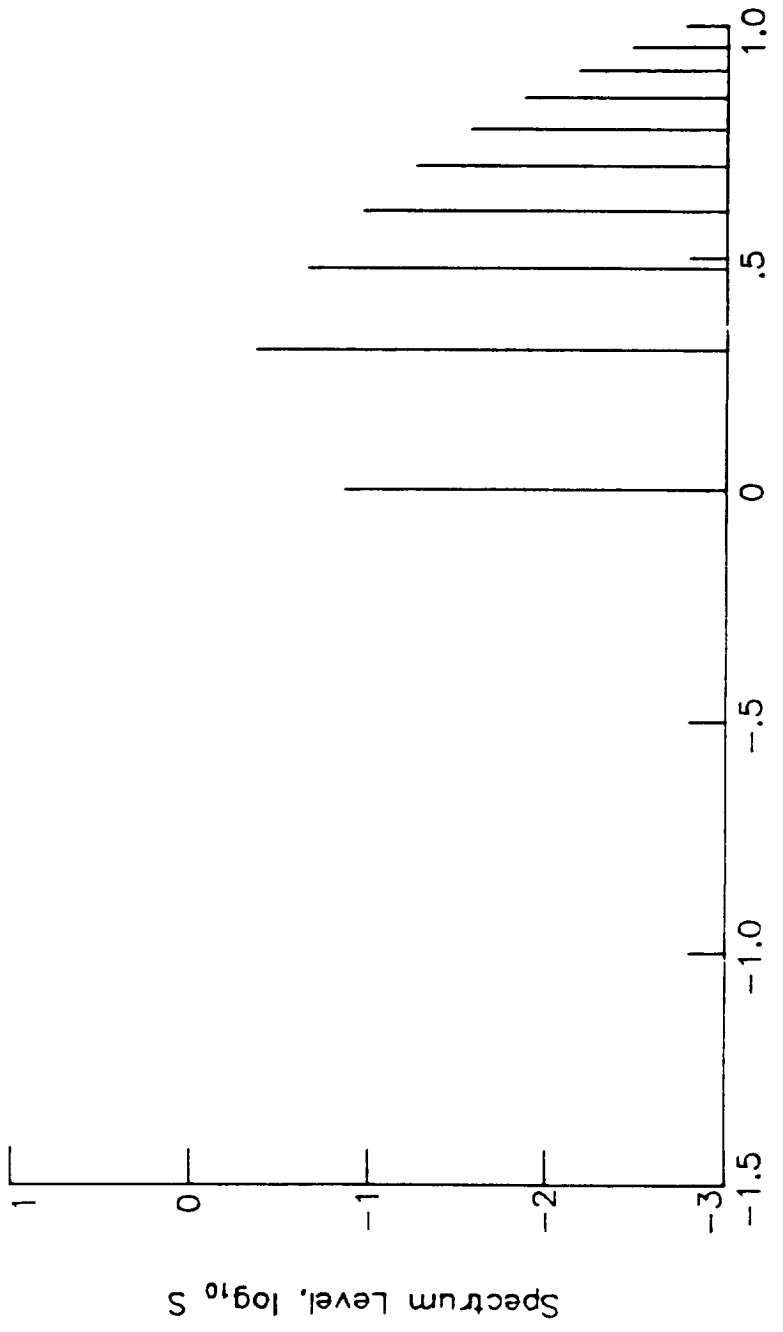

Figure 7.- Spectrum level for inlet and discharge rotor-stator interaction tones with fundamental mode cut-off for fan without inlet guide vanes.

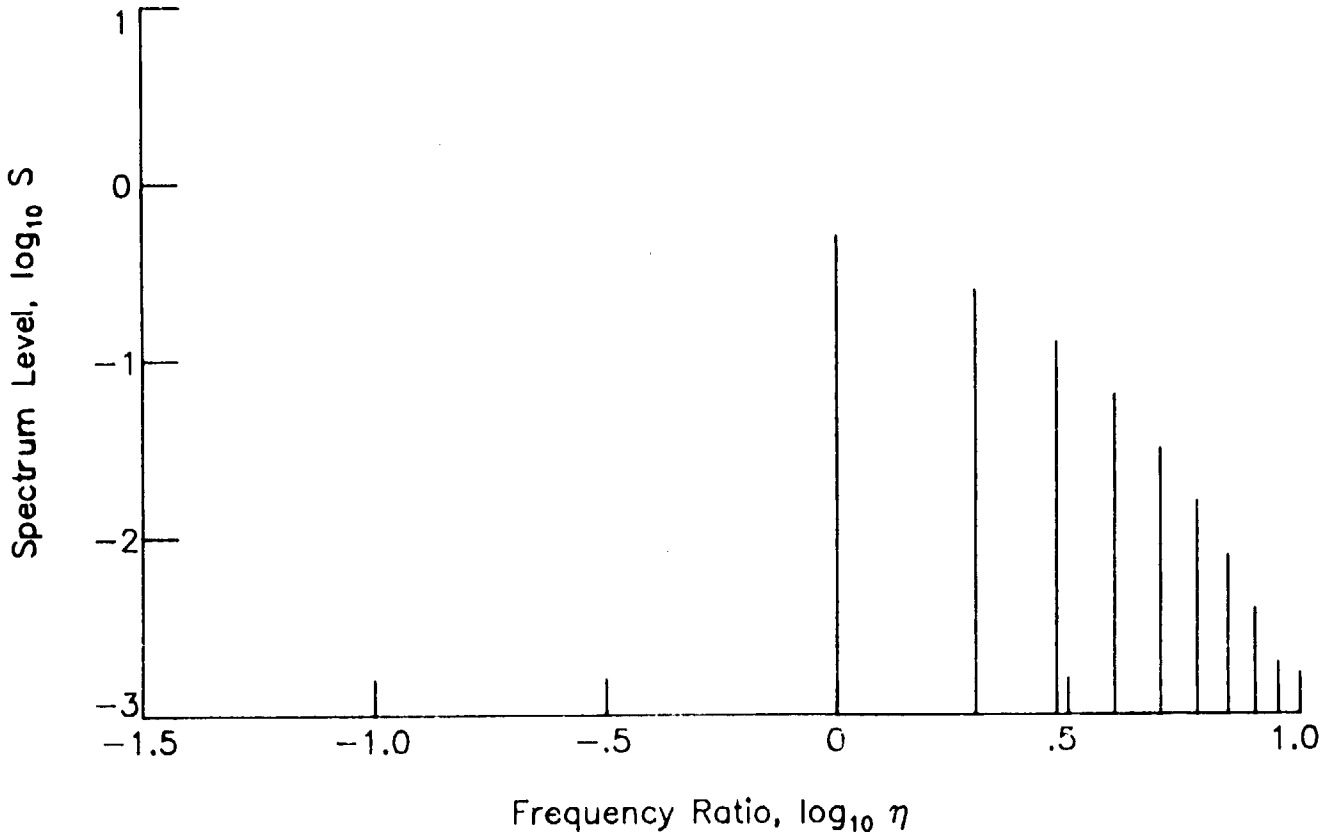

Figure 8.- Spectrum level for inlet and discharge rotor-stator interaction tones without fundamental mode cut-off for fan without inlet guide vanes.

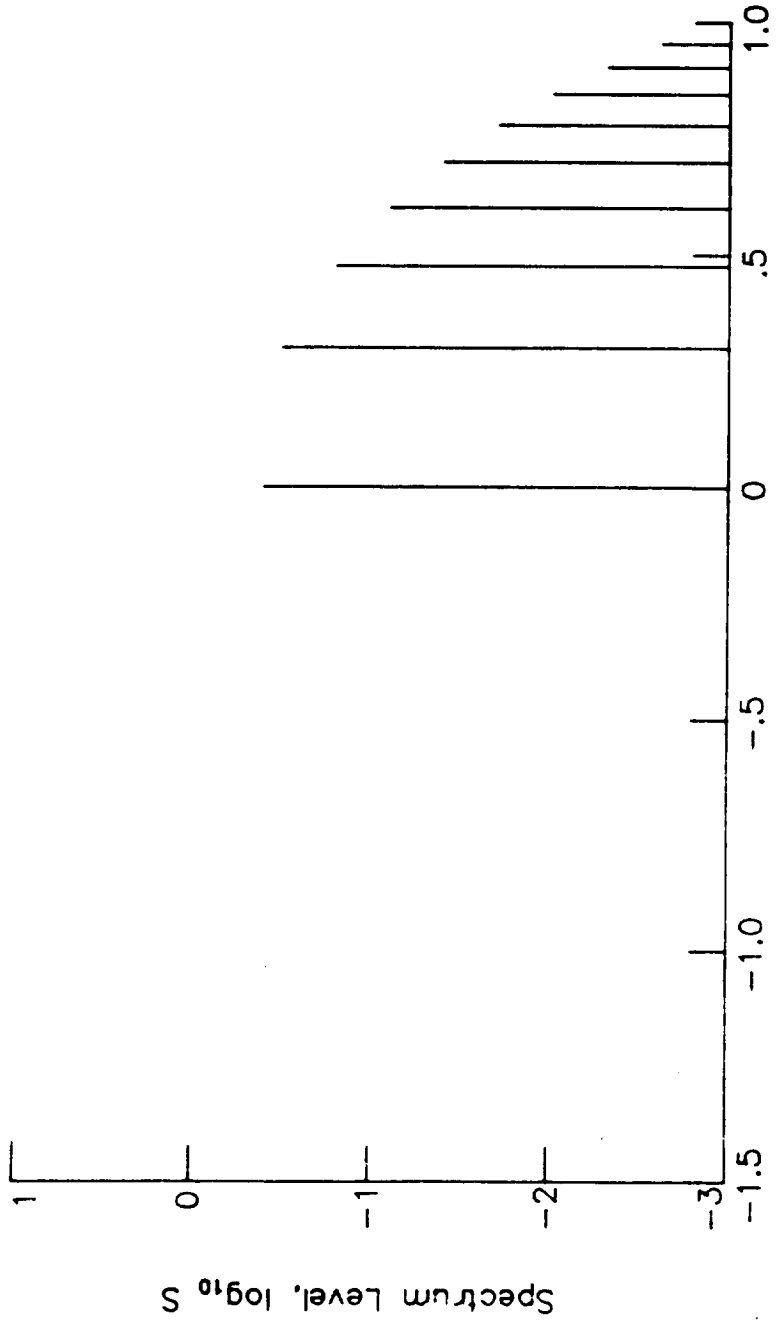

Figure 9.- Spectrum level for inlet and discharge rotor-stator interaction tones with fundamental mode cut-off for fan with inlet guide vanes.

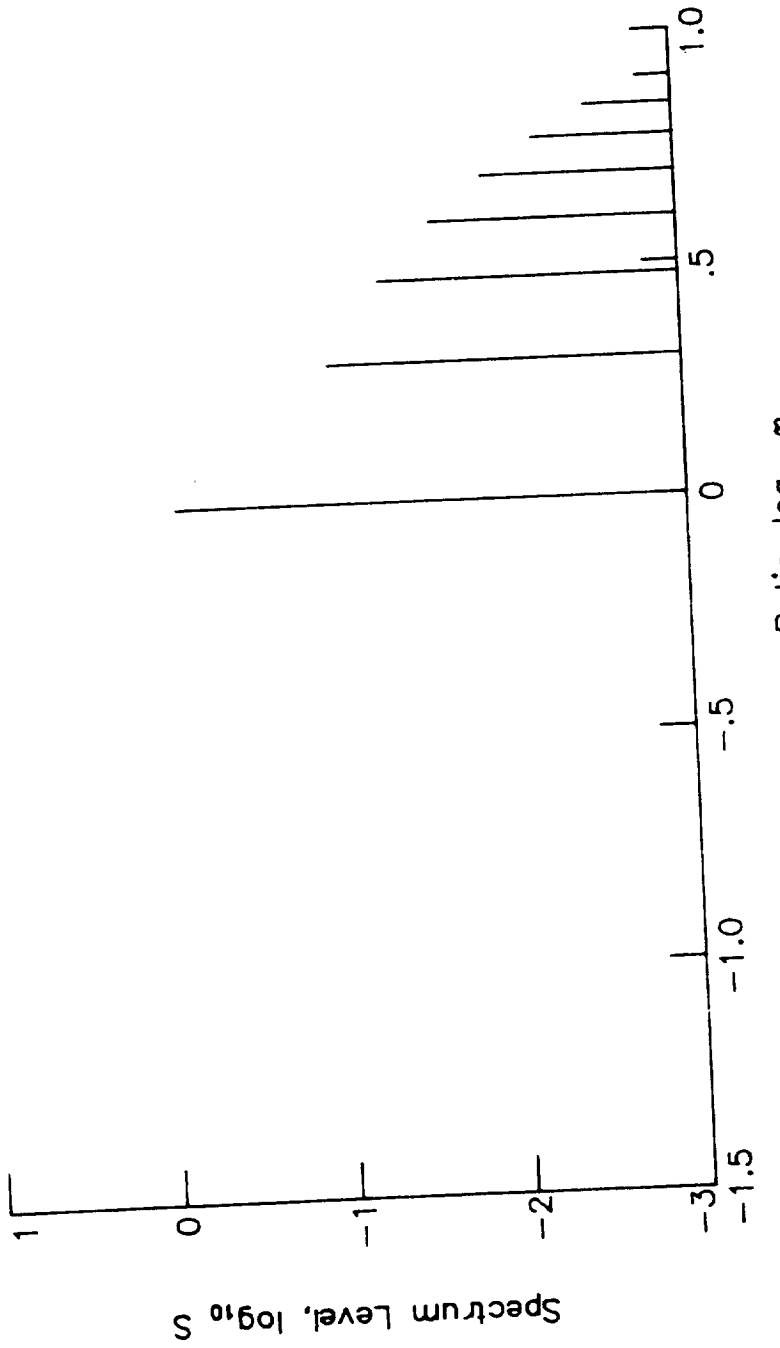

Figure 10.- Spectrum level for inlet and discharge rotor-stator interaction tones without fundamental mode cut-off for fan with inlet guide vanes.

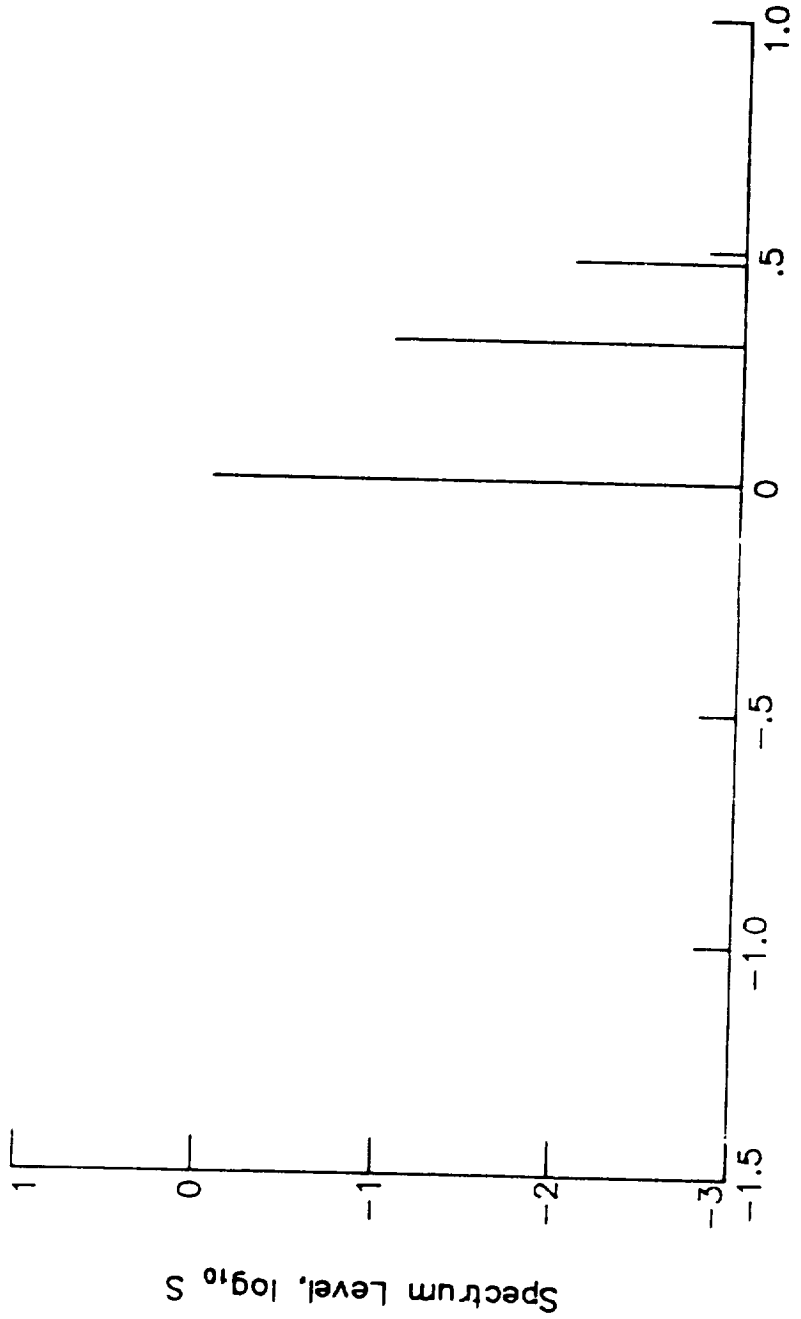

Figure 11.- Spectrum level for inlet flow distortion tones.

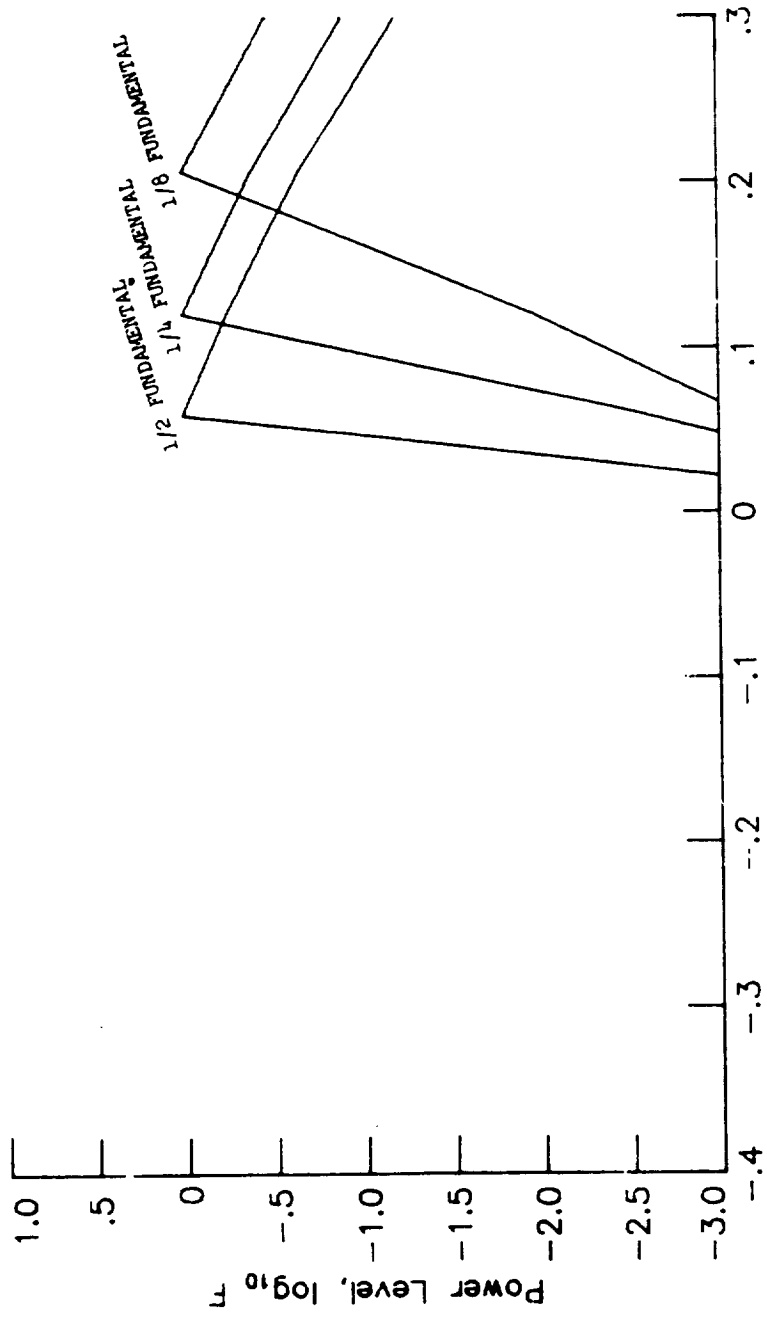

Figure 12.- Power level for combination tone noise.

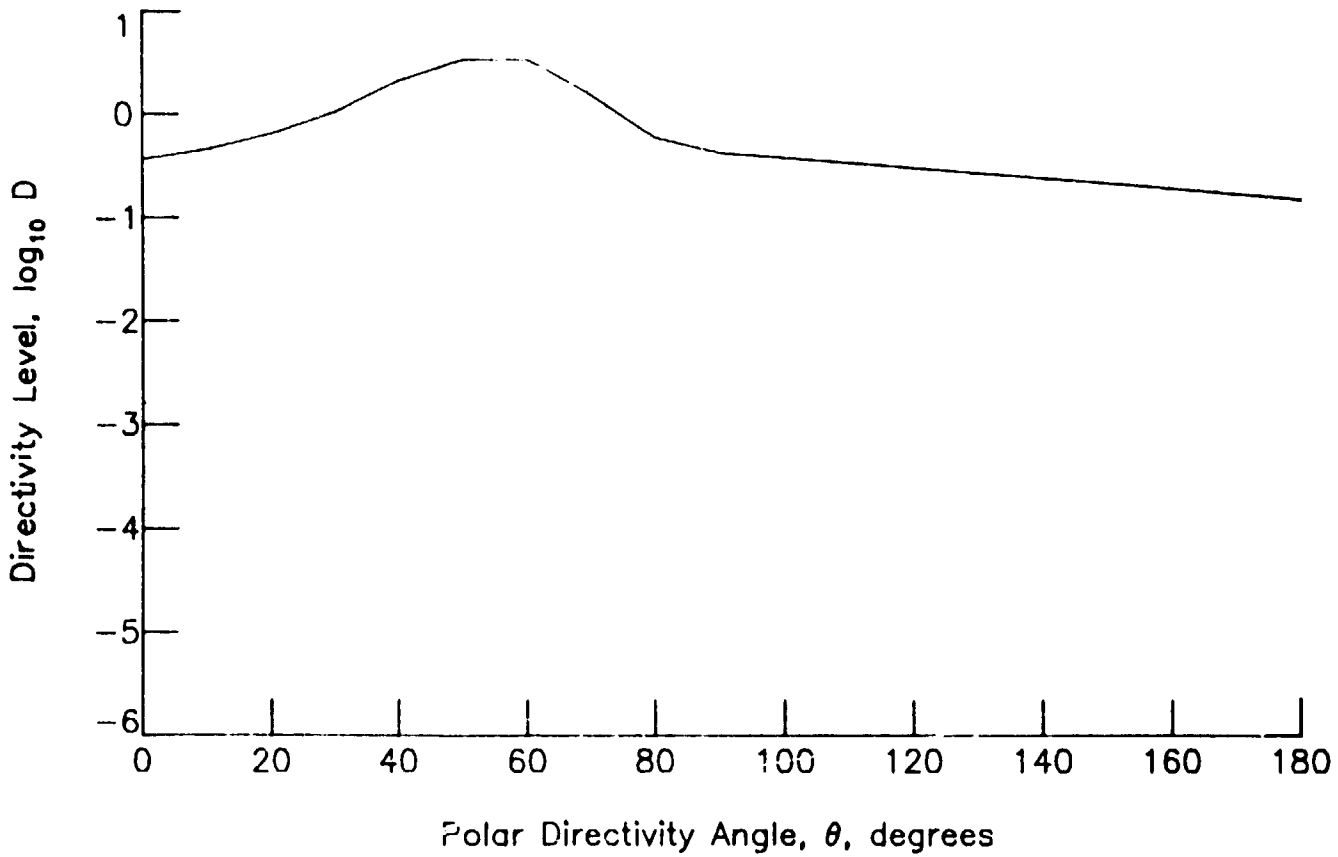

Figure 13.- Directivity level for combination tone noise.

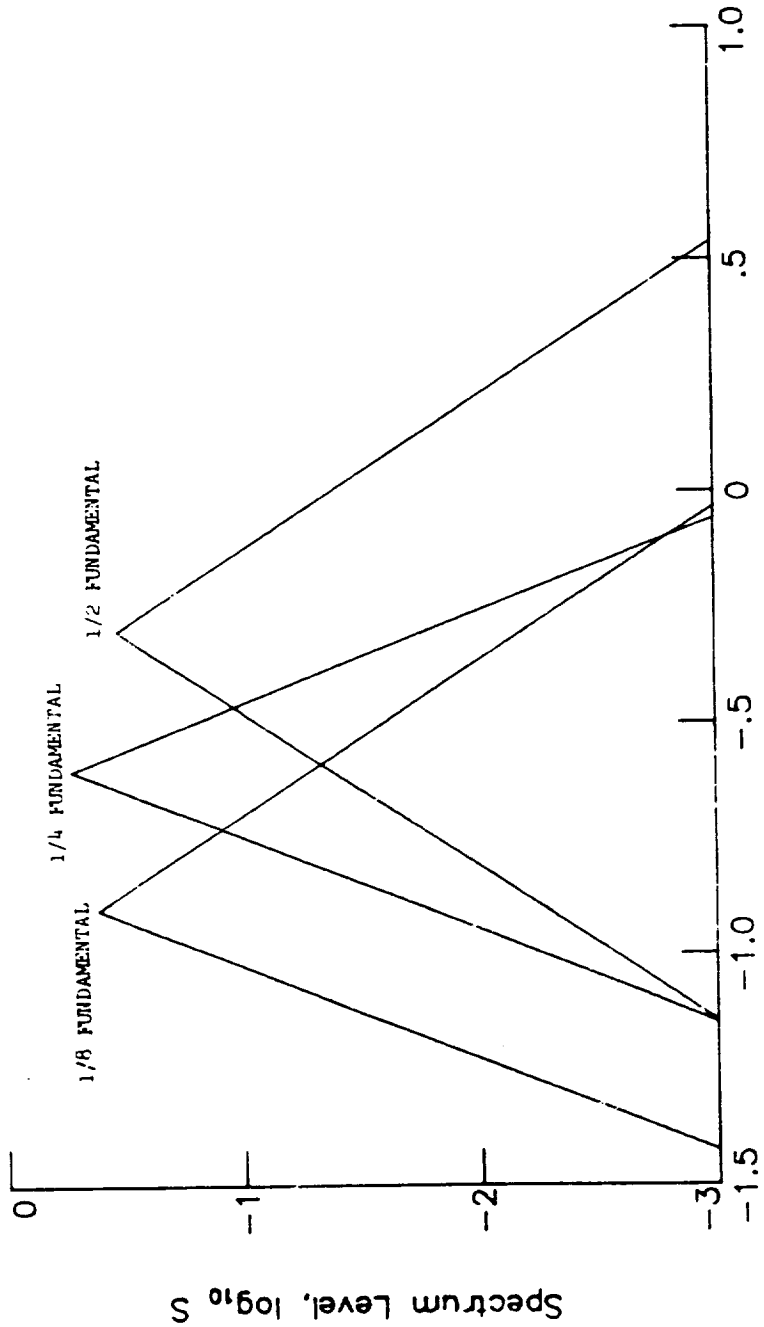

Figure 14.- Spectrum level for combination tone noise.

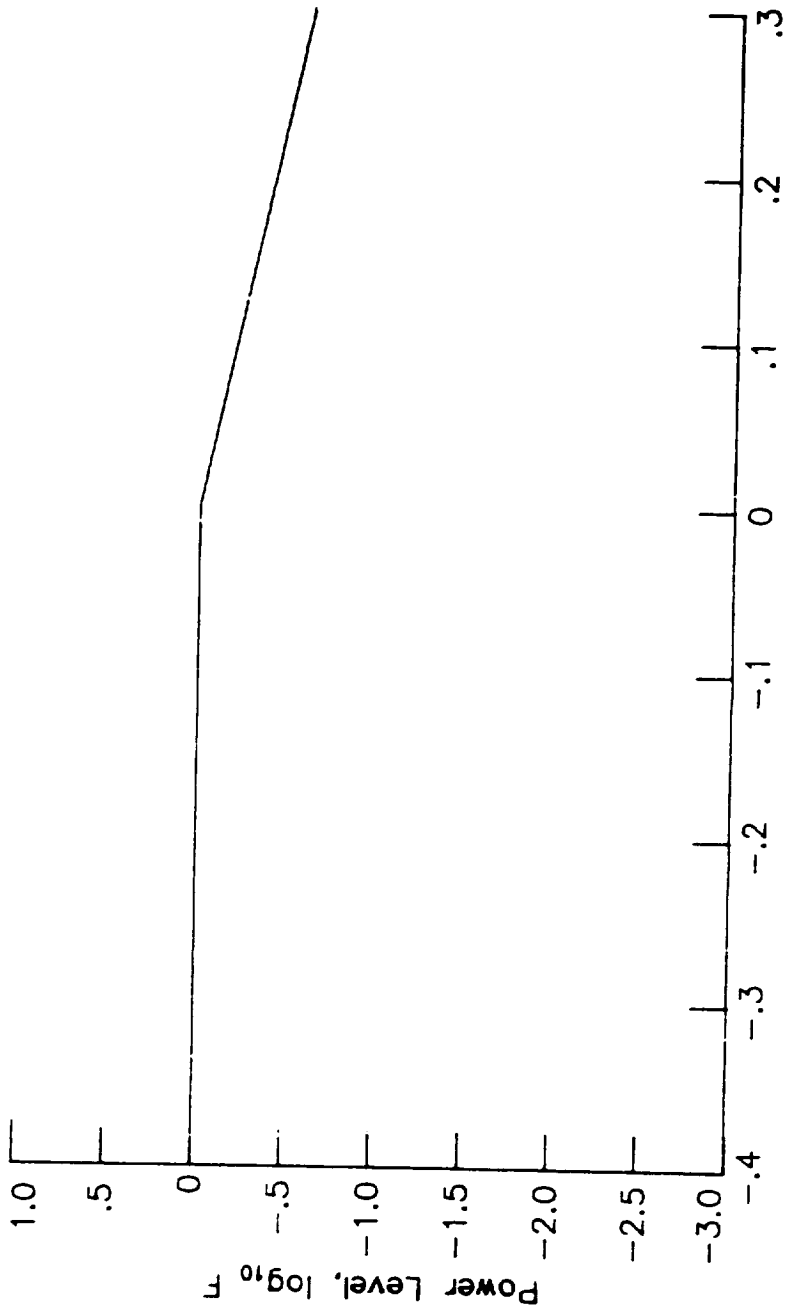

Figure 15.- Power level for discharge broadband noise and discharge rotor-stator interaction tones.

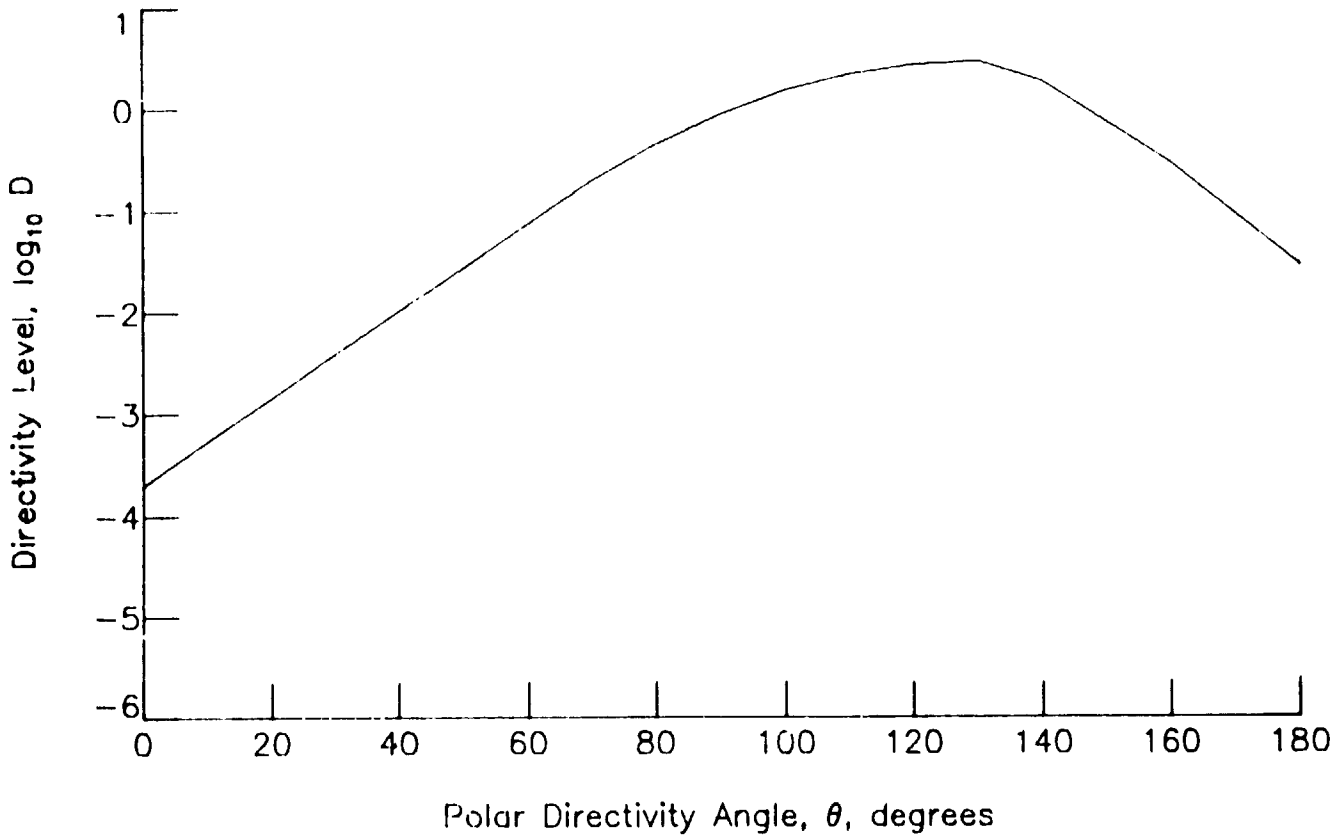

Figure 16.- Directivity level for discharge broadband noise.

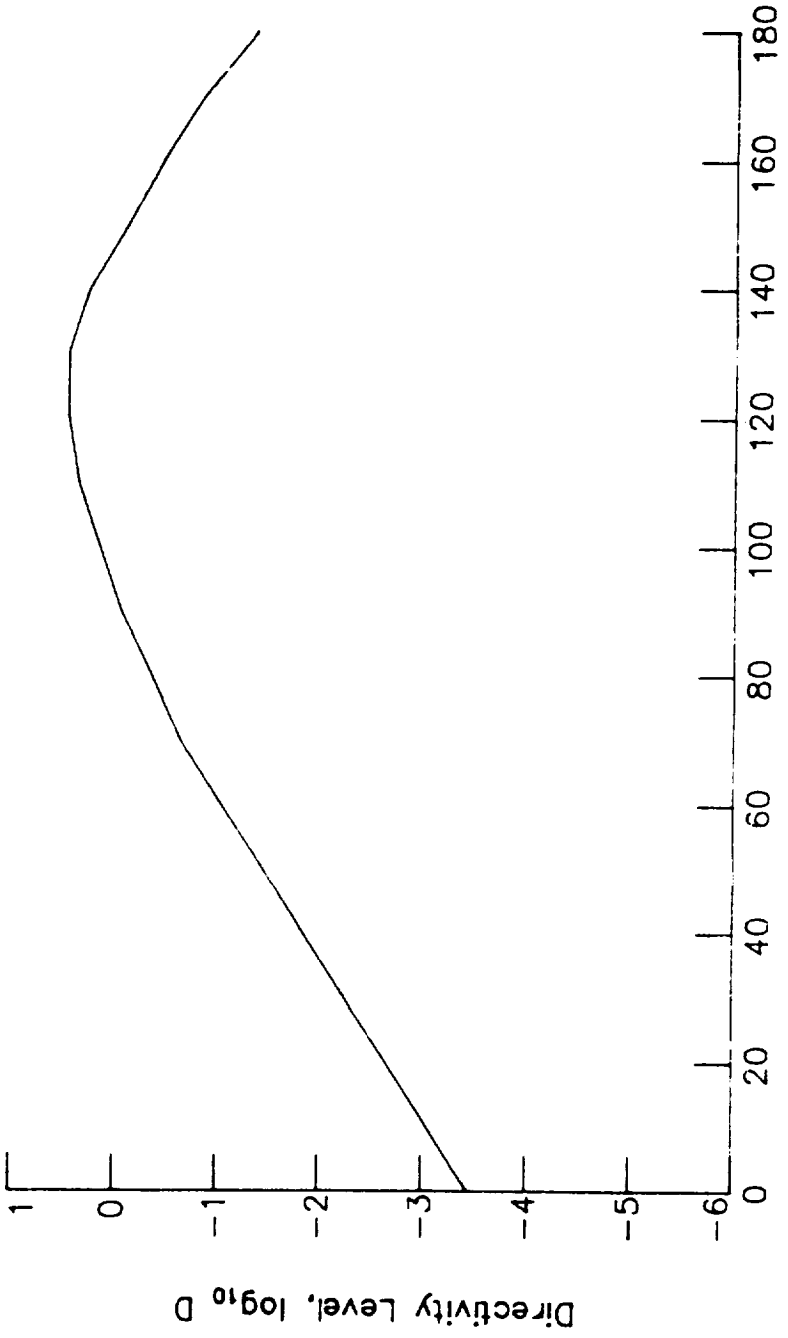

Figure 17.- Directivity level for discharge rotor-stator interaction tones.

8.2 COMBUSTION NOISE MODULE

INTRODUCTION

The Combustion Noise Module predicts the noise from conventional combustors installed in gas turbine engines. The method is based on a proposed appendix by R. K. Matta to SAE ARP 876. The method employs empirical data of core noise from turboshaft, turbojet, and turbofan engines to produce sound spectra as a function of frequency and polar directivity angle.

The method requires input of several parameters. The combustor entrance and exit flow parameters can be provided by the Core Noise Parameters Module or directly by the user. Additional user-provided parameters are required. The module is executed once for each set of values of the input parameters. The output is a table of the mean-square acoustic pressure as a function of frequency, polar directivity angle, and azimuthal directivity angle. Although combustion noise is assumed not to vary with azimuthal directivity angle, it is introduced so that the output table is compatible with other noise tables.

SYMBOLS

A	combustor entrance area, m^2 (ft^2)
A_e	engine reference area, m^2 (ft^2)
c_∞	ambient speed of sound, m/s (ft/s)
D	directivity function
f	frequency, Hz
f_p	spectrum peak frequency, Hz
M_∞	aircraft Mach number
$\dot{m}$	mass flow rate, kg/s (slugs/s)
N	number of engines
$\langle p^2 \rangle^*$	mean-square acoustic pressure, re $\rho_\infty^2 c_\infty^4$
p_{ref}	reference pressure, 2×10^{-5} Pa (4.177×10^{-7} lb/ft^2)
p_t	total pressure, Pa (lb/ft^2)
p_∞	ambient pressure, Pa (lb/ft^2)

r_s distance from source to observer, m (ft)

r_s^* dimensionless distance from source to observer, re $\sqrt{A_e}$

S spectral distribution function

T total temperature, K (^oR)

ΔT_{des} design turbine temperature extraction, K (^oR)

T_∞ ambient temperature, K (^oR)

θ polar directivity angle, deg

Π^* acoustic power, re $\rho_\infty c_\infty^3 A_e$

Π_{ref} reference power, 1×10^{-12} W (7.376×10^{-13} ft-lb/s)

ρ_∞ ambient density, kg/m^3 (slugs/ft^3)

ϕ azimuthal directivity angle, deg

Subscripts:

i entrance

j exit

Superscript:

* dimensionless quantity

INPUT

The combustor entrance and exit parameters are required from either the output of the Core Noise Parameters Module or from the user. Ambient conditions are required for computation of the sound pressure levels. The frequency, polar directivity angle, and azimuthal directivity angle arrays establish the independent variable values for the output table. Finally, the engine reference area, number of engines, combustor entrance area, and distance to observer are required. The range and default values of the input parameters are given in table I.

Input Constants

A^* combustor entrance area, re A_e

A_e engine reference area, m^2 (ft^2)

N number of engines

r_s distance from source to observer, m (ft)

Core Noise Parameters

$\dot{m}_i^*$ combustor entrance mass flow rate, re $\rho_\infty c_\infty A_e$

$p_{t,i}^*$ combustor entrance total pressure, re p_∞

T_i^* combustor entrance total temperature, re T_∞

T_j^* combustor exit total temperature, re T_∞

ΔT_{des}^* design turbine temperature extraction, re T_∞

Ambient Conditions

c_∞ ambient speed of sound, m/s (ft/s)

M_∞ aircraft Mach number

ρ_∞ ambient density, kg/m^3 (slugs/ft^3)

Independent Variable Arrays

f frequency, Hz

θ polar directivity angle, deg

ϕ azimuthal directivity angle, deg

OUTPUT

The output of this module is a table of the mean-square acoustic pressure as a function of frequency, polar directivity angle, and azimuthal directivity angle. In addition, the observer distance r_s is provided for the Propagation Module.

r_s distance from source to observer, m (ft)

Combustor Noise Table

f frequency, Hz

θ polar directivity angle, deg

ϕ azimuthal directivity angle, deg

$\langle p^2(f,\theta,\phi)\rangle^*$ mean-square acoustic pressure, re $\rho_\infty^2 c_\infty^4$

METHOD

The prediction methodology proposed by R. K. Matta is used to compute the combustor noise. Details of the development and validation of the method are given in reference 1. A schematic of a typical combustor is shown in figure 1. The coordinate system and directivity angles are also shown.

The equation for the far-field mean-square acoustic pressure in a 1/3-octave band for a gas turbine combustor is

$$\langle p^2 \rangle^* = \frac{\Pi^* A^*}{4\pi (r_s^*)^2} \frac{D(\theta)\ S(f)}{(1 - M_\infty \cos \theta)^4} \tag{1}$$

The dimensionless source to observer distance r_s^* is defined as

$$r_s^* = r_s / \sqrt{A_e} \tag{2}$$

The acoustic power Π^* is related to the combustor entrance and exit states as

$$\Pi^* = (8.85 \times 10^{-7}) \frac{\dot{m}_i^*}{A^*} \left(\frac{T_j^* - T_i^*}{T_i^*} \right)^2 (p_{t,i}^*)^2 (\Delta T_{des}^*)^{-4} \tag{3}$$

The aircraft Mach number term in equation (1) accounts for forward flight effects.

Two empirical functions are required for equation (1). The directivity function D is a function of the polar directivity angle θ and is given in table II and plotted in figure 2. The spectrum function S is a function of $\log_{10} (f/f_p)$ and is given in table III and plotted in figure 3. The peak frequency f_p is given by

$$f_p = \frac{400}{1 - M_\infty \cos \theta} \tag{4}$$

The mean-square pressure $\langle p^2 \rangle^*$ is now computed from equation (1). The total noise is the mean-square pressure multiplied by the number of engines N. The output of this module is a table of the mean-square acoustic pressure as a function of frequency, polar directivity angle, and azimuthal directivity angle. In addition, printed output is available of the sound pressure level SPL defined as

$$SPL = 10 \log_{10} \langle p^2 \rangle^* + 20 \log_{10} \frac{\rho_\infty c_\infty^2}{p_{ref}} \tag{5}$$

and the power level PWL defined as

$$PWL = 10 \log_{10} \Pi^* + 10 \log_{10} \frac{\rho_\infty c_\infty^3 A_e A^*}{\Pi_{ref}} \qquad (6)$$

REFERENCE

1. Emmerling, J. J.; Kozin, S. B.; and Matta, R. K.: Core Engine Noise Control Program. Volume III, Supplement 1 - Prediction Methods. FAA-RD-74-125, III-I, Mar. 1976. (Available from DTIC as AD A030 376.)

TABLE I.- RANGE AND DEFAULT VALUES OF INPUT PARAMETERS

Input parameter	Minimum	Default	Maximum
A^*	0.01	1	10
A_e, m^2	0.01	$\pi/4$	10
N	1	1	4
r_s, m	0.01	$\sqrt{A_e}$	100
$\dot{m}_i^*$	0	0.2	10
M_∞	0	0	0.9
$p_{t,i}^*$	1	1	30.0
T_i^*	1	1	5.0
T_j^*	1	2	6.0
ΔT_{des}^*	0	0.5	2.0
c_∞, m/s	200	340.294	400
ρ_∞, kg/m^3	0.2	1.225	1.5

TABLE II.- COMBUSTION DIRECTIVITY LEVEL

θ, deg	$\log_{10} D$
0.	-0.85
10.	-0.80
20.	-0.75
30.	-0.70
40.	-0.65
50.	-0.60
60.	-0.54
70.	-0.44
80.	-0.32
90.	-0.16
100.	0.06
110.	0.35
120.	0.50
130.	0.37
140.	0.16
150.	-0.20
160.	-0.55
170.	-0.80
180.	-0.90

TABLE III.- COMBUSTION SPECTRAL LEVEL

$\log_{10} f/f_p$	$\log_{10} S$
-1.1	-4.30
-1.0	-3.85
-0.9	-3.35
-0.8	-2.85
-0.7	-2.40
-0.6	-2.00
-0.5	-1.65
-0.4	-1.35
-0.3	-1.10
-0.2	-0.95
-0.1	-0.80
0.0	-0.80
0.1	-0.85
0.2	-0.95
0.3	-1.15
0.4	-1.40
0.5	-1.65
0.6	-1.95
0.7	-2.35
0.8	-2.70
0.9	-3.15
1.0	-3.55
1.1	-4.00
1.2	-4.40
1.3	-4.75
1.4	-5.25
1.5	-5.70
1.6	-6.20

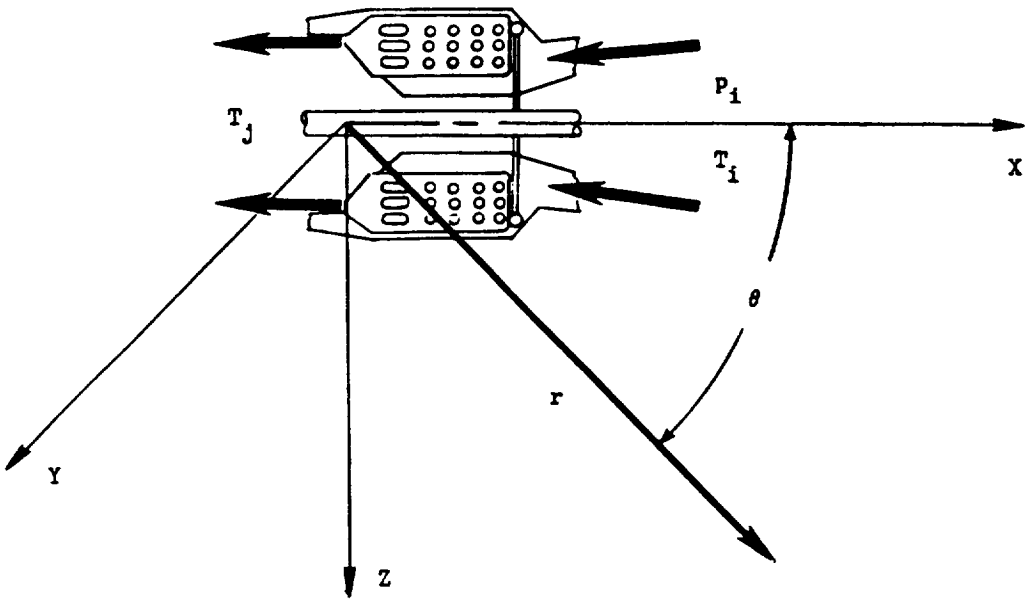

Figure 1.- Schematic diagram of typical gas turbine combustor.

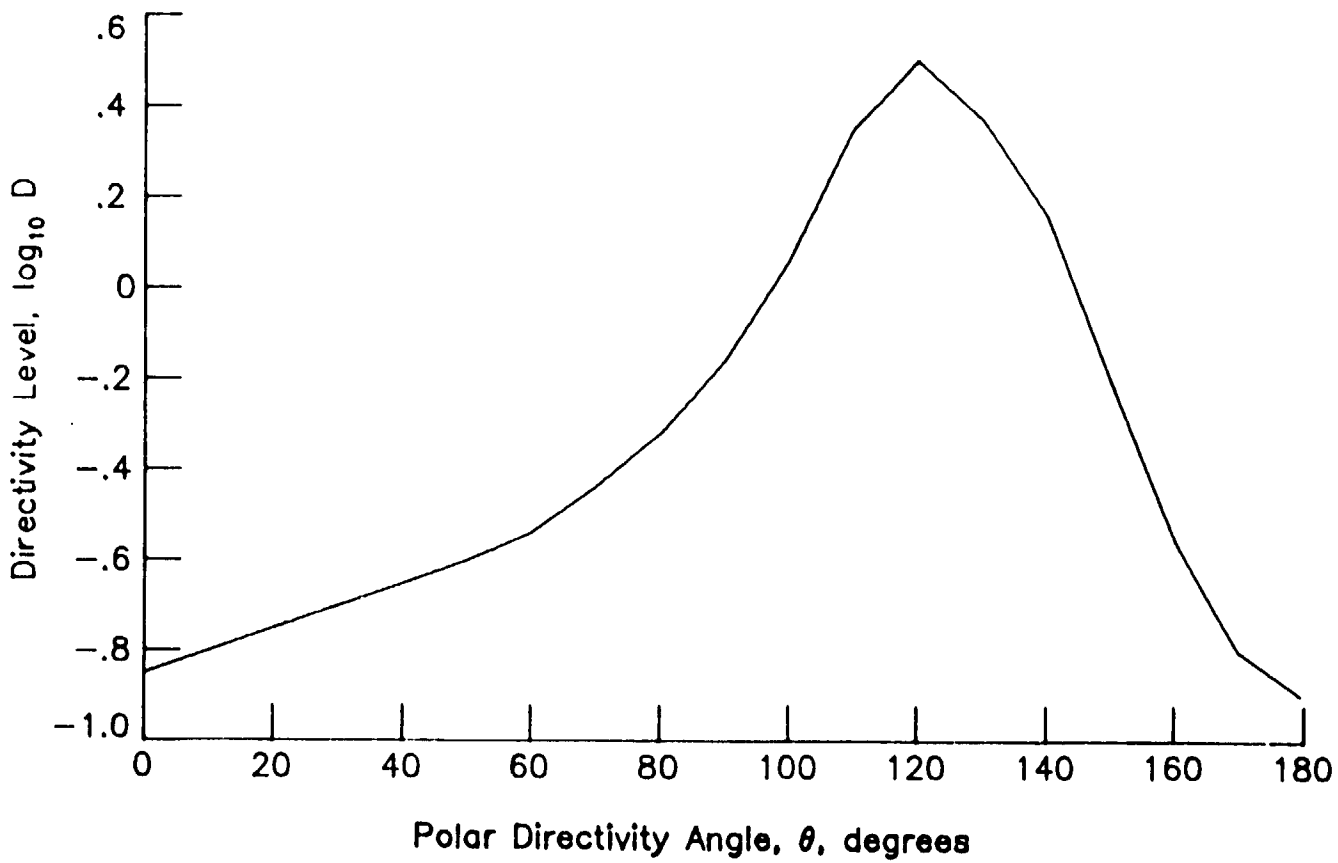

Figure 2.- Combustion noise directivity level.

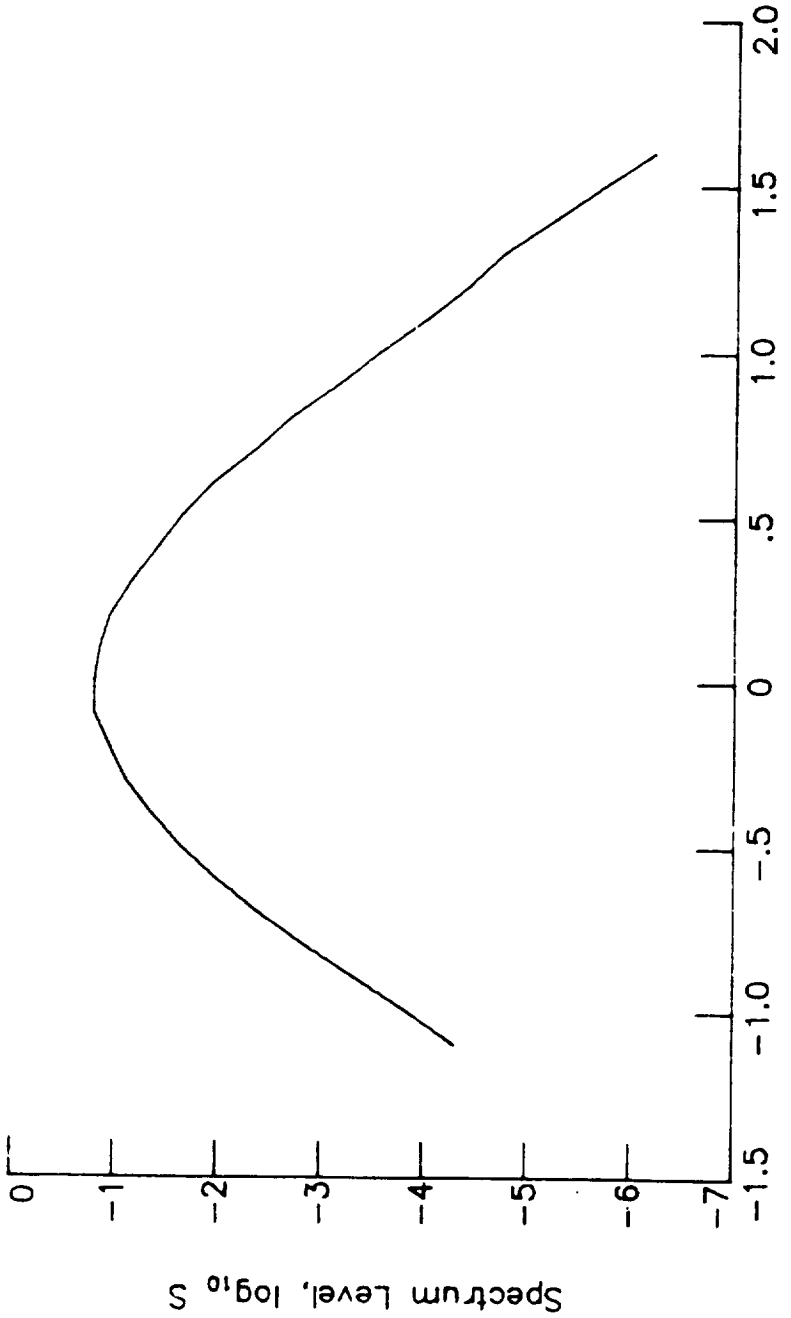

Figure 3.- Combustion noise spectral level.

8.3 TURBINE NOISE MODULE

INTRODUCTION

The Turbine Noise Module predicts the broadband noise and pure tones for an axial flow turbine. The method is based on a method developed by the General Electric Company (ref. 1). The method employs empirical functions to produce sound spectra as a function of frequency and polar directivity angle. Each spectrum is the sum of a broadband noise component and a pure tone component.

The method requires input of several parameters. The turbine entrance and exit flow parameters can be provided by the Turbine Noise Parameters Module or directly by the user. Additional user-provided parameters are required. The module is executed once for each set of values of the input parameters. The output is a table of the mean-square acoustic pressure as a function of frequency, polar directivity angle, and azimuthal directivity angle. Although turbine noise is assumed not to vary with azimuthal directivity angle, it is introduced so that the output table is compatible with other noise tables.

SYMBOLS

A	turbine inlet cross-sectional area, m^2 (ft^2)
A_e	engine reference area, m^2 (ft^2)
a,b	components
B	number of rotor blades
c_∞	ambient speed of sound, m/s (ft/s)
D	directivity function
d	turbine rotor diameter, m (ft)
f	frequency, Hz
f_b	blade passing frequency, Hz
$\acute{f}$	fuel-to-air ratio
h^*	specific enthalpy, re RT_∞
h_a	absolute humidity, percent mole fraction
K	constant

M_∞	aircraft Mach number
N	rotational speed, Hz
N_e	number of engines
n	tone harmonic number
$\langle p^2 \rangle$	mean-square acoustic pressure, re $\rho_\infty^2 c_\infty^4$
P_{ref}	reference pressure, 2×10^{-5} Pa (4.177×10^{-7} lb/ft^2)
r_s	distance from source to observer, m (ft)
r_s^*	dimensionless distance from source to observer, re $\sqrt{A_e}$
R	gas constant, m^2/(K-s^2) (ft^2/($^\circ$R-s^2))
S	spectrum function
T	temperature, K ($^\circ$R)
U_t	blade tip speed, m/s (ft/s)
η	frequency parameter
θ	polar directivity angle, deg
W^*	acoustic power, re $\rho_\infty c_\infty^3 A$
W_{ref}	reference power, 1×10^{-12} W (7.376×10^{-13} ft-lb/s)
ρ_∞	ambient density, kg/m^3 (slugs/ft^3)
ϕ	azimuthal directivity angle, deg

Subscripts:

i	entrance
j	exit
s	static
t	total
∞	ambient

Superscript:

*	dimensionless quantity

INPUT

The turbine parameters are required from either the output of the Turbine Noise Parameters Module or from the user. Ambient conditions are required for computation of sound pressure levels. The frequency, polar directivity angle, and azimuthal directivity arrays establish the independent variable values for the output table. The turbine inlet cross-sectional area and number of rotor blades are required for the geometric description of the turbine. Finally, the engine reference area, number of engines, and distance to the observer are required. The range and default values of the input parameters are given in table I.

Input Constants

A_e engine reference area, m^2 (ft^2)

N_e number of engines

r_s distance from source to observer, m (ft)

Turbine Geometry

A^* turbine inlet cross-sectional area, re A_e

B number of rotor blades

d^* turbine rotor diameter, re $\sqrt{A_e}$

Turbine Noise Parameters

f fuel-to-air ratio

N^* rotational speed, re c_∞/d

$T^*_{t,i}$ entrance total temperature, re T_∞

$T^*_{s,j}$ exit static temperature, re T_∞

Ambient Conditions

c_x ambient speed of sound, m/s (ft/s)

h_a absolute humidity, percent mole fraction

M_x aircraft Mach number

ρ_x ambient density, kg/m^3 ($slugs/ft^3$)

Independent Variable Arrays

f	frequency, Hz
θ	polar directivity angle, deg
ϕ	azimuthal directivity angle, deg

OUTPUT

The output to this module is a table of the mean-square acoustic pressure as a function of frequency, polar directivity angle, and azimuthal directivity angle. In addition, the observer distance r_s is provided for the Propagation Module.

r_s	distance from source to observer, m (ft)

Turbine Noise Table

f	frequency, Hz
θ	polar directivity angle, deg
ϕ	azimuthal directivity angle, deg
$\langle p^2(f,\theta,\phi)\rangle^*$	mean-square acoustic pressure, re $\rho_\infty^2 c_\infty^4$

METHOD

The prediction method presented in reference 1 is used to compute the far-field noise. A schematic of a typical turbine is shown in figure 1. The coordinate system and directivity angles are also shown. The general equations for the prediction method are presented. This presentation is followed by a detailed discussion of the method for each turbine noise component.

The equation for the far-field mean-square acoustic pressure for a turbine is

$$\langle p^2\rangle^* = \frac{\Pi^* A^*}{4\pi (r_s^*)^2} \frac{D(\theta)\ S(\eta)}{(1 - M_\infty \cos\theta)^4} \qquad (1)$$

In equation (1), Π^* is the overall power, D is the directivity function, and S is the spectrum function. The source to observer distance r_s is expressed in dimensionless form as

$$r_s^* = r_s / \sqrt{A_e} \qquad (2)$$

The forward velocity effect is accounted for by the Doppler factor $(1 - M_\infty \cos \theta)^4$. The frequency parameter η is defined as

$$\eta = (1 - M_\infty \cos \theta)\frac{f}{f_b} \tag{3}$$

where the blade passing frequency f_b is

$$f_b = \frac{N^* B c_\infty}{d^* \sqrt{A_e}} \tag{4}$$

The acoustic power for the turbine Π^* is expressed as

$$\Pi^* = K\left(\frac{h^*_{t,i} - h^*_{s,j}}{h^*_{t,i}}\right)^a (U^*_T)^b \tag{5}$$

The constants K, a, and b are determined from empirical data of the particular noise source being considered. The difference between the entrance specific total enthalpy $h^*_{t,i}$ and the exit specific static enthalpy $h^*_{s,j}$ is the ideal work extraction of the turbine. Each specific enthalpy is computed from the input temperatures, the fuel-to-air ratio f, and the absolute humidity h_a with the appropriate Gas Properties Utility. The rotor tip speed U^*_T is a function of the rotational speed and is given by

$$U^*_T = \pi N^* \tag{6}$$

As indicated by equation (1), each turbine noise source has its own directivity function D and spectrum function S. By using these functions and the acoustic power, the mean-square acoustic pressure is computed as a function of frequency and polar directivity angle for a given set of input parameters. The broadband noise is expressed as 1/3-octave-band data. The pure tones are values at discrete frequencies. The pure tones must be added to the appropriate 1/3-octave band so that a total 1/3-octave-band turbine noise spectrum is determined. For a given value of the 1/3-octave-band center frequency parameter η, the lowest harmonic number that falls within the band is

$$n_\ell = [10^{-1/20}\,\eta] + 1 \tag{7}$$

and the highest harmonic number is

$$n_u = [10^{1/20}\,\eta] \tag{8}$$

where [ ] indicates the integer part of the enclosed real number. If $n_\ell > n_u$, then there are no tones within the band. If $n_\ell \leq n_u$, then there are $n_u - n_\ell + 1$ tones within the band. The pure tone mean-square pressures for each harmonic number n are then added to the appropriate band. The tones are propagated to the observer as 1/3-octave-band data.

The empirical constants and functions used to compute the acoustic power for turbine noise are given in table II. The directivity and spectrum functions are given in tables III and IV, respectively. Each turbine noise component is described in detail in the following two sections.

Turbine Broadband Noise

Turbine broadband noise is associated with random unsteadiness or turbulence in the flow passing the blading. Some of the sources of this random, unsteady flow are turbulence in boundary layers, blade wakes and vortices, and entrance flow. Although prediction of individual sources of broadband noise is beyond the scope of this module, the total broadband noise produced by the turbine is predicted.

The acoustic power due to broadband noise from the turbine is

$$\Pi^* = (8.589 \times 10^{-5}) \left(\frac{h^*_{t,i} - h^*_{s,j}}{h^*_{t,i}} \right)^{1.27} (U^*_T)^{-1.27} \tag{9}$$

The directivity function D is given in table III and plotted in figure 2. The spectrum function S is given in table IV and plotted in figure 3. The mean-square acoustic pressure is then computed by equation (1).

Turbine Pure Tone Noise

Discrete tone generation is associated with lift fluctuations on rotor or stator blades. These tones occur at frequencies that are harmonics of the turbine blade passing frequency. The average far-field characteristics are predicted.

The acoustic power due to turbine pure tone noise is

$$\Pi^* = (1.162 \times 10^{-9}) \left(\frac{h^*_{t,i} - h^*_{s,j}}{h^*_{t,i}} \right)^{1.46} (U^*_T)^{-4.02} \tag{10}$$

The directivity function D is given in table III and plotted in figure 4. The spectrum function S is given by

$$S = 0.6838 \times 10^{-(n-1)/2} \tag{11}$$

which is plotted in figure 5. The mean-square acoustic pressure is then computed by equation (1).

Output Computation

The mean-square acoustic pressure for a turbine is the sum of the two components. It is computed for each desired value of the frequency, polar directivity angle, and azimuthal directivity angle. The total noise is the mean-square acoustic pressure multiplied by the number of engines N_e for the output table. In addition, printed output is available of the sound pressure level SPL defined as

$$SPL = 10 \log_{10} \langle p^2 \rangle^* + 20 \log_{10} \frac{\rho_\infty c_\infty^2}{p_{ref}} \tag{12}$$

and the power level PWL defined as

$$PWL = 10 \log_{10} \mathcal{W}^* + 10 \log_{10} \frac{\rho_\infty c_\infty^3 A^* A_e}{\mathcal{W}_{ref}} \tag{13}$$

REFERENCE

1. Matta, R. K.; Sandusky, G. T.; and Doyle, V. L.: GE Core Engine Noise Investigation - Low Emission Engines. FAA-RD-77-4, Feb. 1977. (Available from DTIC as AD A048 590.)

TABLE I.- RANGE AND DEFAULT VALUES OF INPUT PARAMETERS

Input parameter	Minimum	Default	Maximum
A_e, m^2	0.01	$\pi/4$	10
N_e	1	1	4
r_s, m	0.01	$\sqrt{A_e}$	100
A^*	0.1	1	10
B	2	20	500
d^*	0.01	1	100
M_∞	0	0	0.9
δ	0	0	0.06767
N^*	0	0.3	0.5
$T^*_{t,i}$	0.5	3	6
$T^*_{s,j}$	0.5	2	4
c_∞, m/s	200	340.294	400
h_∞, %	0	0	4
ρ_∞, kg m^3	0.2	1.225	1.5

TABLE II.- CONSTANTS FOR TURBINE ACOUSTIC POWER

Source	K	a	b
Broadband	8.589×10^{-5}	1.27	-1.27
Pure tone	1.162×10^{-4}	1.46	-4.02

TABLE III.- TURBINE NOISE DIRECTIVITY LEVELS

θ, deg	Broadband directivity level, $\log_{10} D$	Tone directivity level, $\log_{10} D$
0.	-0.789	-1.911
10.	-0.689	-1.671
20.	-0.599	-1.471
30.	-0.509	-1.261
40.	-0.409	-1.061
50.	-0.319	-0.851
60.	-0.219	-0.641
70.	-0.129	-0.431
80.	-0.029	-0.231
90.	0.071	-0.021
100.	0.151	0.189
110.	0.221	0.389
120.	0.231	0.589
130.	0.211	0.259
140.	0.111	-0.191
150.	-0.029	-0.591
160.	-0.229	-0.931
170.	-0.549	-1.271
180.	-0.869	-1.611

TABLE IV.- TURBINE BROADBAND NOISE SPECTRUM

$\log_{10} \eta$	$\log_{10} S$
-0.903	-1.884
-0.796	-1.604
-0.699	-1.444
-0.602	-1.304
-0.502	-1.184
-0.398	-1.084
-0.301	-1.004
-0.201	-0.924
-0.097	-0.844
0.000	-0.784
0.097	-1.004
0.204	-1.204
0.301	-1.384
0.602	-1.924

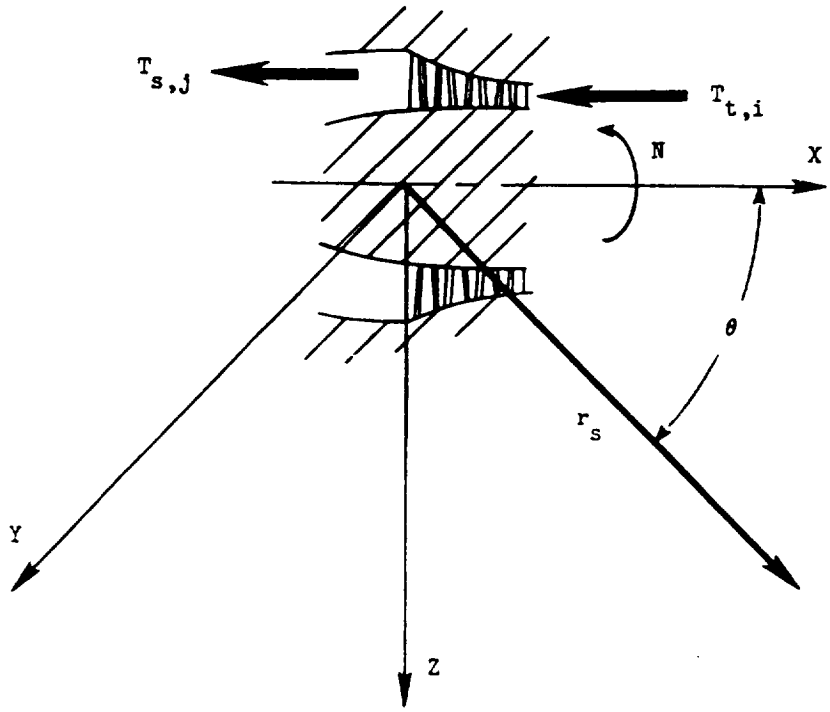

Figure 1.- Schematic diagram of typical axial flow turbine.

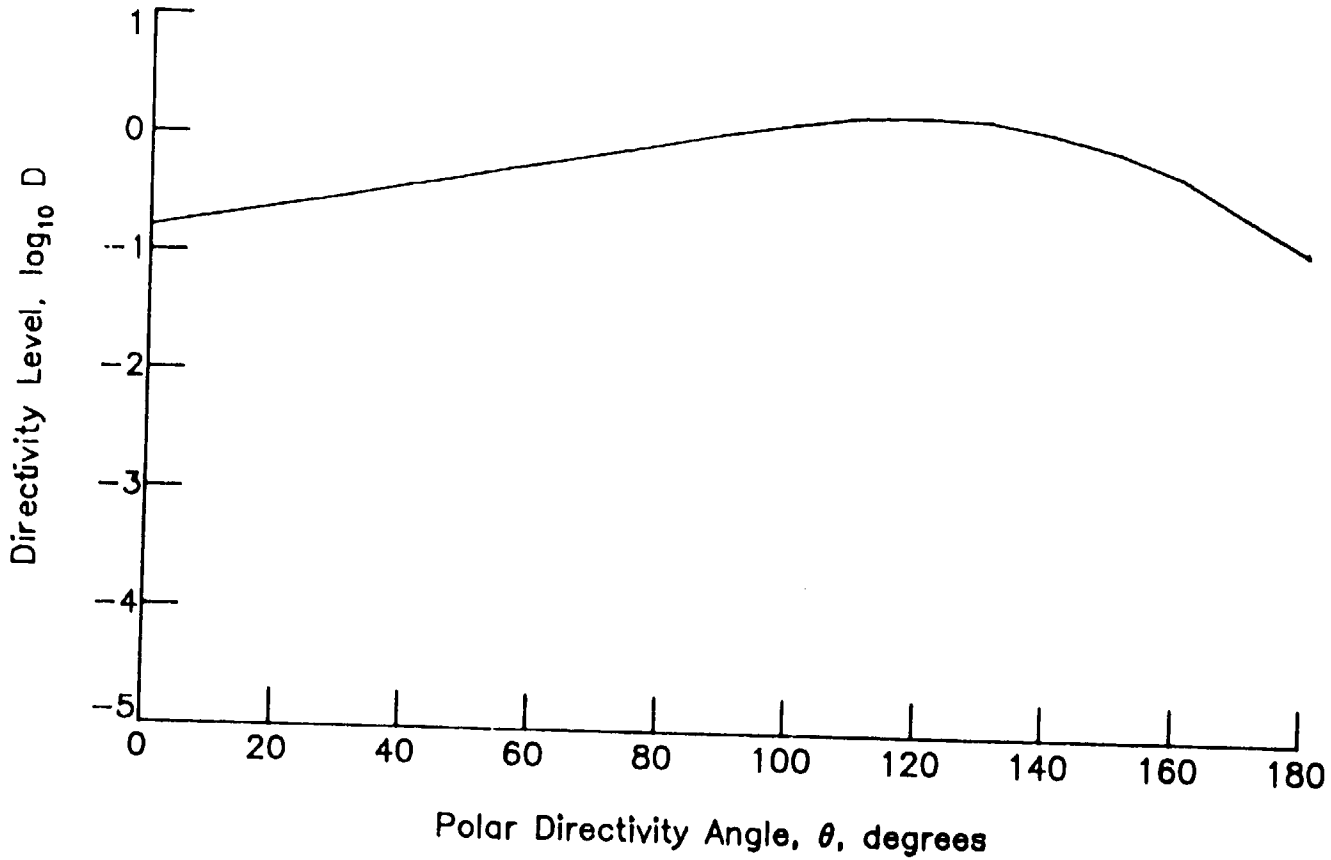

Figure 2.- Directivity level for turbine broadband noise.

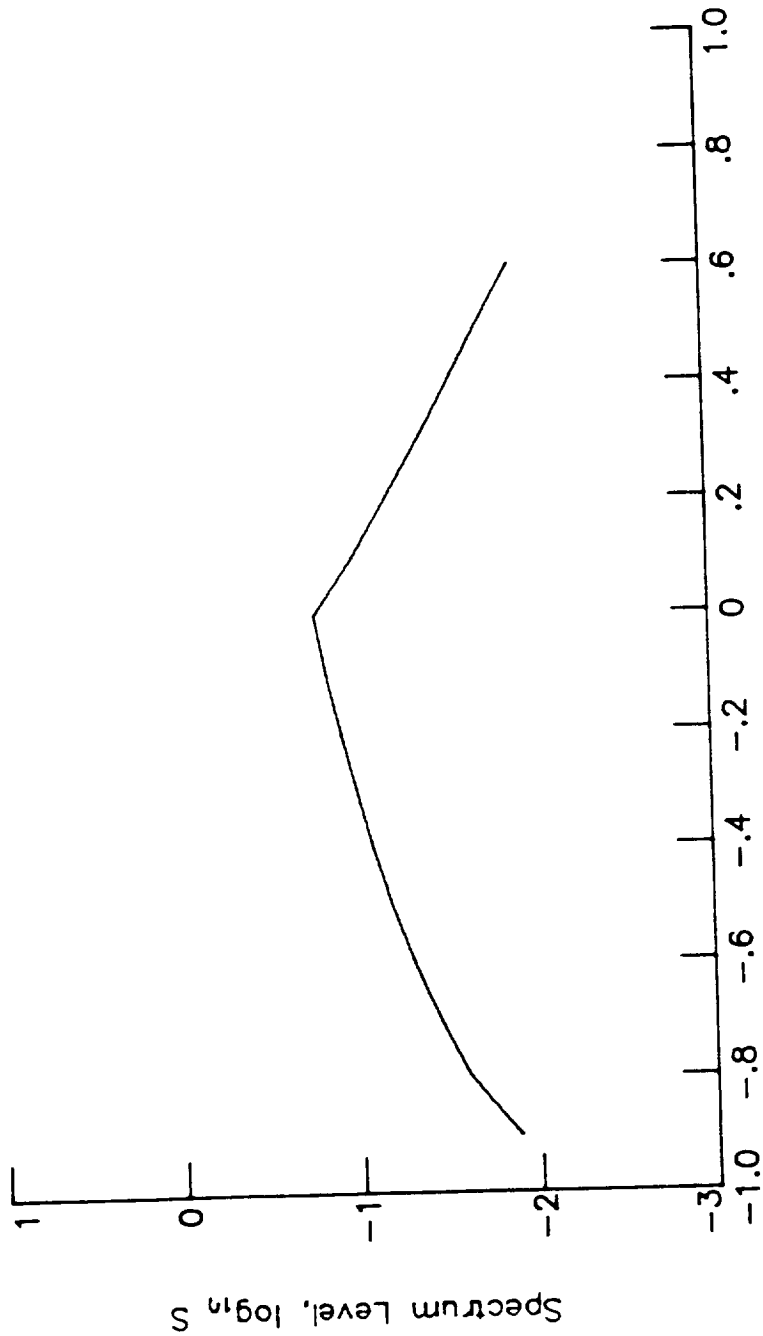

Figure 3.- Spectrum level for turbine broadband noise.

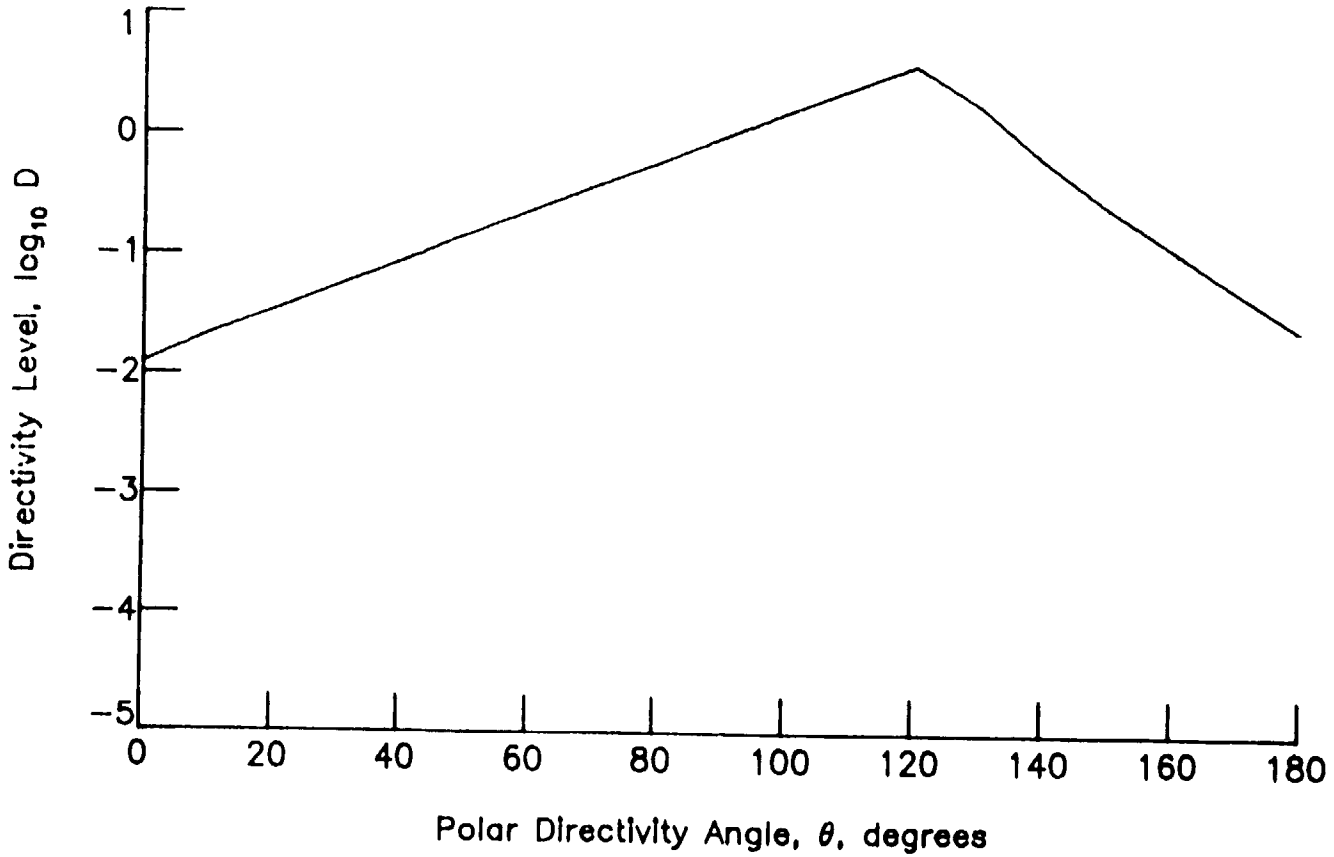

Figure 4.- Directivity level for turbine tone noise.

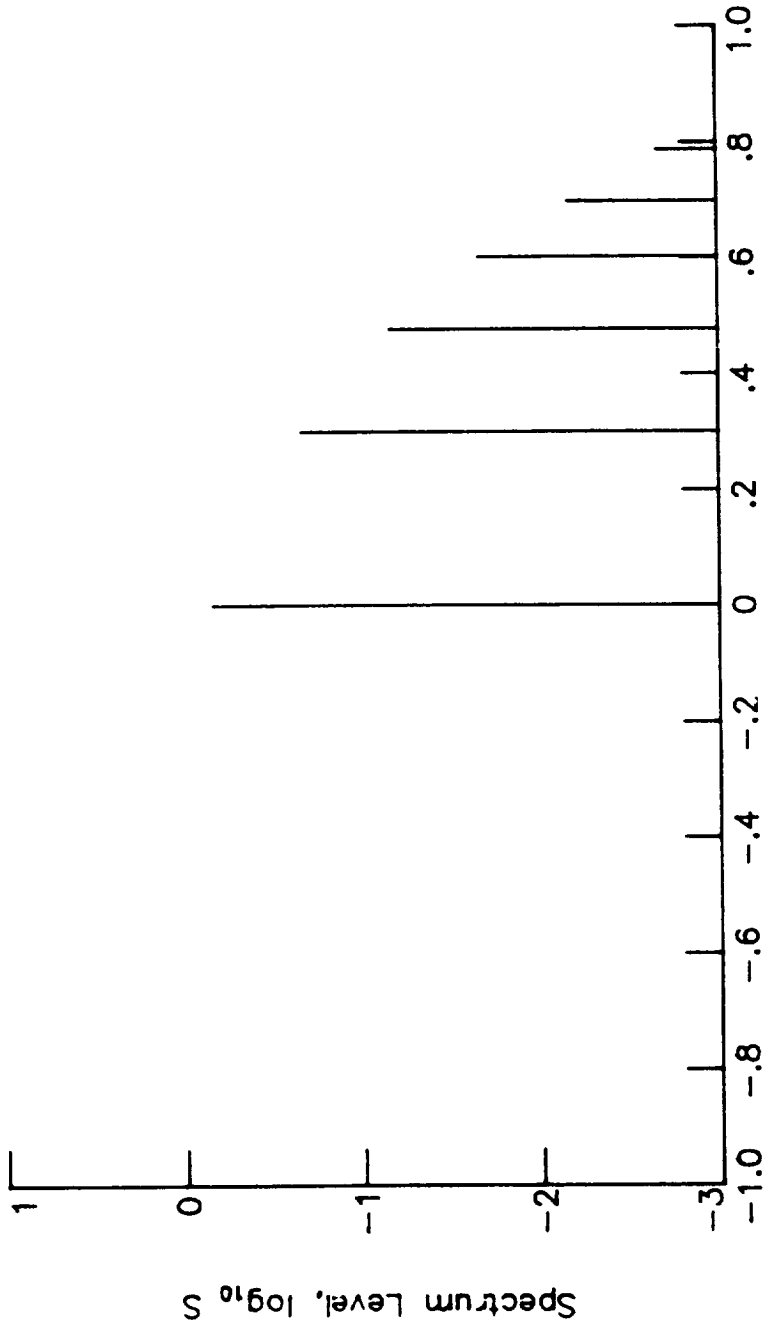

Figure 5.- Spectrum level for turbine tone noise.

8.4 SINGLE STREAM CIRCULAR JET NOISE MODULE

INTRODUCTION

The Single Stream Circular Jet Noise Module predicts the single stream jet mixing noise from shock-free circular nozzles. The method is based on SAE ARP 876 (ref. 1). The method employs empirical data tabulated in terms of relevant dimensionless groups to produce sound spectra as a function of frequency and polar directivity angle.

The method requires input of several parameters. The nozzle exit flow parameters can be provided by the Jet Noise Parameters Module or directly by the user. Additional user-provided parameters are required. The module is executed once for each set of values of the input parameters. The output is a table of the mean-square acoustic pressure as a function of frequency, polar directivity angle, and azimuthal directivity angle. Although jet exhaust noise is assumed not to vary with azimuthal directivity angle, it is introduced so that the output table is compatible with other noise tables.

SYMBOLS

A_e	engine reference area, m^2 (ft^2)
A_j	fully expanded jet area, m^2 (ft^2)
c_∞	ambient speed of sound, m/s (ft/s)
D	directivity function
d_j	fully expanded jet diameter, m (ft)
F	spectral distribution factor
f	frequency, Hz
f^*	Helmholtz number, $f\sqrt{A_e}/c_\infty$
M_∞	aircraft Mach number
m	forward velocity index
N	number of engines
P	power deviation factor
$\langle p^2 \rangle^*$	mean-square acoustic pressure, re $\rho_\infty^2 c_\infty^4$

P_{ref} reference pressure, 2×10^{-5} Pa (4.177×10^{-7} lb/ft^2)

r_s distance from nozzle exit to observer, m (ft)

r_s^* dimensionless distance from nozzle exit to observer, re $\sqrt{A_e}$

S_c corrected Strouhal number, $fd_j/\xi V_j$

T_j jet total temperature, K (^oR)

T_∞ ambient temperature, K (^oR)

V_j exhaust jet velocity, m/s (ft/s)

δ angle between flight vector and engine inlet axis, deg

θ polar directivity angle, deg

ξ Strouhal number correction factor

Π^* acoustic power, re $\rho_\infty c_\infty^3 A_j$

Π_{ref} reference power, 1×10^{-12} W (7.376×10^{-13} ft-lb/s)

ρ_j jet density, kg/m^3 (slugs/ft^3)

ρ_∞ ambient density, kg/m^3 (slugs/ft^3)

ϕ azimuthal directivity angle, deg

ω density exponent

Superscript:

* dimensionless quantity

INPUT

The jet parameters are required from either the output of the Jet Noise Parameters Module or the user. Ambient conditions are required for computation of the Strouhal number and sound pressure levels. The frequency, polar directivity angle, and azimuthal directivity angle arrays establish the independent variable values for the output table. Finally, the engine reference area, number of engines, engine axis offset, and distance to the pseudo-observer are required. The range and default values of the input parameters are given in table I.

Input Constants

A_e engine reference area, m^2 (ft^2)

N number of engines

r_s distance from nozzle exit to pseudo-observer, m (ft)

δ angle between flight vector and engine inlet axis, deg

Jet Noise Parameters

A_j^* area of jet, re A_e

T_j^* jet total temperature, re T_∞

V_j^* jet velocity, re c_∞

ρ_j^* jet density, re ρ_∞

Ambient Conditions

c_∞ speed of sound, m/s (ft/s)

M_∞ aircraft Mach number

ρ_∞ density, kg/m^3 ($slugs/ft^3$)

Independent Variable Arrays

f frequency, Hz

θ polar directivity angle, deg

ψ azimuthal directivity angle, deg

OUTPUT

The output of this module is a table of the mean-square pressure as a function of frequency, polar directivity angle, and azimuthal directivity angle. In addition, pseudo-observer distance r_s is provided for the Propagation Module.

r_s distance from nozzle exit to pseudo-observer, m (ft)

Single Stream Circular Jet Noise Table

f frequency, Hz

θ polar directivity angle, deg

ψ azimuthal directivity angle, deg

$\langle p^2(f,\theta,\psi)\rangle^*$ mean-square acoustic pressure, re $\rho_\infty^2 c_\infty^4$

METHOD

The prediction methodology presented in reference 1 is used to compute the far-field noise. A schematic of a typical exhaust jet nozzle is shown in figure 1. The coordinate system and directivity angles are also shown. Whenever empirical functions require extrapolation, the last value is used, except for spectra which are linearly extrapolated.

The equation for the far-field mean-square acoustic pressure in a 1/3-octave band for a stationary jet is

$$\langle p^2 \rangle^* = \frac{\Pi^* A_j^*}{4\pi \left(r_s^{*2}\right)} D(\theta, V_j^*)\ F(S_c, \theta, V_j^*, T_j^*) \tag{1}$$

In equation (1), Π^* is the overall power, D is the directivity function, and F is the spectral distribution function. Each of these functions is discussed separately. The observer distance r_s is expressed in dimensionless form as

$$r_s^* = r_s / \sqrt{A_e} \tag{2}$$

The acoustic power Π^* is given by

$$\Pi^* = (6.67 \times 10^{-5})(\rho_j^*)^{\omega}(V_j^*)^8 P(V_j^*) \tag{3}$$

which is a variation of the classic V^8 law. Two empirical functions are required for equation (3). The density exponent ω is a function of $\log_{10} V_j^*$ and is given in table II and plotted in figure 2. The power deviation factor P is the deviation of the acoustic power from the V^8 law. It is expressed as a function of $\log_{10} V_j^*$ in table III and plotted in figure 3.

The normalized directivity function D of equation (1) is an empirical function of the polar directivity angle θ and velocity ratio $\log_{10} V_j^*$. It expresses the variation of the mean-square pressure with θ and is normalized such that

$$\frac{1}{2}\int_0^{\pi} D(\theta, V_j^*) \sin\theta\, d\theta = 1 \tag{4}$$

The directivity function for a single stream circular jet is given in table IV and plotted in figure 4.

The normalized spectral distribution factor F is an empirical function of corrected Strouhal number $\log_{10} S_c$, polar directivity angle θ, velocity ratio $\log_{10} V_j^*$, and temperature ratio T_j^*. The corrected Strouhal number S_c is defined as

$$S_c = \frac{f^* d_j^*}{\xi V_j^*} \tag{5}$$

where the jet diameter d_j^* is

$$d_j^* = \sqrt{\frac{4A_j^*}{\pi}} \tag{6}$$

and ξ is the Strouhal number correction factor. The Strouhal number correction factor is an empirical function of the velocity ratio $\log_{10} V_j^*$ and the polar directivity angle θ as shown in table V and figure 5. The normalized spectral distribution factor F is defined such that the summation over 1/3-octave-band Strouhal numbers is

$$\sum_{S_c} F(S_c, \theta, V_j^*, T_j^*) = 1 \tag{7}$$

and is given in table VI and plotted in figure 6.

Equation (1) is valid for a stationary jet ($M_\infty = 0$). To incorporate forward flight effects, equation (1) should be rewritten as

$$\langle p^2 \rangle^* = \frac{\Pi^* A_j^*}{4\pi (r_s^*)^2} \frac{D(\theta, V_j^*)\, F(S_c, \theta, V_j^*, T_j^*)}{1 - M_\infty \cos(\theta - \delta)} \left(\frac{V_j^* - M_\infty}{V_j^*} \right)^{m(\theta)} \tag{8}$$

The exponent $m(\theta)$ is the forward velocity index given in table VII and figure 7 as taken from reference 2, and δ is the angle between the flight vector and the engine inlet axis. In addition, the relative jet velocity must be taken into account by computing the corrected Strouhal number as

$$S_c = \frac{f^* d_j^*}{\xi (V_j^* - M_\infty)} \tag{9}$$

The mean-square acoustic pressure can be computed for each desired value of the frequency, polar directivity angle, and azimuthal directivity angle. The total noise is the mean-square acoustic pressure multiplied by the number of engines N for the output table. In addition, printed output is available of the mean-square pressure $\langle p^2 \rangle^*$, sound pressure level SPL defined as

$$SPL = 10 \log_{10} \langle p^2 \rangle^* + 10 \log_{10} \frac{\rho_\infty^2 c_\infty^4}{p_{ref}^2} \tag{10}$$

and the power level PWL defined as

$$PWL = 10 \log_{10} \Pi^* - 10 \log_{10} \frac{\Pi_{ref}}{\rho_\infty c_\infty^3 A_j^* A_e} \tag{11}$$

REFERENCES

1. Gas Turbine Jet Exhaust Noise Prediction. ARP 876, Soc. Automot. Eng., Mar. 1978.

2. Hoch, R. G.; Duponchel, J. P.; Cocking, B. J.; and Bryce, W. D.: Studies of the Influence of Density on Jet Noise. SNECMA and NGTE paper presented at the First International Symposium on Air Breathing Engines (Marseille, France), June 19-23, 1972.

TABLE I.- RANGE AND DEFAULT VALUES OF INPUT PARAMETERS

Input parameter	Minimum	Default	Maximum
A_e, m^2	0.01	$\pi/4$	10
N	1	1	4
r_s, m	0.01	$\sqrt{A_e}$	100
δ, deg	0	0	30
A_j^*	0.0001	1	10
T_j^*	0.7	1	4
V_j^*	0	1.0	2.5
M_∞	0	0	0.9
ρ_j^*	0.2	1.0	1.2
c_∞, m/s	200	340.294	400
ρ_∞, kg/m^3	0.2	1.225	1.5

TABLE II.- DENSITY EXPONENT ω

$\log_{10} V_j/c_\infty$	ω
-.450	-1.000
-.400	-.900
-.350	-.760
-.300	-.580
-.250	-.410
-.200	-.220
-.150	0.000
-.100	.220
-.050	.500
0.000	.770
.050	1.070
.100	1.390
.150	1.740
.200	1.950
.250	2.000

TABLE III.- POWER DEVIATION LEVEL $\log_{10} P$

$\log_{10} V_j/c_\infty$	$\log_{10} P$
-.400	-.130
-.350	-.130
-.300	-.130
-.250	-.130
-.200	-.130
-.150	-.120
-.100	-.100
-.050	-.050
0.000	0.000
.050	.100
.100	.210
.150	.320
.200	.410
.250	.430
.300	.410
.350	.310
.400	.140

TABLE IV.- POLAR DIRECTIVITY LEVEL $\log_{10} D$

θ, deg	$\log_{10} D$ for $\log_{10} V_j/c_\infty$ of -								
	-0.400	-0.350	-0.300	-0.250	-0.200	-0.150	-0.100	-0.050	0.000
0.000	-.480	-.520	-.550	-.600	-.630	-.670	-.720	-.800	-.860
10.000	-.460	-.500	-.530	-.580	-.610	-.650	-.700	-.780	-.840
20.000	-.430	-.470	-.500	-.550	-.580	-.620	-.670	-.750	-.810
30.000	-.390	-.430	-.460	-.510	-.550	-.590	-.640	-.720	-.800
40.000	-.370	-.380	-.420	-.460	-.510	-.540	-.600	-.680	-.770
50.000	-.340	-.350	-.370	-.430	-.480	-.510	-.560	-.650	-.740
60.000	-.290	-.330	-.330	-.400	-.430	-.470	-.510	-.590	-.700
70.000	-.250	-.270	-.290	-.340	-.380	-.430	-.470	-.570	-.640
80.000	-.210	-.230	-.240	-.280	-.320	-.360	-.410	-.490	-.570
90.000	-.140	-.160	-.190	-.220	-.250	-.280	-.330	-.390	-.470
100.000	-.070	-.090	-.100	-.130	-.150	-.170	-.210	-.270	-.320
110.000	.030	.020	0.000	-.020	-.030	-.040	-.060	-.090	-.130
120.000	.140	.130	.130	.110	.120	.120	.130	.110	.090
130.000	.230	.240	.250	.250	.270	.290	.290	.310	.340
140.000	.310	.340	.350	.370	.380	.410	.440	.470	.520
150.000	.370	.390	.420	.450	.470	.510	.530	.580	.630
160.000	.400	.440	.470	.490	.510	.540	.560	.570	.610
170.000	.450	.460	.470	.510	.560	.590	.610	.560	.510
180.000	.450	.490	.520	.540	.560	.590	.610	.540	.460

TABLE IV.- Concluded

θ, deg	$\log_{10} D$ for $\log_{10} V_j/c_\infty$ of -							
	0.050	0.100	0.150	0.200	0.250	0.300	0.350	0.400
0.000	-.970	-1.090	-1.230	-1.340	-1.410	-1.460	-1.440	-1.370
10.000	-.950	-1.070	-1.210	-1.320	-1.390	-1.440	-1.420	-1.350
20.000	-.920	-1.040	-1.180	-1.290	-1.360	-1.410	-1.390	-1.320
30.000	-.910	-1.030	-1.150	-1.270	-1.320	-1.370	-1.360	-1.300
40.000	-.880	-1.020	-1.130	-1.230	-1.290	-1.320	-1.310	-1.260
50.000	-.850	-1.000	-1.100	-1.180	-1.240	-1.270	-1.250	-1.210
60.000	-.810	-.970	-1.050	-1.130	-1.170	-1.200	-1.190	-1.150
70.000	-.770	-.910	-1.000	-1.050	-1.090	-1.110	-1.090	-1.050
80.000	-.680	-.820	-.900	-.960	-.990	-1.000	-.970	-.920
90.000	-.580	-.690	-.780	-.830	-.850	-.850	-.810	-.750
100.000	-.410	-.530	-.600	-.650	-.670	-.640	-.590	-.500
110.000	-.200	-.290	-.350	-.380	-.360	-.330	-.250	-.110
120.000	.050	-.010	-.030	0.000	.040	.120	.200	.310
130.000	.320	.310	.350	.430	.520	.580	.630	.670
140.000	.570	.600	.650	.690	.730	.740	.730	.630
150.000	.700	.760	.770	.710	.650	.560	.490	.390
160.000	.630	.670	.650	.580	.420	.240	.100	0.000
170.000	.450	.370	.350	.330	.170	.040	-.110	-.200
180.000	.380	.270	.250	.230	.090	-.010	-.160	-.250

TABLE V.- STROUHAL NUMBER CORRECTION FACTOR, ξ

V_j/c_∞	ξ for θ of -							
	120°	130°	135°	140°	150°	160°	165°	170°
1.400	1.000	1.000	1.000	1.000	1.000	1.000	1.000	1.000
1.500	1.000	1.000	1.000	1.000	1.000	.995	.980	.930
1.600	1.000	1.000	1.000	1.000	1.000	.885	.840	.740
1.700	1.000	1.000	1.000	1.000	.965	.760	.680	.600
1.800	1.000	1.000	1.000	.990	.870	.660	.580	.510
1.900	1.000	1.000	1.000	.950	.775	.590	.510	.440
2.000	1.000	1.000	.981	.900	.710	.540	.450	.390
2.100	1.000	1.000	.955	.860	.660	.500	.410	.350
2.200	1.000	1.000	.920	.830	.630	.470	.380	.320
2.300	1.000	.985	.895	.810	.610	.445	.360	.300
2.400	1.000	.970	.880	.795	.595	.430	.350	.280
2.500	1.000	.955	.870	.790	.590	.420	.340	.270

TABLE VI.- NORMALIZED SPECTRAL DISTRIBUTION LEVEL $-10 \log_{10} F$

(a) $T_j/T_\infty = 1.0$; $\log_{10} V_j/c_\infty = 0.100$

$\log_{10} S_c$	$-10 \log_{10} F$ for θ of -									
	90°	100°	110°	120°	130°	140°	150°	160°	170°	180°
-2.000	41.400	41.633	43.833	48.233	47.267	47.800	48.233	43.400	40.500	39.533
-1.600	32.600	32.700	34.100	36.100	35.400	34.600	34.100	30.600	28.500	27.800
-1.300	26.000	26.000	26.800	27.000	26.500	24.700	23.500	21.000	19.500	19.000
-1.150	22.900	22.500	23.200	23.400	23.100	21.100	19.400	16.900	15.400	14.900
-1.000	19.300	19.500	19.500	20.000	20.000	17.500	15.300	13.000	11.620	11.160
-.824	16.500	16.500	16.500	17.000	17.000	14.100	11.800	9.800	8.600	8.200
-.699	14.800	14.900	14.500	15.000	15.000	12.500	10.100	8.400	7.380	7.040
-.602	13.800	13.800	13.300	13.800	13.800	11.200	9.500	8.400	7.740	7.520
-.500	12.700	13.000	12.200	12.800	12.500	10.200	9.500	9.100	8.860	8.780
-.398	11.900	12.000	11.600	12.000	11.600	9.600	9.800	10.300	10.600	10.700
-.301	11.500	11.300	11.100	11.500	11.000	9.500	10.300	11.600	12.380	12.640
-.222	11.100	10.900	11.000	11.300	10.800	9.700	11.100	12.800	13.820	14.160
0.000	11.000	10.900	10.900	11.000	11.000	10.900	14.000	16.300	17.680	18.140
.477	12.900	12.900	12.900	12.900	14.000	16.500	20.500	24.000	26.100	26.800
1.000	17.500	17.500	17.500	17.500	19.000	23.300	27.800	32.500	35.320	36.260
1.600	25.000	25.000	25.000	25.000	26.500	31.000	36.500	42.000	45.300	46.400
1.700	26.250	26.250	26.250	26.250	27.750	32.283	37.950	43.583	46.963	48.090

TABLE VI.- Continued

(b) $T_j/T_\infty = 2.0$; $\log_{10} V_j/c_\infty = 0.100$

$\log_{10} S_c$	$-10 \log_{10} F$ for 0 of -									
	90°	100°	110°	120°	130°	140°	150°	160°	170°	180°
-2.000	38.200	40.767	42.500	44.400	46.333	46.067	47.200	42.467	39.627	38.680
-1.600	29.800	31.300	32.500	33.600	34.200	32.600	32.800	30.200	28.640	28.120
-1.300	23.500	24.200	25.000	25.500	25.100	22.500	22.000	21.000	20.400	20.200
-1.150	20.500	21.100	21.700	22.100	21.100	18.900	17.400	16.700	16.280	16.140
-1.000	17.800	18.000	18.500	18.800	17.500	15.200	13.500	12.000	11.100	10.800
-.824	15.300	15.000	15.300	15.300	14.100	12.000	9.800	8.500	7.720	7.460
-.699	13.500	13.100	13.500	13.500	12.200	10.200	8.000	7.600	7.360	7.280
-.602	12.300	12.000	12.300	12.300	11.100	9.600	7.500	7.600	7.660	7.680
-.500	11.500	11.000	11.200	11.200	10.300	9.400	8.200	8.600	8.840	8.920
-.398	11.000	10.300	10.600	10.600	9.900	9.700	10.000	10.600	10.960	11.080
-.301	10.700	10.100	10.300	10.300	9.900	10.100	11.700	13.000	13.780	14.040
-.222	10.700	10.100	10.200	10.200	10.000	10.700	13.200	15.100	16.240	16.620
0.000	11.100	11.000	11.000	11.000	11.300	13.200	17.500	20.000	21.500	22.000
.477	14.300	14.700	14.500	15.000	17.000	20.700	26.700	31.000	33.580	34.440
1.000	19.500	20.000	20.200	21.500	24.500	29.700	37.000	42.700	46.120	47.260
1.600	27.000	27.100	27.000	29.200	33.100	40.200	49.100	56.600	61.100	62.600
1.700	28.250	28.283	28.133	30.483	34.533	41.950	51.117	58.917	63.597	65.157

TABLE VI.- Continued

(c) $T_j/T_\infty = 2.0$; $\log_{10} V_j/c_\infty = 0.125$

$\log_{10} S_c$	$-10 \log_{10} F$ for θ of -									
	90°	100°	110°	120°	130°	140°	150°	160°	170°	180°
-2.000	38.200	40.767	42.500	44.400	46.333	46.067	47.200	42.467	39.627	38.680
-1.600	29.600	31.300	32.500	33.600	34.200	32.000	32.800	30.200	28.640	28.120
-1.300	23.500	24.200	25.000	25.500	25.100	22.500	22.000	21.000	20.400	20.200
-1.150	20.500	21.100	21.700	22.100	21.100	16.900	17.400	17.100	16.920	16.860
-1.000	17.600	18.000	18.500	18.800	17.500	15.200	13.500	13.500	13.500	13.500
-.824	15.300	15.000	15.300	15.300	14.100	12.000	10.100	10.700	11.060	11.180
-.699	13.500	13.100	13.500	13.500	12.200	10.200	9.000	10.000	10.600	10.800
-.602	12.300	12.000	12.300	12.300	11.100	9.600	8.500	9.500	10.100	10.300
-.500	11.500	11.000	11.200	11.200	10.300	9.400	8.300	9.000	9.420	9.560
-.398	11.000	10.300	10.600	10.600	9.900	9.700	9.000	9.000	9.000	9.000
-.301	10.700	10.100	10.300	10.300	9.900	10.100	10.700	10.000	9.580	9.440
-.222	10.700	10.100	10.200	10.200	10.000	10.700	12.500	11.800	11.380	11.240
0.000	11.100	11.000	11.000	11.000	11.300	13.200	16.600	16.500	16.440	16.420
.477	14.300	14.700	14.500	15.000	17.000	20.700	25.800	26.800	27.400	27.600
1.000	19.500	20.000	20.200	21.500	24.500	29.700	36.000	38.000	39.200	39.600
1.600	27.000	27.100	27.000	29.200	33.100	40.200	47.600	51.000	53.040	53.720
1.700	28.250	28.283	28.133	30.483	34.533	41.950	49.533	53.167	55.347	56.073

TABLE VI.- Continued

(d) $T_j/T_\infty = 2.0$; $\log_{10} V_j/c_\infty = 0.150$

$\log_{10} S_c$	-10 $\log_{10}$ F for θ of -									
	90°	100°	110°	120°	130°	140°	150°	160°	170°	180°
-2.000	38.200	40.767	42.500	44.400	46.333	46.067	47.200	42.467	39.627	38.680
-1.600	29.800	31.300	32.500	33.600	34.200	32.600	32.800	30.200	28.640	28.120
-1.300	23.500	24.200	25.000	25.500	25.100	22.500	22.000	21.000	20.400	20.200
-1.150	20.500	21.100	21.700	22.100	21.100	18.900	17.400	17.100	16.920	16.860
-1.000	17.800	18.000	18.500	18.800	17.500	15.200	13.500	13.500	13.500	13.500
-.824	15.300	15.000	15.300	15.300	14.100	12.000	10.100	10.700	11.060	11.180
-.699	13.500	13.100	13.500	13.500	12.200	10.200	9.000	10.000	10.600	10.800
-.602	12.300	12.000	12.300	12.300	11.100	9.600	8.500	9.500	10.100	10.300
-.500	11.500	11.000	11.200	11.200	10.300	9.400	8.300	9.000	9.420	9.560
-.398	11.000	10.300	10.600	10.600	9.900	9.700	8.800	8.500	8.320	8.260
-.301	10.700	10.100	10.300	10.300	9.900	10.100	10.500	9.500	8.900	8.700
-.222	10.700	10.100	10.200	10.200	10.000	10.700	11.700	10.700	10.100	9.900
0.000	11.100	11.000	11.000	11.000	11.300	13.200	15.600	14.800	14.320	14.160
.477	14.300	14.700	14.500	15.000	17.000	20.700	24.000	23.500	23.200	23.100
1.000	19.500	20.000	20.200	21.500	24.500	29.700	33.000	33.500	33.800	33.900
1.600	27.000	27.100	27.000	29.200	33.100	40.200	43.500	44.100	44.460	44.580
1.700	28.250	28.283	28.133	30.483	34.533	41.950	45.250	45.867	46.237	46.360

TABLE VI.- Continued

(c) $T_j/T_\infty = 2.0$; $\log_{10} V_j/c_\infty = 0.175$

$\log_{10} S_c$	$-10 \log_{10} F$ for θ of -									
	90°	100°	110°	120°	130°	140°	150°	160°	170°	180°
-2.000	38.200	40.767	42.500	44.400	46.333	46.067	47.200	42.467	39.627	38.680
-1.600	29.800	31.300	32.500	33.600	34.200	32.600	32.800	30.200	28.640	28.120
-1.300	23.500	24.200	25.000	25.500	25.100	22.500	22.000	21.000	20.400	20.200
-1.150	20.500	21.100	21.700	22.100	21.100	18.900	17.400	17.300	17.240	17.220
-1.000	17.800	18.000	18.500	18.800	17.500	15.200	13.700	14.000	14.180	14.240
-.824	15.300	15.000	15.300	15.300	14.100	12.000	10.700	11.700	12.300	12.500
-.699	13.500	13.100	13.500	13.500	12.200	10.200	9.800	11.000	11.720	11.960
-.602	12.300	12.000	12.300	12.300	11.100	9.600	9.300	10.300	10.900	11.100
-.500	11.500	11.000	11.200	11.200	10.300	9.400	9.000	9.000	9.000	9.000
-.398	11.000	10.300	10.600	10.600	9.900	9.700	8.300	8.100	7.980	7.940
-.301	10.700	10.100	10.300	10.300	9.900	10.100	9.700	9.000	8.580	8.440
-.222	10.700	10.100	10.200	10.200	10.000	10.700	10.800	10.100	9.680	9.540
0.000	11.100	11.000	11.000	11.000	11.300	13.200	14.400	14.000	13.760	13.680
.477	14.300	14.700	14.500	15.000	17.000	20.700	22.000	22.000	22.000	22.000
1.000	19.500	20.600	20.200	21.500	24.500	29.700	30.500	31.000	31.300	31.400
1.600	27.000	27.100	27.000	29.200	33.100	40.200	40.000	41.200	41.920	42.160
1.700	28.250	28.283	28.133	30.483	34.533	41.950	41.583	42.900	43.690	43.953

TABLE VI.- Continued

(f) $T_j/T_\infty = 2.5$; $\log_{10} V_j/c_\infty = 0.100$

$\log_{10} S_c$	$-10 \log_{10} F$ for θ of -									
	90°	100°	110°	120°	130°	140°	150°	160°	170°	180°
-2.000	38.567	40.133	41.867	44.467	45.867	46.100	45.833	41.700	39.220	38.393
-1.600	29.900	30.800	32.000	33.000	33.200	32.500	31.700	28.900	27.220	26.660
-1.300	23.400	23.800	24.600	24.400	23.700	22.300	21.100	19.300	18.220	17.860
-1.150	20.400	20.800	21.400	20.900	19.800	18.200	16.600	15.100	14.080	13.740
-1.000	17.800	17.900	18.100	17.200	16.200	14.100	12.600	11.200	10.360	10.080
-.824	15.000	14.900	14.800	13.900	12.800	10.500	8.600	8.200	7.960	7.880
-.699	13.200	13.000	13.000	12.200	10.900	9.300	7.400	7.500	7.560	7.580
-.602	12.200	11.900	12.000	11.200	10.200	9.100	7.300	7.900	8.140	8.220
-.500	11.300	11.100	11.100	10.500	9.800	9.200	8.900	9.500	9.860	9.980
-.398	10.800	10.500	10.500	10.200	9.900	10.000	11.100	11.800	12.220	12.360
-.301	10.400	10.400	10.400	10.200	10.200	11.000	13.000	14.300	15.080	15.340
-.222	10.600	10.400	10.500	10.300	10.700	12.000	14.600	16.200	17.160	17.480
0.000	11.200	11.100	11.200	11.600	12.800	15.300	19.200	21.600	23.040	23.520
.477	14.700	14.800	15.400	16.500	18.900	23.400	29.100	33.200	35.660	36.480
1.000	20.500	20.500	21.300	22.900	26.200	32.300	40.000	45.700	49.120	50.260
1.600	28.500	28.400	28.500	30.800	34.700	42.600	52.400	60.300	65.040	66.620
1.700	29.833	29.717	29.700	32.117	36.117	44.317	54.467	62.733	67.693	69.347

TABLE VI.- Continued

(g) $T_j/T_\infty = 2.5$; $\log_{10} V_j/c_\infty = 0.125$

$\log_{10} S_c$	$-10 \log_{10} F$ for θ of -									
	90°	100°	110°	120°	130°	140°	150°	160°	170°	180°
-2.000	38.567	40.133	41.867	44.467	45.867	46.100	45.833	41.700	39.220	38.393
-1.600	29.900	30.800	32.000	33.000	33.200	32.500	31.700	28.900	27.220	26.660
-1.300	23.400	23.800	24.600	24.400	23.700	22.300	21.100	19.300	18.220	17.860
-1.150	20.400	20.800	21.400	20.900	19.800	18.200	16.800	15.900	15.360	15.180
-1.000	17.800	17.900	18.100	17.200	16.200	14.100	12.600	13.000	13.240	13.320
-.824	15.000	14.900	14.800	13.900	12.800	10.500	8.800	11.000	12.320	12.760
-.699	13.200	13.000	13.000	12.200	10.900	9.300	7.800	10.000	11.320	11.760
-.602	12.200	11.900	12.000	11.200	10.200	9.100	7.800	9.100	9.880	10.140
-.500	11.300	11.100	11.100	10.500	9.800	9.200	9.000	8.400	8.040	7.920
-.398	10.800	10.500	10.500	10.200	9.900	10.000	10.800	8.900	7.760	7.380
-.301	10.400	10.400	10.400	10.200	10.200	11.000	12.700	10.700	9.500	9.100
-.222	10.600	10.400	10.500	10.300	10.700	12.000	14.400	12.500	11.360	10.980
0.000	11.200	11.100	11.200	11.600	12.800	15.300	18.900	17.700	16.980	16.740
.477	14.700	14.800	15.400	16.500	18.900	23.400	28.700	29.000	29.180	29.240
1.000	20.500	20.500	21.300	22.900	26.200	32.300	39.400	41.200	42.280	42.640
1.600	28.500	28.400	28.500	30.800	34.700	42.600	51.800	55.200	57.240	57.920
1.700	29.833	29.717	29.700	32.117	36.117	44.317	53.867	57.533	59.733	60.467

TABLE VI.- Continued

(h) $T_j/T_\infty = 2.5$; $\log_{10} V_j/c_\infty = 0.150$

$\log_{10} S_c$	$-10 \log_{10} F$ for θ of -									
	90°	100°	110°	120°	130°	140°	150°	160°	170°	180°
-2.000	38.567	40.133	41.867	44.467	45.867	46.100	45.833	41.700	39.220	38.393
-1.600	29.900	30.800	32.000	33.000	33.200	32.500	31.700	28.900	27.220	26.660
-1.300	23.400	23.800	24.600	24.400	23.700	22.300	21.100	19.300	18.220	17.860
-1.150	20.400	20.800	21.400	20.900	19.800	18.200	16.800	15.900	15.360	15.180
-1.000	17.800	17.900	18.100	17.200	16.200	14.100	13.000	13.000	13.000	13.000
-.824	15.000	14.900	14.800	13.900	12.800	11.100	10.800	11.000	11.120	11.160
-.699	13.200	13.000	13.000	12.200	10.900	9.900	9.900	10.000	10.060	10.080
-.602	12.200	11.900	12.000	11.200	10.200	9.300	9.000	9.100	9.160	9.180
-.500	11.300	11.100	11.100	10.500	9.800	9.200	8.800	8.400	8.160	8.080
-.398	10.600	10.500	10.500	10.200	9.900	9.600	9.700	8.700	8.100	7.900
-.301	10.400	10.400	10.400	10.200	10.200	10.300	11.700	10.300	9.460	9.180
-.222	10.600	10.400	10.500	10.300	10.700	11.500	13.100	11.800	11.020	10.760
0.000	11.200	11.100	11.200	11.600	12.800	14.800	17.100	16.200	15.660	15.480
.477	14.700	14.800	15.400	16.500	18.900	22.400	25.500	25.700	25.820	25.860
1.000	20.500	20.500	21.300	22.900	26.200	31.300	35.000	36.100	36.760	36.980
1.600	28.500	28.400	28.500	30.800	34.700	41.500	45.800	48.100	49.480	49.940
1.700	29.633	29.717	29.700	32.117	36.117	43.200	47.600	50.100	51.600	52.100

TABLE VI.- Continued

(i) $T_j/T_\infty = 2.5$; $\log_{10} V_j/c_\infty = 0.175$

$\log_{10} S_c$	$-10 \log_{10} F$ for θ of -									
	90°	100°	110°	120°	130°	140°	150°	160°	170°	180°
-2.000	38.567	40.133	41.867	44.467	45.867	46.100	45.833	41.700	39.220	38.393
-1.600	29.900	30.800	32.000	33.000	33.200	32.500	31.700	28.900	27.220	26.660
-1.300	23.400	23.600	24.600	24.400	23.700	22.300	21.100	19.300	18.220	17.860
-1.150	20.400	20.800	21.400	20.900	19.800	18.200	16.800	16.000	15.520	15.360
-1.000	17.800	17.900	18.100	17.200	16.200	14.100	13.000	13.100	13.160	13.180
-.824	15.000	14.900	14.800	13.900	12.800	11.100	11.000	11.400	11.640	11.720
-.699	13.200	13.000	13.000	12.200	10.900	9.900	10.100	10.300	10.420	10.460
-.602	12.200	11.900	12.000	11.200	10.200	9.300	9.300	9.400	9.460	9.480
-.500	11.300	11.100	11.100	10.500	9.800	9.200	9.000	8.400	8.040	7.920
-.398	10.800	10.500	10.500	10.200	9.900	9.500	9.500	8.600	8.060	7.880
-.301	10.400	10.400	10.400	10.200	10.200	10.100	11.100	9.900	9.180	8.940
-.222	10.600	10.400	10.500	10.300	10.700	11.000	12.200	11.200	10.600	10.400
0.000	11.200	11.100	11.200	11.600	12.800	14.100	15.700	15.000	14.580	14.440
.477	14.700	14.600	15.400	16.500	18.900	21.700	22.800	23.000	23.120	23.160
1.000	20.500	20.500	21.300	22.900	26.200	30.200	31.000	31.800	32.280	32.440
1.600	28.500	28.400	28.500	30.800	34.700	40.000	40.200	42.000	43.080	43.440
1.700	29.833	29.717	29.700	32.117	36.117	41.633	41.733	43.700	44.880	45.273

TABLE VI.- Continued

(j) $T_j/T_\infty = 2.5$; $\log_{10} V_j/c_\infty = 0.200$

$\log_{10} S_c$	$-10 \log_{10} F$ for θ of -									
	90°	100°	110°	120°	130°	140°	150°	160°	170°	180°
-2.000	38.567	40.133	41.867	44.467	45.867	46.100	45.833	41.700	39.220	38.393
-1.600	29.900	30.800	32.000	33.000	33.200	32.500	31.700	28.900	27.220	26.660
-1.300	23.400	23.800	24.600	24.400	23.700	22.300	21.100	19.300	18.220	17.860
-1.150	20.400	20.800	21.400	20.900	19.800	18.200	16.800	16.000	15.520	15.360
-1.000	17.800	17.900	18.100	17.200	16.200	14.100	13.000	13.100	13.160	13.180
-.824	15.000	14.900	14.600	13.900	12.800	11.100	11.000	11.400	11.640	11.720
-.699	13.200	13.000	13.000	12.200	10.900	9.900	10.100	10.300	10.420	10.460
-.602	12.200	11.900	12.000	11.200	10.200	9.300	9.300	9.400	9.460	9.480
-.500	11.300	11.100	11.100	10.500	9.800	9.200	9.000	8.400	8.040	7.920
-.398	10.800	10.500	10.500	10.200	9.900	9.500	9.500	8.600	8.060	7.880
-.301	10.400	10.400	10.400	10.200	10.200	10.100	10.800	9.700	9.040	8.820
-.222	10.600	10.400	10.500	10.300	10.700	11.000	11.900	10.800	10.140	9.920
0.000	11.200	11.100	11.200	11.600	12.800	13.700	15.100	14.300	13.820	13.660
.477	14.700	14.800	15.400	16.500	18.900	20.600	21.900	21.400	21.100	21.000
1.000	20.500	20.500	21.300	22.900	26.200	28.600	29.400	29.400	29.400	29.400
1.600	28.500	28.400	28.500	30.800	34.700	38.200	37.900	38.500	38.860	38.980
1.700	29.833	29.717	29.700	32.117	36.117	39.767	39.317	40.017	40.437	40.577

TABLE VI.- Continued

(k) $T_j/T_\infty = 2.5$; $\log_{10} V_j/c_\infty = 0.225$

$\log_{10} S_c$	$-10 \log_{10} F$ for θ of -									
	90°	100°	110°	120°	130°	140°	150°	160°	170°	180°
-2.000	38.567	40.133	41.867	44.467	45.867	46.100	45.833	41.700	39.220	38.393
-1.600	29.900	30.800	32.000	33.000	33.200	32.500	31.700	28.900	27.220	26.660
-1.300	23.400	23.800	24.600	24.400	23.700	22.300	21.100	19.300	18.220	17.860
-1.150	20.400	20.800	21.400	20.900	19.800	18.200	16.800	16.000	15.520	15.360
-1.000	17.800	17.900	18.100	17.200	16.200	14.100	13.000	13.100	13.160	13.180
-.824	15.000	14.900	14.800	13.900	12.800	11.100	11.000	11.400	11.640	11.720
-.699	13.200	13.000	13.000	12.200	10.900	9.900	10.100	10.300	10.420	10.460
-.602	12.200	11.900	12.000	11.200	10.200	9.300	9.300	9.400	9.460	9.480
-.500	11.300	11.100	11.100	10.500	9.800	9.200	9.000	8.400	8.040	7.920
-.398	10.800	10.500	10.500	10.200	9.900	9.500	9.500	8.600	8.060	7.880
-.301	10.400	10.400	10.400	10.200	10.200	10.100	10.700	9.700	9.100	8.900
-.222	10.600	10.400	10.500	10.300	10.700	10.800	11.700	10.800	10.260	10.080
0.000	11.200	11.100	11.200	11.600	12.800	13.700	14.600	13.900	13.480	13.340
.477	14.700	14.800	15.400	16.500	18.900	20.100	20.800	20.500	20.320	20.260
1.000	20.500	20.500	21.300	22.900	26.200	27.400	27.700	28.100	28.340	28.420
1.600	28.500	28.400	28.500	30.800	34.700	36.200	35.600	36.500	37.040	37.220
1.700	29.833	29.717	29.700	32.117	36.117	37.667	36.917	37.900	38.490	38.687

TABLE VI.- Continued

(1) $T_j/T_\infty = 3.0$; $\log_{10} V_j/c_\infty = 0.100$

$\log_{10} S_c$	-10 $\log_{10}$ F for θ of -									
	90°	100°	110°	120°	130°	140°	150°	160°	170°	180°
-2.000	38.967	39.667	42.067	43.167	44.500	44.867	43.333	40.333	38.533	37.933
-1.600	30.300	30.800	32.600	32.500	32.500	31.800	30.000	27.000	25.200	24.600
-1.300	23.800	24.000	25.500	24.500	23.500	22.600	20.000	17.000	15.200	14.600
-1.150	20.400	21.000	21.600	21.000	19.500	17.300	15.300	13.000	11.620	11.160
-1.000	17.500	17.800	17.600	17.800	14.500	12.500	11.300	10.000	9.220	8.960
-.824	14.500	14.300	14.200	14.300	10.200	9.000	8.500	8.100	7.860	7.780
-.699	12.900	12.500	12.300	12.500	9.200	8.100	8.000	7.900	7.840	7.820
-.602	11.900	11.400	11.000	11.300	9.000	8.100	8.500	8.500	8.500	8.500
-.500	11.200	10.600	10.300	10.600	9.100	9.000	10.000	10.500	10.800	10.900
-.398	10.900	10.300	10.200	10.300	9.800	10.500	12.300	13.300	13.900	14.100
-.301	10.900	10.300	10.000	10.300	10.700	12.300	14.300	15.900	16.860	17.180
-.222	11.000	10.400	10.000	10.400	11.500	13.600	16.200	17.700	18.600	18.900
0.000	11.500	11.400	11.200	11.500	14.500	17.500	21.000	23.300	24.680	25.140
.477	15.100	15.100	15.200	16.400	21.500	26.200	31.400	35.000	37.160	37.880
1.000	21.200	21.200	21.500	24.100	29.500	35.500	42.800	48.100	51.280	52.340
1.600	29.000	29.000	29.500	33.500	39.000	46.500	56.000	63.100	67.360	68.780
1.700	30.300	30.300	30.833	35.067	40.583	48.333	58.200	65.600	70.040	71.520

TABLE VI.- Continued

(m) $T_j/T_\infty = 3.0$; $\log_{10} V_j/c_\infty = 0.125$

$\log_{10} S_c$	$-10 \log_{10} F$ for θ of -									
	90°	100°	110°	120°	130°	140°	150°	160°	170°	180°
-2.000	38.967	39.867	42.067	43.167	44.500	44.867	43.333	40.333	38.533	37.933
-1.600	30.300	30.800	32.600	32.500	32.500	31.800	30.000	27.000	25.200	24.600
-1.300	23.600	24.000	25.500	24.500	23.500	22.000	20.000	17.000	15.200	14.600
-1.150	20.400	21.000	21.600	21.000	19.500	17.300	15.500	13.200	11.800	11.360
-1.000	17.500	17.800	17.600	17.800	14.500	12.700	11.700	11.000	10.580	10.440
-.824	14.500	14.360	14.200	14.300	10.200	10.100	10.300	9.700	9.340	9.220
-.699	12.900	12.500	12.300	12.500	9.200	9.500	9.300	9.300	9.300	9.300
-.602	11.900	11.400	11.000	11.300	9.000	8.900	8.900	8.900	8.900	8.900
-.500	11.200	10.600	10.300	10.600	9.100	8.500	8.900	9.200	9.380	9.440
-.398	10.900	10.300	10.200	10.300	9.800	10.000	9.700	10.500	10.980	11.140
-.301	10.900	10.300	10.000	10.300	10.700	11.500	11.700	12.600	13.140	13.320
-.222	11.000	10.400	10.000	10.400	11.500	13.000	13.200	14.500	15.280	15.540
0.000	11.500	11.400	11.200	11.500	14.500	16.500	17.700	19.800	21.060	21.480
.477	15.100	15.100	15.200	16.400	21.500	25.000	27.500	31.000	33.100	33.800
1.000	21.200	21.200	21.500	24.100	29.500	34.100	37.800	43.100	46.280	47.340
1.600	29.000	29.000	29.500	33.500	39.000	44.500	49.800	57.500	62.120	63.660
1.700	30.300	30.300	30.833	35.067	40.583	46.233	51.800	59.900	64.760	66.380

TABLE VI.- Continued

(n) $T_j/T_\infty = 3.0$; $\log_{10} V_j/c_\infty = 0.150$

$\log_{10} S_c$	$-10 \log_{10} F$ for 0 of -									
	90°	100°	110°	120°	130°	140°	150°	160°	170°	180°
-2.000	38.967	39.867	42.067	43.167	44.500	44.867	43.333	40.333	38.533	37.933
-1.600	30.300	30.800	32.600	32.500	32.500	31.800	30.000	27.000	25.200	24.600
-1.300	23.800	24.000	25.500	24.500	23.500	22.000	20.000	17.000	15.200	14.600
-1.150	20.400	21.000	21.600	21.000	19.500	17.300	15.800	13.500	12.120	11.660
-1.000	17.500	17.800	17.600	17.800	14.500	13.000	12.500	11.500	10.900	10.700
-.824	14.500	14.300	14.200	14.300	10.200	10.500	10.600	10.500	10.440	10.420
-.699	12.900	12.500	12.300	12.500	9.200	9.700	9.600	10.000	10.240	10.320
-.602	11.900	11.400	11.000	11.300	9.000	9.400	9.100	9.500	9.740	9.820
-.500	11.200	10.600	10.300	10.600	9.100	8.900	9.000	9.400	9.640	9.720
-.398	10.900	10.300	10.200	10.300	9.800	9.500	9.500	10.000	10.300	10.400
-.301	10.900	10.300	10.000	10.300	10.700	11.200	11.100	11.600	11.900	12.000
-.222	11.000	10.400	10.000	10.400	11.500	12.500	12.500	13.100	13.460	13.580
0.000	11.500	11.400	11.200	11.500	14.500	16.100	16.500	17.600	18.260	18.480
.477	15.100	15.100	15.200	16.400	21.300	24.200	25.000	27.500	29.000	29.500
1.000	21.200	21.200	21.500	24.100	29.000	32.900	34.000	38.500	41.200	42.100
1.600	29.000	29.000	29.500	33.500	38.000	42.600	44.500	50.700	54.420	55.660
1.700	30.300	30.300	30.833	35.067	39.500	44.217	46.250	52.733	56.623	57.920

TABLE VI.- Continued

(o) $T_j/T_\infty = 3.0$; $\log_{10} V_j/c_\infty = 0.175$

$\log_{10} S_c$	$-10 \log_{10} F$ for θ of -									
	90°	100°	110°	120°	130°	140°	150°	160°	170°	180°
-2.000	38.967	39.867	42.067	43.167	44.500	44.667	43.333	40.333	38.533	37.933
-1.600	30.300	30.800	32.600	32.500	32.500	31.800	30.000	27.000	25.200	24.600
-1.300	23.800	24.000	25.500	24.500	23.500	22.000	20.000	17.000	15.200	14.600
-1.150	20.400	21.000	21.600	21.000	19.500	17.300	16.000	14.000	12.800	12.400
-1.000	17.500	17.800	17.600	17.800	14.500	13.200	13.000	12.100	11.560	11.380
-.824	14.500	14.300	14.200	14.300	10.200	10.800	11.000	11.300	11.480	11.540
-.699	12.900	12.500	12.300	12.500	9.200	10.100	10.100	10.700	11.060	11.180
-.602	11.900	11.400	11.000	11.300	9.000	9.700	9.300	10.000	10.420	10.560
-.500	11.200	10.600	10.300	10.600	9.100	9.300	9.100	9.500	9.740	9.820
-.398	10.900	10.300	10.200	10.300	9.800	9.500	9.500	9.500	9.500	9.500
-.301	10.900	10.300	10.000	10.300	10.700	10.600	10.500	11.000	11.300	11.400
-.222	11.000	10.400	10.000	10.400	11.500	12.000	11.700	12.300	12.660	12.780
0.000	11.500	11.400	11.200	11.500	14.500	15.400	15.400	16.300	16.840	17.020
.477	15.100	15.100	15.200	16.400	21.000	22.500	23.000	24.500	25.400	25.700
1.000	21.200	21.200	21.500	24.100	28.000	30.400	31.500	33.500	34.700	35.100
1.600	29.000	29.000	29.500	33.500	36.000	39.500	41.300	43.900	45.460	45.980
1.700	30.300	30.300	30.833	35.067	37.333	41.017	42.933	45.633	47.253	47.793

TABLE VI.- Continued

(p) $T_j/T_\infty = 3.0$; $\log_{10} V_j/c_\infty = 0.200$

$\log_{10} S_c$	$-10 \log_{10} F$ for 0 of -									
	90°	100°	110°	120°	130°	140°	150°	160°	170°	180°
-2.000	38.967	39.867	42.067	43.167	44.500	44.867	42.933	40.333	38.773	38.253
-1.600	30.300	30.800	32.600	32.500	32.500	31.800	30.000	27.000	25.200	24.600
-1.300	23.800	24.000	25.500	24.500	23.500	22.000	20.300	17.000	15.020	14.360
-1.150	20.400	21.000	21.600	21.000	19.500	17.300	16.300	14.200	12.940	12.520
-1.000	17.500	17.800	17.600	17.800	14.500	13.500	13.500	12.500	11.900	11.700
-.824	14.500	14.300	14.200	14.300	11.300	11.300	11.500	11.600	11.660	11.680
-.699	12.900	12.500	12.300	12.500	9.500	10.500	10.500	11.100	11.460	11.580
-.602	11.900	11.400	11.000	11.300	8.500	10.100	9.500	10.300	10.780	10.940
-.500	11.200	10.600	10.300	10.600	6.800	9.600	9.200	9.500	9.680	9.740
-.398	10.900	10.300	10.200	10.300	9.600	9.500	9.500	9.500	9.500	9.500
-.301	10.900	10.300	10.000	10.300	10.700	10.400	10.400	10.500	10.560	10.580
-.222	11.000	10.400	10.000	10.400	11.500	11.500	11.500	11.700	11.820	11.860
0.000	11.500	11.400	11.200	11.500	14.500	14.300	14.600	15.100	15.400	15.500
.477	15.100	15.100	15.200	16.400	20.100	20.500	21.500	22.300	22.780	22.940
1.000	21.200	21.200	21.500	24.100	26.500	27.000	29.000	30.500	31.400	31.700
1.600	29.000	29.000	29.500	33.500	34.000	34.500	37.500	40.000	41.500	42.000
1.700	30.300	30.300	30.833	35.067	35.250	35.750	36.917	41.583	43.183	43.717

TABLE VI.- Continued

(q) $T_j/T_\infty = 3.0$; $\log_{10} V_j/c_\infty = 0.225$

$\log_{10} S_c$	$-10 \log_{10} F$ for θ of -									
	90°	100°	110°	120°	130°	140°	150°	160°	170°	180°
-2.000	38.967	39.867	42.067	43.167	44.500	44.667	42.667	40.333	38.933	38.467
-1.600	30.300	30.800	32.600	32.500	32.500	31.600	30.000	27.000	25.200	24.600
-1.300	23.800	24.000	25.500	24.500	23.500	22.000	20.500	17.000	14.900	14.200
-1.150	20.400	21.000	21.600	21.000	19.500	17.300	16.600	14.200	12.760	12.280
-1.000	17.500	17.800	17.600	17.800	14.500	13.500	13.500	12.500	11.900	11.700
-.824	14.500	14.300	14.200	14.300	11.300	11.300	11.500	11.600	11.660	11.680
-.699	12.900	12.500	12.300	12.500	9.500	10.500	10.500	11.100	11.460	11.580
-.602	11.900	11.400	11.000	11.300	8.500	10.100	9.700	10.400	10.820	10.960
-.500	11.200	10.600	10.300	10.600	8.800	9.600	9.300	9.500	9.620	9.660
-.398	10.900	10.300	10.200	10.300	9.600	9.500	9.500	9.500	9.500	9.500
-.301	10.900	10.300	10.000	10.300	10.700	10.400	10.400	10.500	10.560	10.580
-.222	11.000	10.400	10.000	10.400	11.500	11.500	11.300	11.700	11.940	12.020
0.000	11.500	11.400	11.200	11.500	14.500	14.300	14.300	14.400	14.460	14.480
.477	15.100	15.100	15.200	16.400	20.100	20.500	21.000	20.600	20.360	20.280
1.000	21.200	21.200	21.500	24.100	26.500	27.000	26.000	27.500	27.200	27.100
1.600	29.000	29.000	29.500	33.500	34.000	34.500	36.300	35.000	34.220	33.960
1.700	30.300	30.300	30.833	35.067	35.250	35.750	37.683	36.250	35.390	35.103

TABLE VI.- Continued

(c) $T_j/T_\infty = 3.5$; $\log_{10} V_j/c_\infty = 0.100$

$\log_{10} S_c$	$-10 \log_{10} F$ for θ of -									
	90°	100°	110°	120°	130°	140°	150°	160°	170°	180°
-2.000	36.800	39.900	42.567	43.767	45.933	45.267	44.867	38.600	34.840	33.587
-1.600	30.000	30.700	31.900	32.300	33.000	31.800	30.200	25.800	23.160	22.280
-1.300	23.400	23.800	23.900	23.700	23.300	21.700	19.200	16.200	14.400	13.800
-1.150	20.300	20.600	20.400	19.900	18.700	17.300	14.700	12.900	11.820	11.460
-1.000	17.000	17.000	17.300	16.100	13.700	12.500	11.000	10.000	9.400	9.200
-.824	14.100	14.000	14.000	12.700	9.400	8.600	7.700	8.000	8.180	8.240
-.699	12.600	12.400	12.500	11.200	8.300	7.700	7.200	8.600	9.440	9.720
-.602	11.600	11.600	11.400	10.500	8.200	7.800	7.700	10.000	11.380	11.840
-.500	11.000	11.000	10.900	10.100	8.600	8.700	9.400	12.000	13.560	14.080
-.398	10.600	10.600	10.500	10.000	9.800	10.500	11.900	14.600	16.220	16.760
-.301	10.600	10.400	10.400	10.200	11.000	12.500	14.000	16.800	18.480	19.040
-.222	10.600	10.500	10.500	10.600	11.900	13.900	16.000	18.800	20.480	21.040
0.000	11.400	11.300	11.400	12.300	15.500	18.200	21.100	24.500	26.540	27.220
.477	15.000	15.100	15.900	16.600	22.800	27.300	32.300	36.700	39.340	40.220
1.000	21.900	21.900	22.600	26.100	31.100	37.600	44.500	50.600	54.260	55.480
1.600	29.900	29.900	30.400	34.800	40.800	49.100	58.600	66.400	71.080	72.640
1.700	31.233	31.233	31.700	36.250	42.417	51.017	60.950	69.033	73.883	75.500

TABLE VI.- Continued

(s) $T_j/T_\infty = 3.5$; $\log_{10} V_j/c_\infty = 0.125$

$\log_{10} S_c$	$-10 \log_{10} F$ for θ of -									
	90°	100°	110°	120°	130°	140°	150°	160°	170°	180°
-2.000	38.800	39.900	42.567	43.767	45.933	45.267	44.867	38.600	34.840	33.587
-1.600	30.000	30.700	31.900	32.300	33.000	31.800	30.200	25.800	23.160	22.280
-1.300	23.400	23.800	23.900	23.700	23.300	21.700	19.200	16.200	14.400	13.800
-1.150	20.300	20.600	20.400	19.900	18.700	17.300	14.700	13.000	11.980	11.640
-1.000	17.000	17.000	17.300	16.100	13.700	12.500	11.000	10.200	9.720	9.560
-.824	14.100	14.000	14.000	12.700	9.400	8.600	7.700	8.300	8.660	8.780
-.699	12.600	12.400	12.500	11.200	8.300	7.700	7.200	8.800	9.760	10.080
-.602	11.600	11.600	11.400	10.500	8.200	7.800	7.700	10.100	11.540	12.020
-.500	11.000	11.000	10.900	10.100	8.600	8.700	9.400	11.800	13.240	13.720
-.398	10.600	10.600	10.500	10.000	9.800	10.500	11.900	14.100	15.420	15.860
-.301	10.600	10.400	10.400	10.200	11.000	12.500	14.000	16.300	17.680	18.140
-.222	10.600	10.500	10.500	10.600	11.900	13.900	16.000	18.100	19.360	19.780
0.000	11.400	11.300	11.400	12.300	15.500	18.200	21.100	23.100	24.300	24.700
.477	15.000	15.100	15.900	18.600	22.800	27.300	32.300	34.100	35.180	35.540
1.000	21.900	21.900	22.600	26.100	31.100	37.600	44.500	46.400	47.540	47.920
1.600	29.900	29.900	30.400	34.800	40.800	49.100	58.600	60.500	61.640	62.020
1.700	31.233	31.233	31.700	36.250	42.417	51.017	60.950	62.850	63.990	64.370

TABLE VI.- Continued

(t) $T_j/T_\infty = 3.5$; $\log_{10} V_j/c_\infty = 0.150$

$\log_{10} S_c$	$-10 \log_{10} F$ for θ of -									
	90°	100°	110°	120°	130°	140°	150°	160°	170°	180°
-2.000	38.800	39.900	42.567	43.767	45.933	45.267	44.867	38.600	34.840	33.587
-1.600	30.000	30.700	31.900	32.300	33.000	31.800	30.200	25.800	23.160	22.280
-1.300	23.400	23.800	23.900	23.700	23.300	21.700	19.200	16.200	14.400	13.800
-1.150	20.300	20.600	20.400	19.900	18.700	17.300	14.800	13.200	12.240	11.920
-1.000	17.000	17.000	17.300	16.100	13.700	12.600	11.100	10.700	10.460	10.380
-.824	14.100	14.000	14.000	12.700	9.400	9.400	8.900	9.500	9.860	9.980
-.699	12.600	12.400	12.500	11.200	8.300	8.400	8.700	9.200	9.500	9.600
-.602	11.600	11.600	11.400	10.500	8.200	8.200	8.400	8.700	8.880	8.940
-.500	11.000	11.000	10.900	10.100	8.600	8.400	8.900	9.100	9.220	9.260
-.398	10.600	10.600	10.500	10.000	9.800	10.200	10.500	11.300	11.780	11.940
-.301	10.600	10.400	10.400	10.200	11.000	12.200	12.700	13.200	13.500	13.600
-.222	10.600	10.500	10.500	10.600	11.900	13.600	14.400	15.100	15.520	15.660
0.000	11.400	11.300	11.400	12.300	15.500	17.600	18.800	19.700	20.240	20.420
.477	15.000	15.100	15.900	18.600	22.800	26.100	28.500	29.900	30.740	31.020
1.000	21.900	21.900	22.600	26.100	31.100	35.900	39.300	41.000	42.020	42.360
1.600	29.900	29.900	30.400	34.800	40.800	46.800	51.500	53.900	55.340	55.820
1.700	31.233	31.233	31.700	36.250	42.417	48.617	53.533	56.050	57.560	58.063

TABLE VI.- Continued

(u) $T_j/T_\infty = 3.5$; $\log_{10} V_j/c_\infty = 0.175$

$\log_{10} S_c$	$-10 \log_{10} F$ for θ of -									
	90°	100°	110°	120°	130°	140°	150°	160°	170°	180°
-2.000	38.800	39.900	42.567	43.767	45.933	45.267	44.867	38.600	34.840	33.587
-1.600	30.000	30.700	31.900	32.300	33.000	31.800	30.200	25.800	23.160	22.280
-1.300	23.400	23.800	23.900	23.700	23.300	21.700	19.200	16.200	14.400	13.800
-1.150	20.300	20.600	20.400	19.900	18.700	17.300	15.000	13.300	12.280	11.940
-1.000	17.000	17.000	17.300	16.100	13.700	12.600	11.700	11.200	10.900	10.800
-.824	14.100	14.000	14.000	12.700	9.400	9.800	10.300	10.600	10.780	10.840
-.699	12.600	12.400	12.500	11.200	8.300	9.200	9.400	10.100	10.520	10.660
-.602	11.600	11.600	11.400	10.500	8.200	8.500	8.800	9.200	9.440	9.520
-.500	11.000	11.000	10.900	10.100	8.600	8.500	8.800	9.100	9.280	9.340
-.398	10.600	10.600	10.500	10.000	9.800	9.900	10.000	9.900	9.840	9.820
-.301	10.600	10.400	10.400	10.200	11.000	11.500	11.500	11.400	11.340	11.320
-.222	10.600	10.500	10.500	10.600	11.900	12.900	12.900	12.900	12.900	12.900
0.000	11.400	11.300	11.400	12.300	15.500	16.800	17.000	16.900	16.840	16.820
.477	15.000	15.100	15.900	18.600	22.800	25.100	25.400	26.200	26.680	26.840
1.000	21.900	21.900	22.600	26.100	31.000	34.000	34.700	36.100	36.940	37.220
1.600	29.900	29.900	30.400	34.800	40.500	44.600	45.500	47.400	48.540	48.920
1.700	31.233	31.233	31.700	36.250	42.083	46.367	47.300	49.283	50.473	50.870

C - 2

TABLE VI.- Continued

(v) $T_j/T_\infty = 3.5$; $\log_{10} V_j/c_\infty = 0.200$

$\log_{10} S_\infty$	$-10 \log_{10} F$ for θ of -									
	95°	100°	110°	120°	130°	140°	150°	160°	170°	180°
-2.000	38.800	39.900	42.567	43.767	45.933	45.267	44.867	38.600	34.840	33.587
-1.600	30.000	30.700	31.900	32.300	33.000	31.800	30.200	25.800	23.160	22.280
-1.300	23.400	23.600	23.900	23.700	23.300	21.700	19.200	16.200	14.400	13.800
-1.150	20.300	20.600	20.400	19.900	18.700	17.300	15.400	13.700	12.680	12.340
-1.000	17.000	17.000	17.300	16.100	13.700	12.700	12.700	12.100	11.740	11.620
-.824	14.100	14.000	14.000	12.700	9.400	10.500	10.700	11.100	11.340	11.420
-.699	12.600	12.400	12.500	11.200	8.300	9.900	9.700	11.000	11.780	12.040
-.602	11.600	11.600	11.400	10.500	8.200	9.200	8.700	10.300	11.260	11.580
-.500	11.000	11.000	10.900	10.100	8.600	8.500	8.600	9.500	10.040	10.220
-.398	10.600	10.600	10.500	10.000	9.800	9.900	9.500	9.900	10.140	10.220
-.301	10.600	10.400	10.400	10.200	11.000	11.200	10.900	10.900	10.900	10.900
-.222	10.600	10.500	10.500	10.600	11.900	12.500	12.200	12.000	11.880	11.840
0.000	11.400	11.300	11.400	12.300	15.300	16.000	15.800	15.900	15.960	15.980
.477	15.000	15.100	15.900	18.600	22.100	23.600	23.600	23.700	23.760	23.780
1.000	21.900	21.900	22.600	26.100	29.900	32.100	32.400	32.600	32.720	32.760
1.600	29.900	29.900	30.400	34.800	38.700	41.700	42.200	42.600	42.840	42.920
1.700	31.233	31.233	31.700	36.250	40.167	43.300	43.833	44.267	44.527	44.613

TABLE VI.- Concluded

(w) $T_j/T_\infty = 3.5$; $\log_{10} V_j/c_\infty = 0.225$

$\log_{10} S_c$	$-10 \log_{10} F$ for θ of -									
	90°	100°	110°	120°	130°	140°	150°	160°	170°	180°
-2.000	38.600	39.900	42.567	43.767	45.933	45.267	44.867	38.600	34.840	33.587
-1.600	30.000	30.700	31.900	32.300	33.000	31.800	30.200	25.800	23.160	22.280
-1.300	23.400	23.800	23.900	23.700	23.300	21.700	19.200	16.200	14.400	13.800
-1.150	20.300	20.600	20.400	19.900	18.700	17.300	15.400	13.700	12.680	12.340
-1.000	17.000	17.000	17.300	16.100	13.700	12.700	12.700	12.100	11.740	11.620
-.824	14.100	14.000	14.000	12.700	9.400	10.500	10.700	11.100	11.340	11.420
-.699	12.600	12.400	12.500	11.200	8.300	9.900	9.700	11.000	11.780	12.040
-.602	11.600	11.600	11.400	10.500	8.200	9.200	8.700	10.300	11.260	11.580
-.500	11.000	11.000	10.900	10.100	8.600	8.500	8.600	9.500	10.040	10.220
-.398	10.600	10.600	10.500	10.000	9.800	9.900	9.500	9.900	10.140	10.220
-.301	10.600	10.400	10.400	10.200	11.000	11.200	10.900	10.900	10.900	10.900
-.222	10.600	10.500	10.500	10.600	11.900	12.500	12.200	12.000	11.880	11.840
0.000	11.400	11.300	11.400	12.300	15.300	16.000	15.800	15.800	15.800	15.800
.477	15.000	15.100	15.900	18.600	22.100	23.600	23.600	23.500	23.440	23.420
1.000	21.900	21.900	22.600	26.100	29.900	32.100	32.400	32.200	32.080	32.040
1.600	29.900	29.900	30.400	34.800	38.700	41.700	42.200	41.800	41.560	41.480
1.700	31.233	31.233	31.700	36.250	40.167	43.300	43.833	43.400	43.140	43.053

TABLE VII.- FORWARD VELOCITY INDEX $m(\theta)$

θ, deg	$m(\theta)$
0.000	3.000
10.000	1.650
20.000	1.100
30.000	.500
40.000	.200
50.000	0.000
60.000	0.000
70.000	.100
80.000	.400
90.000	1.000
100.000	1.900
110.000	3.000
120.000	4.700
130.000	7.000
140.000	8.500
150.000	8.500
160.000	8.500
170.000	8.500
180.000	8.500

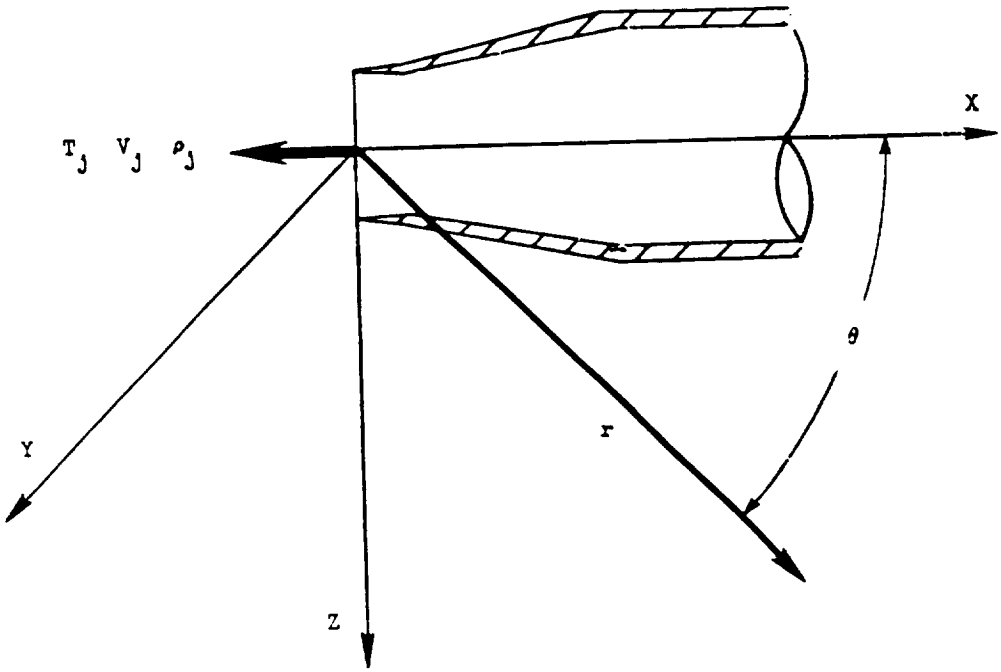

Figure 1.- Schematic diagram of single stream circular nozzle.

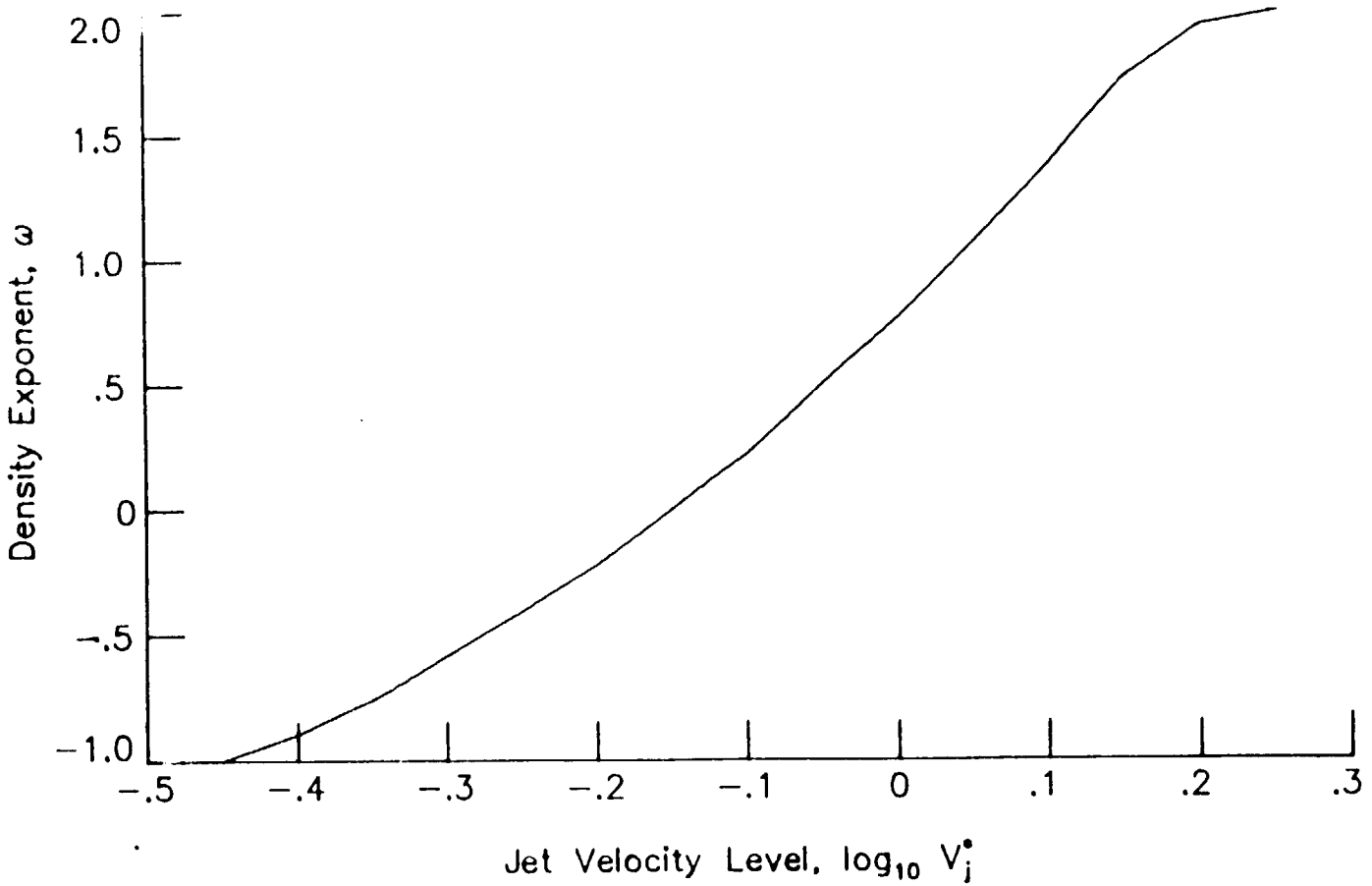

Figure 2.- Density exponent.

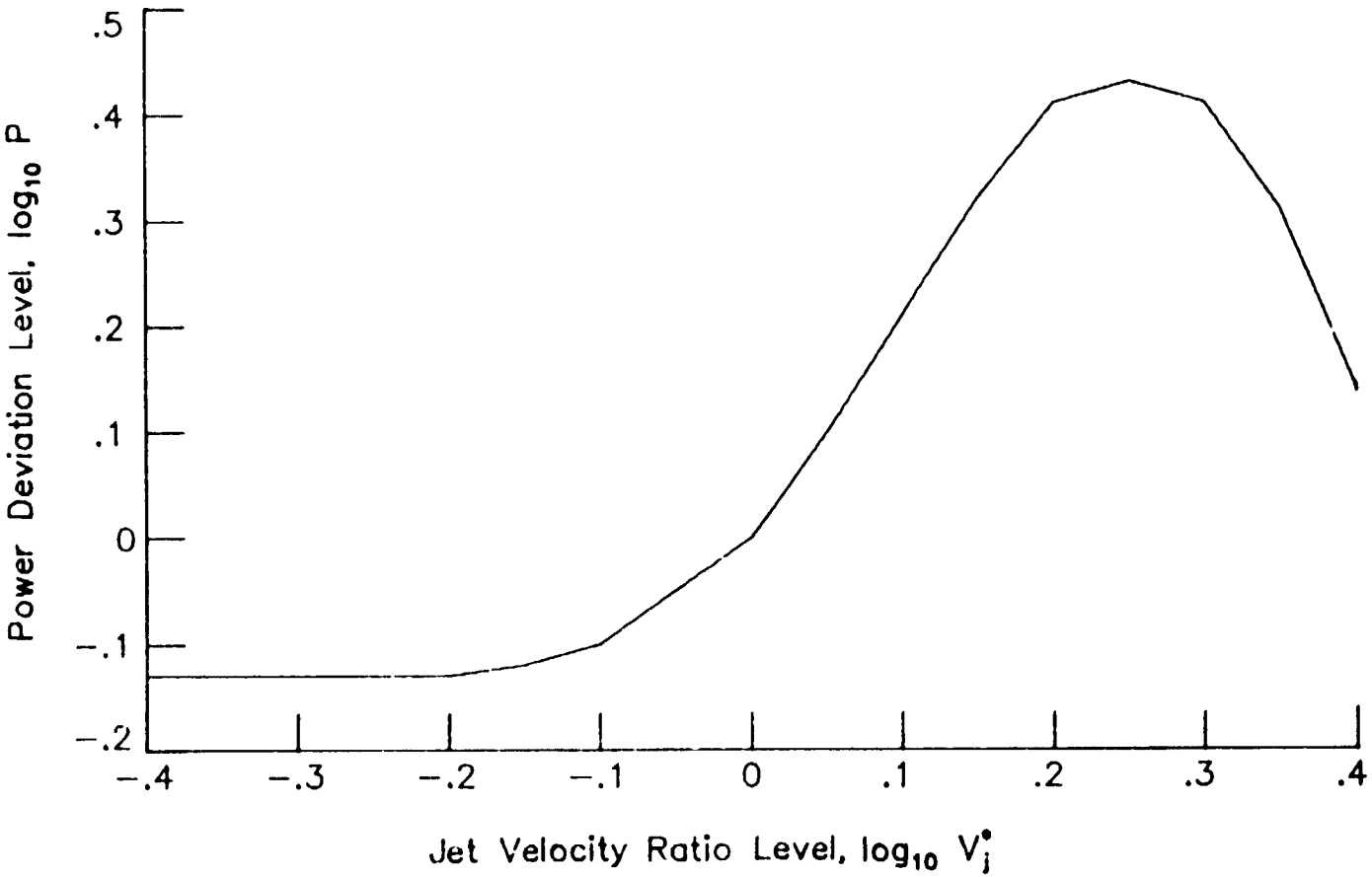

Figure 3.- Power deviation level.

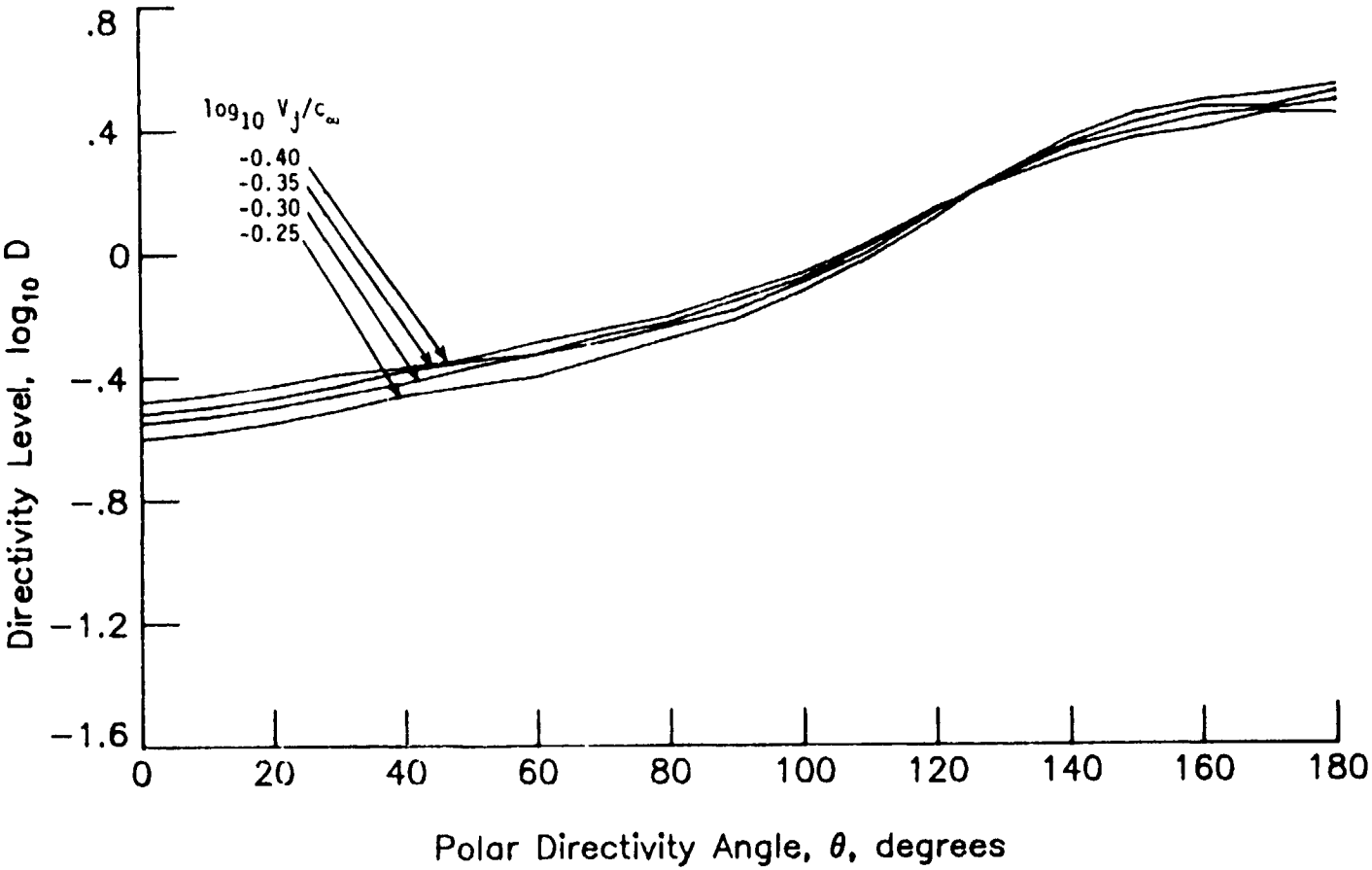

Figure 4.- Normalized polar directivity level.

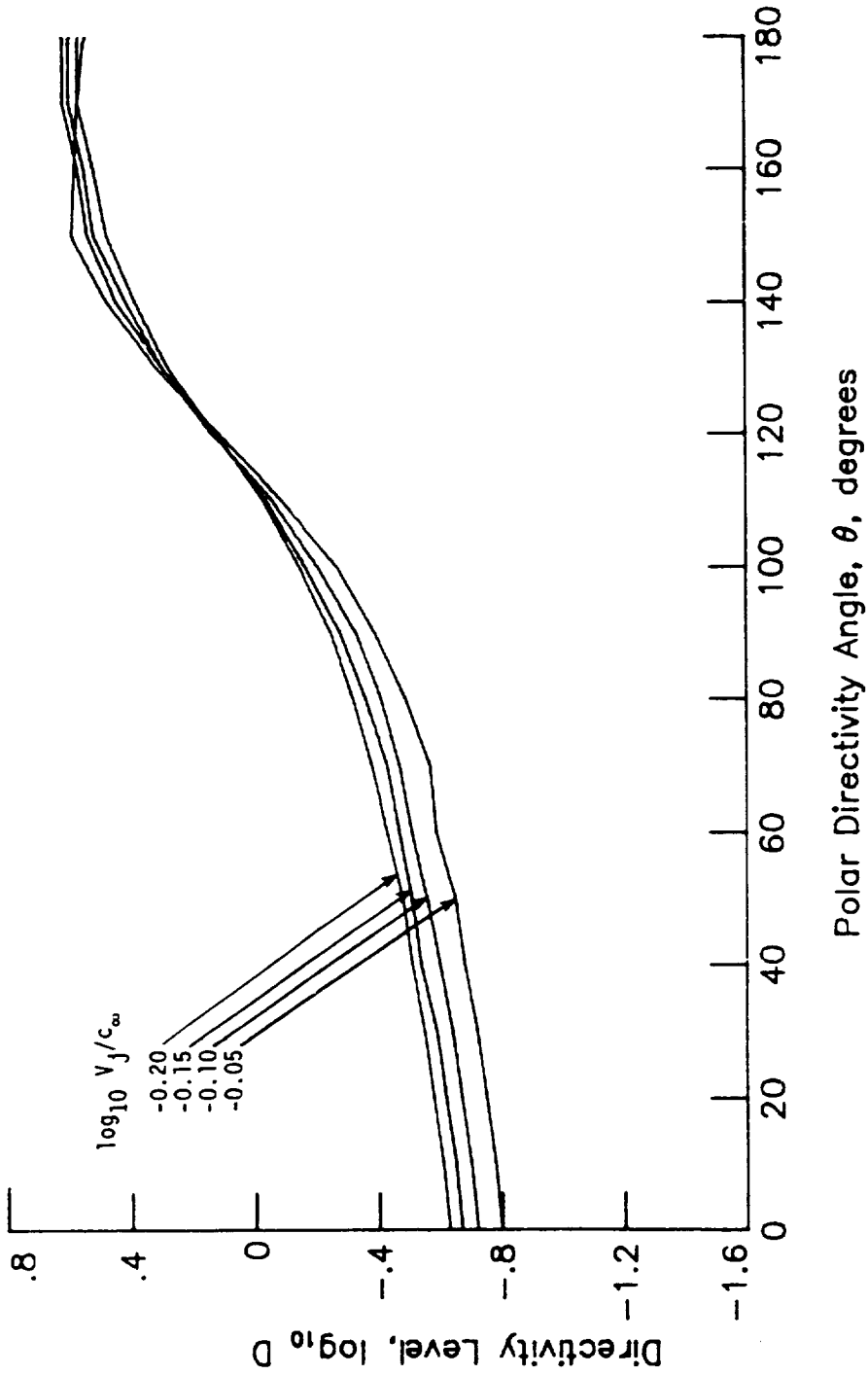

Figure 4.- Continued.

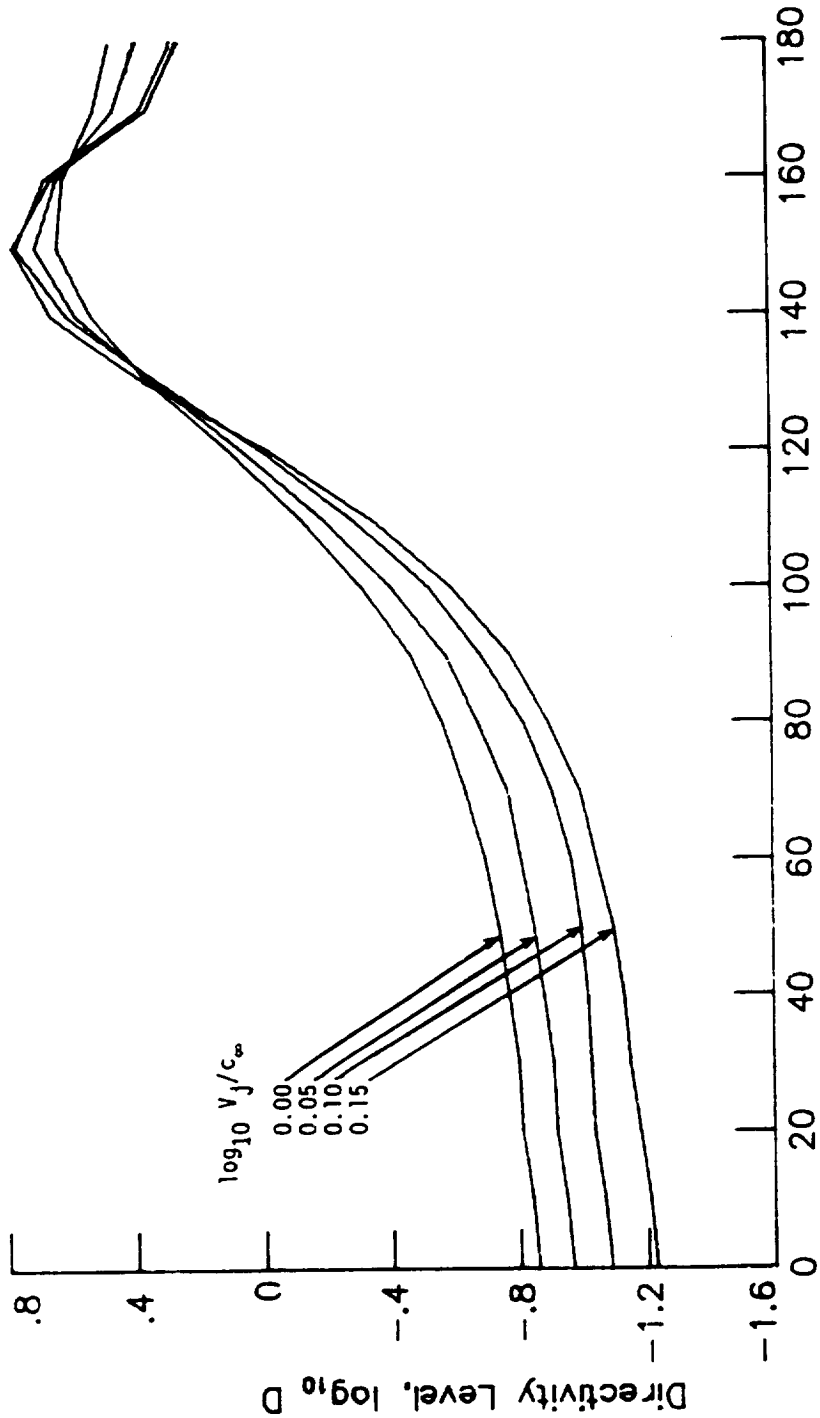

Figure 4.- Continued.

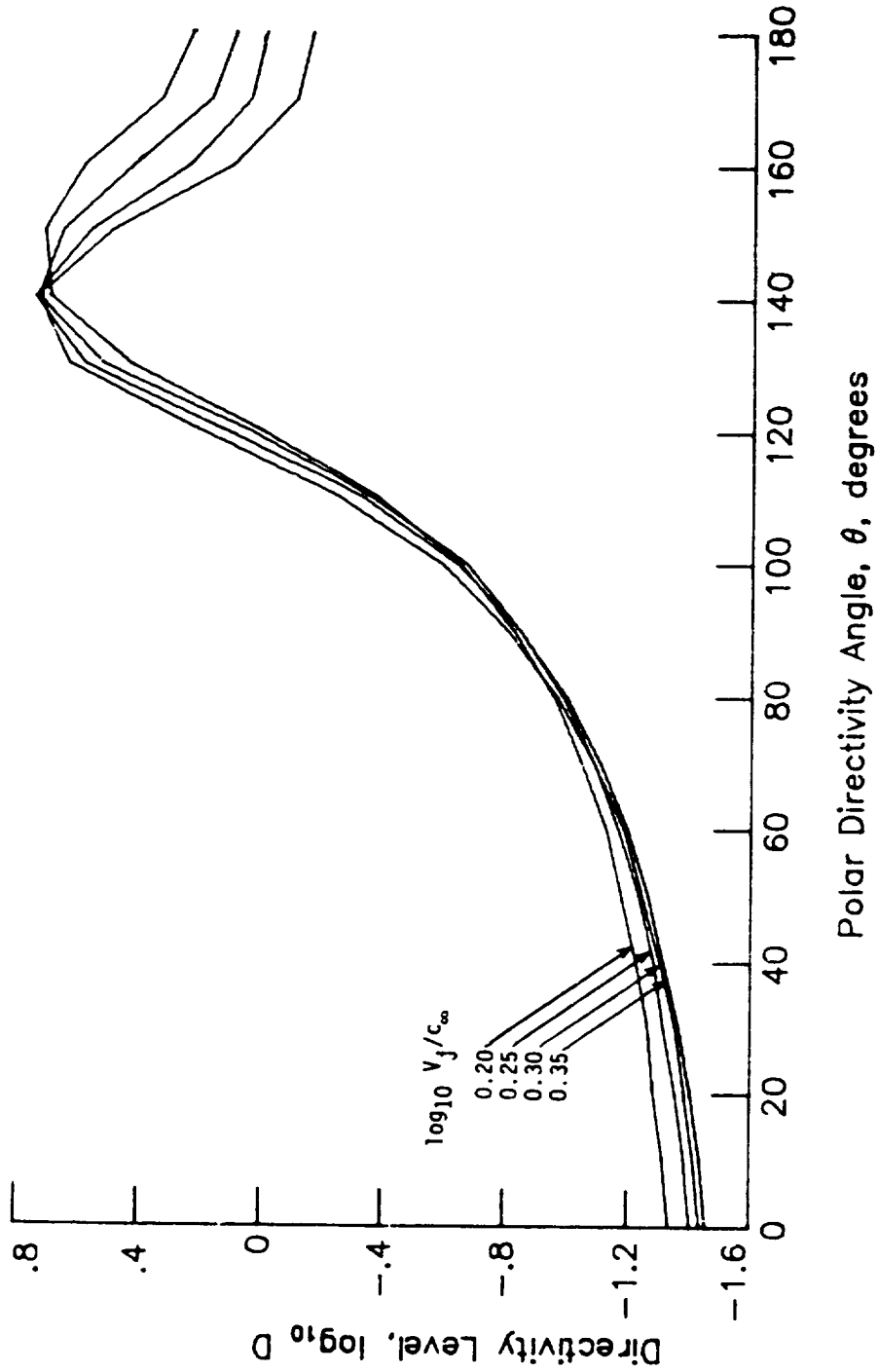

Figure 4.- Continued.

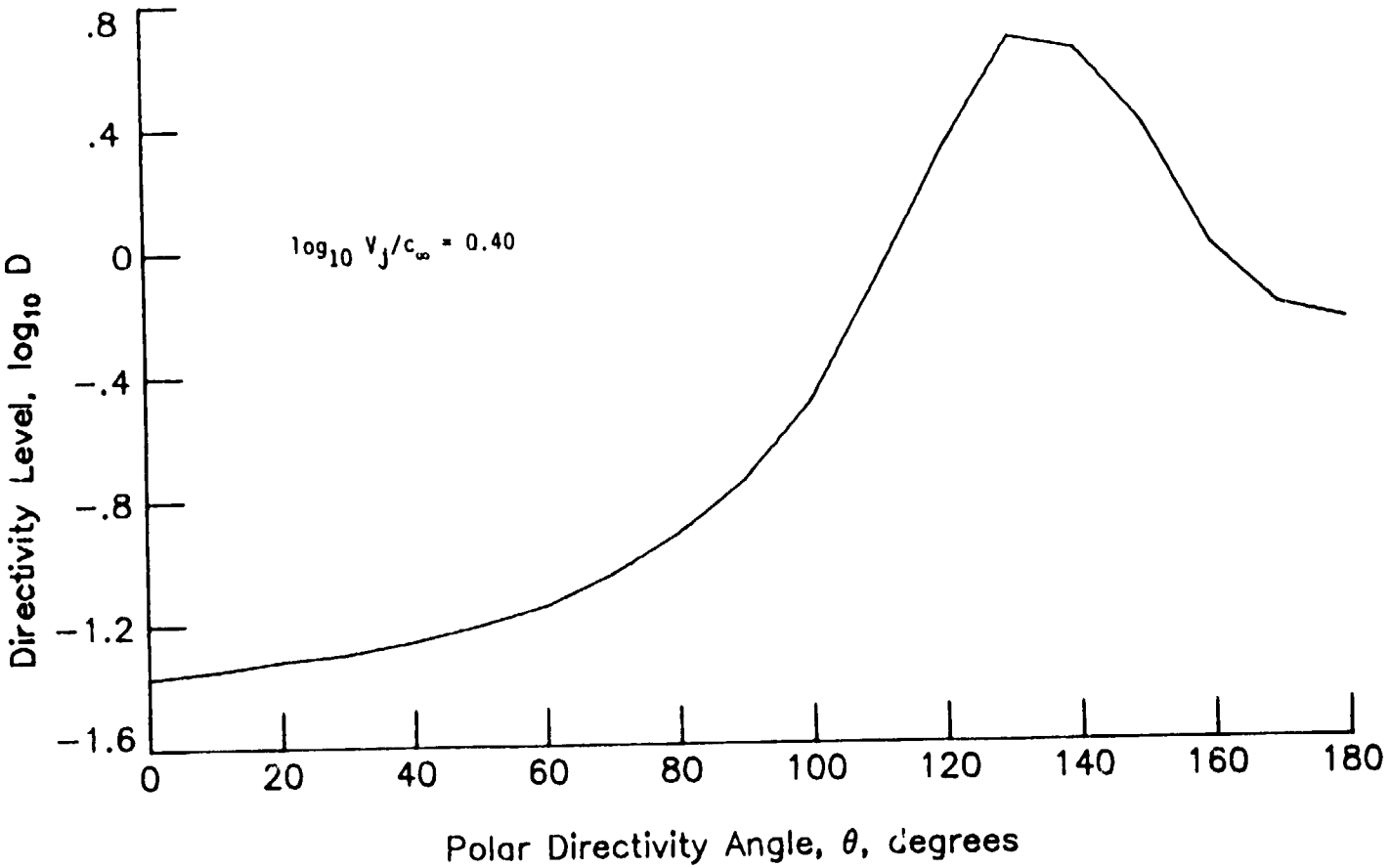

Figure 4.- Concluded.

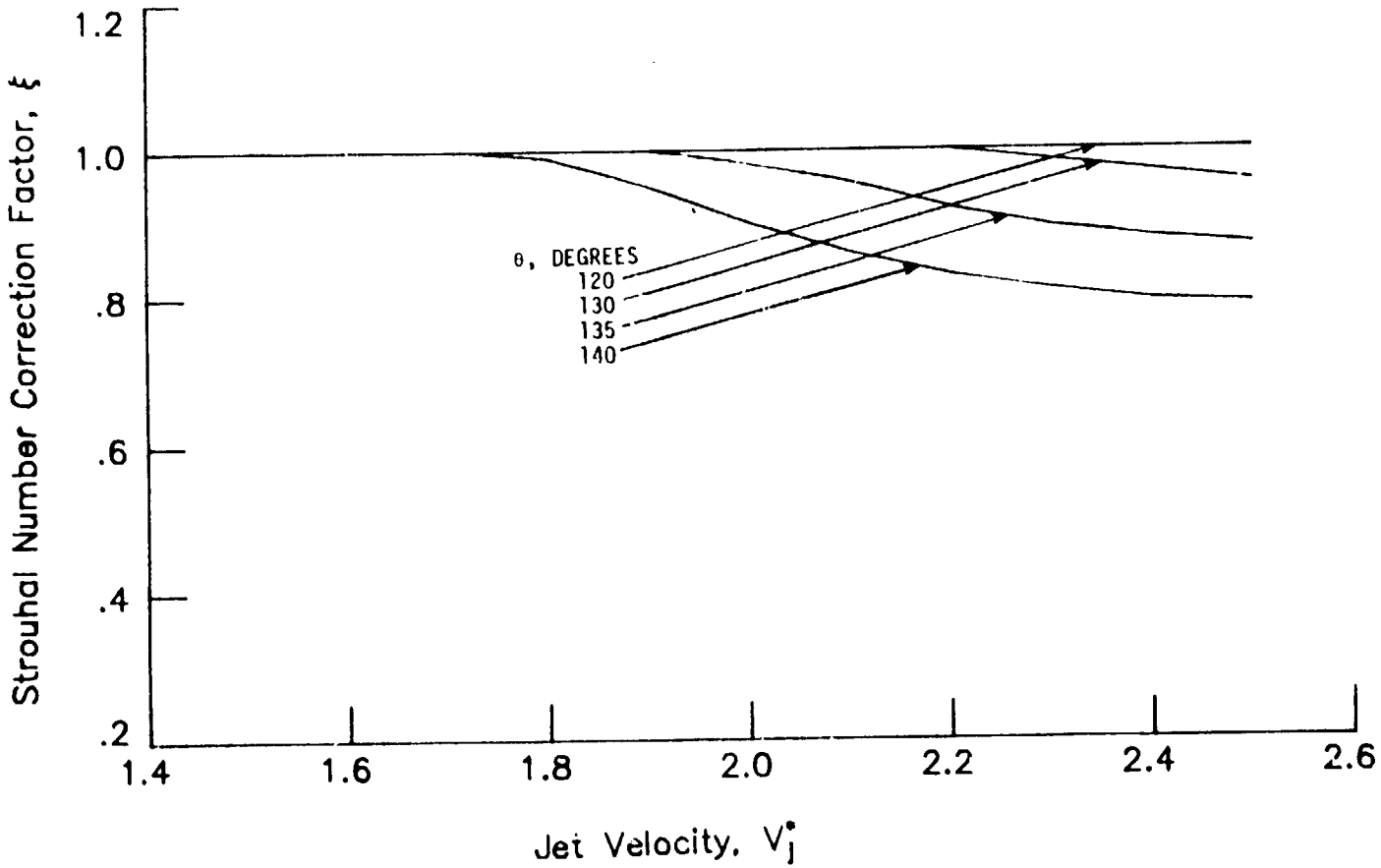

Figure 5.- Strouhal number correction factor.

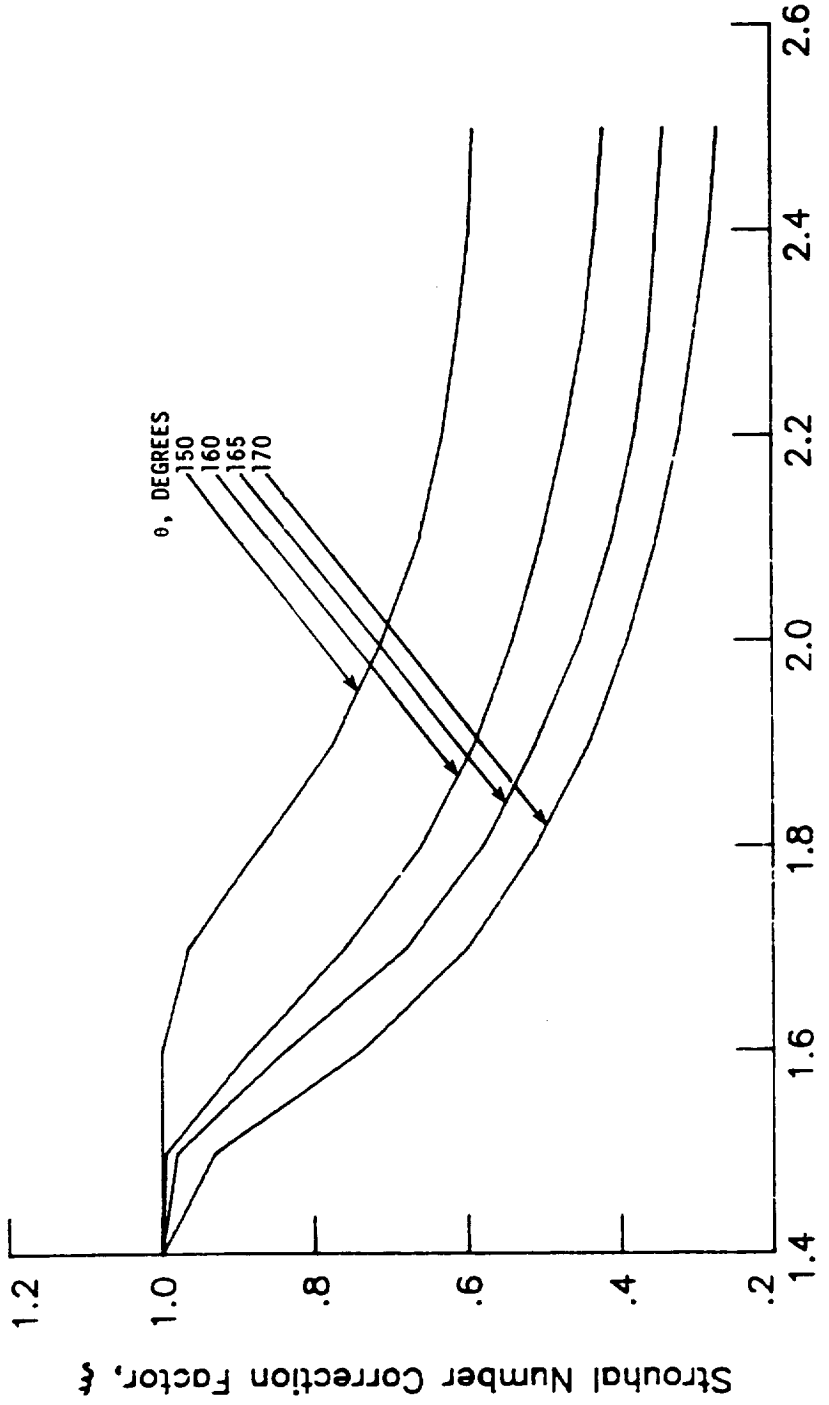

Figure 5.- Concluded.

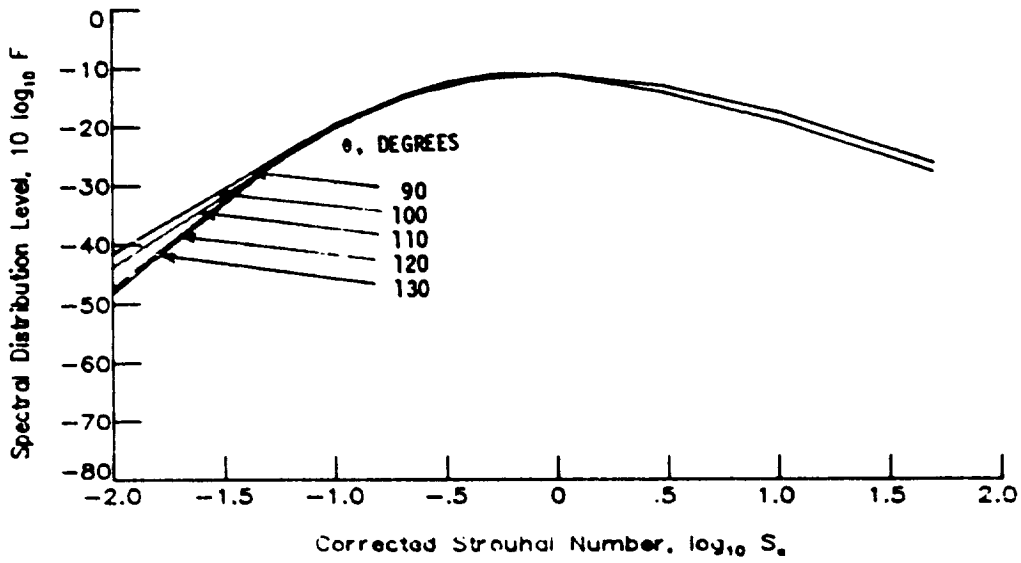

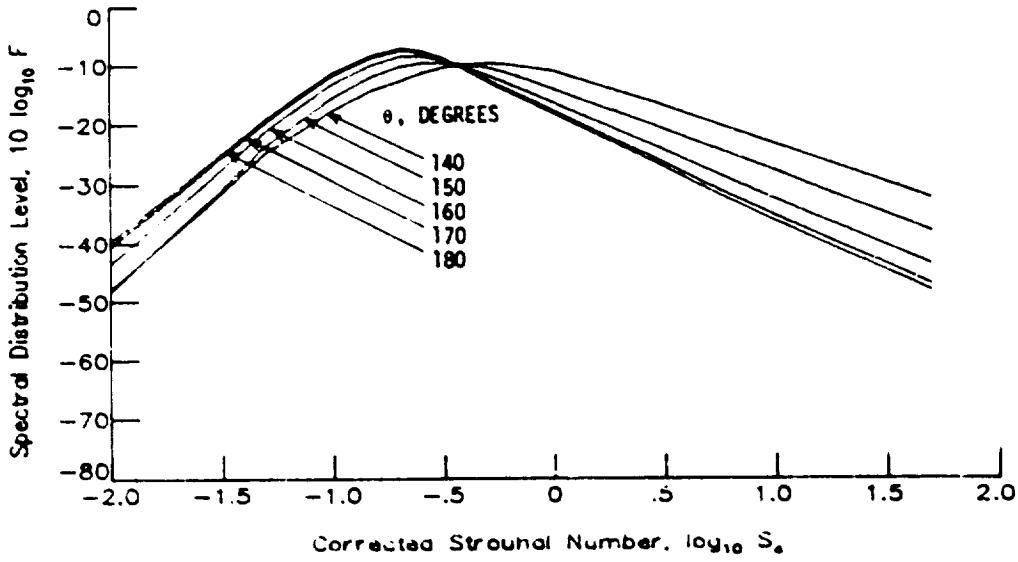

(a) $T_j/T_\infty = 1.0$; $\log_{10} V_j/c_\infty = 0.100$.

Figure 6.- Normalized spectral distribution level.

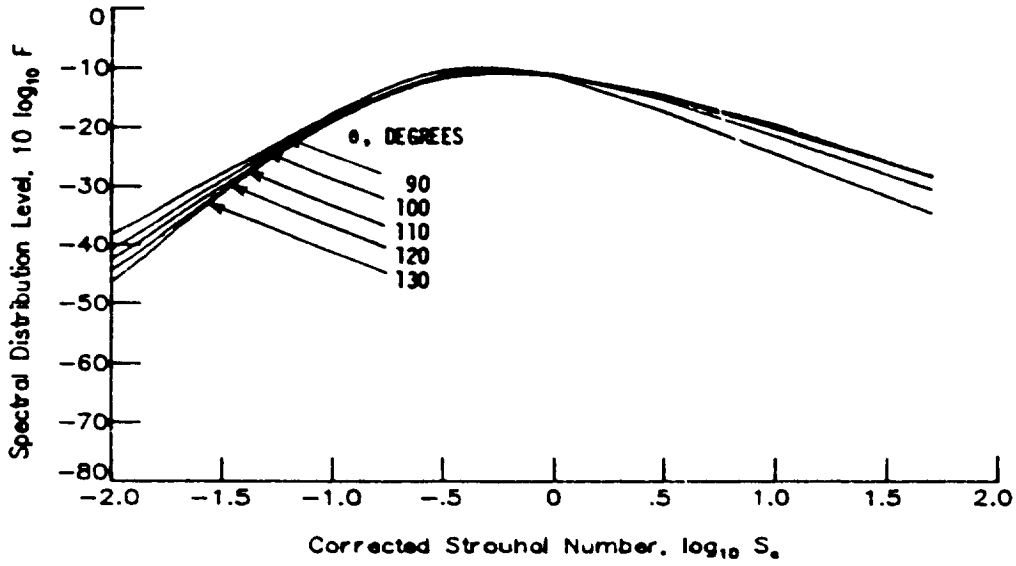

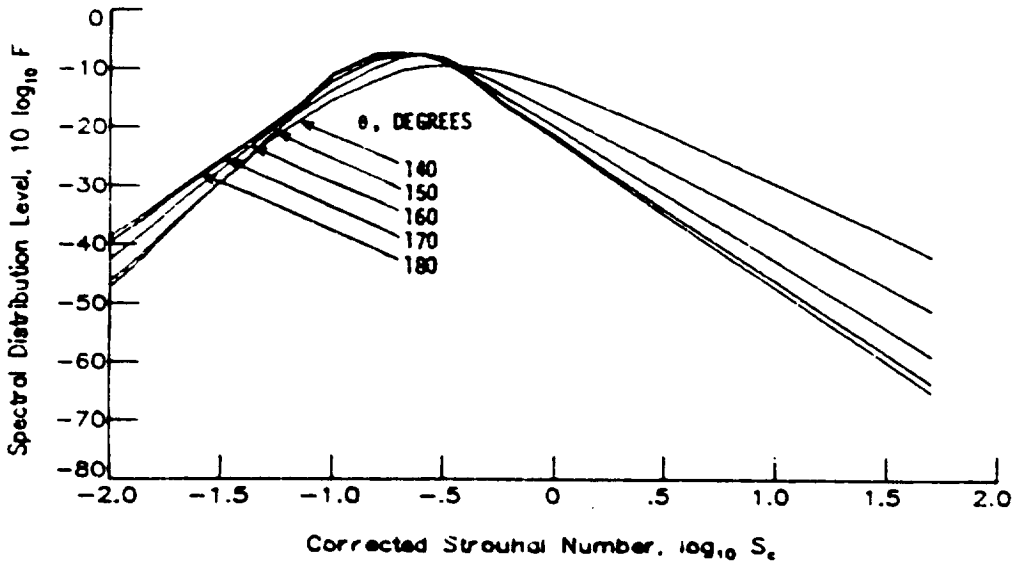

(b) $T_j/T_\infty = 2.0$; $\log_{10} V_j/c_\infty = 0.100$.

Figure 6.- Continued.

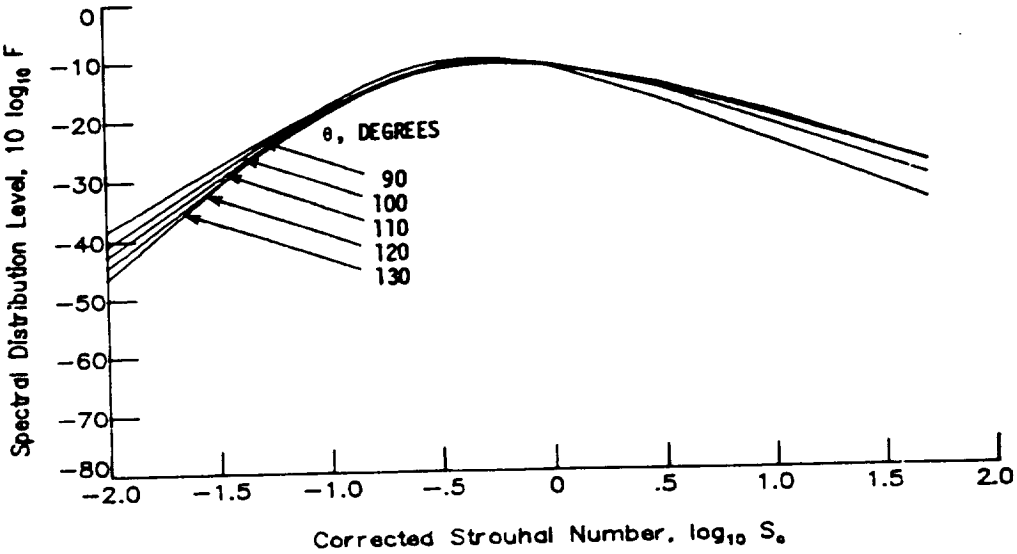

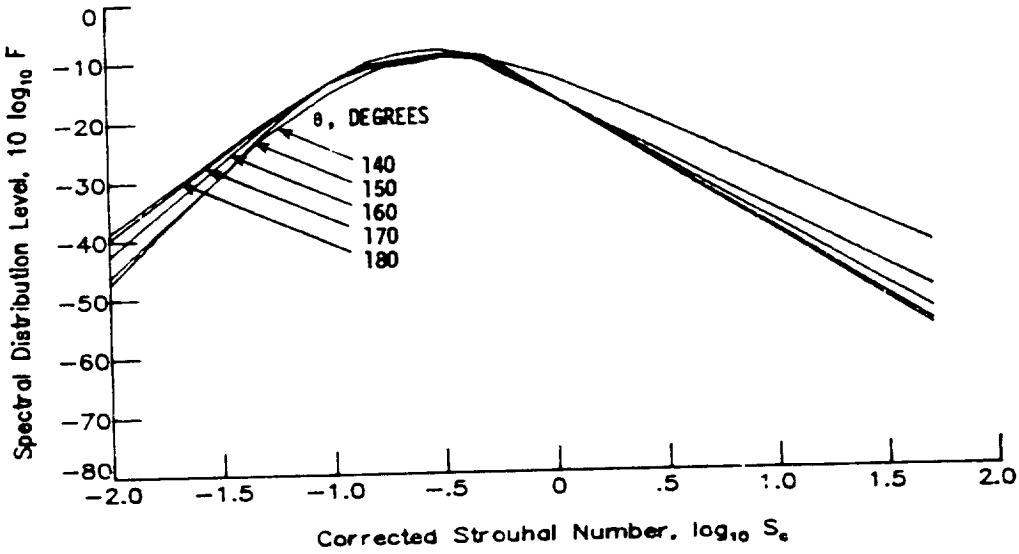

(c) $T_j/T_\infty = 2.0$; $\log_{10} V_j/c_\infty = 0.125$.

Figure 6.- Continued.

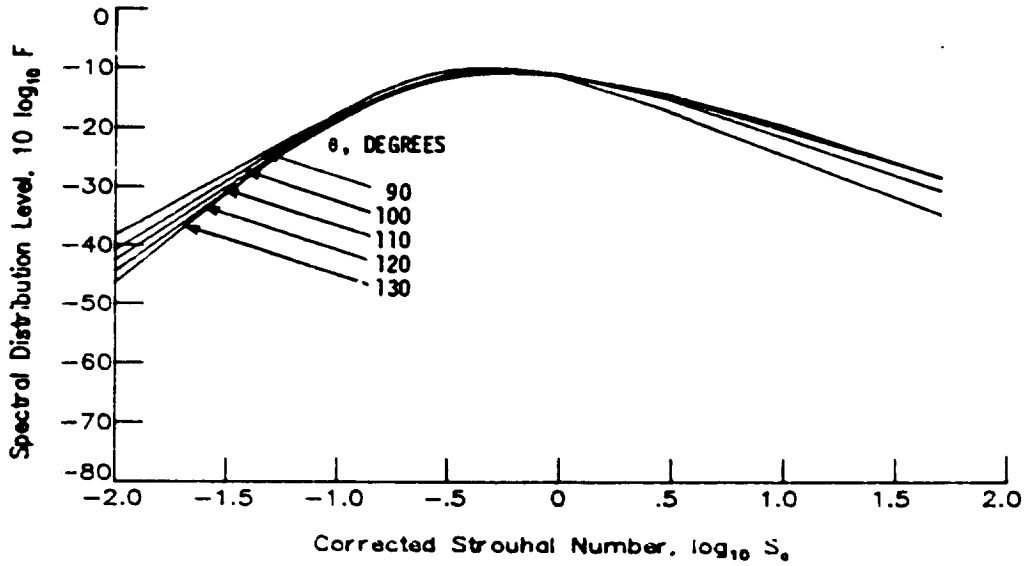

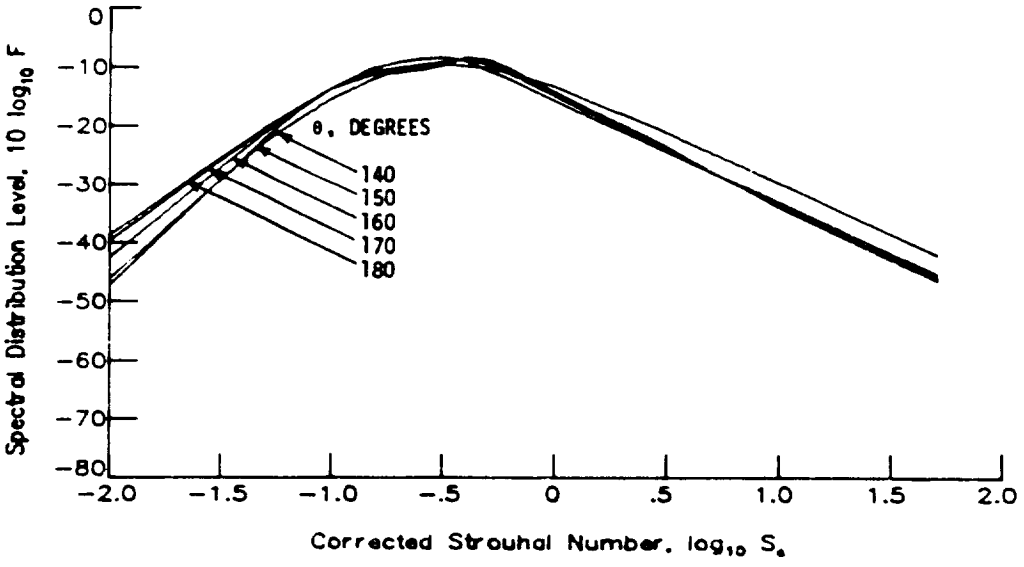

(d) $T_j/T_\infty = 2.0$; $\log_{10} V_j/c_\infty = 0.150$.

Figure 6.- Continued.

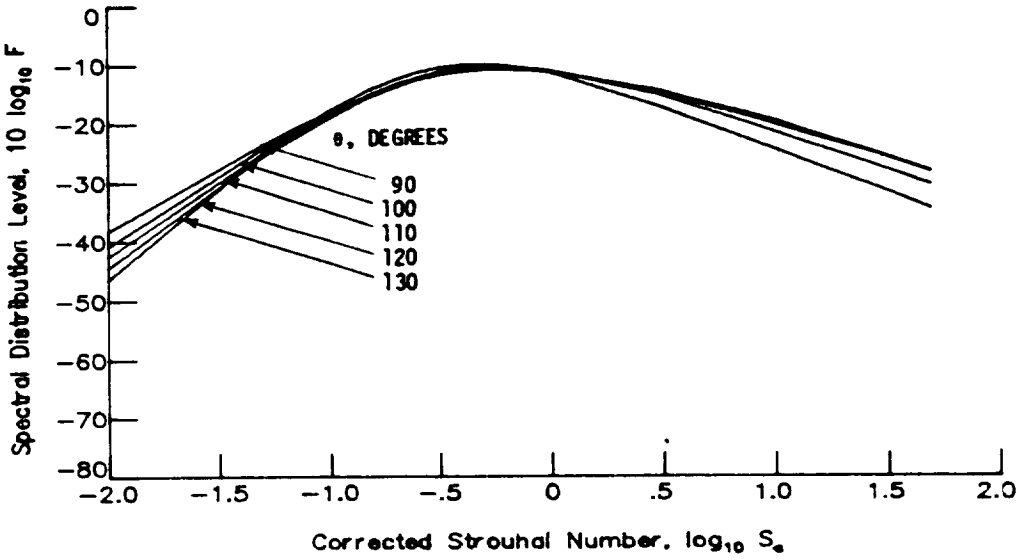

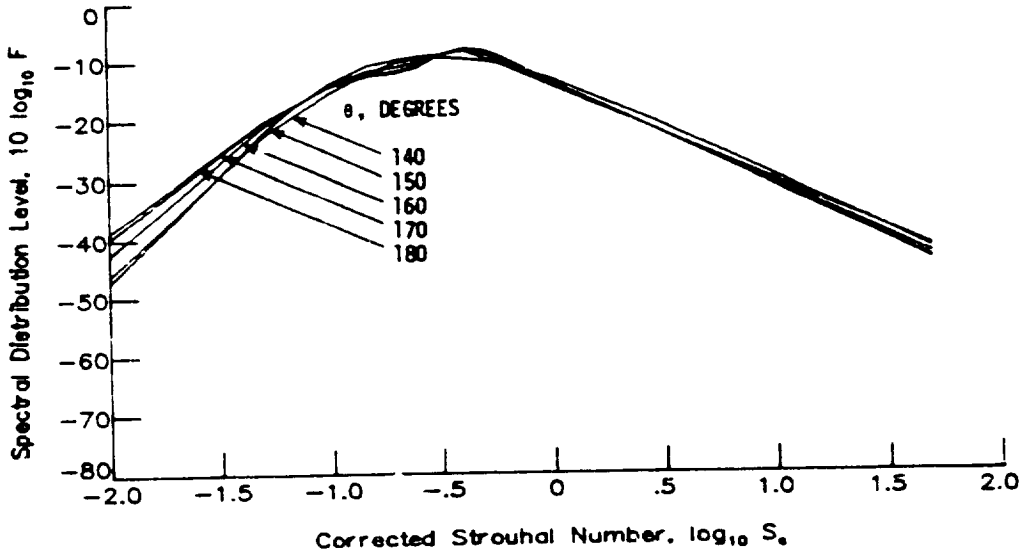

(e) $T_j/T_\infty = 2.0$; $\log_{10} V_j/c_\infty = 0.175$.

Figure 6.- Continued.

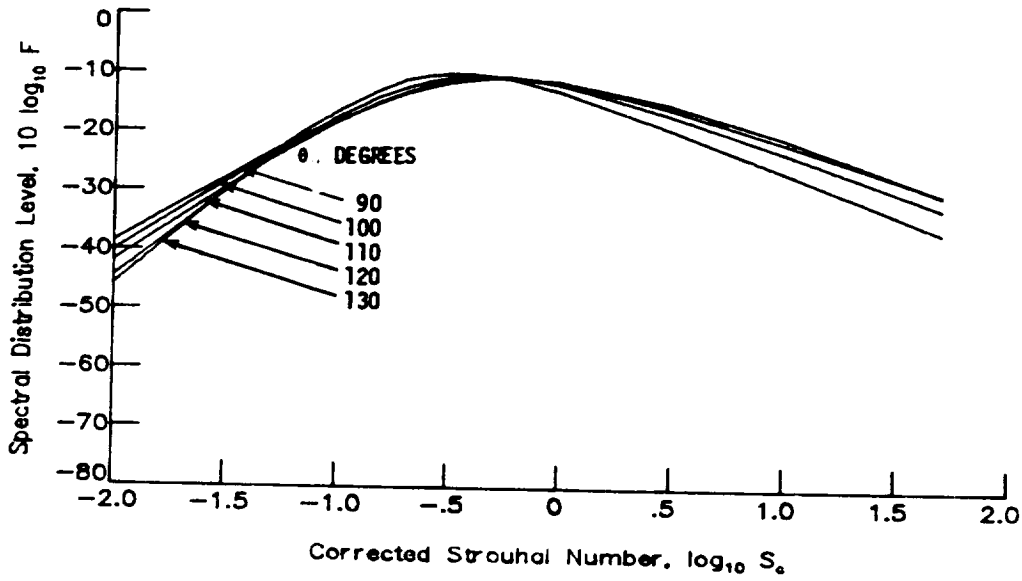

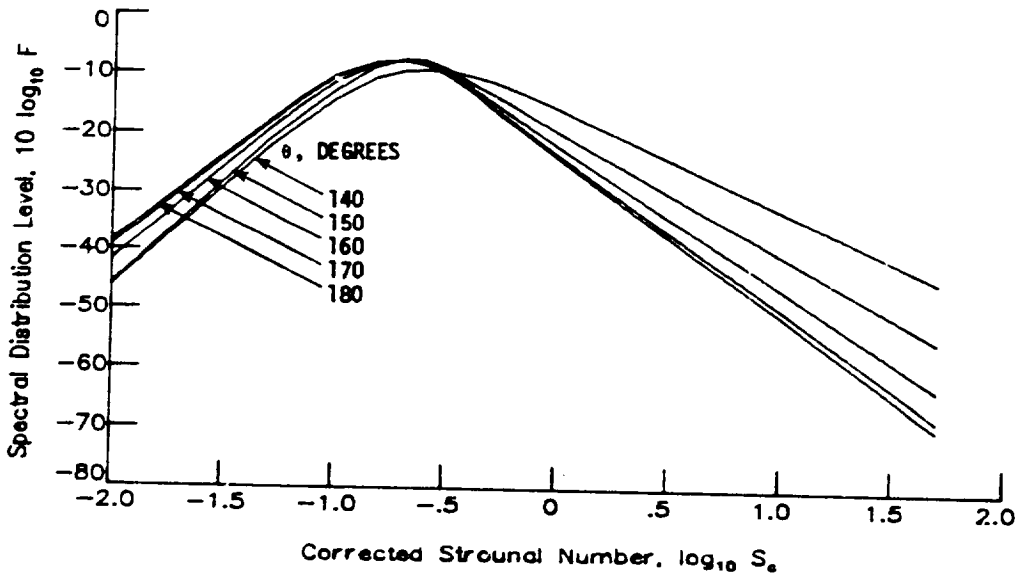

(f) $T_j/T_\infty = 2.5$; $\log_{10} V_j/c_\infty = 0.100$.

Figure 6.- Continued.

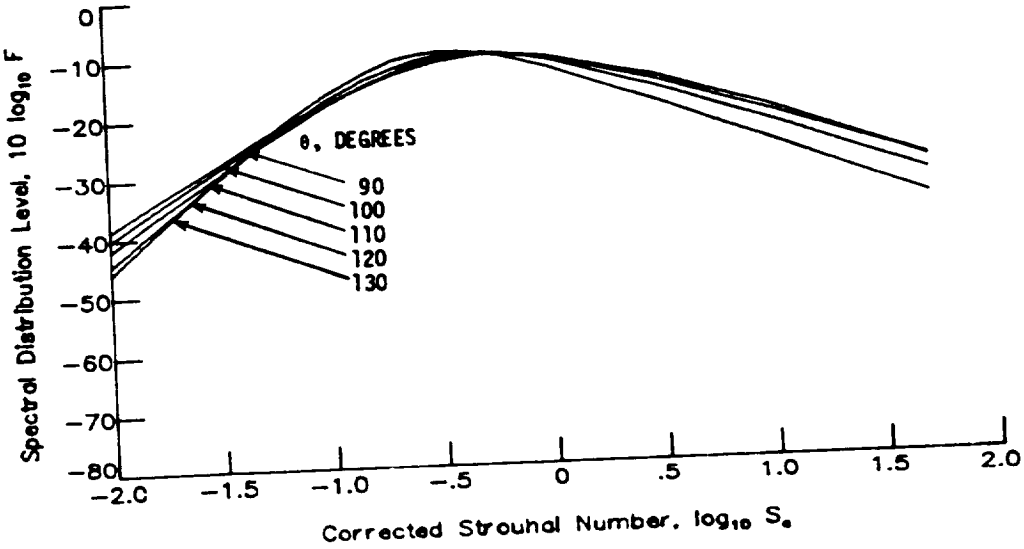

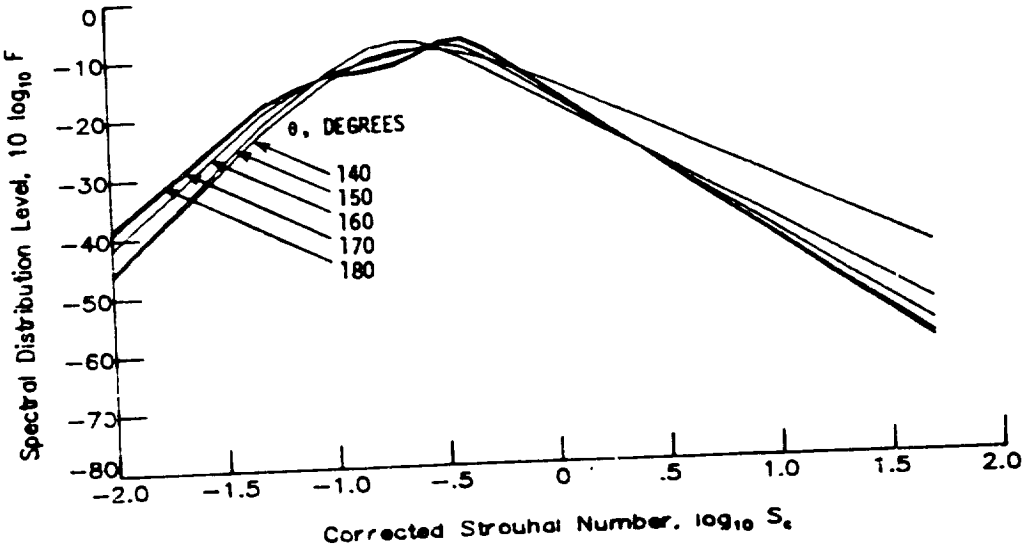

(g) $T_j/T_\infty = 2.5$; $\log_{10} V_j/c_\infty = 0.125$.

Figure 6.- Continued.

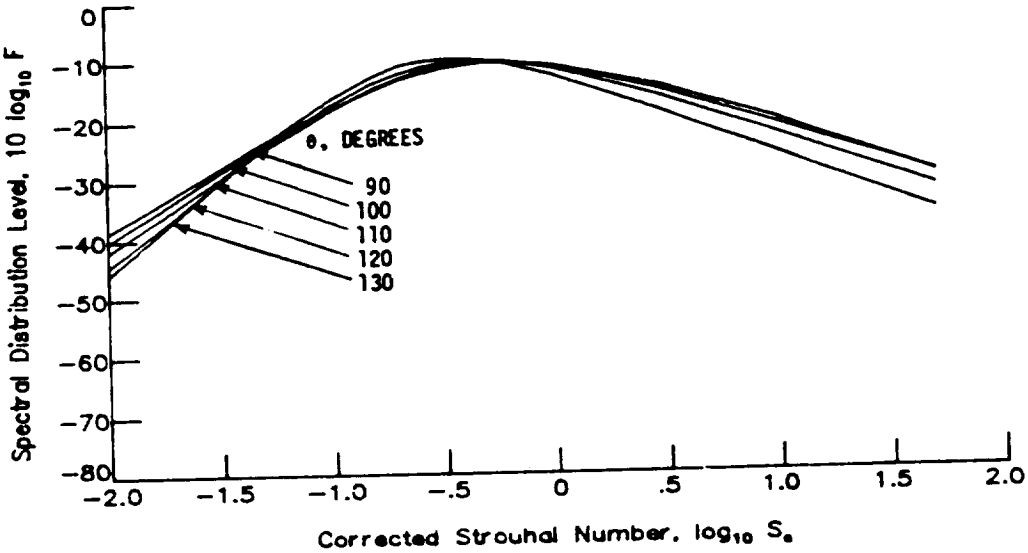

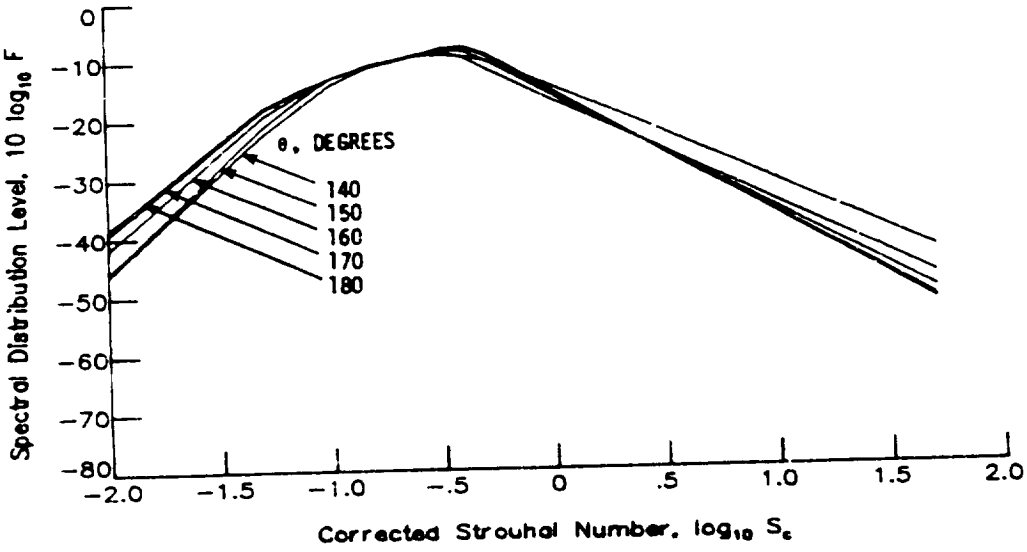

(h) $T_j/T_\infty = 2.5$; $\log_{10} V_j/c_\infty = 0.150$.

Figure 6.- Continued.

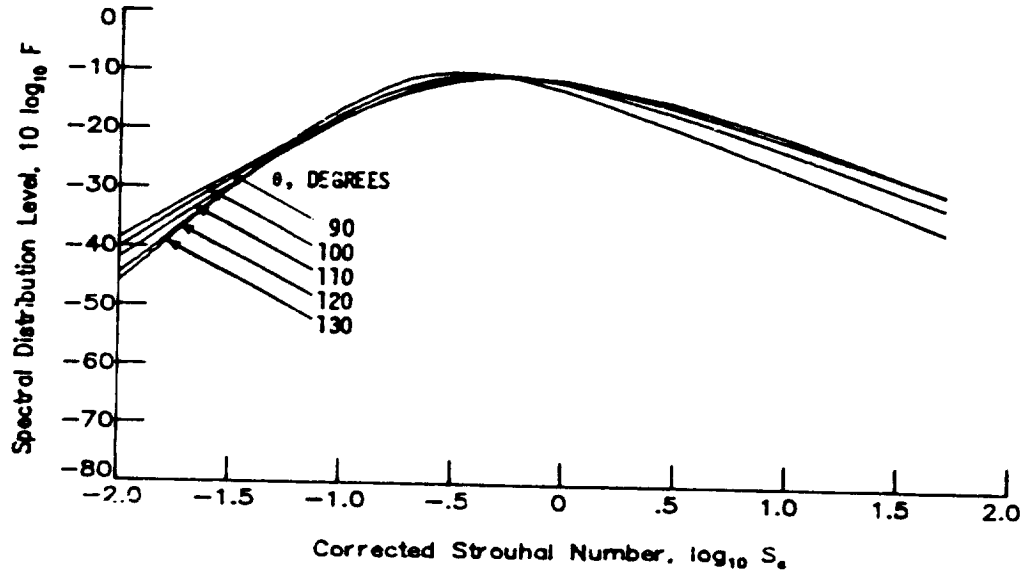

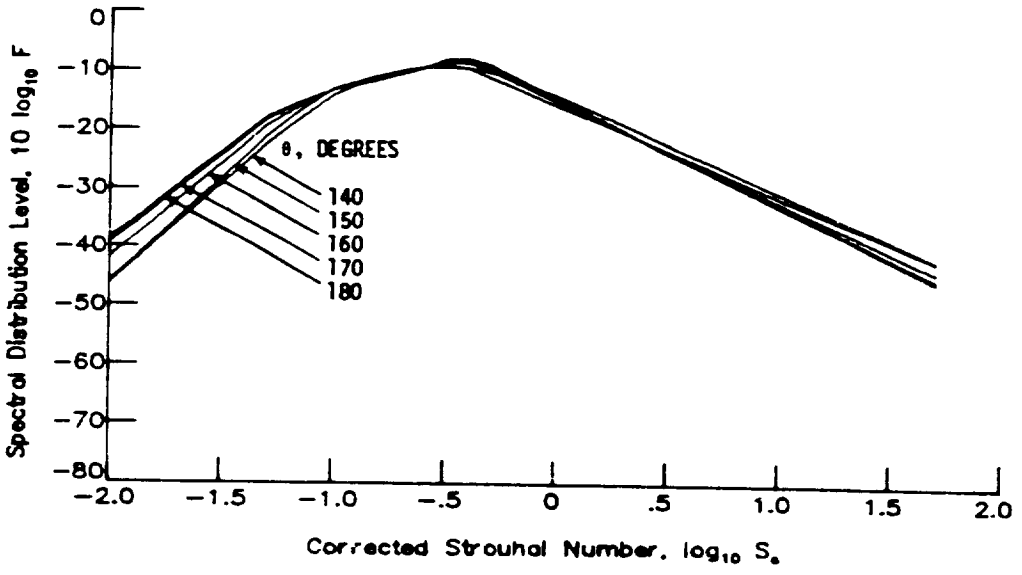

(i) $T_j/T_\infty = 2.5$; $\log_{10} V_j/c_\infty = 0.175$.

Figure 6.- Continued.

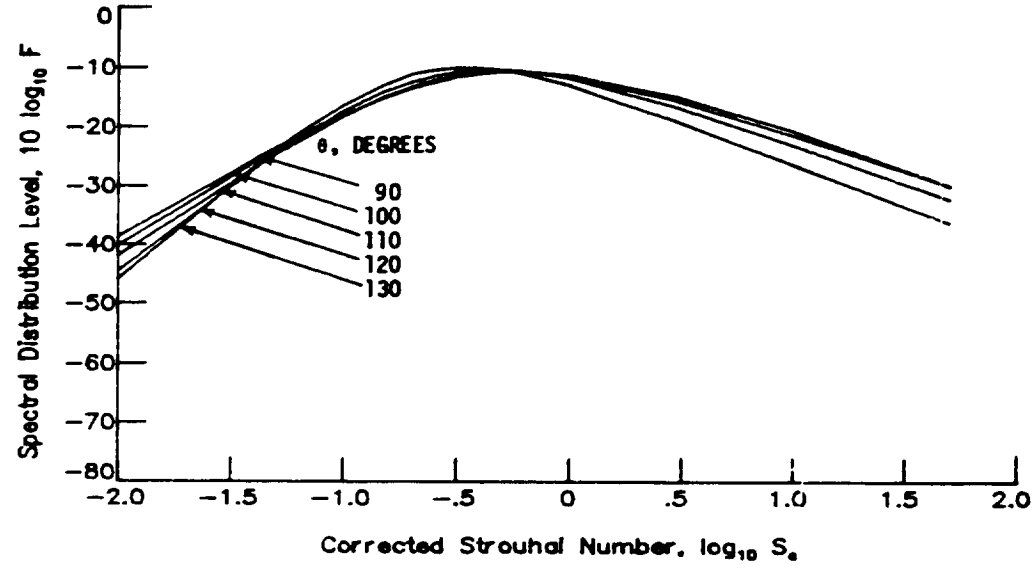

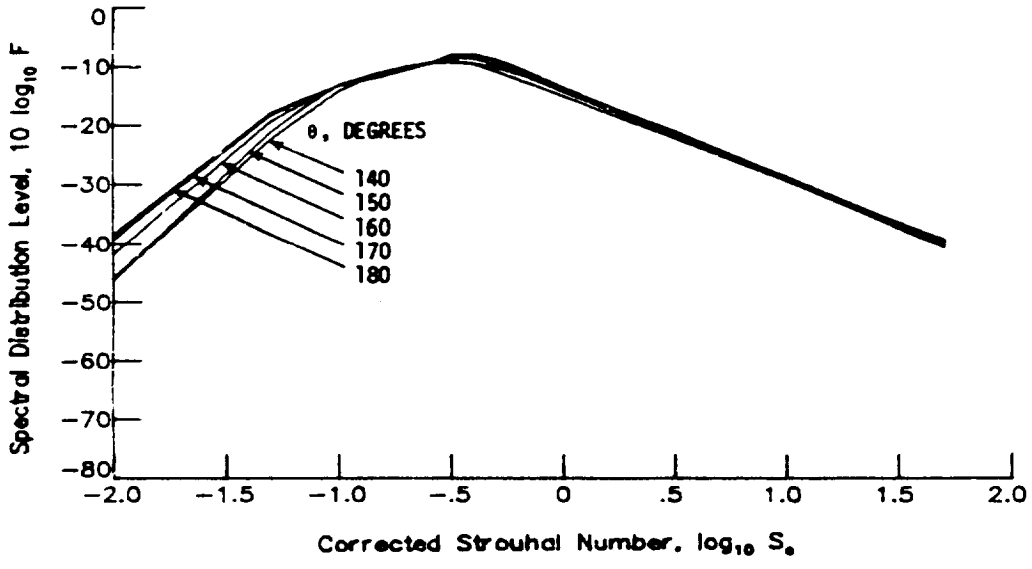

(j) $T_j/T_\infty = 2.5$; $\log_{10} V_j/c_\infty = 0.200$.

Figure 6.- Continued.

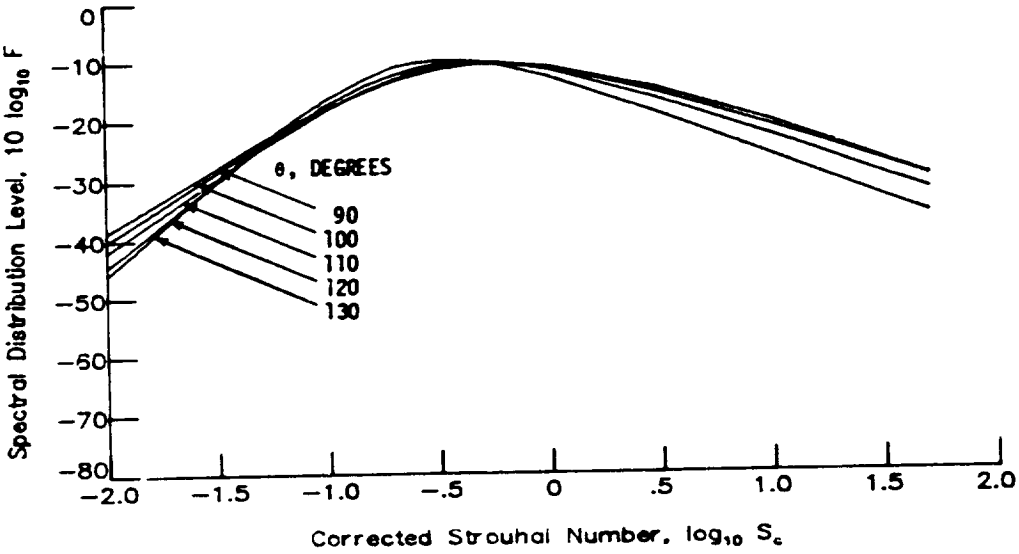

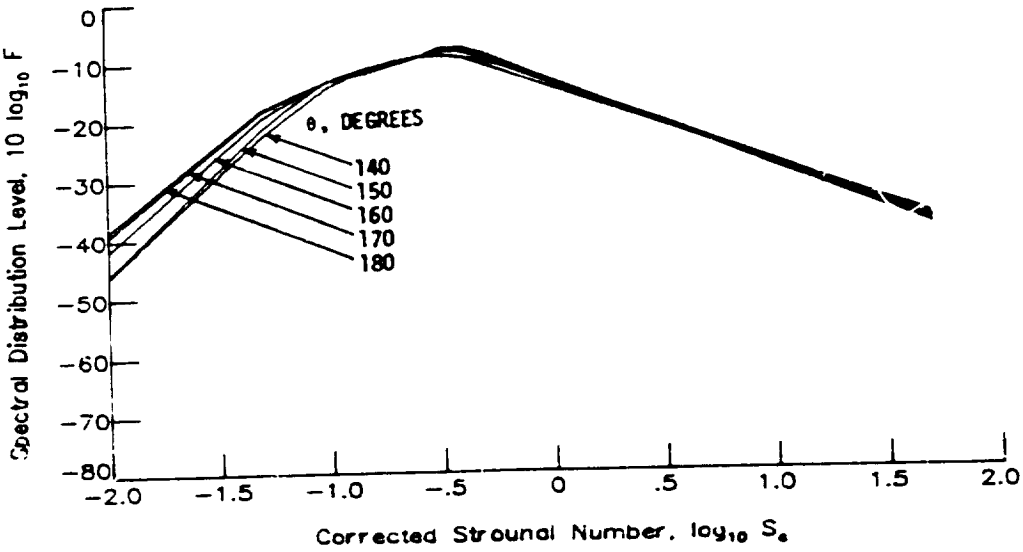

(k) $T_j/T_\infty = 2.5$; $\log_{10} V_j/c_\infty = 0.225$.

Figure 6.- Continued.

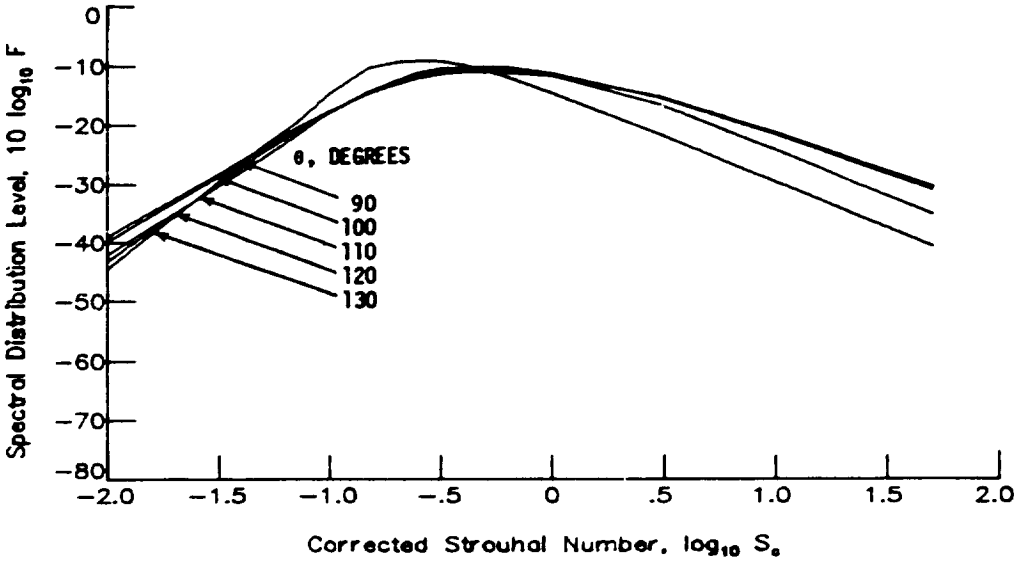

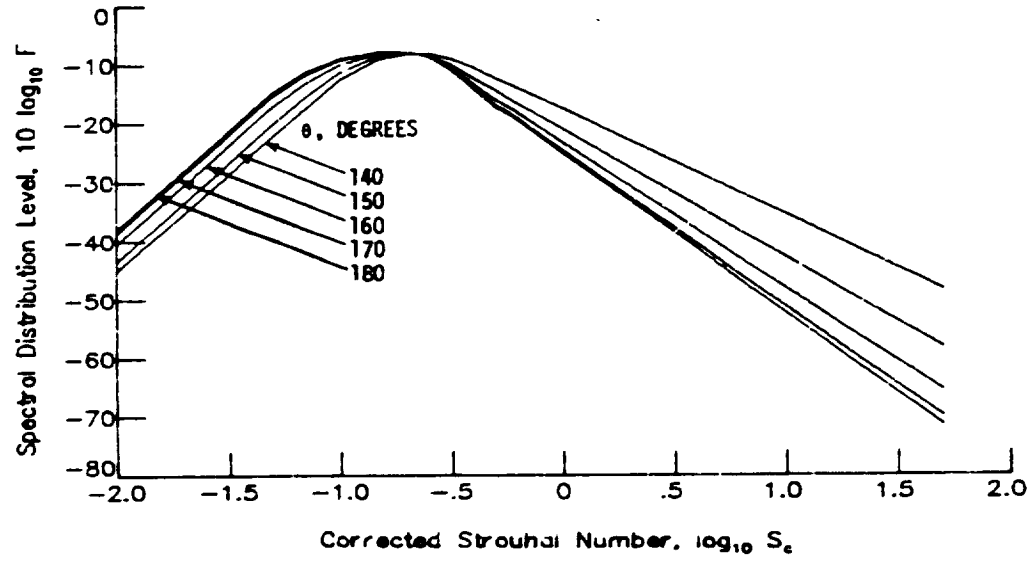

(l) $T_j/T_\infty = 3.0$; $\log_{10} V_j/c_\infty = 0.100$.

Figure 6.- Continued.

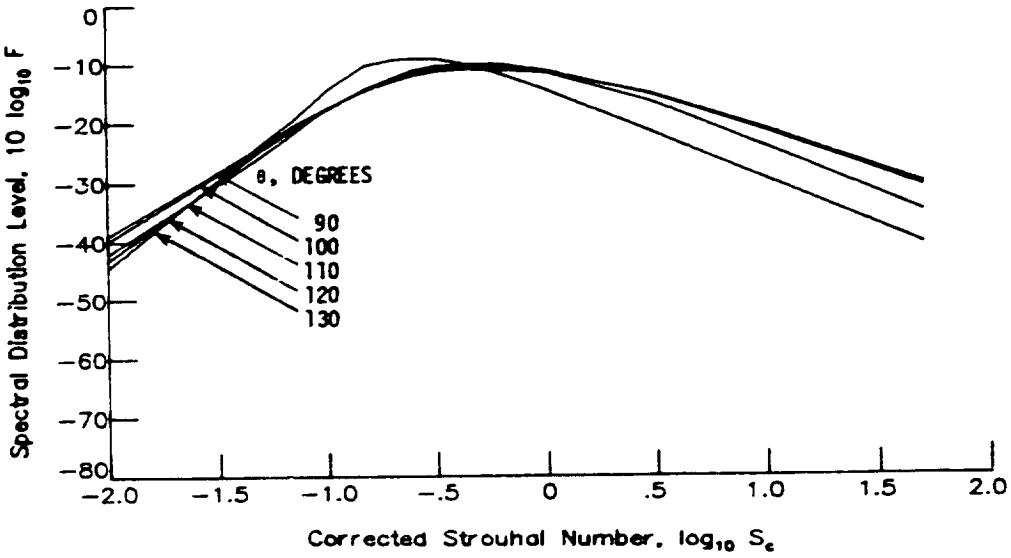

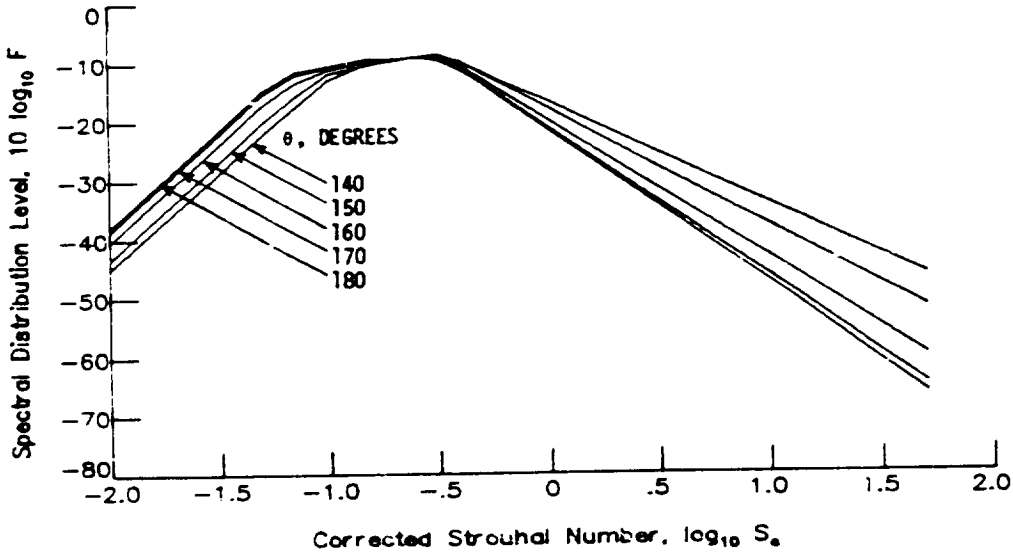

(m) $T_j/T_\infty = 3.0$; $\log_{10} V_j/c_\infty = 0.125$.

Figure 6.- Continued.

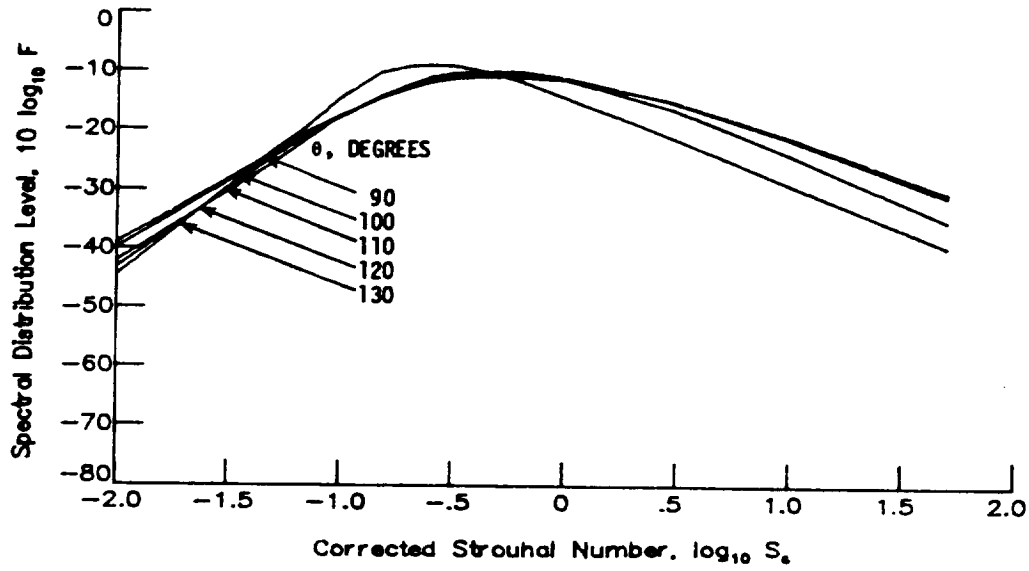

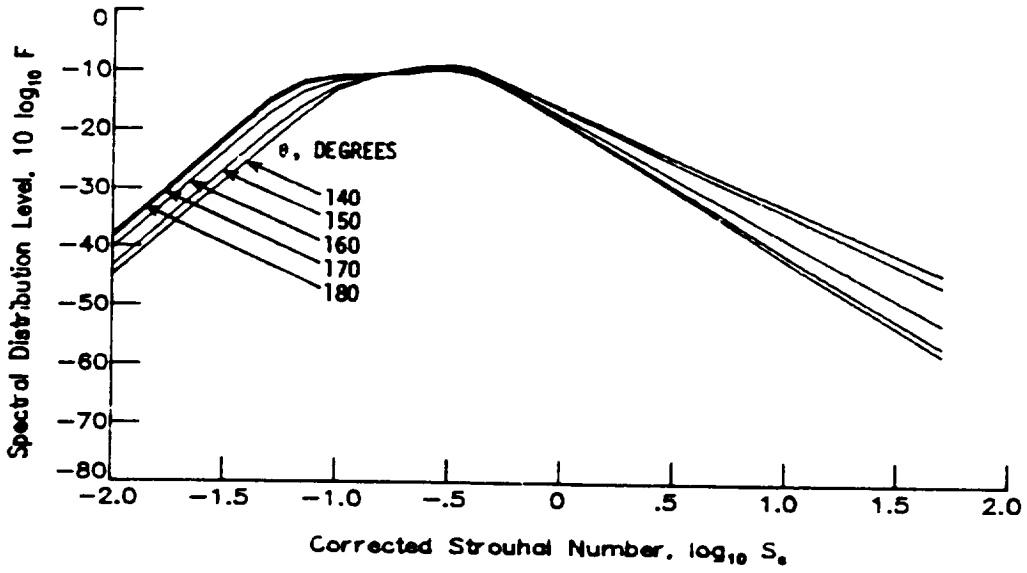

(n) $T_j/T_\infty = 3.0$; $\log_{10} V_j/c_\infty = 0.150$.

Figure 6.- Continued.

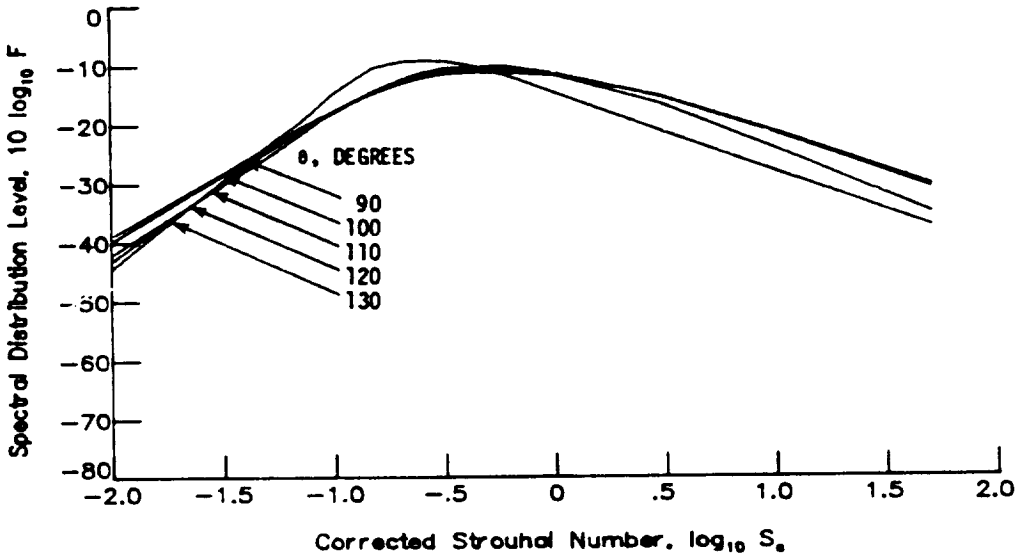

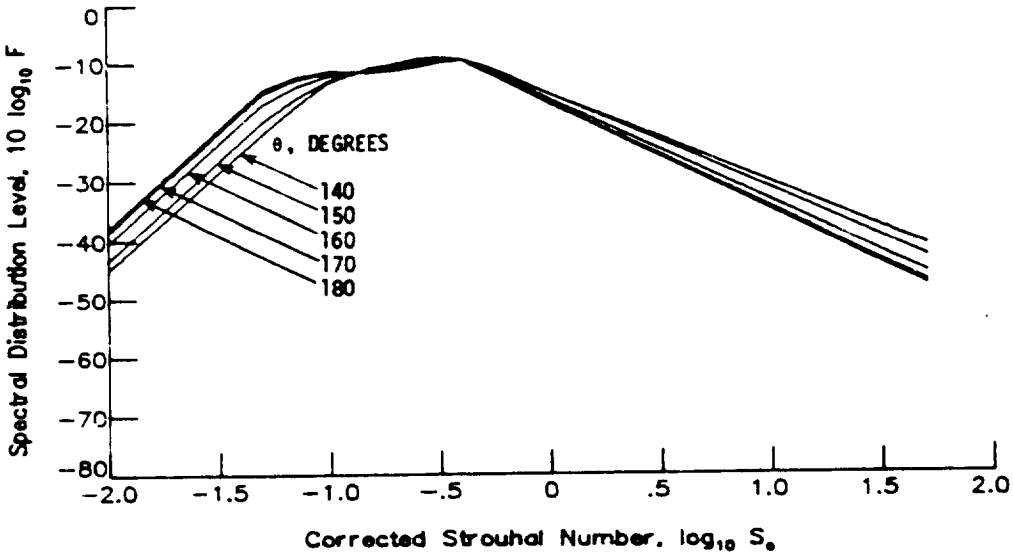

(o) $T_j/T_\infty = 3.0$; $\log_{10} V_j/c_\infty = 0.175$.

Figure 6.- Continued.

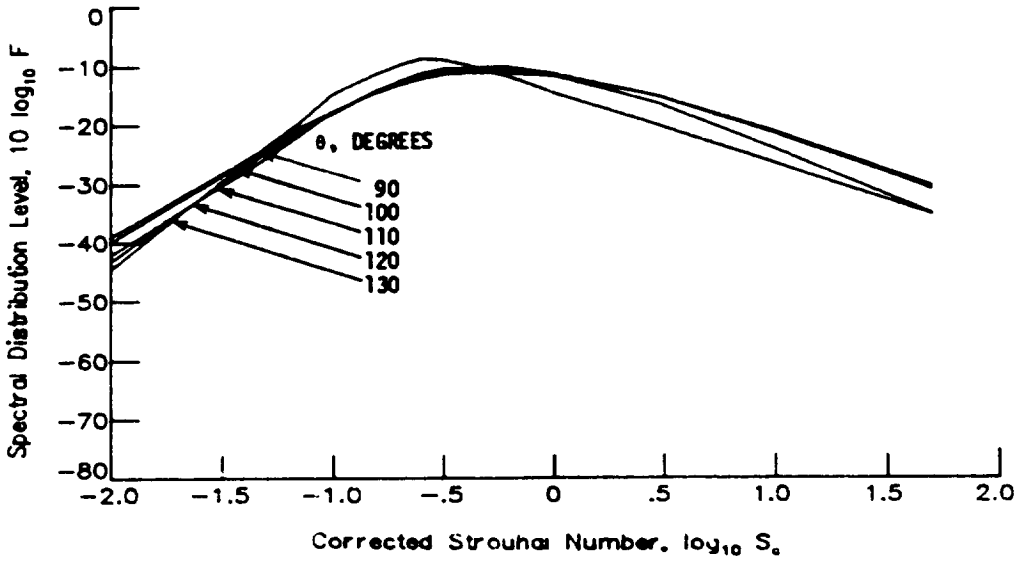

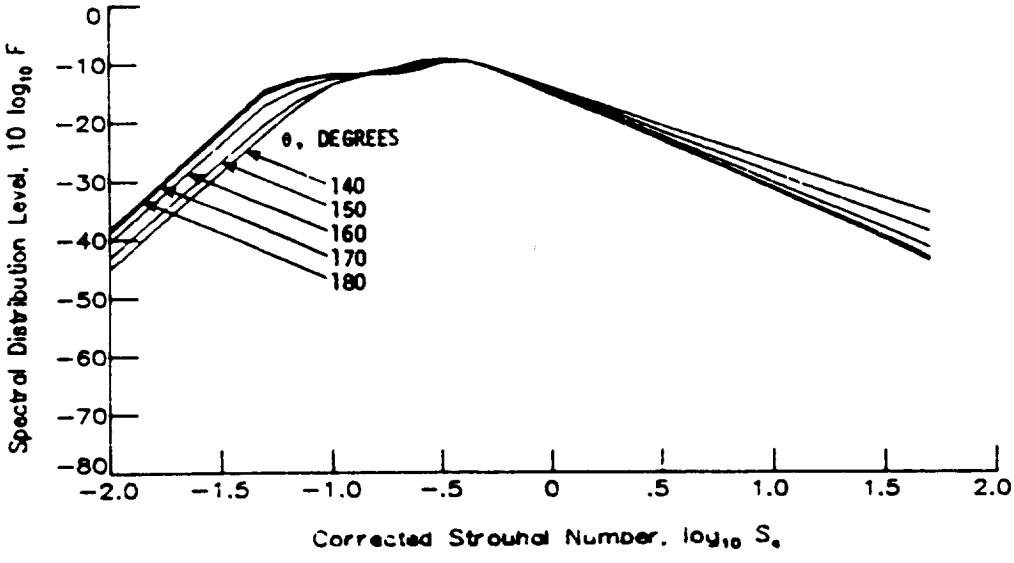

(p) $T_j/T_\infty = 3.0$; $\log_{10} V_j/c_\infty = 0.200$.

Figure 6.- Continued.

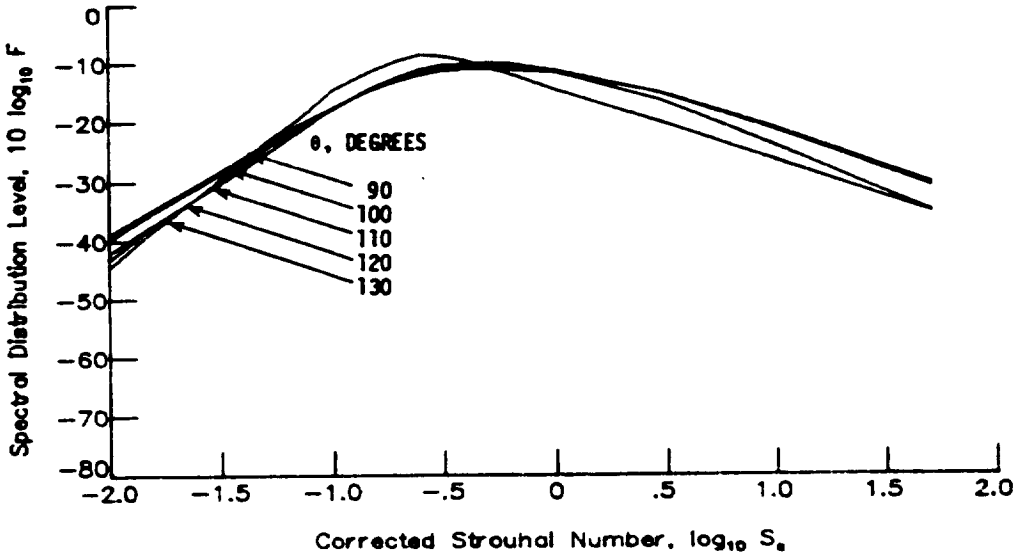

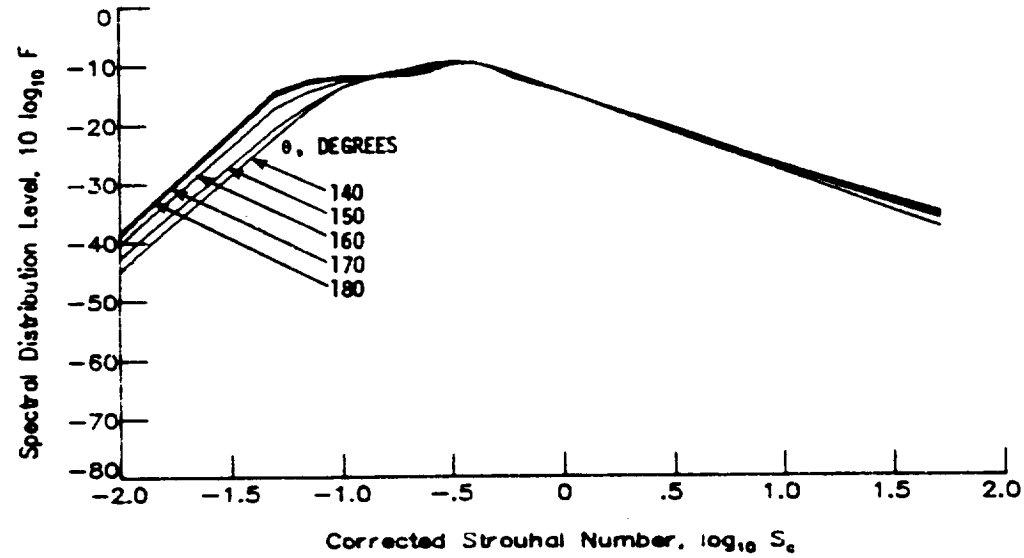

(q) $T_j/T_\infty = 3.0$; $\log_{10} V_j/c_\infty = 0.225$.

Figure 6.- Continued.

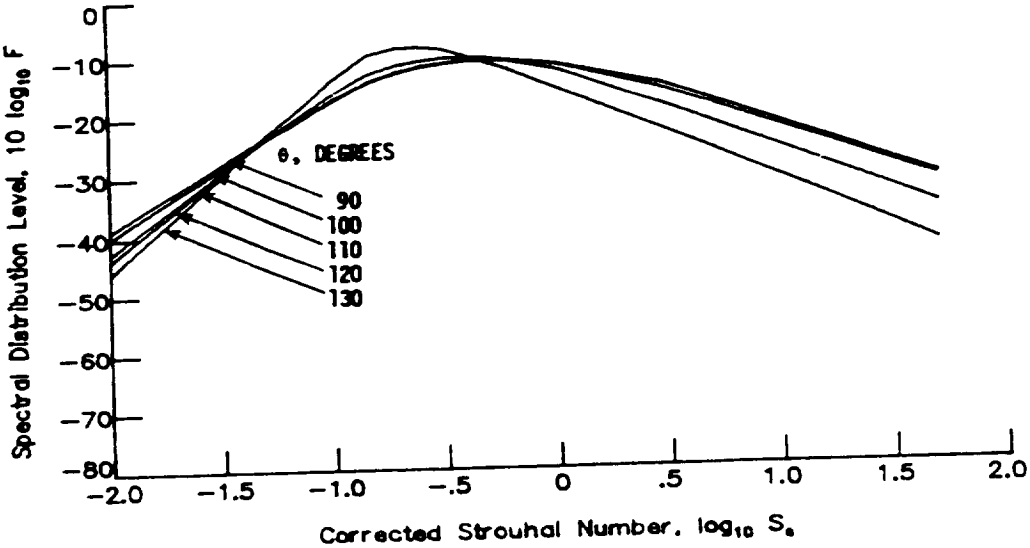

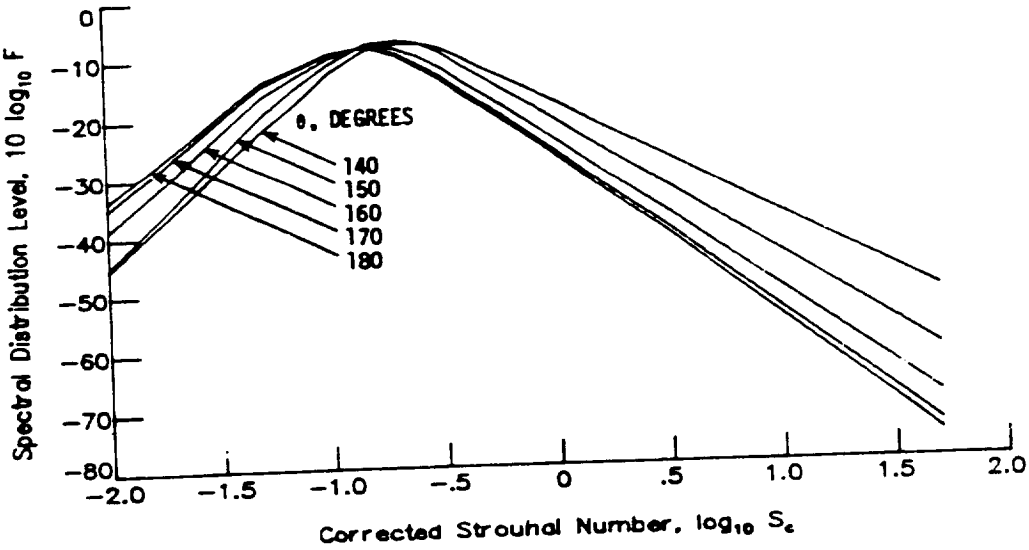

(r) $T_j/T_\infty = 3.5$; $\log_{10} V_j/c_\infty = 0.100$.

Figure 6.- Continued.

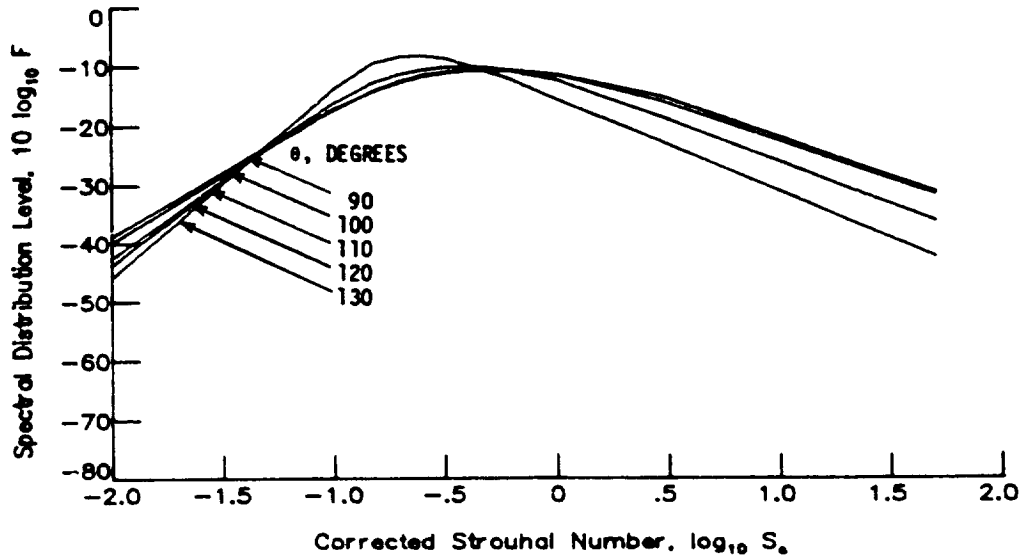

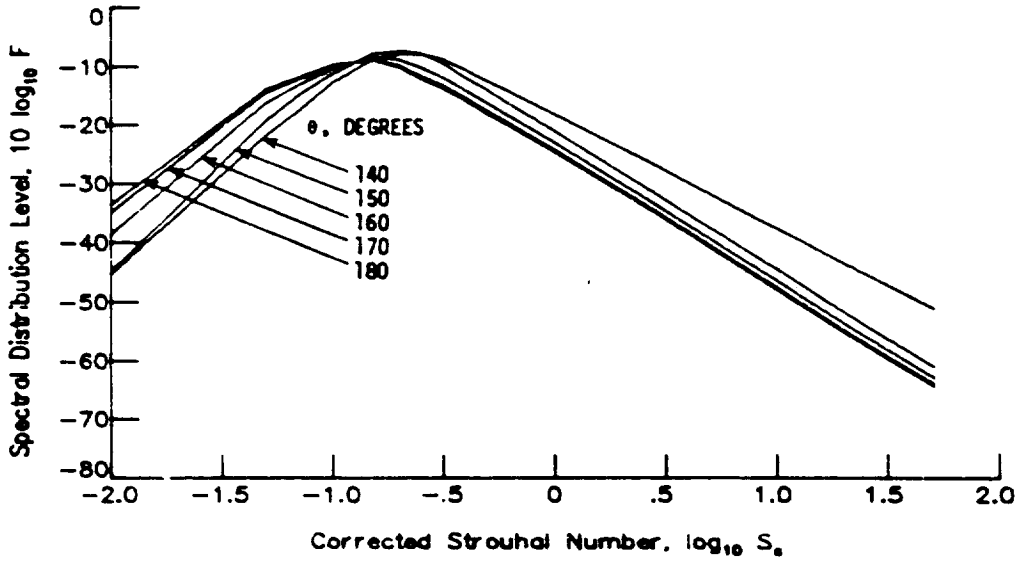

(s) $T_j/T_\infty = 3.5$; $\log_{10} V_j/c_\infty = 0.125$.

Figure 6.- Continued.

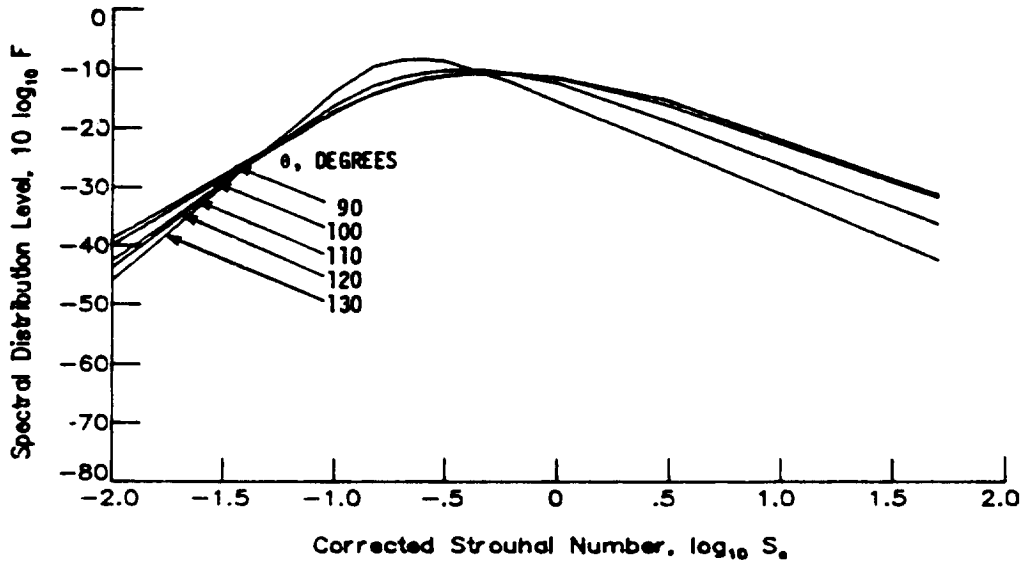

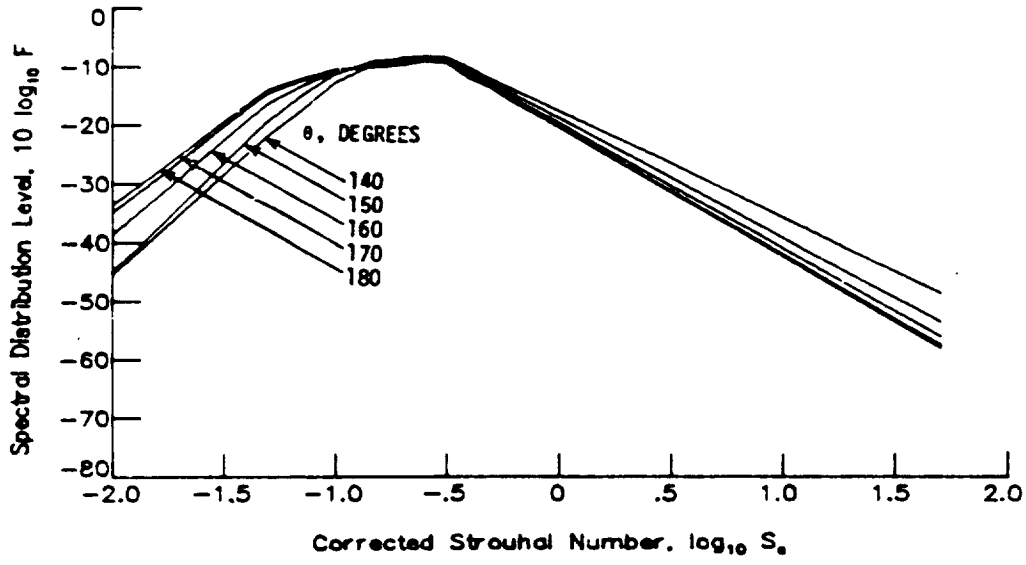

(t) $T_j/T_\infty = 3.5$; $\log_{10} V_j/c_\infty = 0.150$.

Figure 6.- Continued.

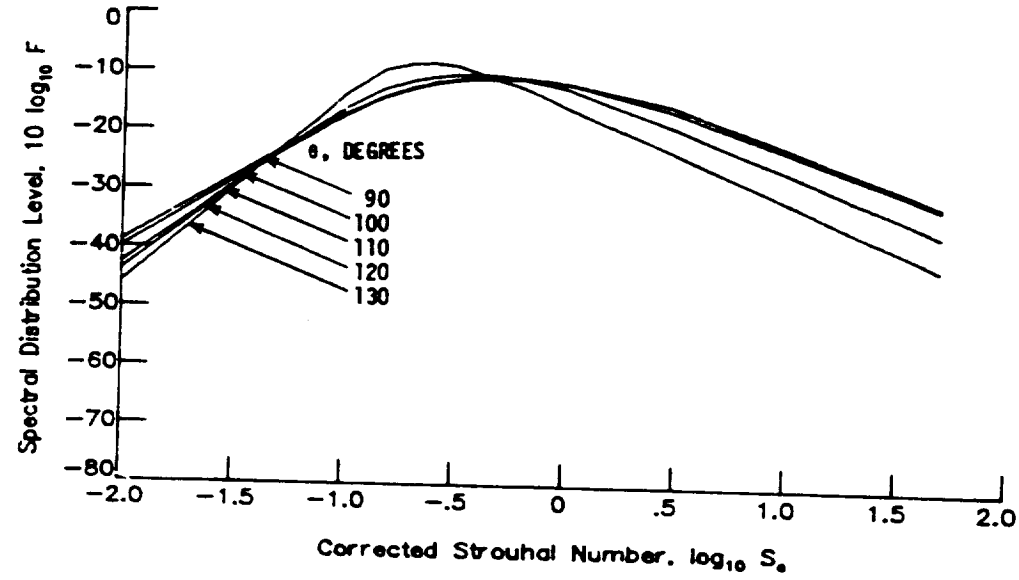

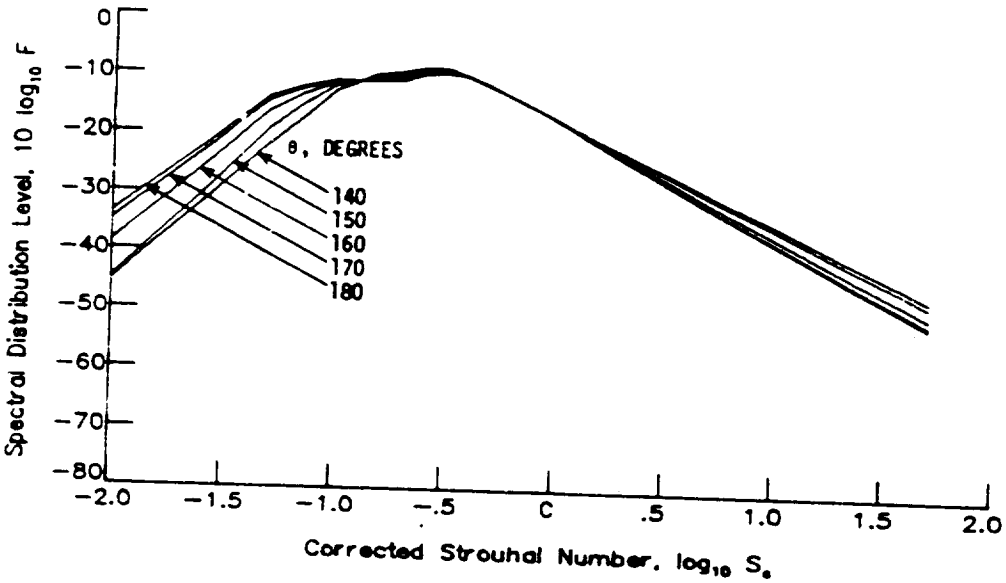

(u) $T_j/T_\infty = 3.5$; $\log_{10} V_j/c_\infty = 0.175$.

Figure 6.- Continued.

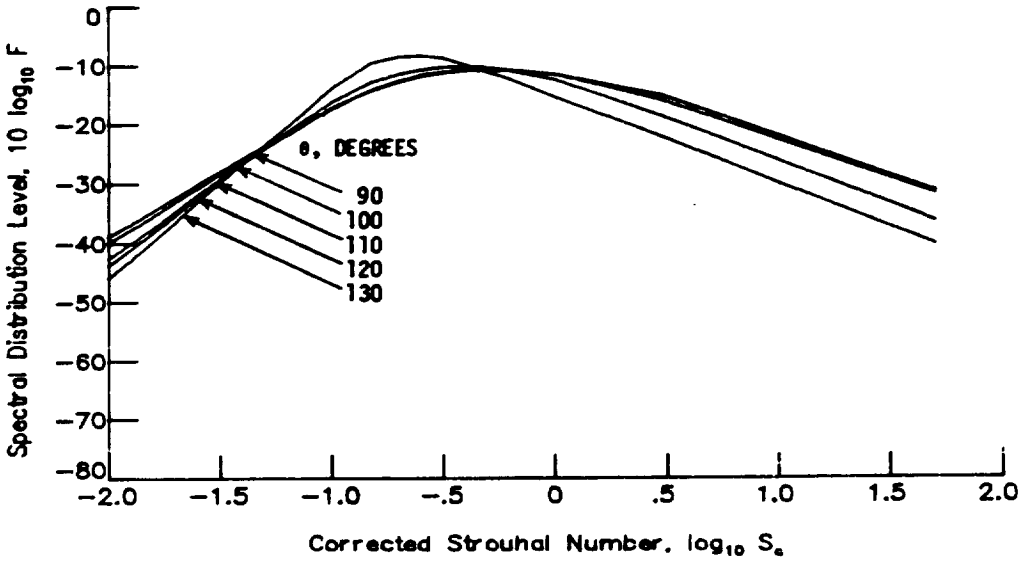

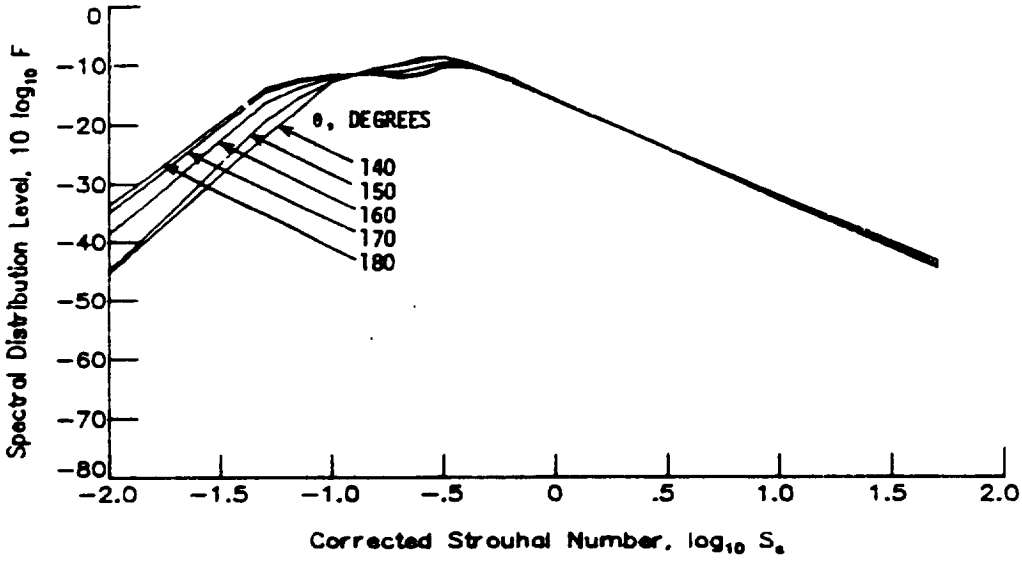

(v) $T_j/T_\infty = 3.5$; $\log_{10} V_j/c_\infty = 0.200$.

Figure 6.- Continued.

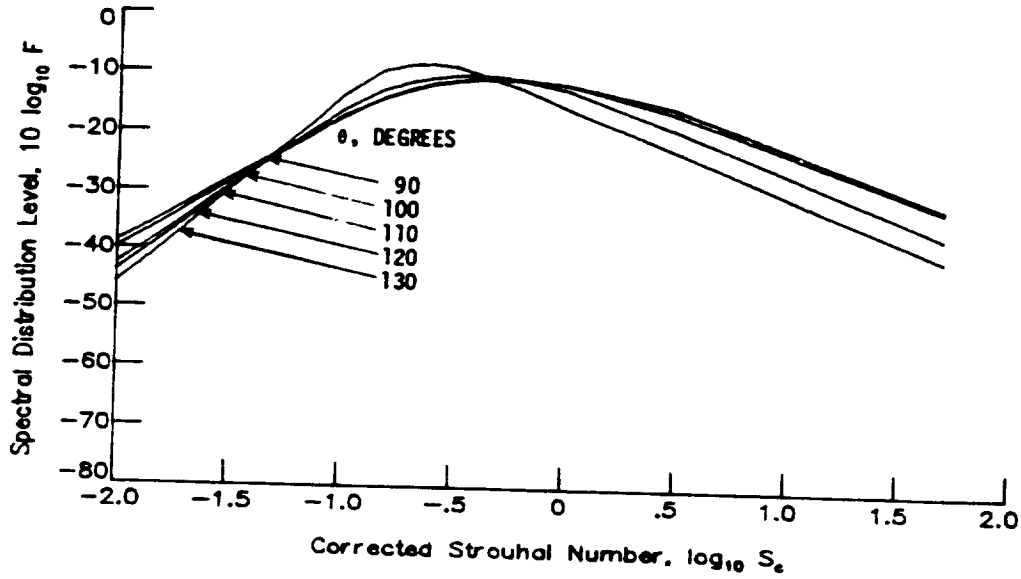

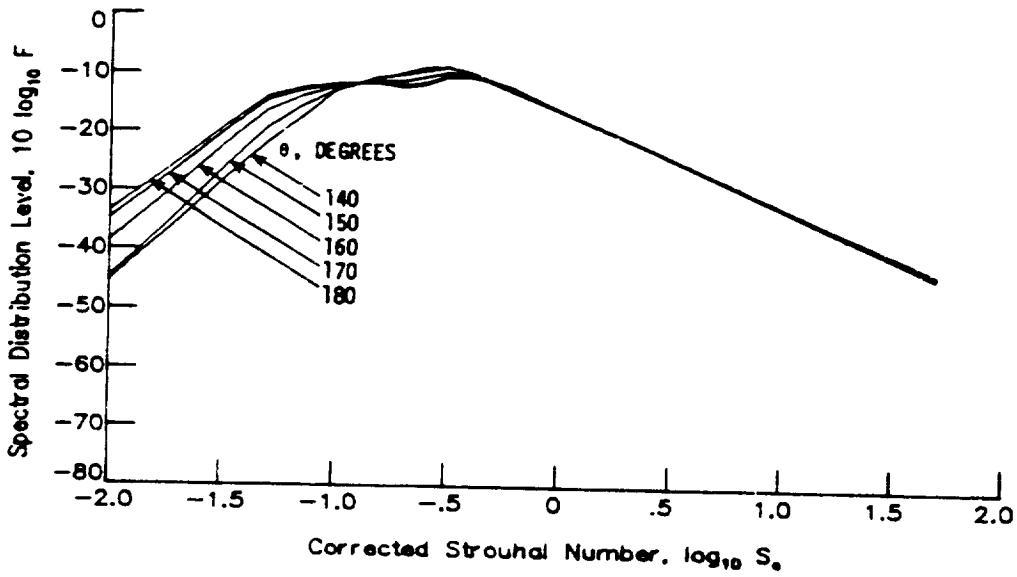

(w) $T_j/T_\infty = 3.5$; $\log_{10} V_j/c_\infty = 0.225$.

Figure 6.- Concluded.

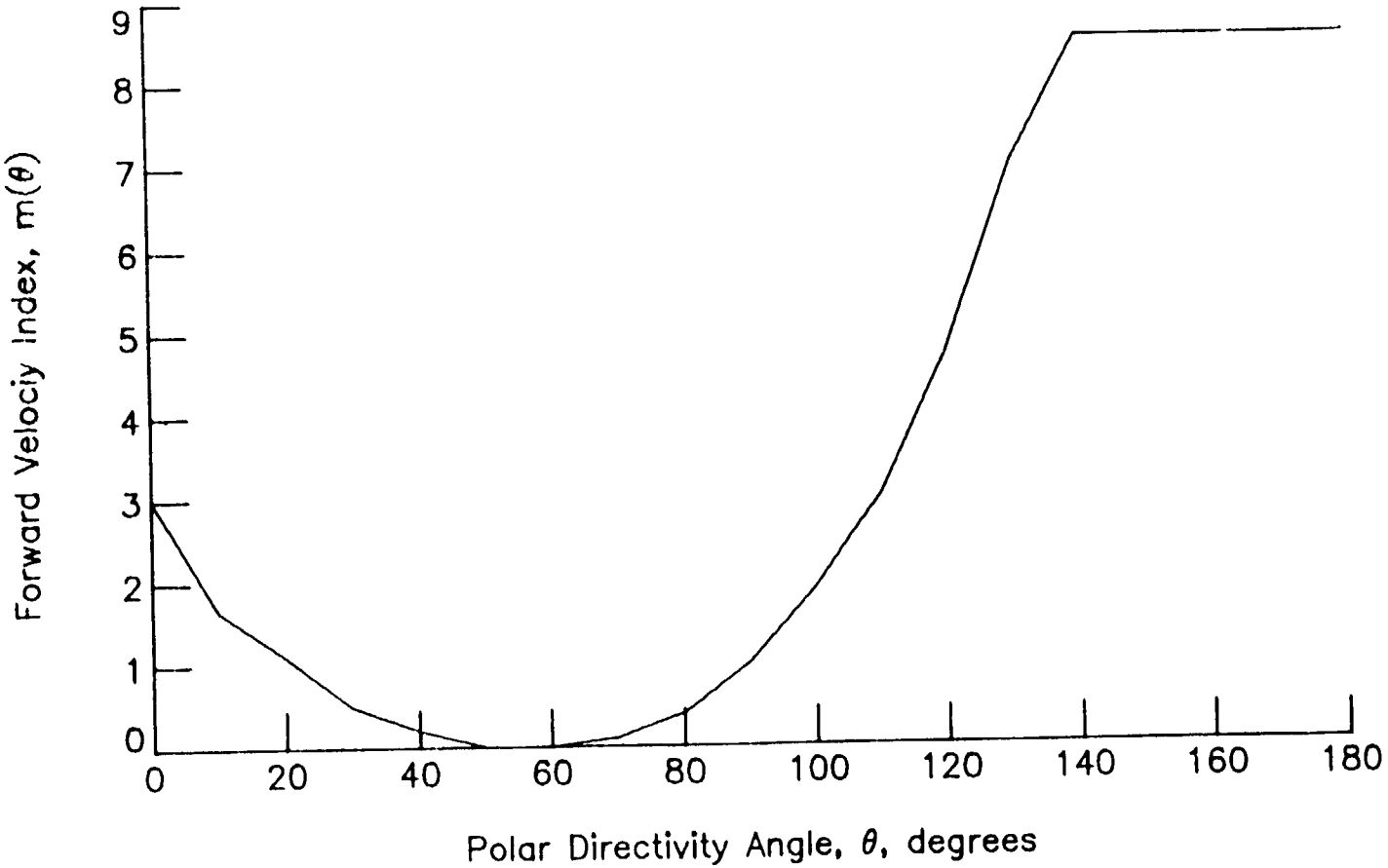

Figure 7.- Forward velocity index.

8.5 CIRCULAR JET SHOCK CELL NOISE MODULE

INTRODUCTION

The Circular Jet Shock Cell Noise Module predicts the broadband shock-associated noise from a single convergent nozzle operating at supercritical pressure ratios. The method is based on the proposed Appendix C by H. K. Tanna to SAE ARP 876. The method employs master spectra functions and a shock cell interference function to produce sound spectra as a function of frequency and polar directivity angle.

The method requires input of several parameters. The jet noise parameters can be provided by the Jet Noise Parameters Module or directly by the user. Additional user-provided parameters are required. The module is executed once for each set of values of the input parameters. The output is a table of the mean-square acoustic pressure as a function of frequency, polar directivity angle, and azimuthal directivity angle. Although jet shock cell noise is assumed not to vary with azimuthal directivity angle, it is introduced so that the output table is compatible with other noise tables.

SYMBOLS

A_e	engine reference area, m^2 (ft^2)
A_j	jet nozzle reference area, m^2 (ft^2)
b	proportional bandwidth constant
C	correlation coefficient spectrum
c_∞	ambient speed of sound, m/s (ft/s)
f	frequency, Hz
f^*	Helmholtz number, $f\sqrt{A_e}/c_\infty$
H	group source strength spectrum
M_j	jet Mach number
M_∞	aircraft Mach number
N_e	number of engines
N_s	number of shocks
$\langle p^2 \rangle^*$	mean-square acoustic pressure, re $\rho_\infty^2 c_\infty^4$
P_{ref}	reference pressure, 2×10^{-5} Pa (4.177×10^{-7} lb/ft^2)

r_s distance from nozzle exit to observer, m (ft)

r_s^* dimensionless distance from nozzle exit to observer, re $\sqrt{A_e}$

T_j jet total temperature, K (^oR)

T_∞ ambient temperature, K (^oR)

V_j fully expanded jet velocity, m/s (ft/s)

W shock cell interference function

β pressure ratio parameter, $\left(M_j^2 - 1\right)^{1/2}$

δ angle between flight vector and engine inlet axis, deg

η exponent

θ polar directivity angle, deg

ρ_∞ ambient density, kg/m^3 (slugs/ft^3)

σ frequency parameter, $7.80\beta(1 - M_\infty \cos\theta)\sqrt{A_j^*}\, f^*$

ϕ azimuthal directivity angle, deg

Superscript:

* dimensionless quantity

INPUT

The jet noise parameters are required from either the Jet Noise Parameters Module or the user. Ambient conditions are required for computation of the frequency parameter and sound pressure levels. The frequency, polar directivity angle, and azimuthal directivity angle arrays establish the independent variable values for the output table. Finally, the engine reference area, number of engines, engine offset angle, and distance to observer are required. The range and default values of the input parameters are given in table I.

Input Constants

A_e engine reference area, m^2 (ft^2)

N_e number of engines

N_s number of shocks

r_s distance from nozzle exit to observer, m (ft)

Jet Noise Parameters

A_j^* area of jet, re A_e

M_j fully expanded jet Mach number

T_j^* jet total temperature, re T_∞

V_j^* fully expanded jet velocity, re c_∞

Ambient Conditions

c_∞ ambient speed of sound, m/s (ft/s)

M_∞ aircraft Mach number

ρ_∞ ambient density, kg/m^3 (slugs/ft^3)

Independent Variable Arrays

f frequency, Hz

θ polar directivity angle, deg

ϕ azimuthal directivity angle, deg

OUTPUT

The output of this module is a table of the mean-square acoustic pressure as a function of frequency, polar directivity angle, and azimuthal directivity angle. In addition, the observer distance r_s is provided for the Propagation Module.

r_s distance from nozzle to observer, m (ft)

Circular Jet Shock Cell Noise Table

f frequency, Hz

θ polar directivity angle, deg

ϕ azimuthal directivity angle, deg

$\langle p^2(f,\theta,\phi)\rangle^*$ mean-square acoustic pressure, re $\rho_\infty^2 c_\infty^4$

METHOD

The prediction methodology proposed by H. K. Tanna is used to compute the shock cell noise. Details of the development and validation of the method are given in references 1 and 2. A schematic of a typical exhaust jet nozzle is shown in figure 1. The coordinate system and directivity angles are also shown. The total jet noise will be the sum of the shock cell and jet mixing noise.

The normalized 1/3-octave-band mean-square pressure for shock associated noise is given by

$$\langle p^2 \rangle^* = (1.920 \times 10^{-3}) \frac{A_j^*}{4\pi (r_s^*)^2} \frac{\left[1 + W(\sigma, \theta, V_j^*)\right]}{\left[1 - M_\infty \cos(\theta - \delta)\right]^4} \beta^n H(\sigma) \qquad (1)$$

The dimensionless source to observer distance r_s^* is defined as

$$r_s^* = r_s / \sqrt{A_e} \qquad (2)$$

and the frequency parameter σ is

$$\sigma = 7.80\beta(1 - M_\infty \cos\theta) \sqrt{A_j^*} f^* \qquad (3)$$

The pressure ratio parameter β is defined as

$$\beta = \left(M_j^2 - 1\right)^{1/2} \qquad (4)$$

and is a measure of the relative shock strength. The pressure ratio parameter β must be greater than 0 for shock cell noise to occur. The exponent of the pressure ratio parameter n depends on the jet Mach number M_j and the jet total temperature T_j^* as

$$n = \begin{cases} 1 & \text{(Unheated jet } (T_j^* < 1.1) \text{ with } \beta > 1) \\ 2 & \text{(Heated jet } (T_j^* \geq 1.1) \text{ with } \beta > 1) \\ 4 & \text{(All jets with } \beta \leq 1) \end{cases} \qquad (5)$$

The shock cell interference function W is a function of the frequency parameter σ, polar directivity angle θ, and velocity ratio V_j^* and is expressed as

$$W = \frac{4}{N_s b} \sum_{k=1}^{N_s - 1} [C(\sigma)]^{k^2} \sum_{m=0}^{N_s - (k+1)} \frac{\sin(b\sigma q_{km}/2)}{b\sigma q_{km}} \cos(\sigma q_{km}) \qquad (6)$$

where

$$q_{km} = \frac{1.70k}{V_j^*} \left[1 - 0.06\left(m + \frac{k+1}{2}\right)\right] (1 + 0.7 V_j^* \cos\theta) \qquad (7)$$

and $b = 0.23077$. The two master spectra, the correlation coefficient spectrum C of equation (6) and the group source strength spectrum H of equation (1), are given in tables II and III and plotted in figures 2 and 3, respectively. For an unheated jet, the value of H should be 2 dB less than the tabulated value. The shock cell interference function W is plotted in figure 4 for a value of $N_s = 8$. Once the mean-square pressure has been computed by equation (1), it is multiplied by the number of engines N_e to produce the total shock cell noise.

The output of this module is a table of the mean-square acoustic pressure $\langle p^2 \rangle^*$ as a function of frequency, polar directivity angle, and azimuthal directivity angle. In addition, printed output is available of the sound pressure level SPL defined as

$$SPL = 10 \log_{10} \langle p^2 \rangle^* + 20 \log_{10} \frac{\rho_\infty c_\infty^2}{p_{ref}} \tag{8}$$

REFERENCES

1. Harper-Bourne, M.; and Fisher, M. J.: The Noise From Shock Waves in Supersonic Jets. Noise Mechanisms, AGARD-CP-131, Mar. 1974, pp. 11-1 - 11-13.

2. Tanna, H. K.; Dean, P. D.; and Burrin, R. H.: The Generation and Radiation of Supersonic Jet Noise. Volume IV - Shock-Associated Noise Data. AFAPL-TR-76-65, Volume IV, U.S. Air Force, Sept. 1976.

TABLE I.- RANGE AND DEFAULT VALUES OF INPUT PARAMETERS

Input parameter	Minimum	Default	Maximum
A_e, m^2	0.01	$\pi/4$	10
N_e	1	1	4
N_s	2	8	10
r_s, m	0.01	$\sqrt{A_e}$	100
A_j^*	0.0001	1	10
M_∞	0	0	0.9
M_j	0	1.414	2.0
T_j^*	0.7	1	6
V_j^*	0	1	3.5
δ, deg	0	0	30
c_∞, m/s	200	340.294	400
ρ_∞, kg/m^3	0.2	1.225	1.5

TABLE II.- CORRELATION COEFFICIENT SPECTRUM

$\log_{10} \sigma$	C
-.700	.703
-.600	.703
-.500	.710
-.400	.714
-.300	.719
-.200	.724
-.100	.729
0.000	.735
.100	.740
.200	.740
.300	.740
.400	.735
.500	.714
.600	.681
.700	.635
.800	.579
.900	.520
1.000	.460
1.100	.400
1.200	.345
1.300	.290
1.400	.235
1.500	.195
1.600	.150
1.700	.100
1.800	.060
1.900	.030
2.000	.015

TABLE III.- GROUP SOURCE STRENGTH SPECTRUM

$\log_{10} \sigma$	$\log_{10} H$
0.0	-2.69
0.1	-2.31
0.2	-1.94
0.3	-1.59
0.4	-1.33
0.5	-1.10
0.6	-0.94
0.7	-0.88
0.8	-0.91
0.9	-0.99
1.0	-1.09
1.1	-1.17
1.2	-1.30
1.3	-1.42
1.4	-1.55
1.5	-1.67
1.6	-1.81
1.7	-1.92
1.8	-2.06
1.9	-2.18
2.0	-2.30
2.1	-2.42
2.2	-2.54
2.3	-2.66
2.4	-2.78
2.5	-2.90

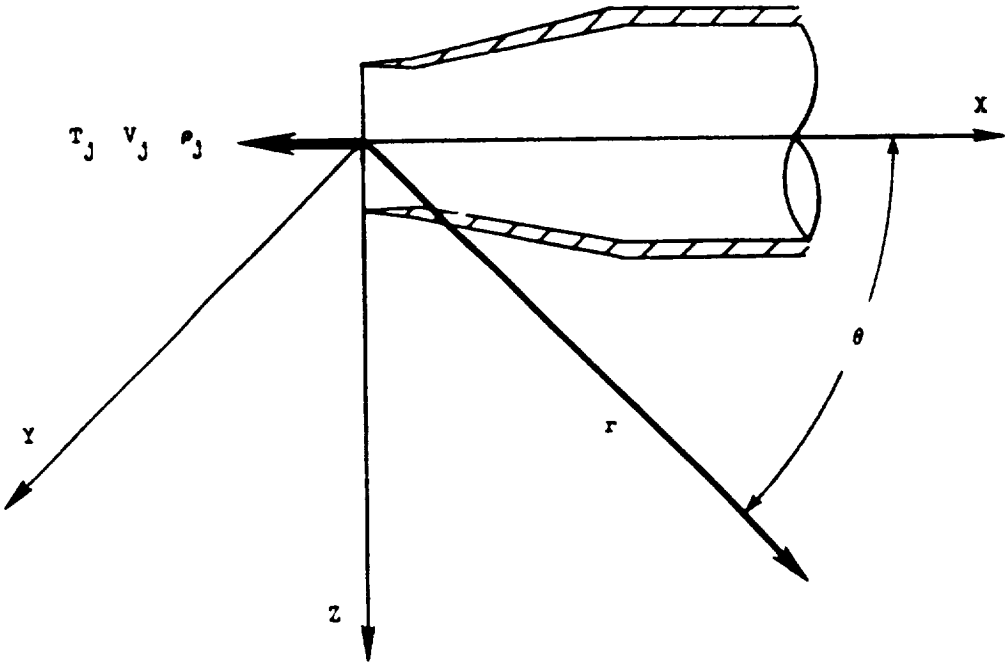

Figure 1.- Schematic diagram of single stream circular nozzle.

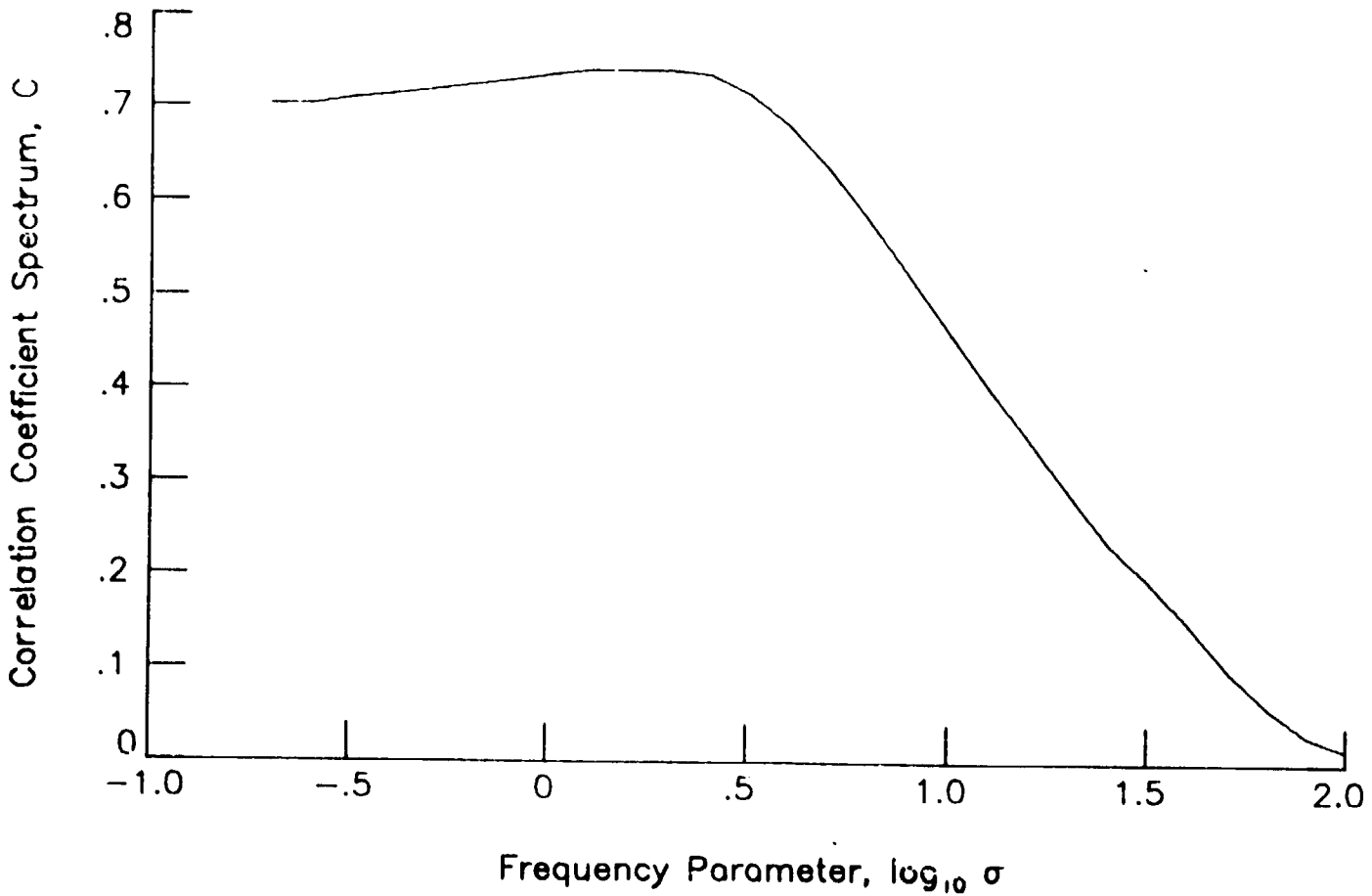

Figure 2.- Correlation coefficient spectrum.

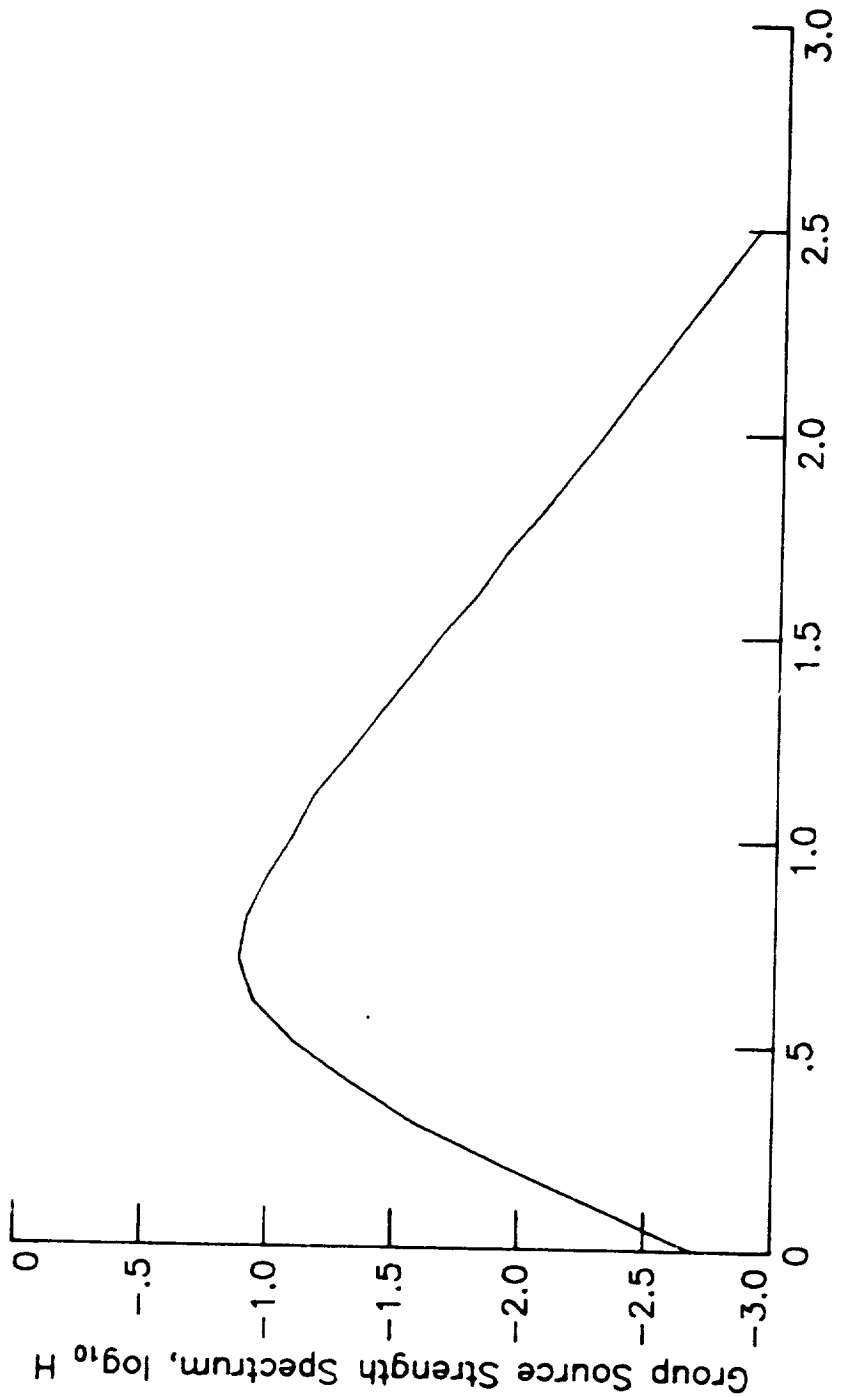

Figure 3.- Group source strength spectrum.

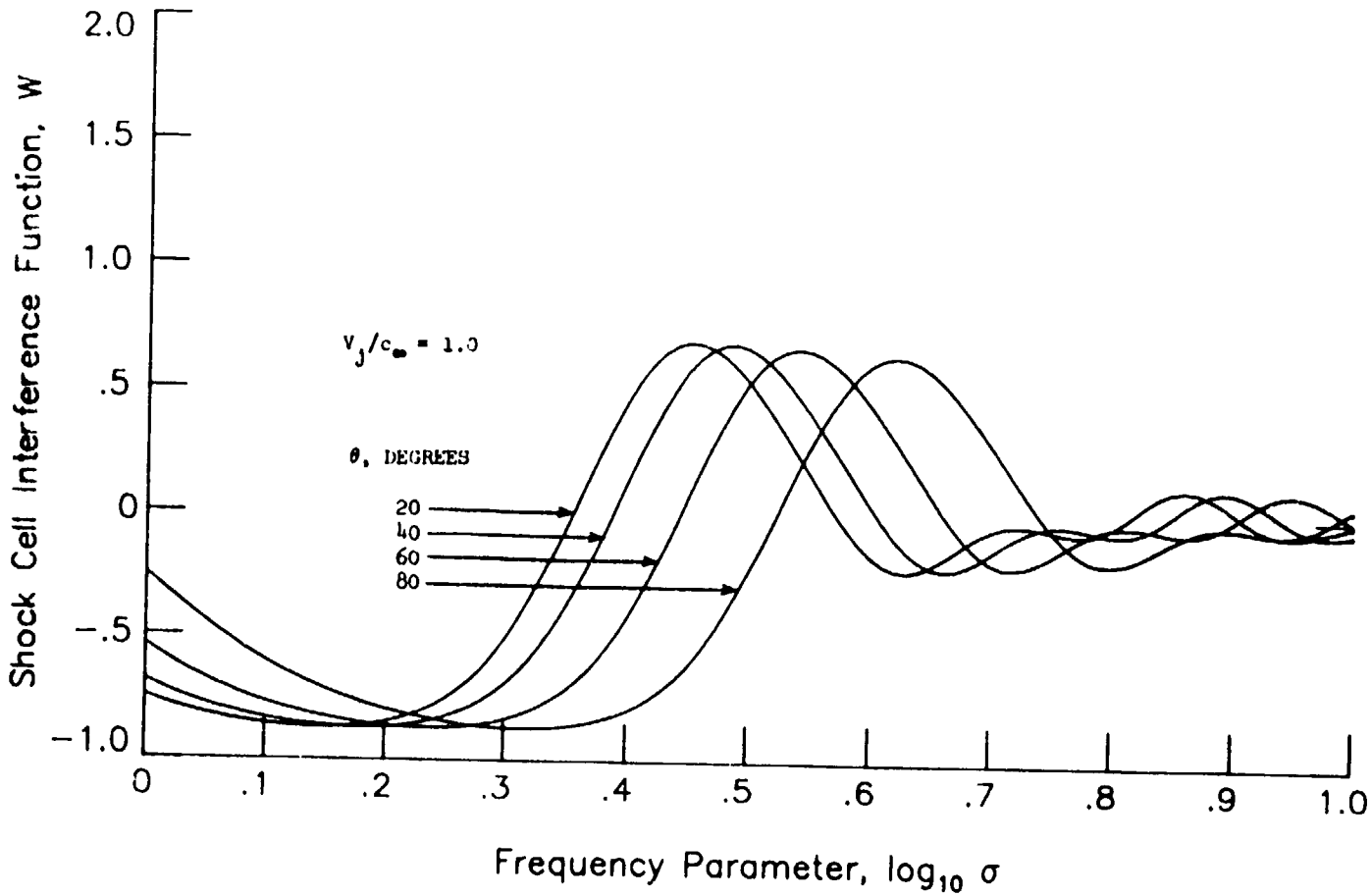

Figure 4.- Shock cell interference function.

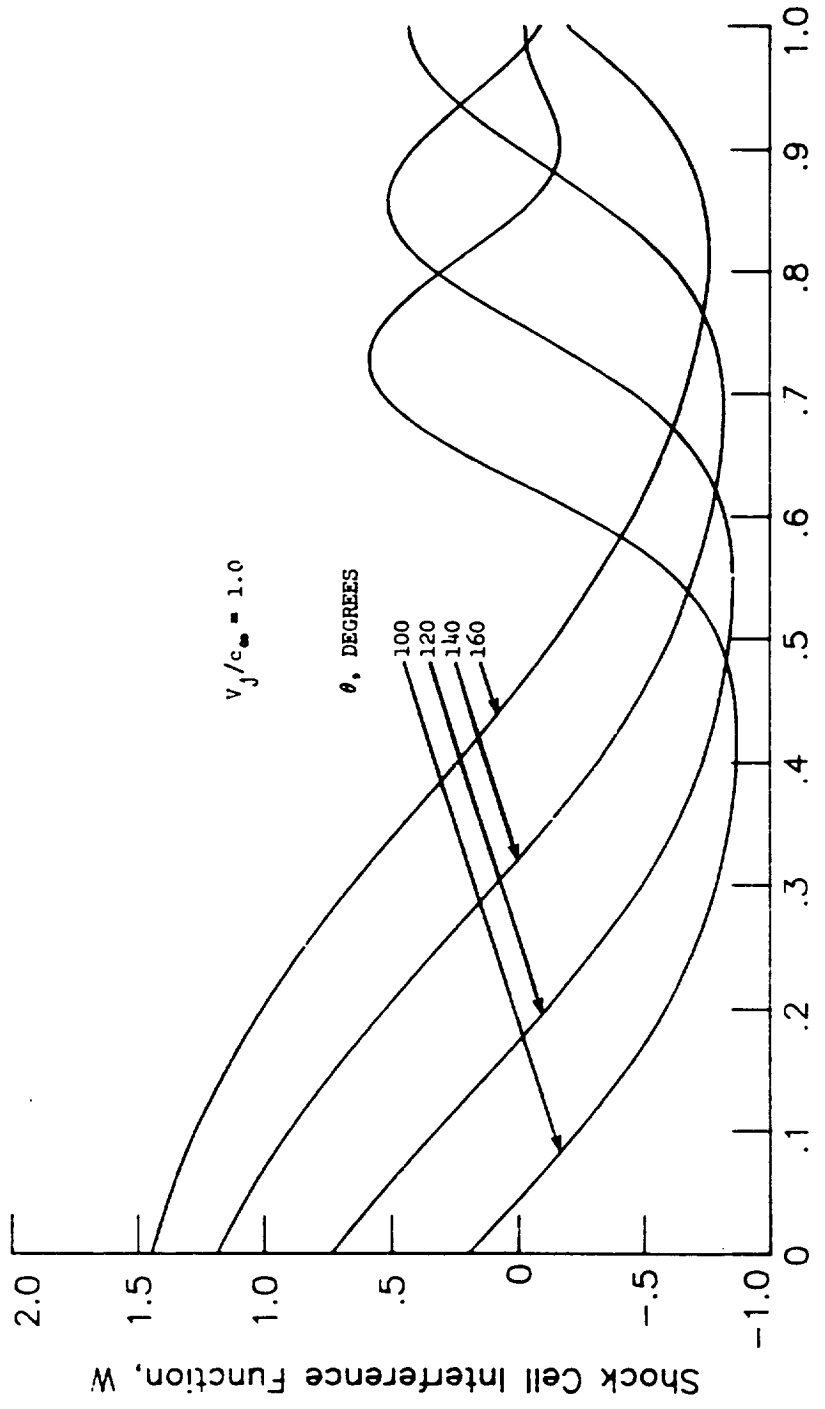

Figure 4.- Continued.

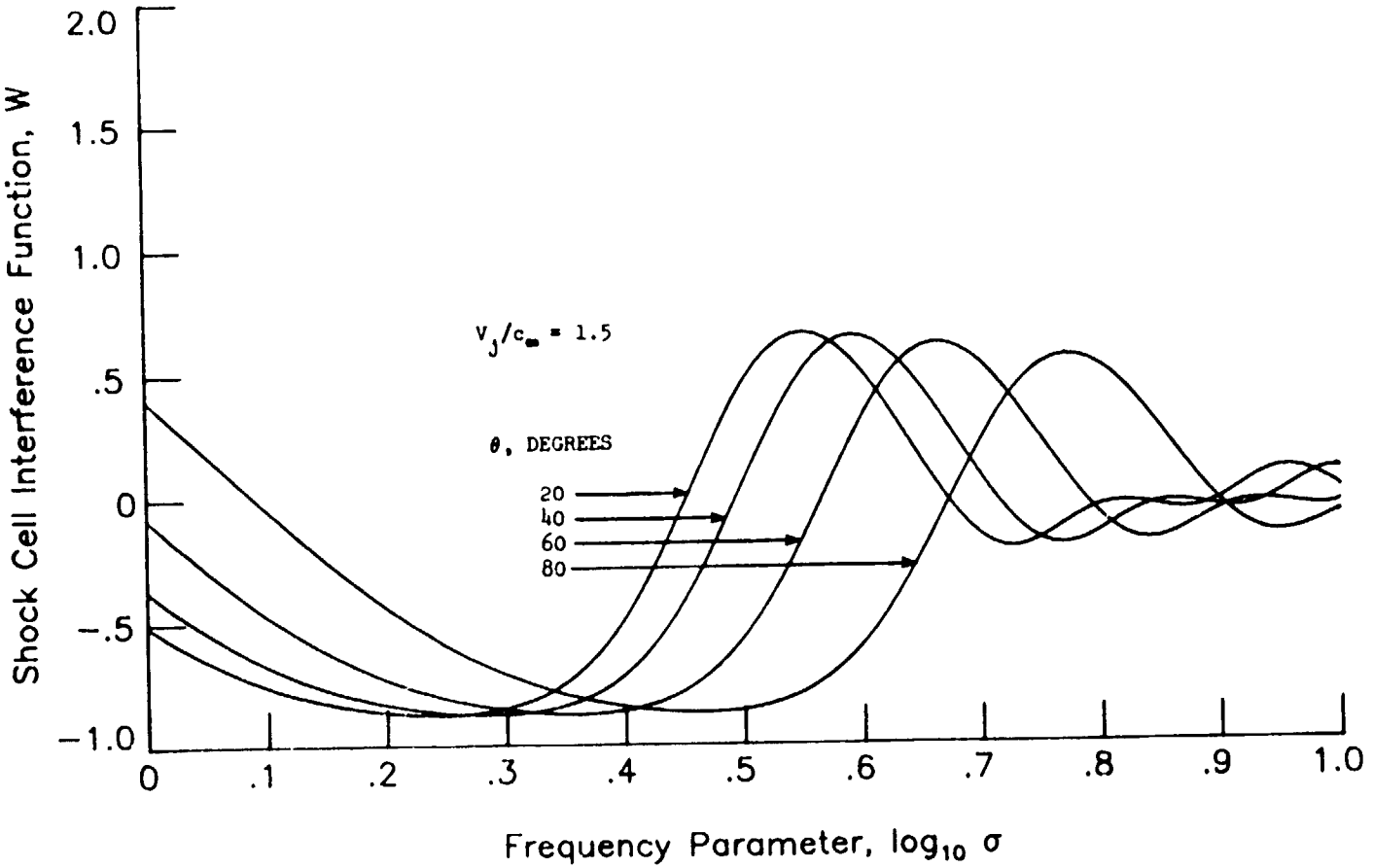

Figure 4.- Continued.

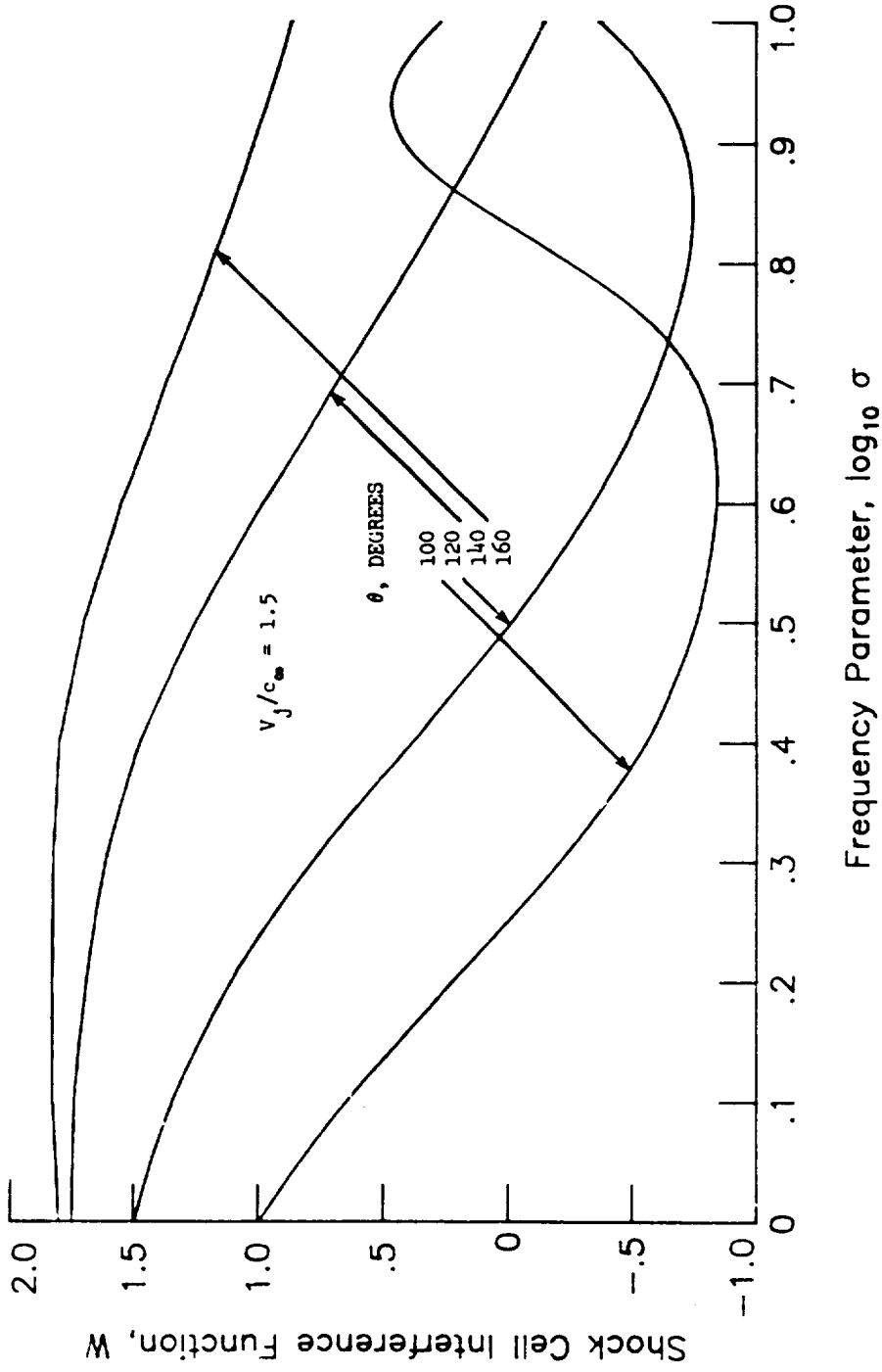

Figure 4.- Continued.

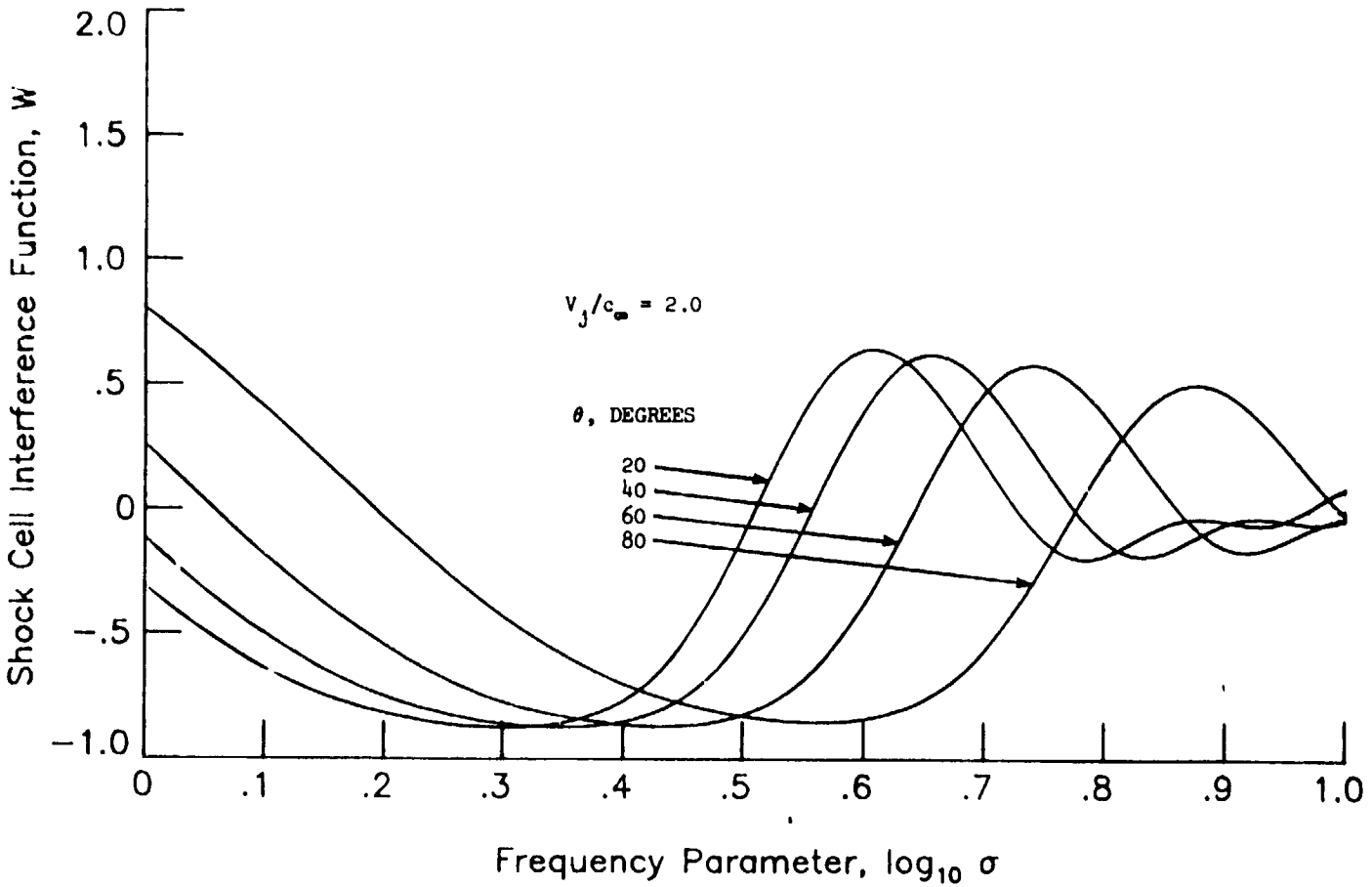

Figure 4.- Continued.

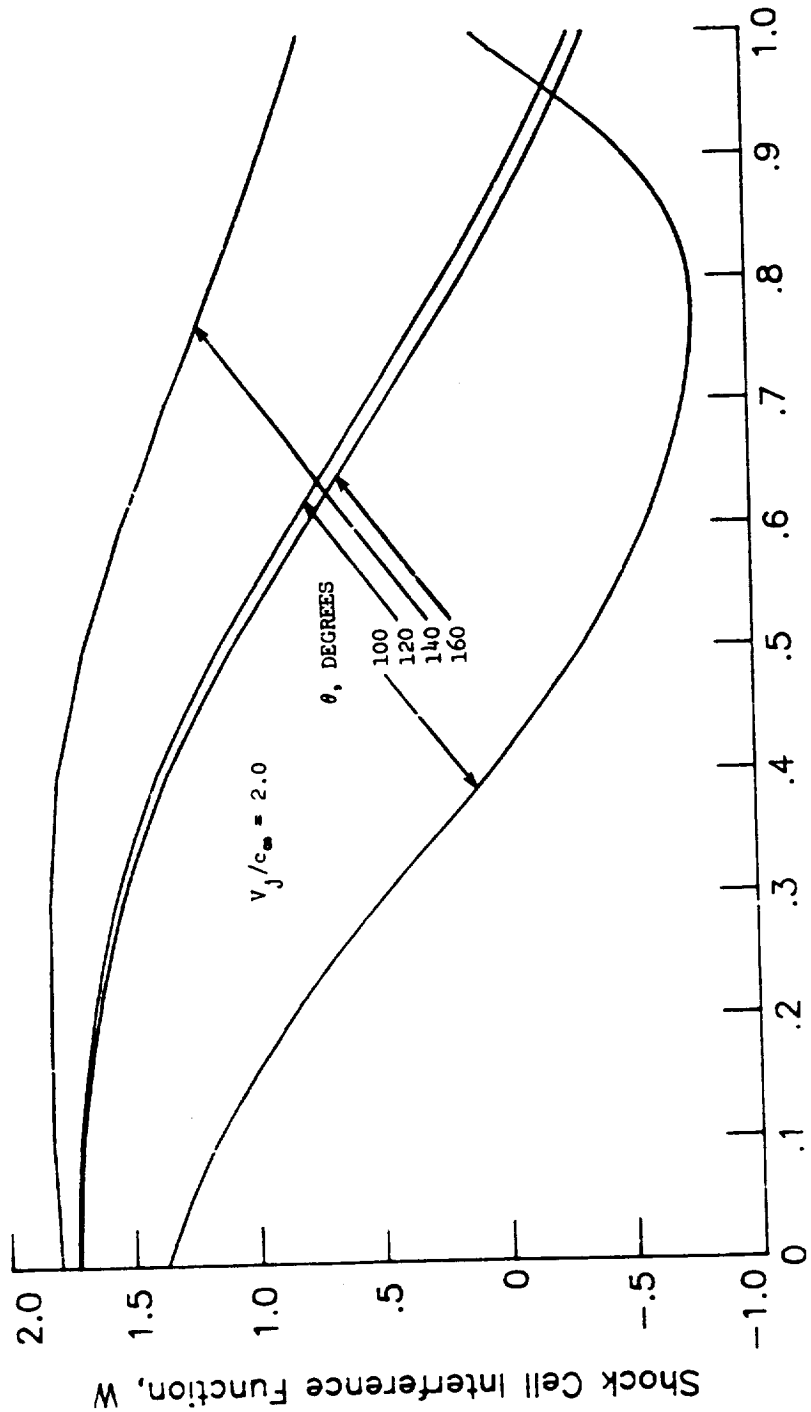

Figure 4.- Concluded.

8.6 STONE JET NOISE MODULE

INTRODUCTION

The Stone Jet Noise Module predicts the far-field mean-square acoustic pressure for single stream and coaxial circular jets. Included in the prediction are both jet mixing noise and shock-turbulence interaction noise. The method used is that developed by J. R. Stone as presented in references 1 and 2. For coaxial nozzles, the method is limited to jets whose core jet velocity is greater than the secondary jet velocity. Further, only the core jet velocity may be supersonic.

The method requires input of several parameters. The nozzle exit flow parameters can be provided by the Jet Noise Parameters Module or directly by the user. Additional user-provided parameters are required. The module is executed once for each set of values of the input parameters. The output is a table of the mean-square acoustic pressure as a function of frequency, polar directivity angle, and azimuthal directivity angle. Jet exhaust noise is assumed independent of the azimuthal directivity angle; however, the prediction is tabulated as a (constant) function of azimuthal angle so that the output table is compatible with other noise tables.

SYMBOLS

A_e engine reference area, m^2 (ft^2)

A_j fully expanded jet area, m^2 (ft^2)

c_∞ ambient speed of sound, m/s (ft/s)

D_m directivity function for jet mixing noise

D_s directivity function for shock noise

d_e equivalent diameter, m (ft)

d_h hydraulic diameter, m (ft)

d_j jet diameter, m (ft)

d_p^* plug diameter, m (ft)

F_m spectral distribution factor for jet mixing noise

F_s spectral distribution factor for shock noise

f frequency, Hz

f_s	frequency shift parameter
G_c	configuration factor for mean-square pressure for coaxial nozzle
G_p	configuration factor for mean-square pressure for plug nozzle
g_c	configuration factor for Strouhal number for coaxial nozzle
g_p	configuration factor for Strouhal number for plug nozzle
H_m	forward flight effects factor
M	Mach number
M_∞	aircraft Mach number
m	exponent
N	number of engines
$\langle p^2 \rangle^*$	mean-square acoustic pressure, re $\rho_\infty^2 c_\infty^4$
$\langle p^2(\sqrt{A_e}, 90^o) \rangle^*$	mean-square acoustic pressure at the reference distance $\sqrt{A_e}$ at $\theta = 90^o$, re $\rho_\infty^2 c_\infty^4$
p_{ref}	reference pressure, 2×10^{-5} Pa (4.177×10^{-7} lb/ft^2)
R_d	ratio of hydraulic diameter to equivalent diameter
r_s	distance from source to observer, m (ft)
S_m	Strouhal number for jet mixing noise
S_s	Strouhal number for jet shock cell noise
T	fully expanded jet temperature, K (^oR)
T_∞	ambient temperature, K (^oR)
V	fully expanded jet velocity, m/s (ft/s)
β	pressure ratio parameter, $\left(M_1^2 - 1\right)^{1/2}$
δ	angle between flight vector and engine inlet axis, deg
θ	polar directivity angle, deg
θ'	modified directivity angle, $(V_1^*)^{0.1}\theta$, deg
θ_m	Mach angle, deg
ρ	fully expanded jet density, kg/m^3 (slugs/ft^3)
ρ_∞	ambient density, kg/m^3 (slugs/ft^3)

ϕ azimuthal directivity angle, deg

ω density exponent

ω_o stationary jet density exponent

Subscripts:

1 primary stream

2 secondary stream

Superscript:

* dimensionless value

INPUT

The jet parameters are required from either the output of the Jet Noise Parameters Module or the user. Ambient conditions are required. The frequency, polar directivity angle, and azimuthal directivity angle arrays establish the independent variable values for the output table. Finally, the engine reference area, number of engines, engine axis offset, and distance to the pseudo-observer are required. The range and default values of the input parameters are given in table I.

Input Constants

A_e engine reference area, m^2 (ft^2)

N number of engines

r_s distance from nozzle exit to pseudo-observer, m (ft)

δ angle between flight vector and engine inlet axis, deg

Jet Noise Parameters

Primary Stream

$A^*_{j,1}$ primary fully expanded jet area, re A_e

$d^*_{e,1}$ actual primary stream equivalent diameter, re $\sqrt{A_e}$

$d^*_{h,1}$ actual primary stream hydraulic diameter, re $\sqrt{A_e}$

M_1 primary stream Mach number

T^*_1 primary stream total temperature, re T_∞

V_1^* primary stream jet velocity, re c_∞

ρ_1^* primary stream jet density, re ρ_∞

Secondary Stream

$A_{j,2}^*$ secondary fully expanded jet area, re A_e

M_2 secondary stream Mach number

T_2^* secondary stream total temperature, re T_∞

V_2^* secondary stream jet velocity, re c_∞

ρ_2^* secondary stream jet density, re ρ_∞

Ambient Conditions

c_∞ ambient sound speed, m/s (ft/s)

M_∞ aircraft Mach number

ρ_∞ ambient density, kg/m^3 ($slugs/ft^3$)

Independent Variable Arrays

f frequency, Hz

θ polar directivity angle, deg

ψ azimuthal directivity angle, deg

OUTPUT

The output of this module is a table of the mean-square acoustic pressure as a function of frequency, polar directivity angle, and azimuthal directivity angle. In addition the pseudo-observer distance r_s is provided for the Propagation Module.

r_s distance from nozzle exit to pseudo-observer, m (ft)

Stone's Method Jet Noise Table

f frequency, Hz

θ polar directivity angle, deg

ψ azimuthal directivity angle, deg

$\langle p^2(f,\theta,\psi)\rangle^*$ mean-square acoustic pressure, re $\rho_\infty^2 c_\infty^4$

METHOD

The prediction method developed in references 1 and 2 is used to compute the mean-square acoustic pressure in the far field. The method uses empirically determined functions to provide the directivity and spectral content of the field with the computed overall mean-square acoustic pressure at $\theta = 90^\circ$, $\langle p^2(\sqrt{A_e}, 90^\circ)\rangle^*$, used to fix the amplitude throughout the field.

This module can be used to predict the noise for several exhaust nozzle types including both subsonic and supersonic single stream circular nozzles, both with and without plugs, and coaxial jets.

The prediction schemes for all nozzle types are developed from two basic equations, one each for jet mixing noise and shock-turbulence interaction noise, each of which is empirically determined. Furthermore, configuration factors are used to adjust the levels predicted for single stream circular nozzles to those for single stream plug nozzles or coaxial nozzles. Illustrations of these various configurations, also showing the coordinate axis and directivity angles, are provided in figure 1.

Jet Mixing Noise

The equation used to calculate the jet mixing noise at a distance r_s from the nozzle exit is

$$\langle p^2(r_s^*, \theta)\rangle^* = \frac{\langle p^2(\sqrt{A_e}, 90^\circ)\rangle^*}{(r_s^*)^2}\left[\frac{1 + (0.124V_1^*)^2}{(1 + 0.62V_1^* \cos\theta)^2 + (0.124V_1^*)^2}\right]^{3/2} \times D_m(\theta')\, F_m(S_m, \theta')\, H_m(M_\infty, \theta, V_1^*, \rho_1^*, T_1^*)\, G_c G_p \qquad (1)$$

In this equation $\langle p^2(\sqrt{A_e}, 90^\circ)\rangle^*$ is the mean-square acoustic pressure for a stationary jet calculated at the reference distance $\sqrt{A_e}$ from the nozzle exit at $\theta = 90^\circ$, r_s^* is the dimensionless distance from the nozzle exit r_s referred to $\sqrt{A_e}$, $F_m(S_m, \theta')$ is a spectral distribution function, $H_m(M_\infty, \theta, V_1^*, \rho_1^*, T_1^*)$ is the forward flight effects factor, G_c and G_p are configuration factors, and $D_m(\theta')$ provides directivity information. Each of these factors is now considered in detail.

The mean-square acoustic pressure at the reference distance and $\theta = 90^\circ$, $\langle p^2(\sqrt{A_e}, 90^\circ)\rangle^*$, is calculated through use of the following equation:

$$\langle p^2(\sqrt{A_e}, 90^o)\rangle^* = \frac{2.502 \times 10^{-6} A^*_{j,1} (\rho^*_1)^{\omega_o} (V^*_1)^{7.5}}{\left[1 + (0.124 V^*_1)^2\right]^{3/2}} \tag{2}$$

Here, $A^*_{j,1}$ is the fully expanded jet area, ρ^*_1 and V^*_1 are the fully expanded jet density and velocity, respectively, with all three quantities evaluated for the primary stream, and nondimensionalized by A_e, ρ_∞, and c_∞, respectively. The density exponent ω_o is an empirically determined function of V^*_1 given by

$$\omega_o = \frac{2(V^*_1)^{3.5} - 0.6}{(V^*_1)^{3.5} + 0.6} \tag{3}$$

The factor $F_m(S_m, \theta')$ is a function of the modified directivity angle $\theta' = \theta(V^*_1)^{0.1}$ and the jet mixing noise Strouhal number S_m calculated by

$$S_m = \frac{f^* d^*_{j,1}\left[1 - M_\infty \cos(\theta - \delta)\right](T^*_1)^{0.4(1+\cos\theta')}}{V^*_1(1 - M_\infty/V^*_1)} \times \left\{\frac{\left[1 + 0.62(V^*_1 - M_\infty)\cos\theta\right]^2 + \left[0.124(V^*_1 - M_\infty)\right]^2}{(1 + 0.62V^*_1\cos\theta)^2 + (0.124V^*_1)^2}\right\}^{1/2} g_c g_p \tag{4}$$

In this equation f^* is the Helmholtz number given as

$$f^* = \frac{f\sqrt{A_e}}{c_\infty} \tag{5}$$

M_∞ is the aircraft Mach number, and $d^*_{j,1}$ is the jet diameter given as

$$d^*_{j,1} = \sqrt{\frac{4A^*_{j,1}}{\pi}} \tag{6}$$

Further δ is the angle between the flight vector and the engine inlet axis, in degrees, and T^*_1 is the fully expanded primary jet temperature nondimensionalized by T_∞. The function $F_m(S_m, \theta')$ is normalized such that the summation over 1/3-octave Strouhal number is unity:

$$\sum_{S_m} F_m(S_m,\theta') = 1 \tag{7}$$

and is tabulated in table II and plotted in figure 2.

The function $D_m(\theta')$ contains directivity information and is given in table III and plotted in figure 3.

The factors g_c and g_p are configuration factors which are discussed when the configuration factors G_c and G_p of equation (1) are considered. The forward flight effects factor $H_m(M_\infty,\theta,V_1^*,\rho_1^*,T_1^*)$ is given by

$$H_m(M_\infty,\theta,V_1^*,\rho_1^*,T_1^*) = \left\{ \frac{(1 + 0.62V_1^* \cos\theta)^2 + (0.124V_1^*)^2}{\left[1 + 0.62(V_1^* - M_\infty)\cos\theta\right]^2 + \left[0.124(V_1^* - M_\infty)\right]^2} \right\}^{3/2}$$

$$\times \frac{(1 - M_\infty/V_1)^5 (\rho_1^*)^{\omega-\omega_0}}{1 - M_\infty \cos(\theta - \delta)} \tag{8}$$

where

$$\omega - \omega_0 = \frac{1.8\left\{\left[V_1^*(1 - M_\infty/V_1^*)^{2/3}\right]^{3.5} - (V_1^*)^{3.5}\right\}}{\left\{0.6 + \left[V_1^*(1 - M_\infty/V_1^*)^{2/3}\right]^{3.5}\right\}\left[0.6 + (V_1^*)^{3.5}\right]} \tag{9}$$

The function H_m is normalized such that it is unity if $M_\infty = 0$ for all values of the remaining parameters:

$$H_m(0,\theta,V_1^*,\rho_1^*,T_1^*) = 1 \tag{10}$$

The configuration factors G_p and G_c take the mean-square acoustic pressure predicted for a single stream circular nozzle and adjust it to predict the mean-square acoustic pressure for plug and single nozzles, respectively. The factor G_p is given by

$$G_p = \begin{cases} \left(0.10 + \dfrac{2R_d^2}{1 + R_d^2}\right)^{0.3} & \text{(Nozzle with plug)} \\ 1 & \text{(Nozzle without plug)} \end{cases} \tag{11}$$

In this equation,

$$R_d = d^*_{h,1} / d^*_{e,1} \tag{12}$$

With $d^*_{h,1}$, the plug nozzle hydraulic diameter, given by

$$d^*_{h,1} = \sqrt{\frac{4A^*_{j,1}}{\pi} + (d^*_p)^2} - d^*_p \tag{13}$$

and $d^*_{e,1}$, the nozzle equivalent diameter, given by

$$d^*_{e,1} = \sqrt{\frac{4A^*_{j,1}}{\pi}}$$

where $A^*_{j,1}$ is the primary nozzle area and d^*_p is the plug diameter; these quantities are nondimensionalized by A_e and $\sqrt{A_e}$, respectively. The factor G_c is given by

$$G_c = \begin{cases} \left(\frac{T^*_1}{T^*_2}\right)^{1/2} \left\{ \left(1 - V^*_2/V^*_1\right)^m + \frac{1.2\left[1 + A^*_{j,2}(V^*_2)^2 / A^*_{j,1}(V^*_1)^2\right]^4}{\left(1 + A^*_{j,2}/A^*_{j,1}\right)^3} \right\} & \text{(Coaxial nozzle)} \\ 1 & \text{(Single nozzle)} \end{cases} \tag{14}$$

The exponent m is given by

$$m = \begin{cases} 1.1\sqrt{A^*_{j,2}/A^*_{j,1}} & \left(A^*_{j,2}/A^*_{j,1} < 29.7\right) \\ 6 & \left(A^*_{j,2}/A^*_{j,1} \geq 29.7\right) \end{cases} \tag{15}$$

The factor g_p or g_c adjusts the Strouhal number S_m for a single stream circular jet to that for a plug nozzle or a single nozzle, respectively. These factors are given by

$$g_p = \begin{cases} (R_d)^{0.4} & \text{(Nozzle with plug)} \\ 1 & \text{(Nozzle without plug)} \end{cases} \tag{16}$$

and

$$q_c = \begin{cases} \left(1 - T_2^* f_s / T_1^*\right)^{-1} & \text{(Coaxial nozzle)} \\ 1 & \text{(Single nozzle)} \end{cases} \tag{17}$$

where f_s is an empirically determined function of the area ratio parameter $1 + A_{j,2}^*/A_{j,1}^*$ and the velocity ratio V_2^*/V_1^*. This function is tabulated in table IV and plotted in figure 4.

Shock Noise

The 1/3-octave-band mean-square acoustic pressure due to shock-turbulence interaction noise is calculated through use of the following equation:

$$\langle p^2 \rangle^* = \frac{(3.15 \times 10^{-4}) A_{j,1}^*}{(r_s^*)^2} \frac{\beta^4}{1 - \beta^4} \frac{F_s(S_s)\, D_s(\theta, M_1)\, G_c}{1 - M_\infty \cos(\theta - \delta)} \tag{18}$$

In this equation δ is the pressure ratio parameter as follows:

$$\delta = \left(M_1^2 - 1\right)^{1/2} \tag{19}$$

which must be greater than zero for shock cell noise to occur.

The function $D_s(\theta, M_1)$ provides the dependence of the shock cell noise, for a stationary jet, on the directivity angle θ and the fully expanded primary stream Mach number M_1. This function is given by

$$D_s(\theta, M_1) = \begin{cases} 1 & (\theta \le \theta_m) \\ 1.189 & (\theta > \theta_m) \end{cases}$$

where θ_m is the Mach angle defined by

$$\theta_m = \text{Arcsin}\,(1/M_1) \tag{20}$$

The spectral content of the shock noise is provided through the function $F_s(S_s)$ which depends on the Strouhal number S_s:

$$S_s = \frac{f^* d_{h,1}^*}{0.70 V_1^*} \beta \left[1 - M_\infty \cos(\theta - \delta)\right] \left[(1 + 0.7 V_1^* \cos\theta)^2 + (0.14 V_1^*)^2\right]^{1/2} \tag{21}$$

The function $F_s(S_s)$ is tabulated in table V and plotted in figure 5.

The total far-field jet noise will be the sum of the shock noise and the jet mixing noise.

The mean-square acoustic pressure for one engine, which is the sum of the jet mixing noise, as computed by equation (1), and the shock noise, as computed by equation (18), can be computed for each desired value of the frequency, polar directivity angle, and azimuthal directivity angle. The total noise is the mean-square acoustic pressure multiplied by the number of engines N for the output table. In addition, printed output is available of the mean-square pressure $\langle p^2 \rangle^*$ and sound pressure level SPL defined as

$$SPL = 10 \log_{10} \langle p^2 \rangle^* + 10 \log_{10} \frac{\rho_\infty^2 c_\infty^4}{p_{ref}^2} \tag{22}$$

Power level calculations are not performed by this module.

REFERENCES

1. Stone, James R.: Interim Prediction Method for Jet Noise. NASA TM X-71618, 1974.

2. Stone, James R.; and Montegani, Francis J.: An Improved Prediction Method for the Noise Generated in Flight by Circular Jets. NASA TM-81470, 1980.

TABLE I.- RANGE AND DEFAULT VALUES OF INPUT PARAMETERS

Input parameter	Minimum	Default	Maximum
A_e, m^2	0.01	$\pi/4$	10.0
N	1	1	4
r_s, m	0.01	$\sqrt{A_e}$	100
δ, deg	0	0	30
$A^*_{j,1}$	0.0001	1	10
$d^*_{e,1}$	$2 \times 10^{-2}/\sqrt{\pi}$	$2/\sqrt{\pi}$	$\sqrt{40/\pi}$
$d^*_{h,1}$	$2 \times 10^{-2}/\sqrt{\pi}$	$2/\sqrt{\pi}$	$\sqrt{40/\pi}$
M_1	0	1.0	1.25
T^*_1	0.7	1.0	4.0
V^*_1	0	1.0	2.5
ρ^*_1	0.2	1.0	1.2
$A^*_{j,2}$	0	0	10
M_2	0	0	1
T^*_2	0.7	1	4
V^*_2	0	0	2.5
ρ^*_2	0.2	1.0	1.2
c_∞, m/s	300	340.294	400
M_∞	0	0	0.9
ρ_∞, kg/m^3	1.0	1.225	1.5

TABLE II.- JET MIXING NOISE SPECTRAL DISTRIBUTION LEVEL $10 \log_{10} F_m$

$\log_{10} S_m$	$10 \log_{10} F_m$ for θ of -									
	0° to 110°	120°	130°	140°	150°	160°	170°	180°	190°	200°
-1.7	-39.1	-42.4	-43.0	-44.5	-42.4	-36.4	-32.8	-29.4	-25.6	-22.2
-1.6	-36.8	-40.0	-40.2	-41.3	-39.3	-31.9	-28.7	-25.6	-22.2	-19.2
-1.5	-34.5	-37.6	-37.4	-38.2	-36.2	-27.9	-25.0	-22.2	-19.2	-16.6
-1.4	-32.3	-35.2	-34.6	-35.0	-33.1	-24.3	-21.7	-19.2	-16.6	-14.3
-1.3	-30.0	-32.8	-31.8	-31.8	-29.9	-21.1	-18.8	-16.6	-14.3	-12.4
-1.2	-27.7	-30.4	-29.0	-28.7	-26.8	-18.3	-16.3	-14.3	-12.4	-10.9
-1.1	-25.4	-28.0	-26.2	-25.5	-23.6	-15.9	-14.1	-12.4	-10.9	-9.7
-1.0	-23.2	-25.6	-23.4	-22.4	-20.5	-13.8	-12.3	-10.9	-9.7	-8.9
-.9	-21.1	-23.2	-20.6	-19.3	-17.5	-12.1	-10.9	-9.7	-8.9	-8.4
-.8	-19.1	-20.8	-17.8	-16.1	-14.7	-10.8	-9.8	-8.9	-8.4	-8.9
-.7	-17.4	-18.5	-15.2	-13.2	-12.1	-9.9	-9.0	-8.4	-8.9	-9.9
-.6	-15.9	-16.2	-13.1	-11.3	-9.9	-9.2	-8.5	-8.9	-9.9	-11.8
-.5	-14.7	-14.1	-11.5	-10.0	-8.3	-8.7	-9.0	-9.9	-11.8	-13.9
-.4	-13.7	-12.2	-10.2	-9.4	-7.7	-9.2	-10.0	-11.8	-13.9	-16.0
-.3	-12.8	-10.9	-9.6	-9.1	-8.3	-10.2	-11.8	-13.9	-16.0	-18.1
-.2	-12.1	-10.2	-9.3	-9.4	-9.7	-12.0	-13.8	-16.0	-18.1	-20.2
-.1	-11.6	-9.9	-9.6	-9.9	-11.6	-13.9	-15.8	-18.1	-20.2	-22.3
0.0	-11.3	-10.2	-10.2	-10.9	-13.4	-15.8	-17.8	-20.2	-22.3	-24.4
.1	-11.1	-10.6	-11.4	-12.4	-15.2	-17.7	-19.8	-22.3	-24.4	-26.5
.2	-11.2	-11.1	-12.7	-14.0	-17.0	-19.6	-21.8	-24.4	-26.5	-28.6
.3	-11.3	-11.8	-14.0	-15.6	-18.8	-21.5	-23.8	-26.5	-28.6	-30.7
.4	-11.7	-12.7	-15.3	-17.2	-20.6	-23.4	-25.8	-28.6	-30.7	-32.8
.5	-12.3	-13.7	-16.6	-18.8	-22.3	-25.3	-27.8	-30.7	-32.8	-34.9
.6	-13.0	-14.7	-18.0	-20.4	-24.1	-27.2	-29.8	-32.8	-34.9	-37.0
.7	-13.7	-15.8	-19.3	-22.1	-25.9	-29.1	-31.8	-34.9	-37.0	-39.1
.8	-14.6	-16.9	-20.7	-23.7	-27.7	-31.0	-33.8	-37.0	-39.1	-41.2
.9	-15.6	-18.0	-22.0	-25.3	-29.5	-32.9	-35.8	-39.1	-41.2	-43.3
1.0	-16.7	-19.2	-23.4	-26.9	-31.3	-34.8	-37.8	-41.2	-43.3	-45.4
1.1	-17.8	-20.4	-24.7	-28.5	-33.1	-36.7	-39.8	-43.3	-45.4	-47.5
1.2	-18.9	-21.6	-26.1	-30.1	-34.9	-38.6	-41.8	-45.4	-47.5	-49.6
1.3	-20.1	-22.8	-27.5	-31.7	-36.7	-40.5	-43.8	-47.5	-49.6	-51.7
1.4	-21.3	-24.0	-28.8	-33.3	-38.5	-42.4	-45.8	-49.6	-51.7	-53.8
1.5	-22.4	-25.2	-30.2	-34.9	-40.3	-44.3	-47.8	-51.7	-53.8	-55.9
1.6	-23.6	-26.4	-31.5	-36.5	-42.0	-46.2	-49.8	-53.8	-55.9	-58.0
1.7	-24.8	-27.6	-32.8	-38.1	-43.8	-48.1	-51.8	-55.9	-58.0	-60.1
1.8	-26.0	-28.8	-34.1	-39.7	-45.6	-50.0	-53.8	-58.0	-60.1	-62.2
1.9	-27.2	-30.0	-35.5	-41.3	-47.4	-51.9	-55.8	-60.1	-62.2	-64.3

TABLE III.- JET MIXING NOISE DIRECTIVITY LEVEL $10 \log_{10} D_m$

θ, deg	$10 \log_{10} D_m$
110.0	0.00
120.0	-.51
130.0	-1.07
140.0	-1.56
150.0	-1.98
160.0	-2.55
170.0	-3.00
180.0	-3.50
190.0	-4.01
200.0	-4.52

TABLE IV.- FREQUENCY SHIFT PARAMETER f_s

$\log \left(1 + A^*_{j,2}/A^*_{j,1}\right)$	f_s for V^*_2/V^*_1 of -				
	0.20	0.40	0.60	0.80	1.00
0.00	0.00	0.00	0.00	0.00	0.00
.05	.04	.05	.06	.05	.04
.10	.07	.09	.12	.10	.08
.15	.11	.13	.18	.15	.12
.20	.14	.17	.23	.20	.16
.25	.16	.21	.28	.25	.20
.30	.19	.25	.33	.29	.23
.35	.21	.28	.37	.33	.26
.40	.24	.31	.41	.37	.30
.45	.25	.35	.45	.40	.32
.50	.27	.38	.48	.43	.35
.55	.28	.41	.51	.46	.38
.60	.28	.43	.53	.48	.41
.65	.29	.46	.56	.52	.43
.70	.29	.48	.59	.54	.45
.75	.30	.51	.61	.56	.48
.80	.30	.53	.64	.59	.50
.85	.30	.55	.65	.61	.52
.90	.30	.57	.67	.63	.54
.95	.30	.59	.69	.64	.56
1.00	.30	.61	.71	.65	.58
1.05	.30	.63	.73	.68	.60
1.10	.30	.65	.74	.69	.61
1.15	.30	.66	.75	.70	.63
1.20	.30	.68	.77	.72	.65
1.25	.30	.69	.78	.73	.66
1.30	.30	.71	.79	.74	.67
1.35	.30	.72	.81	.75	.69
1.40	.30	.73	.82	.76	.70
1.45	.30	.74	.83	.77	.71
1.50	.30	.76	.84	.78	.73
1.55	.30	.77	.85	.80	.74
1.60	.30	.78	.86	.81	.75

TABLE V.- SHOCK NOISE SPECTRAL DISTRIBUTION

LEVEL $10 \log_{10} F_s$

$\log_{10} S_s$	$10 \log_{10} F_s$
-1.8	-94.60
-1.7	-89.60
-1.6	-84.60
-1.5	-79.60
-1.4	-74.60
-1.3	-69.60
-1.2	-64.60
-1.1	-59.60
-1.0	-54.60
-.9	-49.60
-.8	-44.60
-.7	-39.60
-.6	-34.60
-.5	-29.60
-.4	-24.60
-.3	-19.60
-.2	-14.60
-.1	-9.60
0.0	-7.60
.1	-8.60
.2	-9.60
.3	-10.60
.4	-11.60
.5	-12.60
.6	-13.60
.7	-14.60
.8	-15.60
.9	-16.60
1.0	-17.60
1.1	-18.60
1.2	-19.60
1.3	-20.60
1.4	-21.60
1.5	-22.60
1.6	-23.60
1.7	-24.60
1.8	-25.60

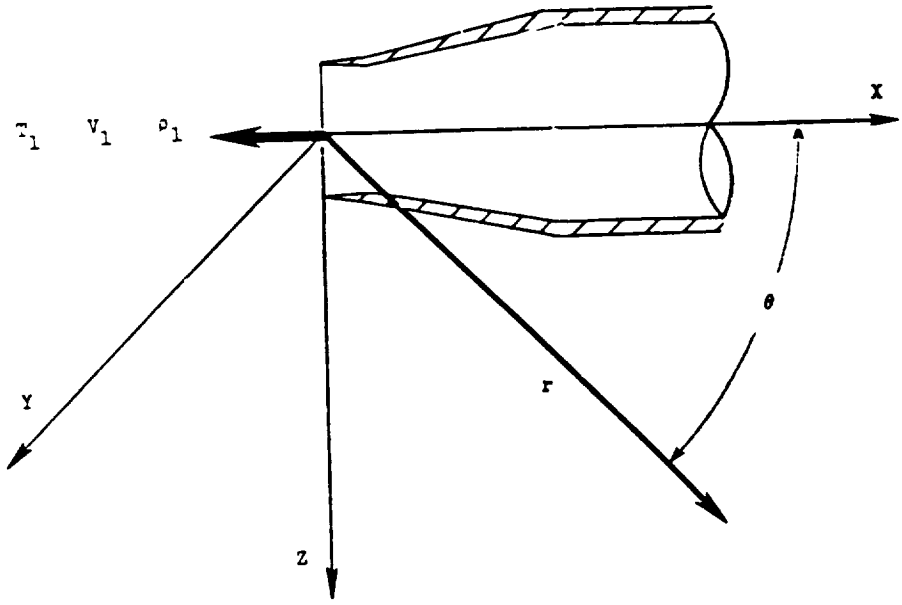

(a) Single stream circular nozzle.

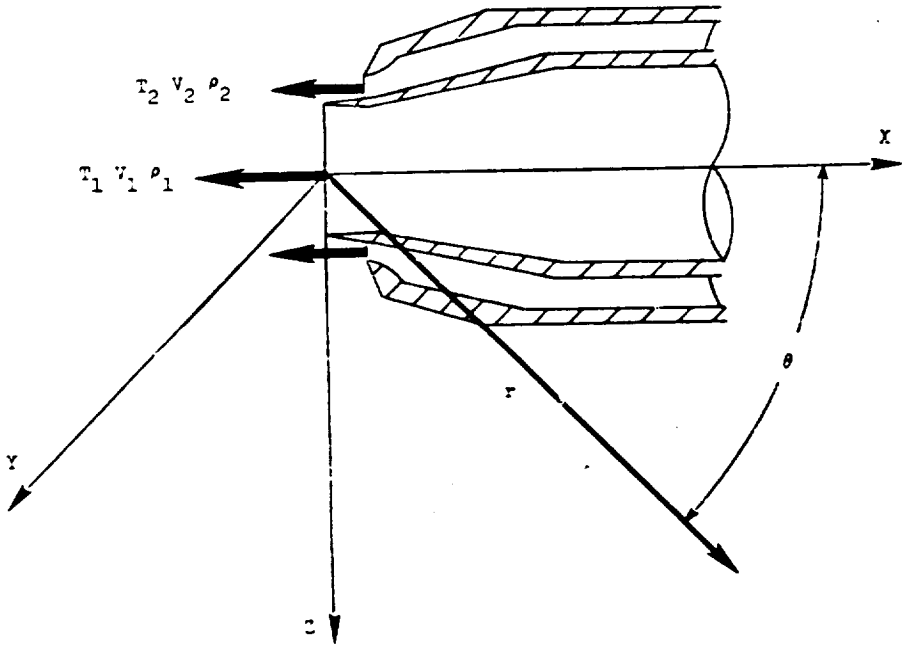

(b) Dual stream coaxial nozzle.

Figure 1.- Schematic diagrams of nozzles.

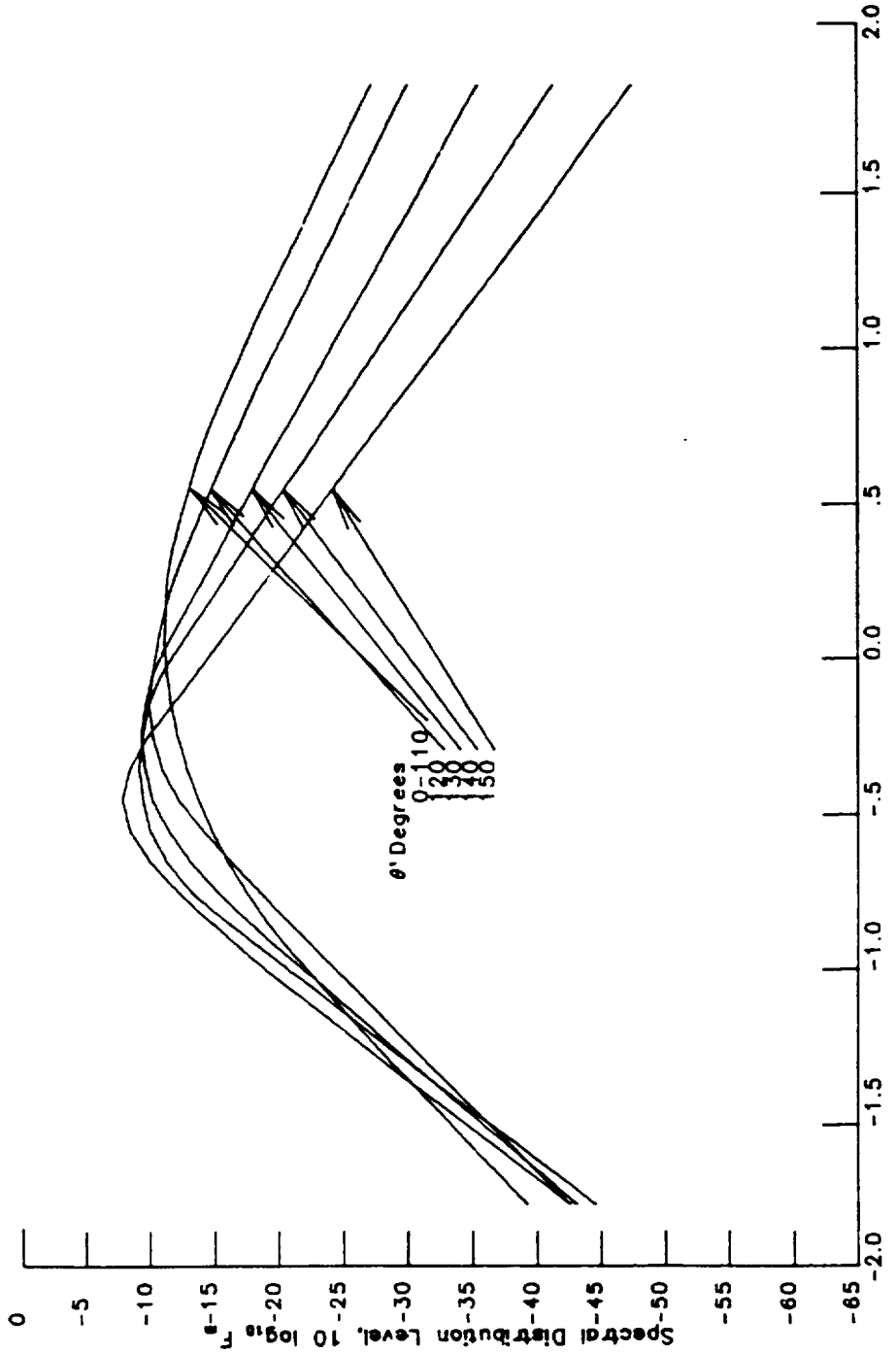

Figure 2.- Jet mixing noise spectral distribution level.

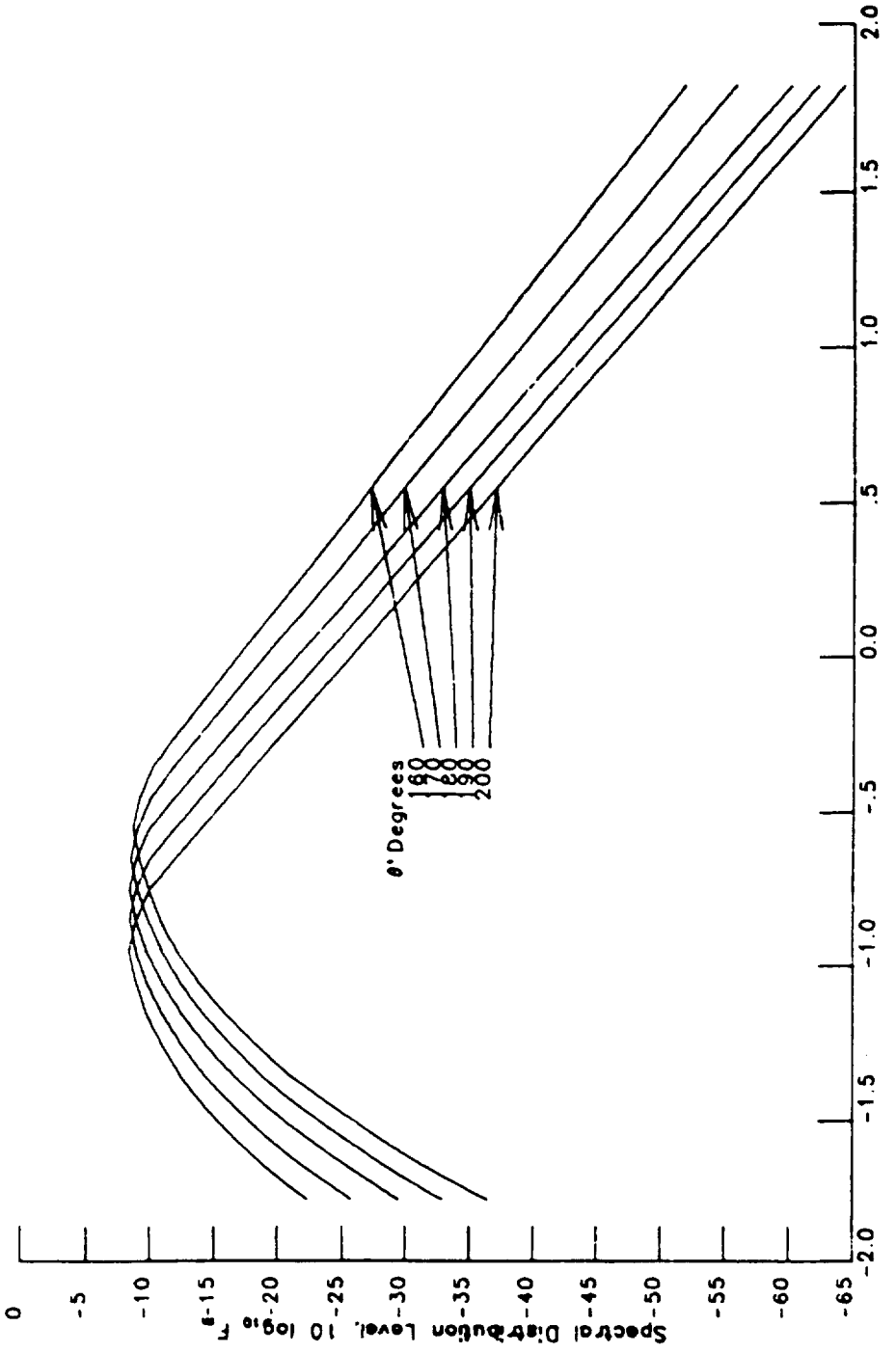

Figure 2.- Concluded.

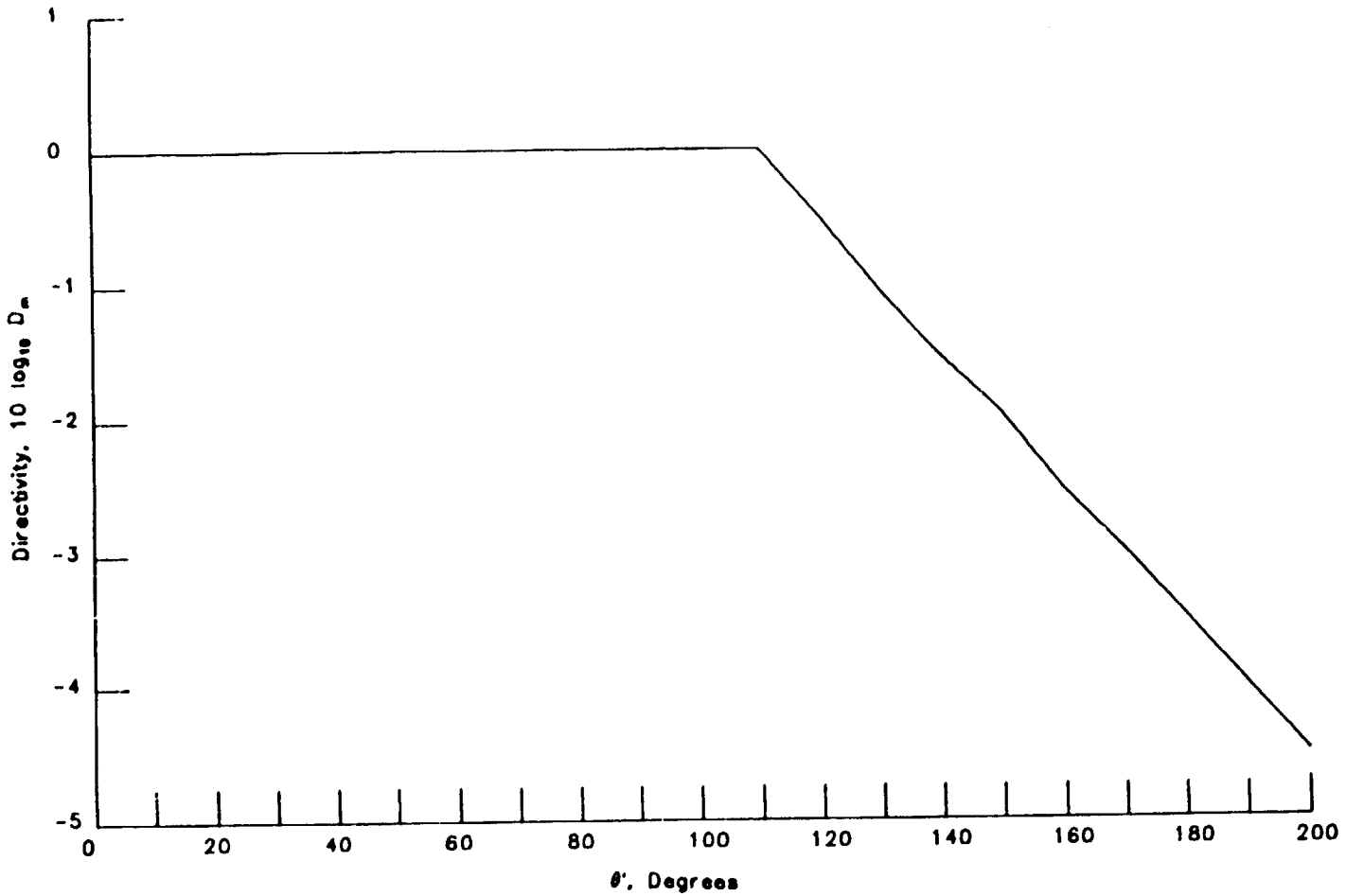

Figure 3.- Jet mixing noise directivity factor $D_m(\theta')$.

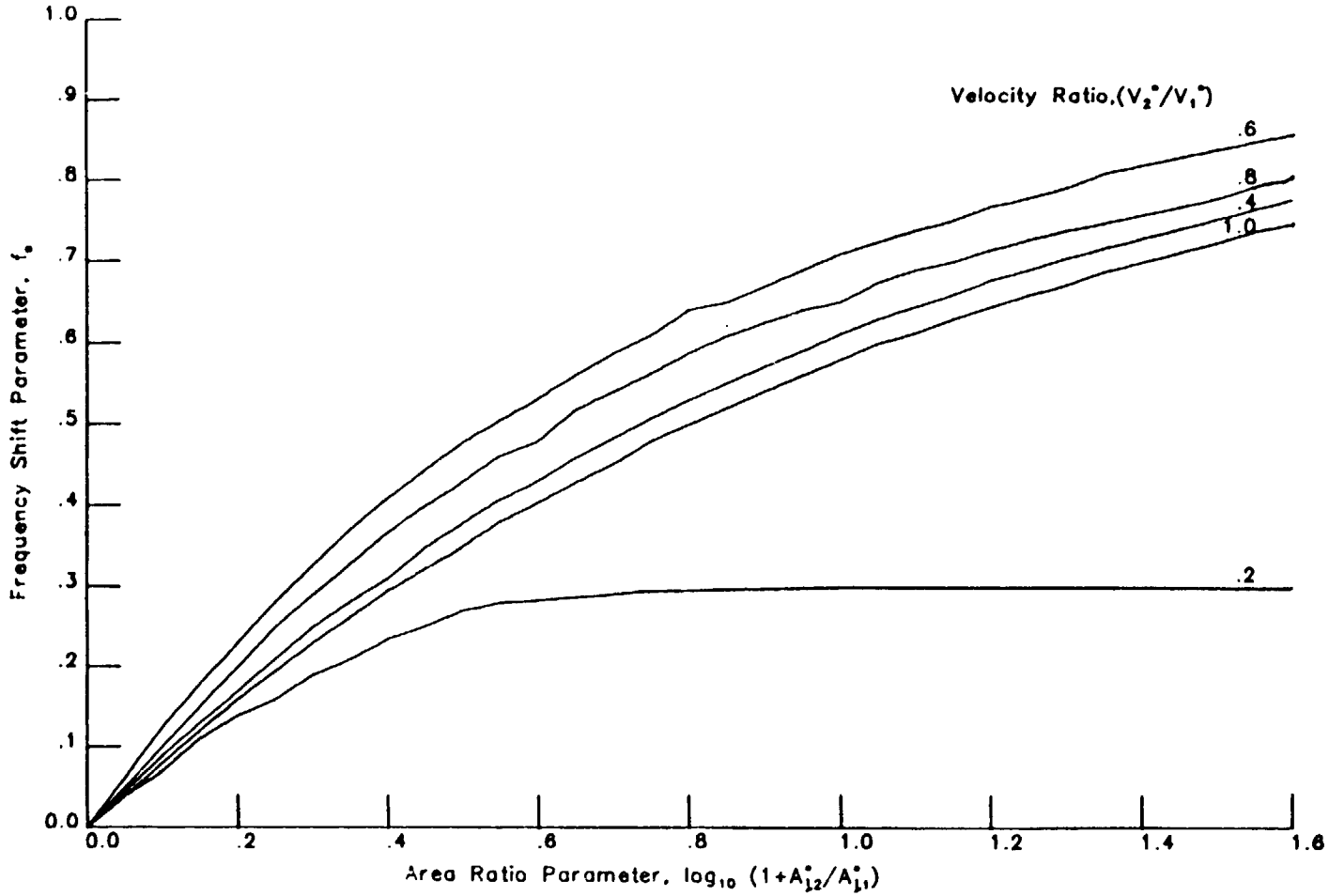

Figure 4.- Frequency shift parameter f_s.

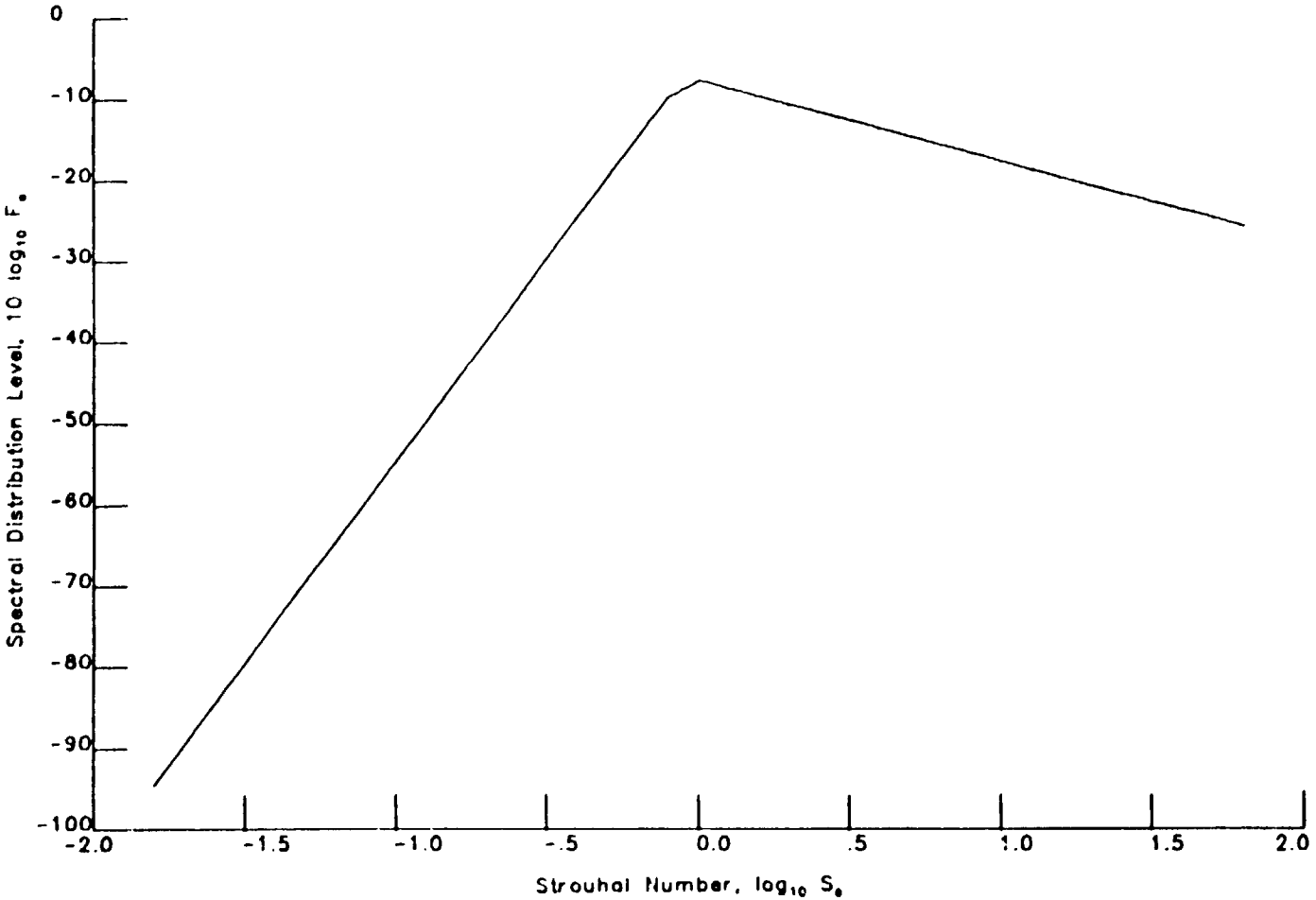

Figure 5.- Shock noise spectral distribution level.

8.7 DUAL STREAM COANNULAR JET NOISE MODULE

INTRODUCTION

The Dual Stream Coannular Jet Noise Module predicts the noise characteristics of a coannular jet exhaust nozzle with an inverted velocity profile. The dual stream jet has a secondary, or outer, flow which has a higher jet velocity than the primary flow. The method converts the coannular jet to an equivalent single stream jet with the same thrust, mass flow, and energy. The prediction is based on the method developed by Pao and Russell as presented in references 1 and 2.

The method requires input of several parameters. The two-nozzle exit flow states can be provided by the Jet Noise Parameters Module or directly by the user. Additional user-provided parameters are required. The module is executed once for each set of values of the input parameters. The output is a table of the mean-square acoustic pressure as a function of frequency, polar directivity angle, and azimuthal directivity angle. Although the jet noise is assumed not to vary with azimuthal directivity angle, it is introduced so that the output table is compatible with other noise tables.

SYMBOLS

A	fully expanded jet area, m^2 (ft^2)
A_e	engine reference area, m^2 (ft^2)
c_∞	ambient speed of sound, m/s (ft/s)
D	directivity function
d_{eq}	equivalent jet diameter, m (ft)
d_h	jet hydraulic diameter, m (ft)
f	frequency, Hz
f^*	Helmholtz number, $f\sqrt{A_e}/c_\infty$
G	spectral distribution function
M_a	aircraft Mach number
m	forward velocity index
$\dot{m}$	mass flow rate, kg/s (slugs/s)

N	number of engines
P	power deviation factor
$\langle p^2 \rangle^*$	mean-square acoustic pressure, re $\rho_\infty^2 c_\infty^4$
p_{ref}	reference pressure, 1×10^{-5} Pa (4.177×10^{-7} lb/ft^2)
r_s	distance from nozzle exit to observer, m (ft)
r_s^*	dimensionless distance from nozzle exit to observer, re $\sqrt{A_e}$
S	Strouhal number
S_1	first peak Strouhal number
S_2	second peak Strouhal number
T	total temperature, K ($^\circ$R)
T_∞	ambient temperature, K ($^\circ$R)
V	jet velocity, m/s (ft/s)
α	relative spectral peak magnitude factor
α'	$= \alpha A_2/A_1$
γ	ratio of specific heats
δ	angle between flight vector and engine inlet axis, deg
θ	polar directivity angle, deg
Π^*	acoustic power, re $\rho_\infty c_\infty^3 A_{eq}$
Π_{ref}	reference power, 1×10^{-12} W (7.376×10^{-13} ft-lb/s)
ρ	jet density, kg/m^3 (slugs/ft^3)
ρ_∞	ambient density, kg/m^3 (slugs/ft^3)
σ	normalized Strouhal number
σ_1	first peak normalized Strouhal number
σ_2	second peak normalized Strouhal number
ϕ	azimuthal directivity angle, deg
ω	density exponent

Subscripts:

eq	equivalent jet
1	primary jet
2	secondary jet

Superscript:

*	dimensionless quantity

INPUT

The primary and secondary jet parameters are required from the output of the Jet Noise Parameters Module or from the user. Ambient conditions are required for computation of the Strouhal number and sound pressure levels. The frequency, polar directivity angle, and azimuthal directivity angle arrays establish the independent variable values for the output table. Finally, the engine reference area, number of engines, engine inlet axis offset, and distance to observer are required. The range and default values of the input parameters are given in table I.

Input Constants

A_e	engine reference area, m^2 (ft^2)
N	number of engines
r_s	distance from nozzle exit to observer, m (ft)
δ	angle between flight vector and engine inlet axis, deg

Primary Jet Parameters

A_1^*	primary jet area, re A_e
T_1^*	primary jet total temperature, re T_∞
V_1^*	primary jet velocity, re c_∞
ρ_1^*	primary jet density, re ρ_∞
γ_1	ratio of specific heats for primary jet

Secondary Jet Parameters

A_2^*	secondary jet area, re A_e
$d_{h,2}^*$	secondary jet hydraulic diameter, re $\sqrt{A_e}$

T_2^* secondary jet total temperature, re T_∞

V_2^* secondary jet velocity, re c_∞

ρ_2^* secondary jet density, re ρ_∞

γ_2 ratio of specific heats for secondary jet

Ambient Conditions

c_∞ ambient speed of sound, m/s (ft/s)

M_∞ aircraft Mach number

ρ_∞ ambient density, kg/m^3 (slugs/ft^3)

Independent Variable Arrays

f frequency, Hz

θ polar directivity angle, deg

ϕ azimuthal directivity angle, deg

OUTPUT

The output of this module is a table of the mean-square acoustic pressure as a function of frequency, polar directivity angle, and azimuthal directivity angle. In addition, the observer distance r_s is provided for the Propagation Module.

r_s distance from nozzle exit to observer, m (ft)

Double Stream Coannular Jet Noise Table

f frequency, Hz

θ polar directivity angle, deg

ϕ azimuthal directivity angle, deg

$\langle p^2(f,\theta,\phi)\rangle^*$ mean-square acoustic pressure, re $\rho_\infty^2 c_\infty^4$

METHOD

The noise prediction method determines the noise characteristics of a single equivalent jet which has the same total thrust, mass flow rate, and energy as the coannular jet. The 1/3-octave-band mean-square acoustic pressure is computed as a function of frequency, polar directivity angle,

and azimuthal directivity angle for the input conditions. The method used has been extracted from references 1 and 2. A schematic of a typical coannular jet nozzle is shown in figure 1.

The mass flow rate of the equivalent jet is given by

$$\dot{m}^*_{eq} = \dot{m}^*_1 + \dot{m}^*_2 \tag{1}$$

where $\dot{m}^* + \rho^* A^* V^*$. The equivalent jet velocity is computed by equating the equivalent jet thrust to the sum of the thrusts of the individual jets as

$$V^*_{eq} = \frac{V^*_1 \dot{m}^*_1 + V^*_2 \dot{m}^*_2}{\dot{m}^*_{eq}} \tag{2}$$

By assuming that the products of combustion do not affect the value of the gas constant, the equivalent jet temperature can be computed from the energy equation as

$$T^*_{eq} = \frac{\dot{m}^*_1 \frac{\gamma_1}{\gamma_1 - 1} T^*_1 + \dot{m}^*_2 \frac{\gamma_2}{\gamma_2 - 1} T^*_2}{\dot{m}^*_1 \frac{\gamma_1}{\gamma_1 - 1} + \dot{m}^*_2 \frac{\gamma_2}{\gamma_2 - 1}} \tag{3}$$

The equivalent specific heat ratio is determined by the mass average

$$\frac{\gamma_{eq}}{\gamma_{eq} - 1} = \frac{\dot{m}^*_1 \frac{\gamma_1}{\gamma_1 - 1} + \dot{m}^*_2 \frac{\gamma_2}{\gamma_2 - 1}}{\dot{m}^*_1 + \dot{m}^*_2} \tag{4}$$

The equivalent jet density is found from the condition that the jet static pressure is equal to the ambient static pressure. Rearranging the perfect gas law yields

$$\rho^*_{eq} = \left[T_{eq} - \frac{\gamma_{eq} - 1}{2} (V^*_{eq})^2 \right]^{-1} \tag{5}$$

and the equivalent jet area is

$$A^*_{eq} = \frac{\dot{m}^*_{eq}}{\rho^*_{eq} V^*_{eq}} \tag{6}$$

The equivalent jet diameter is

$$d_{eq}^* = \left(\frac{4A_{eq}^*}{\pi}\right)^{1/2} \tag{7}$$

The acoustic power Π^* is calculated for the equivalent jet using the single stream circular jet method. A coannular benefit factor Q is added to this relation to account for double stream effects. The resulting expression for the acoustic power is

$$\Pi^* = (6.67 \times 10^{-5})(\rho_{eq}^*)^{\omega}(V_{eq}^*)^8 P(V_{eq}^*) Q(V_{eq}^*, V_2^*/V_1^*) \tag{8}$$

The power deviation factor P is a function of the velocity ratio $\log_{10} V_{eq}^*$ and is given in table II and plotted in figure 2. The density exponent ω is a function of the velocity ratio $\log_{10} V_{eq}^*$ and is given in table III and plotted in figure 3. The coannular benefit factor Q is a function of velocity ratio V_2^*/V_1^* and velocity ratio $\log_{10} V_{eq}^*$ and is given in table IV and plotted in figure 4.

The mean-square pressure is computed from the acoustic power using a normalized directivity function and a normalized spectrum function. For a directivity angle less than 110°, the 1/3-octave-band mean-square pressure is

$$\langle p^2 \rangle^* = \frac{\Pi^* A_{eq}^*}{4\pi (r_s^*)^2} \frac{D(\theta, V_{eq}^*)}{1 - M_\infty \cos(\theta - \delta)} G(\theta, \sigma_1) \left(\frac{V_{eq}^* - M_\infty}{V_{eq}^*}\right)^{m(\theta)} \tag{9}$$

and for directivity angles greater than 110°,

$$\langle p^2 \rangle^* = \frac{\Pi^* A_{eq}^*}{4\pi (r_s^*)^2} \frac{D(\theta, V_{eq}^*)}{1 - M_\infty \cos(\theta - \delta)} \left[\frac{G(\theta, \sigma_1)}{1 + \alpha'} + \frac{\alpha' G(\theta, \sigma_2)}{1 + \alpha'}\right] \left(\frac{V_{eq}^* - M_\infty}{V_{eq}^*}\right)^{m(\vartheta)} \tag{10}$$

where $r_s^* = r_s / \sqrt{A_e}$. The directivity function D in equations (9) and (10) is a function of polar directivity angle θ and velocity ratio $\log_{10} V_{eq}^*$ and is given in table V and plotted in figure 5. The terms which include the aircraft Mach number M_∞ account for forward flight effects. The forward flight index $m(\theta)$ is a function of polar directivity angle ϑ and is given in table VI and plotted in figure 6. The angle δ allows for an offset between the engine inlet axis and the direction of flight. The remaining terms in equations (9) and (10) give the spectral distribution.

.. coannular jet has a spectrum characterized by two peaks. The first peak corresponds to the characteristics of the outer stream and exists for all values of the polar directivity angle. The second peak corresponds to the characteristics of the mixed stream and exists for values of the polar directivity angle greater than 110^{o}. The spectra are expressed in terms of the Strouhal number defined as

$$S = \frac{f^* d^*_{eq}}{V^*_{eq} - M_\infty} (T^*_{eq})^{0.4} \tag{11}$$

The peak Strouhal numbers are a function of polar directivity angle θ and velocity ratio $\log_{10} V^*_{eq}$. The first peak Strouhal number S_1 is given in table VII and plotted in figure 7. The second peak Strouhal number S_2 is given in table VIII and plotted in figure 8. The Strouhal numbers used to define the spectrum shape are normalized with respect to the corresponding peak Strouhal number. The normalized Strouhal numbers σ are defined as

$$\sigma_1 = \frac{1}{S_1} \frac{f^* d^*_{eq}}{V^*_{eq} - M_\infty} (T^*_{eq})^{0.4} \tag{12}$$

and

$$\sigma_2 = \frac{1}{S_2} \frac{f^* d^*_{h,2}}{V^*_{eq} - M_\infty} (T^*_{eq})^{0.4} \tag{13}$$

The two spectral peaks differ in magnitude by a factor α'. This relative magnitude factor is defined as

$$\alpha' = \alpha(V^*_{eq}, V^*_2/V^*_1, \theta) \frac{A^*_2}{A^*_{eq}} \tag{14}$$

The spectral peak magnitude factor α is a function of the equivalent velocity $\log_{10} V^*_{eq}$, the velocity ratio V^*_2/V^*_1, and the polar directivity angle θ. The values of the spectral peak magnitude factor α are given in table IX and plotted in figure 9. The spectral shape is defined by the spectral distribution G as a function of polar directivity angle θ and normalized Strouhal number σ. The values of the spectral distribution G are given in table X and plotted in figure 10.

All of the terms in equations (9) and (10) have been defined. The mean-square acoustic pressure can be computed for each desired value of frequency, polar directivity angle, and azimuthal directivity angle. The total noise is the mean-square acoustic pressure multiplied by the number of engines N for the output table. In addition, printed output is available of the dimensionless mean-square pressure $\langle p^2 \rangle^*$, the sound pressure level SPL defined as

$$SPL = 10 \log_{10} \langle p^2 \rangle^* - 20 \log_{10} \frac{p_{ref}}{\rho_\infty c_\infty^2} \tag{15}$$

and the power level PWL defined as

$$PWL = 10 \log_{10} \Pi^* - 10 \log_{10} \frac{\Pi_{ref}}{\rho_\infty c_\infty^3 A^*_{eq} A_e} \tag{16}$$

REFERENCES

1. Pao, S. Paul: A Correlation of Mixing Noise From Coannular Jets With Inverted Flow Profiles. NASA TP-1301, 1979.

2. Russell, James W.: A Method for Predicting the Noise Levels of Coannular Jets With Inverted Velocity Profiles. NASA CR-3176, 1979.

TABLE I.- RANGE AND DEFAULT VALUES OF INPUT PARAMETERS

Input parameter	Minimum	Default	Maximum
A_e, m^2	0.01	$\pi/4$	10
N	1	1	4
r_s, m	0.01	$\sqrt{A_e}$	100
δ, deg	0	0	30
A_1^*	0.0001	1	10
T_1^*	0.7	1	6
V_1^*	0	1.0	2.5
M_∞	0	0	0.9
ρ_1^*	0.2	1.0	1.2
γ_1	1.3	1.4	1.5
A_2^*	0	0	10
$d_{n,2}^*$	0.01	1	10
T_2^*	0.7	1	6
V_2^*	0	0	2.5
ρ_2^*	0.2	1.0	1.2
γ_2	1.3	1.4	1.5
c_∞, m/s	200	340.294	400
ρ_∞, kg/m^3	0.2	1.225	1.5

TABLE II.- POWER DEVIATION FACTOR $\log_{10} P$

$\log_{10} V_{eq}/c_\infty$	$\log_{10} P$
-.400	-.130
-.350	-.130
-.300	-.130
-.250	-.130
-.200	-.130
-.150	-.120
-.100	-.100
-.050	-.050
0.000	0.000
.050	.100
.100	.210
.150	.320
.200	.410
.250	.430
.300	.410
.350	.310
.400	.140

TABLE III.- DENSITY EXPONENT, ω

$\log_{10} V_{eq}/c_\infty$	ω
-.450	-1.000
-.400	-.900
-.350	-.760
-.300	-.580
-.250	-.410
-.200	-.220
-.150	0.000
-.100	.220
-.050	.500
0.000	.770
.050	1.070
.100	1.390
.150	1.740
.200	1.950
.250	2.000

TABLE IV.- COANNULAR BENEFIT FACTOR $-10 \log_{10} Q$

V_2/V_1	$-10 \log_{10} Q$ for $\log_{10} V_{eq}/c_\infty$ of -						
	0	0.050	0.100	0.150	0.200	0.250	0.300
1.000	0.000	0.000	0.000	0.000	0.000	0.000	0.000
1.100	0.000	.294	.417	.526	.526	.417	.323
1.200	0.000	.588	.833	1.111	1.100	.833	.645
1.300	0.000	.882	1.375	2.200	2.077	1.545	.968
1.400	0.000	1.125	2.000	3.042	2.846	2.278	1.600
1.500	0.000	1.335	2.140	3.250	3.471	2.833	2.167
1.600	0.000	1.423	2.070	3.216	4.043	3.368	2.583
1.700	0.000	1.331	2.000	3.020	4.474	3.895	3.000
1.800	0.000	1.293	1.859	2.800	4.153	4.342	3.385
1.900	0.000	1.147	1.718	2.578	3.696	4.769	3.769
2.000	0.000	1.055	1.577	2.356	3.261	4.627	4.156
2.100	0.000	.968	1.437	2.133	2.907	4.104	4.547
2.200	0.000	.887	1.296	1.926	2.674	3.680	4.778
2.300	0.000	.806	1.155	1.741	2.442	3.280	4.369
2.400	0.000	.725	1.014	1.556	2.209	2.923	3.962
2.500	0.000	.645	.921	1.370	1.979	2.667	3.577
2.600	0.000	.564	.833	1.185	1.771	2.410	3.192
2.700	0.000	.483	.744	1.000	1.563	2.154	2.857
2.800	0.000	.402	.656	.907	1.354	1.911	2.571
2.900	0.000	.322	.568	.813	1.146	1.690	2.286
3.000	0.000	.241	.480	.720	.966	1.468	2.000

TABLE V.- DIRECTIVITY FUNCTION $\log_{10} D$

θ, deg	$\log_{10} D$ for $\log_{10} V_{eq}/c_\infty$ of -							
	0	0.050	0.100	0.150	0.200	0.250	0.300	0.350
0.000	-.860	-.970	-1.155	-1.240	-1.302	-1.344	-1.398	-1.449
10.000	-.840	-.950	-1.135	-1.215	-1.272	-1.314	-1.363	-1.409
20.000	-.820	-.930	-1.110	-1.185	-1.242	-1.284	-1.328	-1.369
30.000	-.800	-.910	-1.085	-1.155	-1.202	-1.244	-1.293	-1.319
40.000	-.770	-.880	-1.055	-1.115	-1.162	-1.204	-1.237	-1.269
50.000	-.740	-.850	-1.025	-1.075	-1.117	-1.154	-1.184	-1.209
60.000	-.700	-.810	-.985	-1.035	-1.072	-1.102	-1.120	-1.139
70.000	-.640	-.770	-.898	-.935	-.968	-.988	-1.016	-1.020
80.000	-.570	-.680	-.760	-.798	-.822	-.843	-.853	-.870
90.000	-.470	-.580	-.641	-.675	-.695	-.706	-.709	-.700
100.000	-.320	-.410	-.471	-.506	-.533	-.547	-.559	-.560
110.000	-.130	-.200	-.246	-.274	-.295	-.308	-.319	-.320
120.000	.090	.050	.014	-.002	-.013	-.016	-.016	-.010
130.000	.340	.320	.304	.304	.303	.306	.312	.320
140.000	.520	.570	.599	.626	.645	.661	.668	.671
150.000	.630	.700	.749	.781	.795	.802	.808	.809
160.000	.610	.630	.655	.614	.597	.573	.560	.550
170.000	.510	.450	.364	.296	.233	.174	.118	.120
180.000	.460	.380	.294	.226	.163	.099	.046	.060

TABLE VI.- FORWARD VELOCITY INDEX $m(\theta)$

θ, deg	$m(\theta)$
0.000	3.000
10.000	1.650
20.000	1.100
30.000	.500
40.000	.200
50.000	0.000
60.000	0.000
70.000	.100
80.000	.400
90.000	1.000
100.000	1.900
110.000	3.000
120.000	4.700
130.000	7.000
140.000	8.500
150.000	8.500
160.000	8.500
170.000	8.500
180.000	8.500

TABLE VII.- FIRST PEAK STROUHAL NUMBER $\log_{10} S_1$

θ, deg	$\log_{10} S_1$ for $\log_{10} V_{eq}/c_\infty$ of -							
	0	0.050	0.100	0.150	0.200	0.250	0.300	0.350
90.000	0.000	0.000	0.000	0.000	0.000	0.000	0.000	0.000
100.000	-.050	-.050	-.050	-.050	-.050	-.050	-.050	-.050
110.000	-.120	-.120	-.120	-.120	-.120	-.120	-.120	-.120
120.000	-.220	-.220	-.220	-.220	-.220	-.220	-.230	-.240
130.000	-.330	-.330	-.330	-.330	-.330	-.350	-.360	-.370
140.000	-.420	-.420	-.420	-.420	-.420	-.450	-.490	-.530
150.000	-.500	-.500	-.500	-.500	-.520	-.570	-.620	-.660
160.000	-.580	-.590	-.610	-.620	-.650	-.770	-.870	-.940
170.000	-.750	-.770	-.790	-.820	-.880	-1.060	-1.170	-1.250

TABLE VIII.- SECOND PEAK STROUHAL NUMBER $\log_{10} S_2$

θ, deg	$\log_{10} S_2$ for $\log_{10} V_{eq}/c_\infty$ of -							
	0	0.050	0.100	0.150	0.200	0.250	0.300	0.350
110.000	-.590	-.590	-.590	-.590	-.590	-.590	-.590	-.590
120.000	-.340	-.350	-.350	-.360	-.370	-.390	-.410	-.450
130.000	-.240	-.240	-.240	-.240	-.250	-.290	-.390	-.520
140.000	-.210	-.200	-.180	-.180	-.250	-.380	-.500	-.660
150.000	-.060	-.120	-.190	-.270	-.360	-.480	-.600	-.890
160.000	-.060	-.130	-.220	-.310	-.430	-.560	-.870	-1.270
170.000	-.030	-.130	-.240	-.360	-.520	-.690	-1.040	-1.340

TABLE IX.- SPECTRAL PEAK MAGNITUDE LEVEL $\log_{10} \alpha$

(a) $\theta = 110^{o}$

V_2/V_1	$\log_{10} \alpha$ for $\log_{10} V_{eq}/c_\infty$ of -							
	0	0.050	0.100	0.150	0.200	0.250	0.300	0.350
1.000	.370	.370	.370	.370	.370	.370	.370	.370
1.100	.370	.370	.370	.370	.370	.370	.370	.370
1.200	.370	.370	.370	.370	.370	.370	.370	.370
1.300	.370	.370	.370	.370	.370	.370	.370	.370
1.400	.370	.370	.370	.370	.370	.370	.370	.370
1.500	.370	.370	.370	.370	.370	.370	.370	.370
1.600	.370	.370	.370	.370	.370	.370	.370	.370
1.700	.370	.370	.370	.370	.370	.370	.370	.370
1.800	.370	.370	.370	.370	.370	.370	.370	.370
1.900	.370	.370	.370	.370	.370	.370	.370	.370
2.000	.370	.370	.370	.370	.370	.370	.370	.370
2.100	.370	.370	.370	.370	.370	.370	.370	.370
2.200	.370	.370	.370	.370	.370	.370	.370	.370

TABLE IX.- Continued

(b) $\theta = 120^{\circ}$

V_2/V_1	$\log_{10} \alpha$ for $\log_{10} V_{eq}/c_\infty$ of -							
	0	0.050	0.100	0.150	0.200	0.250	0.300	0.350
1.000	.358	.358	.358	.358	.358	.358	.358	.358
1.100	.359	.359	.360	.361	.362	.362	.363	.363
1.200	.361	.363	.364	.366	.368	.370	.372	.372
1.300	.370	.370	.370	.370	.370	.372	.375	.380
1.400	.375	.375	.376	.377	.378	.379	.382	.390
1.500	.380	.382	.383	.385	.388	.392	.396	.405
1.600	.381	.386	.392	.399	.402	.405	.411	.420
1.700	.397	.401	.405	.410	.414	.418	.424	.432
1.800	.409	.413	.417	.422	.425	.428	.434	.440
1.900	.425	.428	.431	.435	.436	.440	.446	.455
2.000	.440	.444	.448	.453	.455	.459	.465	.471
2.100	.461	.464	.467	.471	.473	.476	.481	.487
2.200	.461	.464	.467	.471	.473	.476	.481	.487

TABLE IX.- Continued

(c) $\theta = 130^{\circ}$

V_2/V_1	$\log_{10} \alpha$ for $\log_{10} V_{eq}/c_\infty$ of -							
	0	0.050	0.100	0.150	0.200	0.250	0.300	0.350
1.000	-.688	-.543	-.379	-.196	-.010	.159	.297	.380
1.100	-.414	-.304	-.181	-.042	.098	.237	.338	.419
1.200	-.253	-.162	-.060	.054	.175	.292	.373	.448
1.300	-.120	-.041	.047	.146	.223	.331	.407	.482
1.400	-.024	.045	.123	.210	.262	.361	.441	.506
1.500	.078	.134	.197	.268	.336	.407	.476	.528
1.600	.168	.214	.266	.324	.389	.451	.509	.548
1.700	.248	.286	.330	.378	.438	.492	.540	.568
1.800	.316	.349	.386	.428	.482	.530	.569	.588
1.900	.368	.398	.432	.471	.520	.561	.595	.604
2.000	.402	.432	.465	.503	.547	.584	.611	.620
2.100	.415	.446	.481	.521	.561	.597	.621	.630
2.200	.415	.446	.481	.521	.561	.597	.621	.630

TABLE IX.- Continued

(d) $\theta = 140^{\circ}$

V_2/V_1	$\log_{10} \alpha$ for $\log_{10} V_{eq}/c_\infty$ of -							
	0	0.050	0.100	0.150	0.200	0.250	0.300	0.350
1.000	-1.366	-1.224	-1.064	-.885	-.693	-.494	-.341	-.199
1.100	-.990	-.875	-.745	-.600	-.437	-.281	-.138	-.016
1.200	-.689	-.589	-.476	-.350	-.222	-.099	.021	.136
1.300	-.454	-.368	-.273	-.165	-.064	.050	.143	.245
1.400	-.252	-.181	-.101	-.012	.076	.166	.256	.356
1.500	-.059	-.008	.050	.115	.195	.275	.351	.435
1.600	.091	.137	.189	.247	.305	.377	.438	.504
1.700	.209	.251	.298	.351	.401	.461	.512	.568
1.800	.292	.331	.376	.425	.470	.524	.566	.612
1.900	.364	.400	.440	.486	.527	.569	.605	.644
2.000	.429	.460	.495	.535	.572	.608	.638	.672
2.100	.482	.512	.545	.583	.632	.640	.663	.690
2.200	.482	.512	.545	.583	.632	.640	.663	.690

TABLE IX.- Continued

(e) $\theta = 150^{\circ}$

V_2/V_1	$\log_{10} \alpha$ for $\log_{10} V_{eq}/c_\infty$ of -							
	0	0.050	0.100	0.150	0.200	0.250	0.300	0.350
1.000	-2.233	-1.972	-1.679	-1.351	-.989	-.653	-.417	-.281
1.100	-1.666	-1.461	-1.232	-.974	-.687	-.400	-.222	-.062
1.200	-1.362	-1.184	-.963	-.715	-.444	-.220	-.060	.065
1.300	-.965	-.792	-.598	-.380	-.177	-.037	.093	.205
1.400	-.689	-.403	-.308	-.200	-.054	.063	.171	.268
1.500	-.333	-.245	-.146	-.036	.069	.163	.248	.331
1.600	-.169	-.097	-.016	.074	.158	.235	.302	.374
1.700	-.020	.041	.108	.184	.254	.316	.376	.432
1.800	.098	.148	.204	.267	.326	.378	.430	.484
1.900	.211	.254	.303	.357	.407	.454	.504	.548
2.000	.326	.364	.406	.452	.495	.535	.569	.605
2.100	.437	.467	.500	.538	.574	.603	.632	.659
2.200	.536	.573	.612	.657	.688	.713	.737	.757

TABLE IX.- Concluded

(f) $\theta = 165^{\circ}$

V_2/V_1	$\log_{10} \alpha$ for $\log_{10} V_{eq}/c_\infty$ of -							
	0	0.050	0.100	0.150	0.200	0.250	0.300	0.350
1.000	-3.712	-3.231	-2.691	-2.085	-1.503	-.667	.169	.405
1.100	-3.191	-2.777	-2.313	-1.793	-1.248	-.466	.199	.388
1.200	-2.788	-2.412	-1.990	-1.516	-.999	-.329	.221	.376
1.300	-2.265	-1.960	-1.618	-1.234	-.759	-.186	.233	.369
1.400	-1.820	-1.573	-1.295	-.984	-.565	-.091	.242	.364
1.500	-1.567	-1.333	-1.071	-.776	-.419	-.014	.255	.357
1.600	-1.317	-1.107	-.872	-.607	-.309	.045	.259	.354
1.700	-1.094	-.914	-.713	-.487	-.215	.093	.264	.352
1.800	-1.013	-.827	-.617	-.383	-.139	.128	.272	.347
1.900	-.938	-.752	-.542	-.308	-.073	.161	.275	.345
2.000	-.873	-.687	-.477	-.243	-.025	.180	.277	.344
2.100	-.823	-.638	-.431	-.198	.012	.193	.277	.344
2.200	-.781	-.598	-.393	-.162	.039	.199	.277	.344

TABLE X.- SPECTRAL DISTRIBUTION $-\log_{10} G$

σ	$-\log_{10} G$ for θ of -						
	110°	120°	130°	140°	150°	160°	170°
-1.200	2.560	2.672	3.132	3.615	4.130	5.000	5.220
-1.100	2.380	2.452	2.842	3.255	3.740	4.460	4.710
-1.000	2.200	2.232	2.552	2.895	3.350	3.920	4.200
-.900	2.020	2.012	2.262	2.535	2.960	3.320	3.690
-.800	1.840	1.807	2.012	2.225	2.570	2.870	3.160
-.700	1.660	1.627	1.782	1.940	2.220	2.490	2.680
-.600	1.480	1.474	1.572	1.700	1.910	2.130	2.310
-.500	1.324	1.342	1.392	1.475	1.600	1.780	1.980
-.400	1.244	1.242	1.257	1.310	1.390	1.500	1.660
-.300	1.174	1.167	1.142	1.155	1.190	1.250	1.350
-.200	1.124	1.102	1.052	1.025	1.010	1.010	1.050
-.100	1.086	1.057	1.000	.941	.885	.630	.860
0.000	1.074	1.042	.982	.915	.640	.753	.651
.100	1.084	1.054	1.001	.945	.890	.840	.770
.200	1.114	1.098	1.057	1.035	1.000	.990	.970
.300	1.164	1.163	1.152	1.140	1.140	1.150	1.180
.400	1.232	1.234	1.257	1.265	1.290	1.330	1.370
.500	1.324	1.322	1.362	1.395	1.440	1.510	1.550
.600	1.420	1.432	1.482	1.515	1.590	1.670	1.750
.700	1.528	1.552	1.612	1.660	1.740	1.840	1.930
.800	1.649	1.692	1.752	1.795	1.890	2.010	2.130
.900	1.774	1.824	1.892	1.955	2.040	2.180	2.300
1.000	1.899	1.962	2.032	2.105	2.180	2.350	2.500
1.100	2.029	2.097	2.172	2.265	2.350	2.530	2.690
1.200	2.156	2.237	2.322	2.415	2.530	2.710	2.880
1.300	2.271	2.367	2.457	2.570	2.700	2.900	3.060
1.400	2.404	2.502	2.597	2.725	2.890	3.080	3.250
1.500	2.534	2.632	2.737	2.875	3.060	3.250	3.430

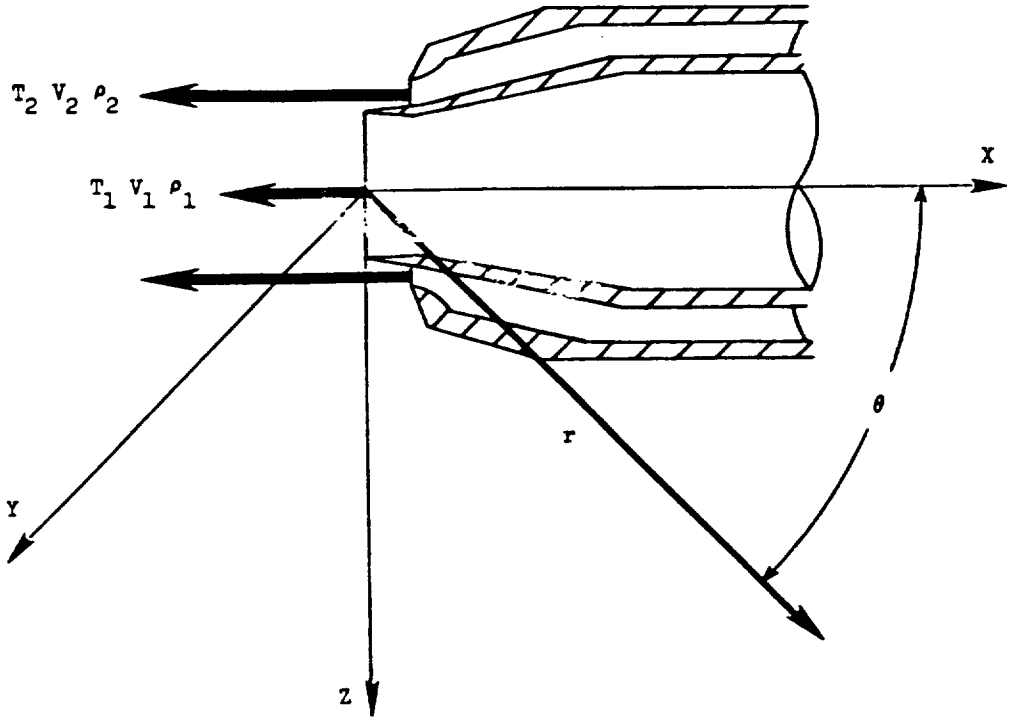

Figure 1.- Schematic diagram of double stream coannular nozzle.

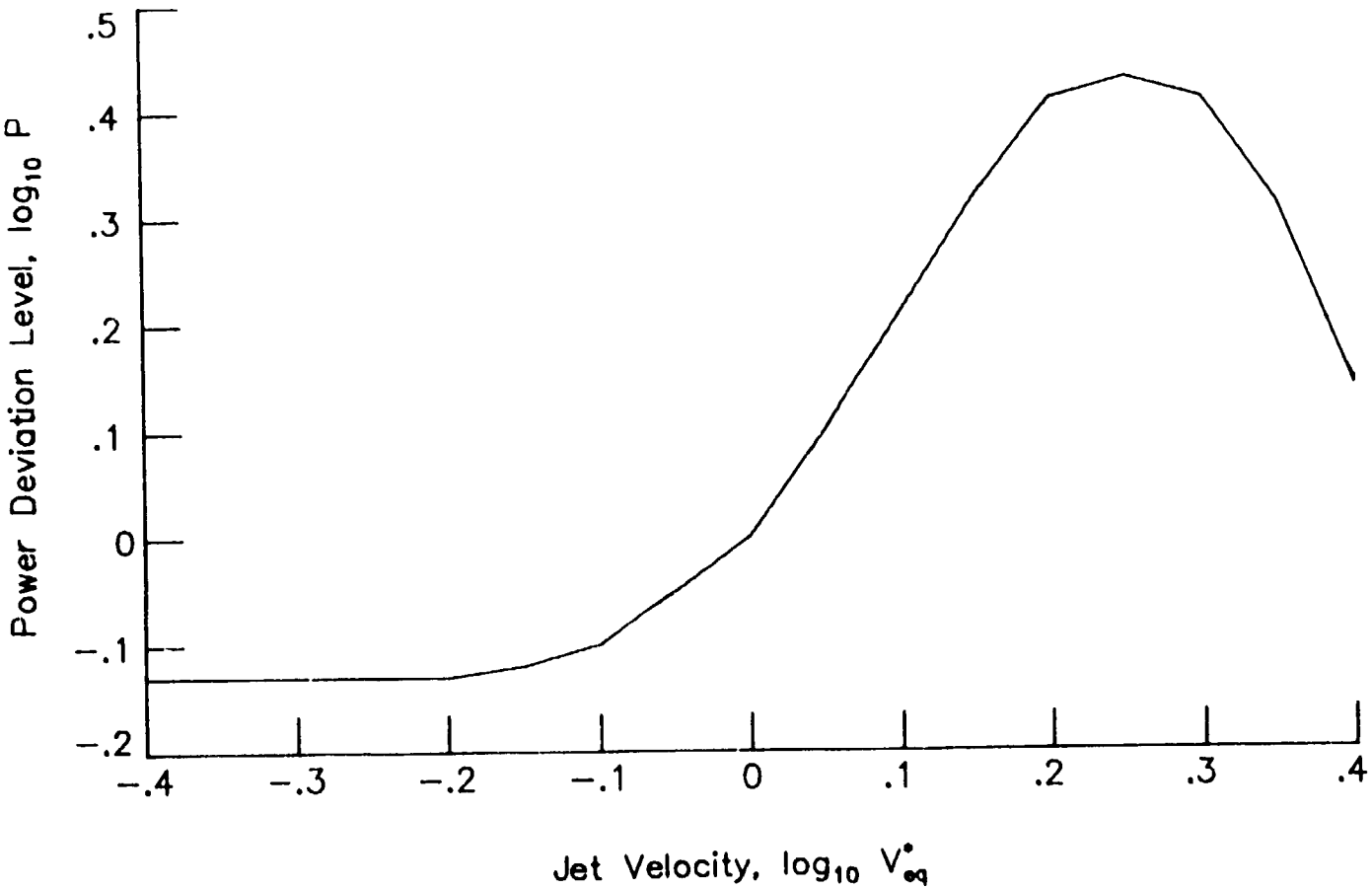

Figure 2.- Power deviation level.

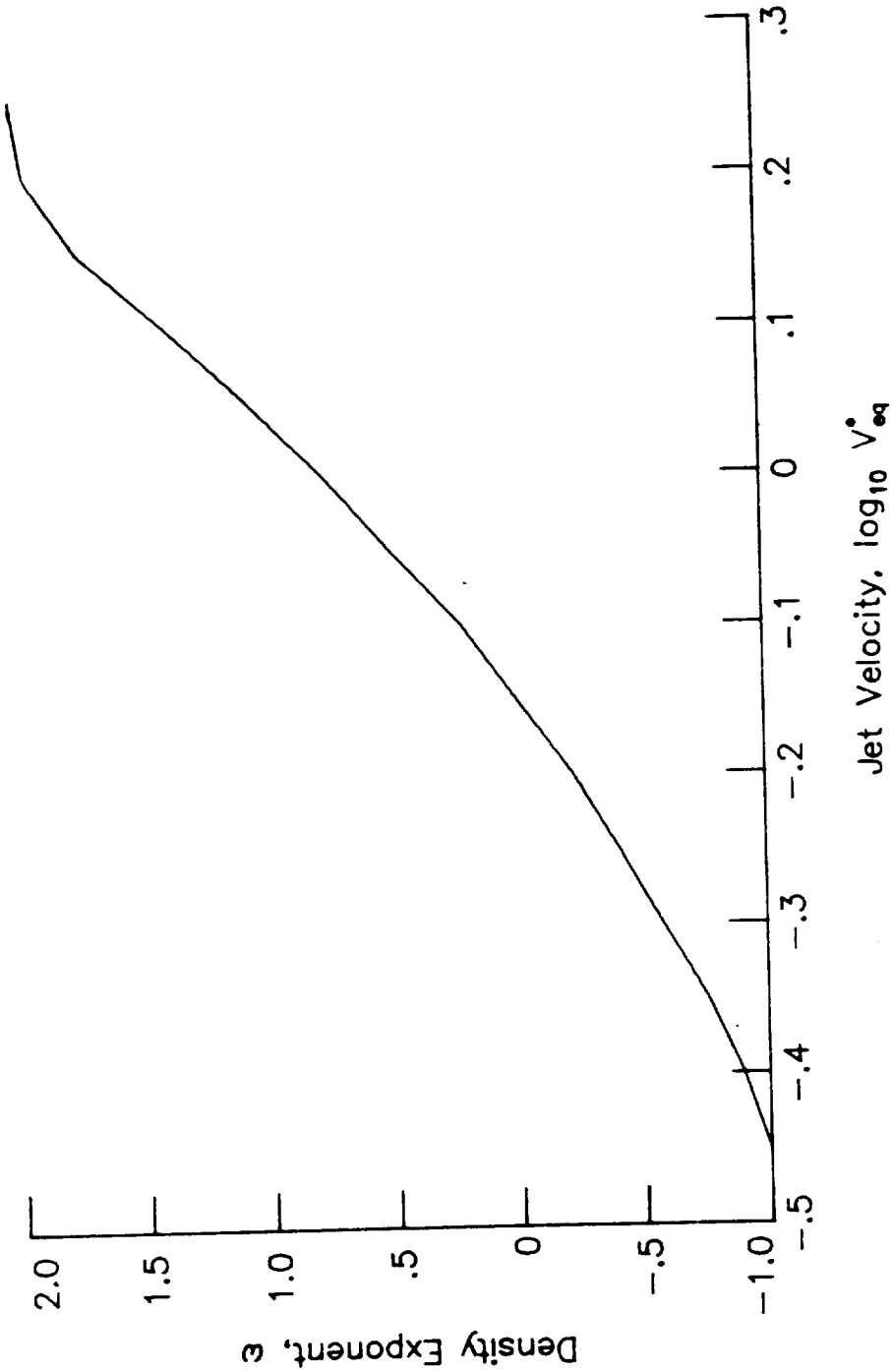

Figure 3.- Density exponent.

C - 3

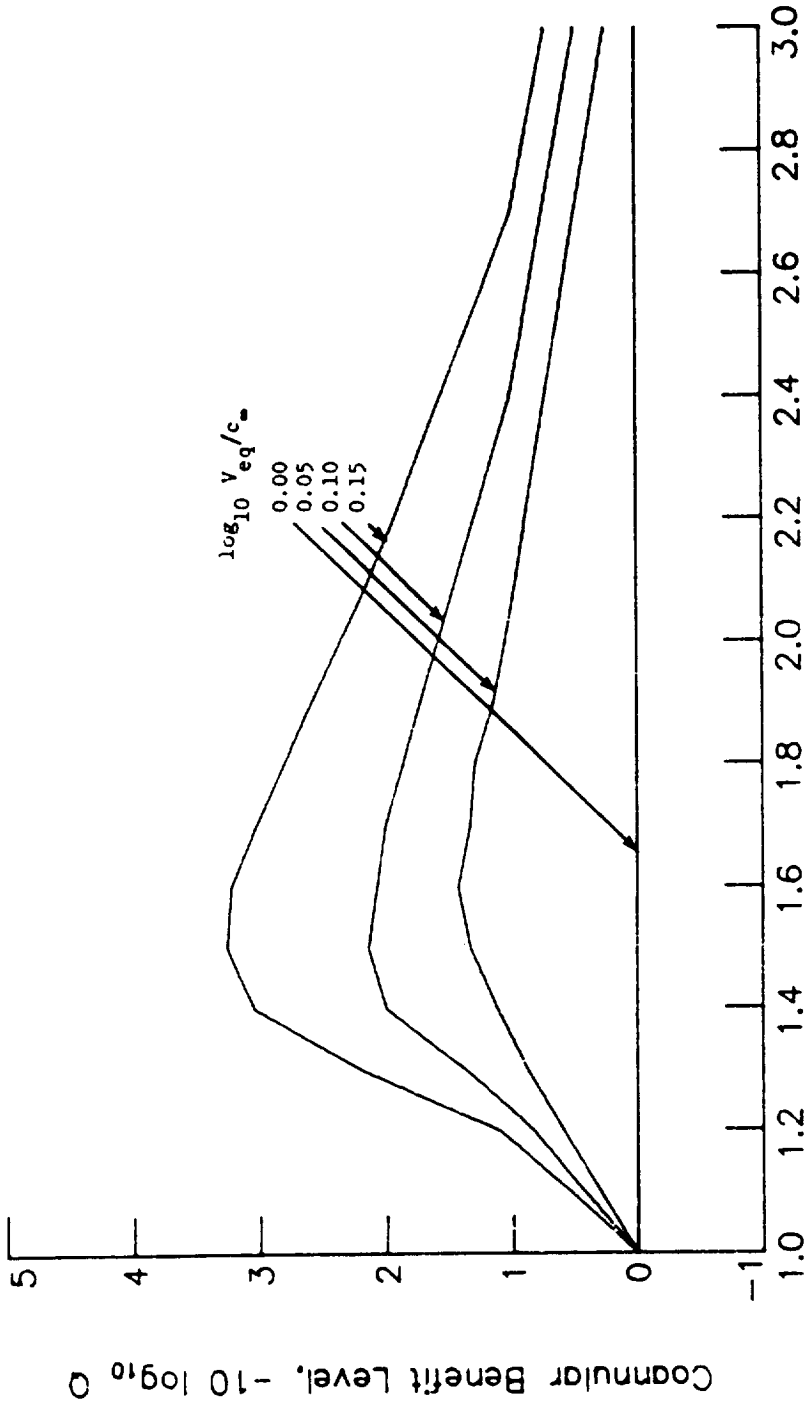

Figure 4.- Coannular benefit level.

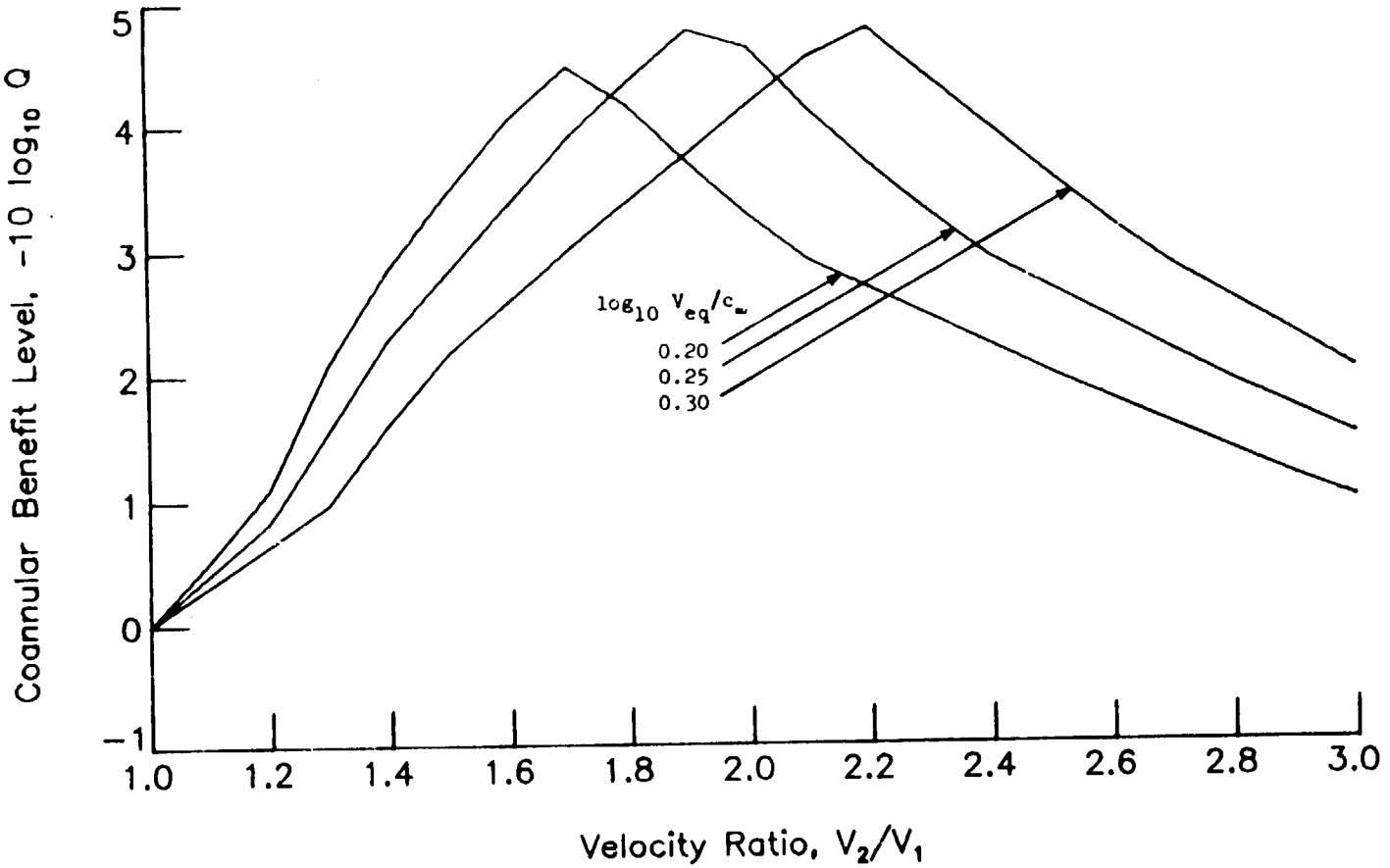

Figure 4.- Concluded.

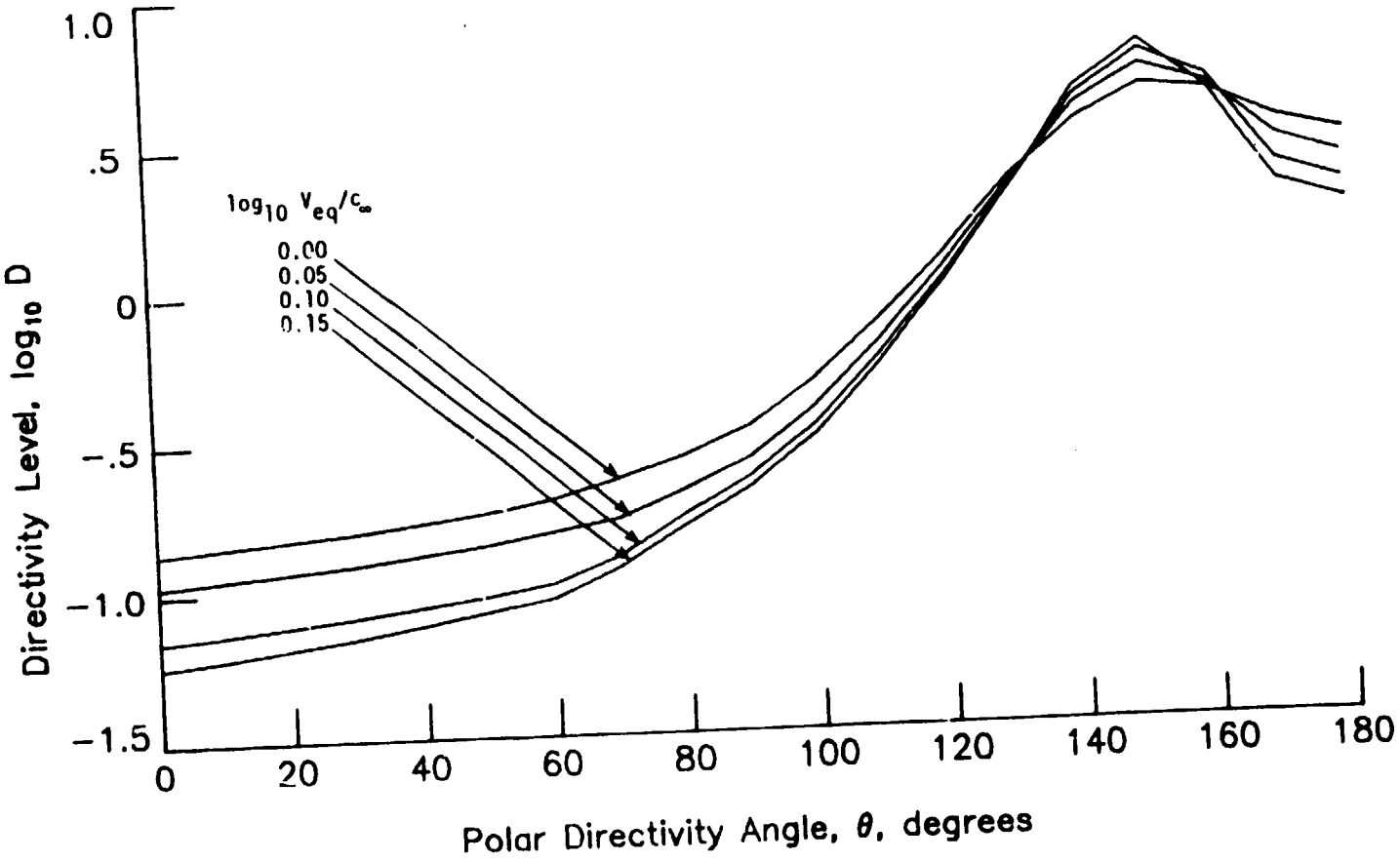

Figure 5.- Directivity level.

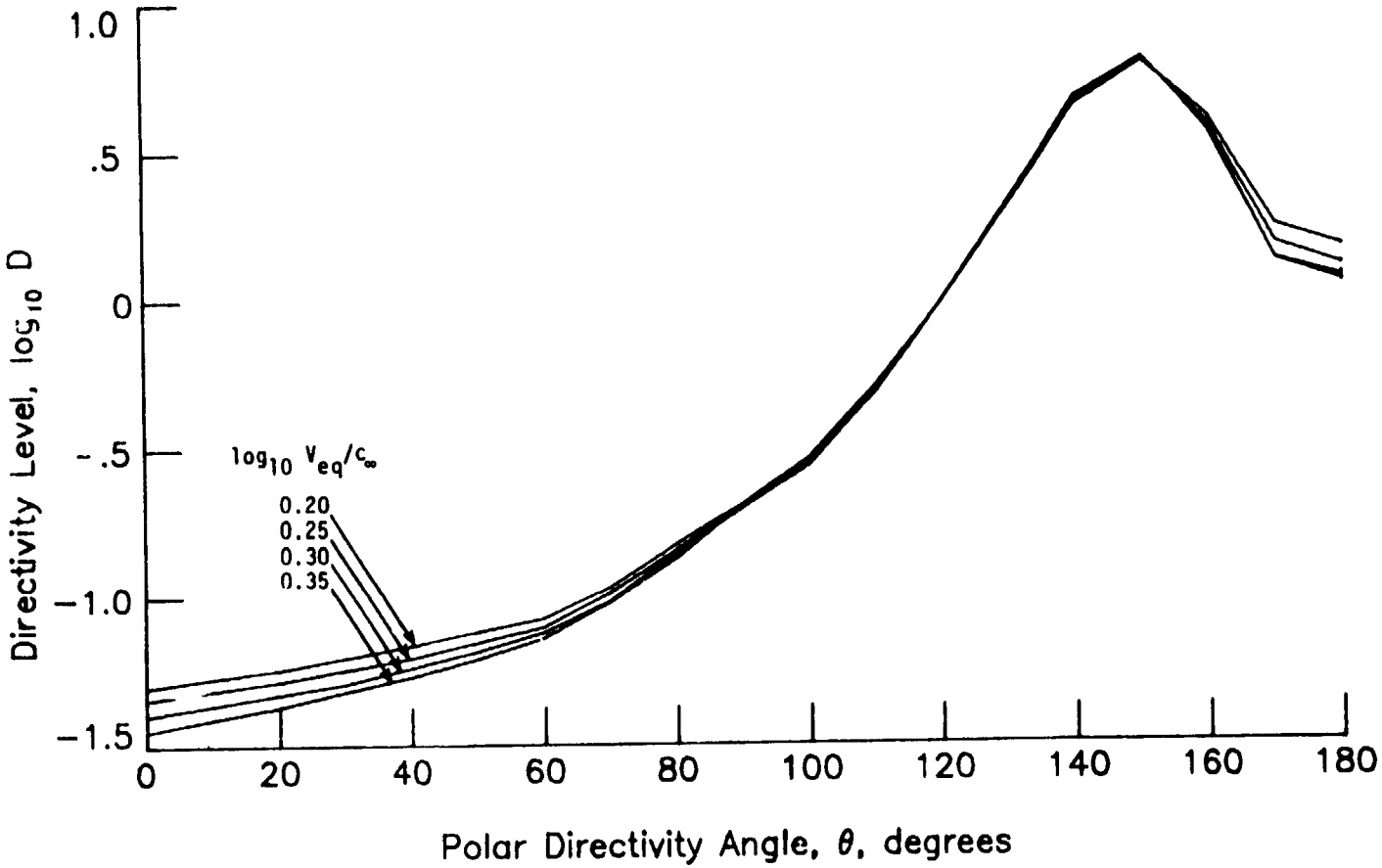

Figure 5.- Concluded.

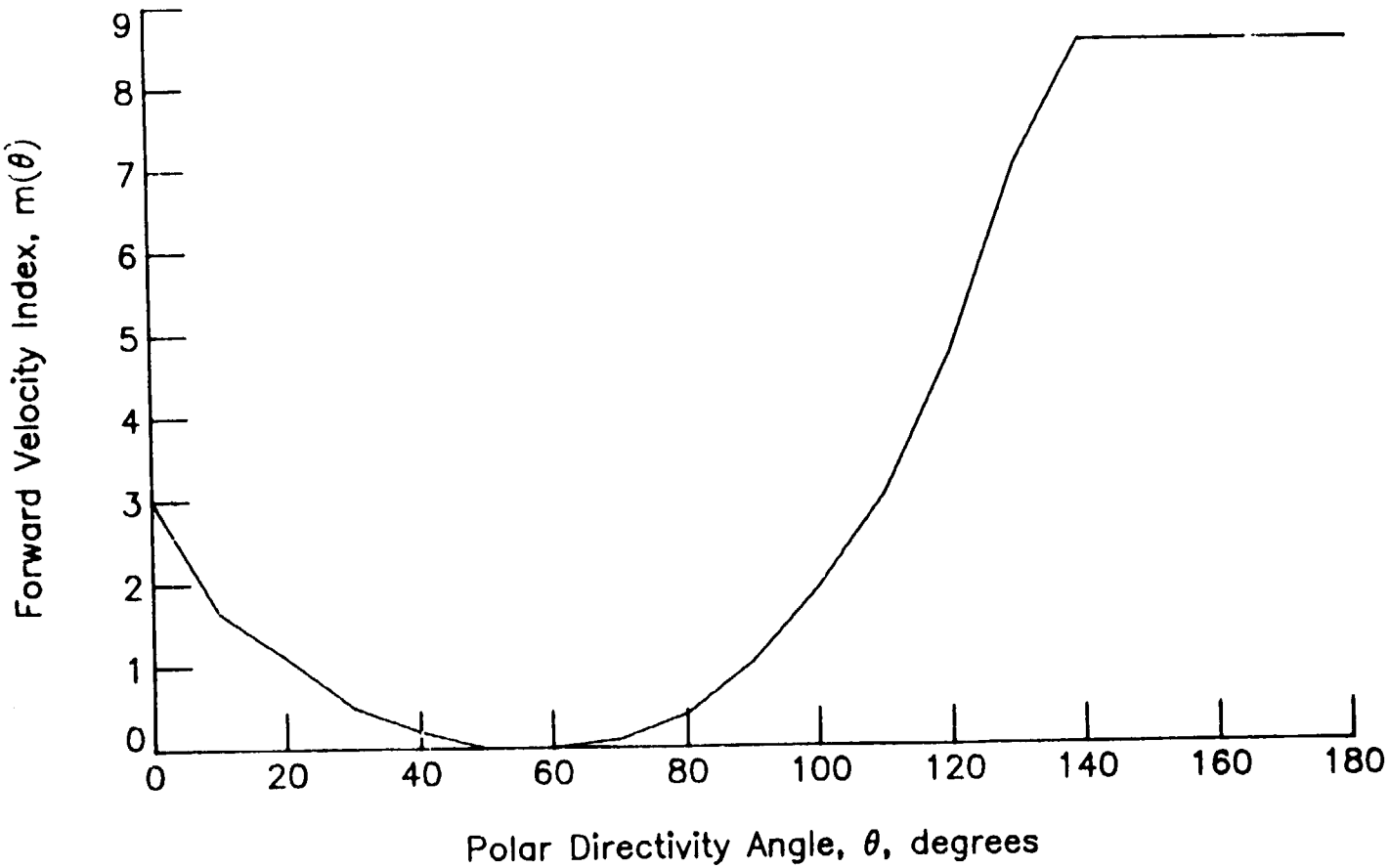

Figure 6.- Forward velocity index.

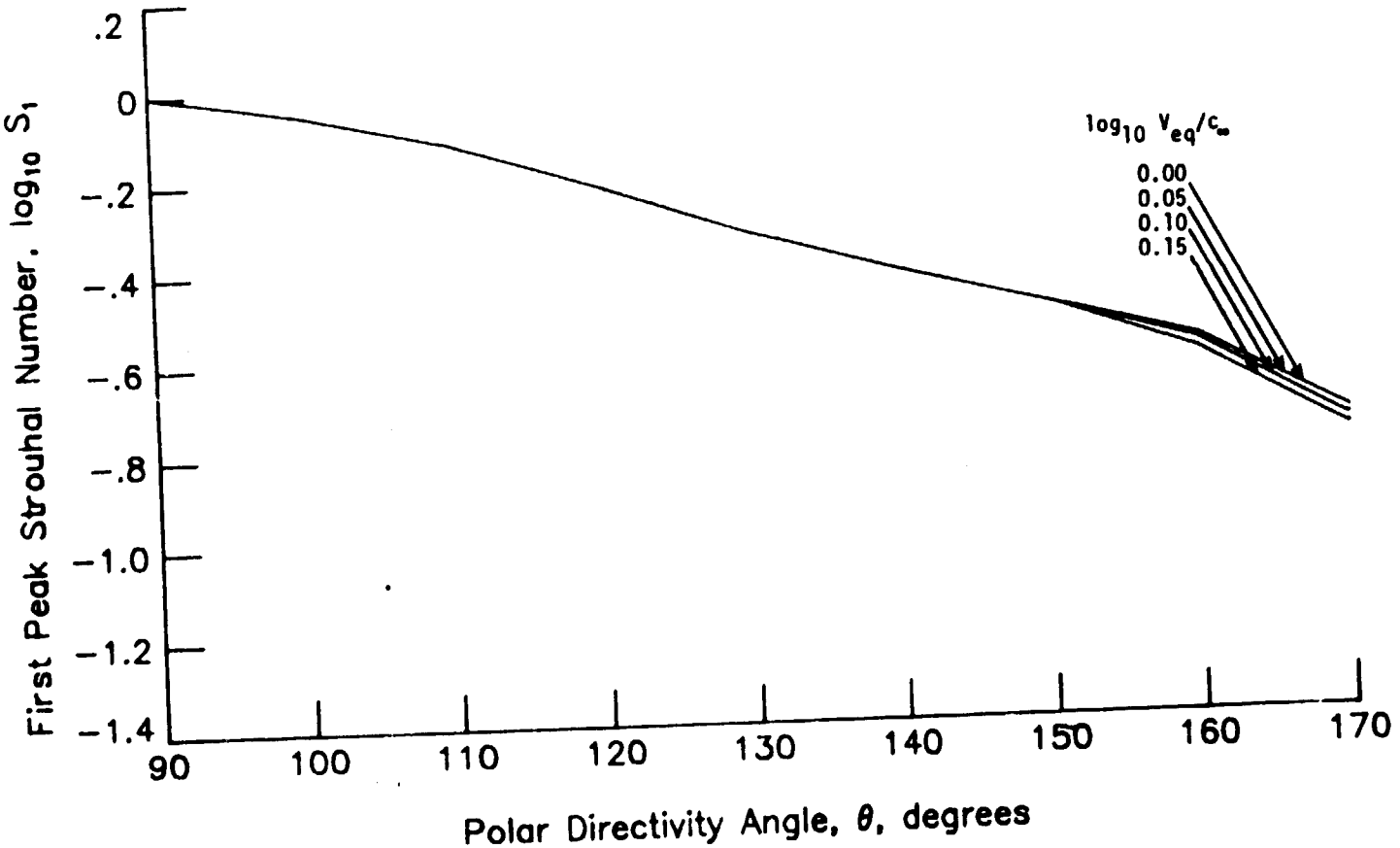

Figure 7.- First peak Strouhal number.

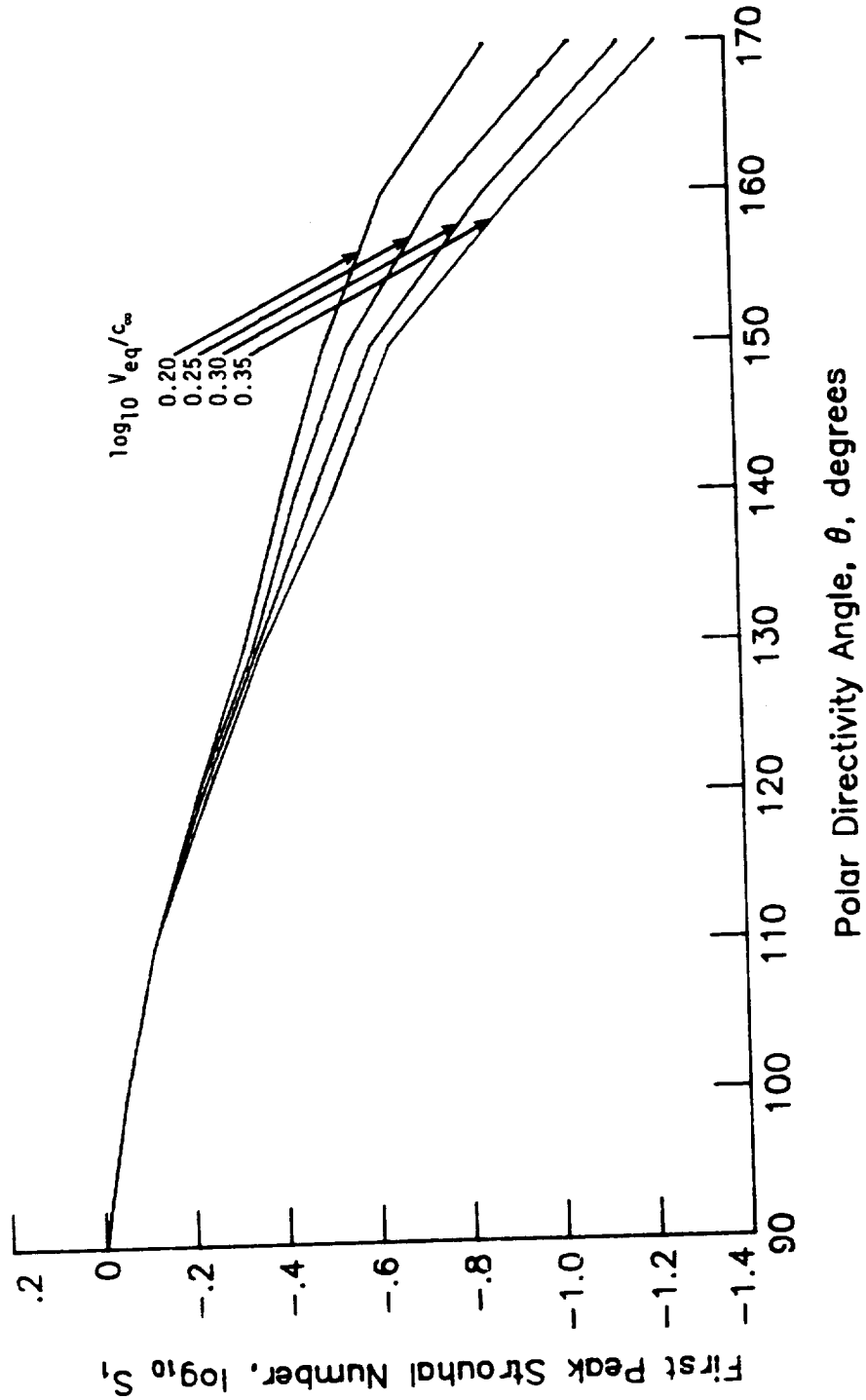

Figure 7.- Concluded.

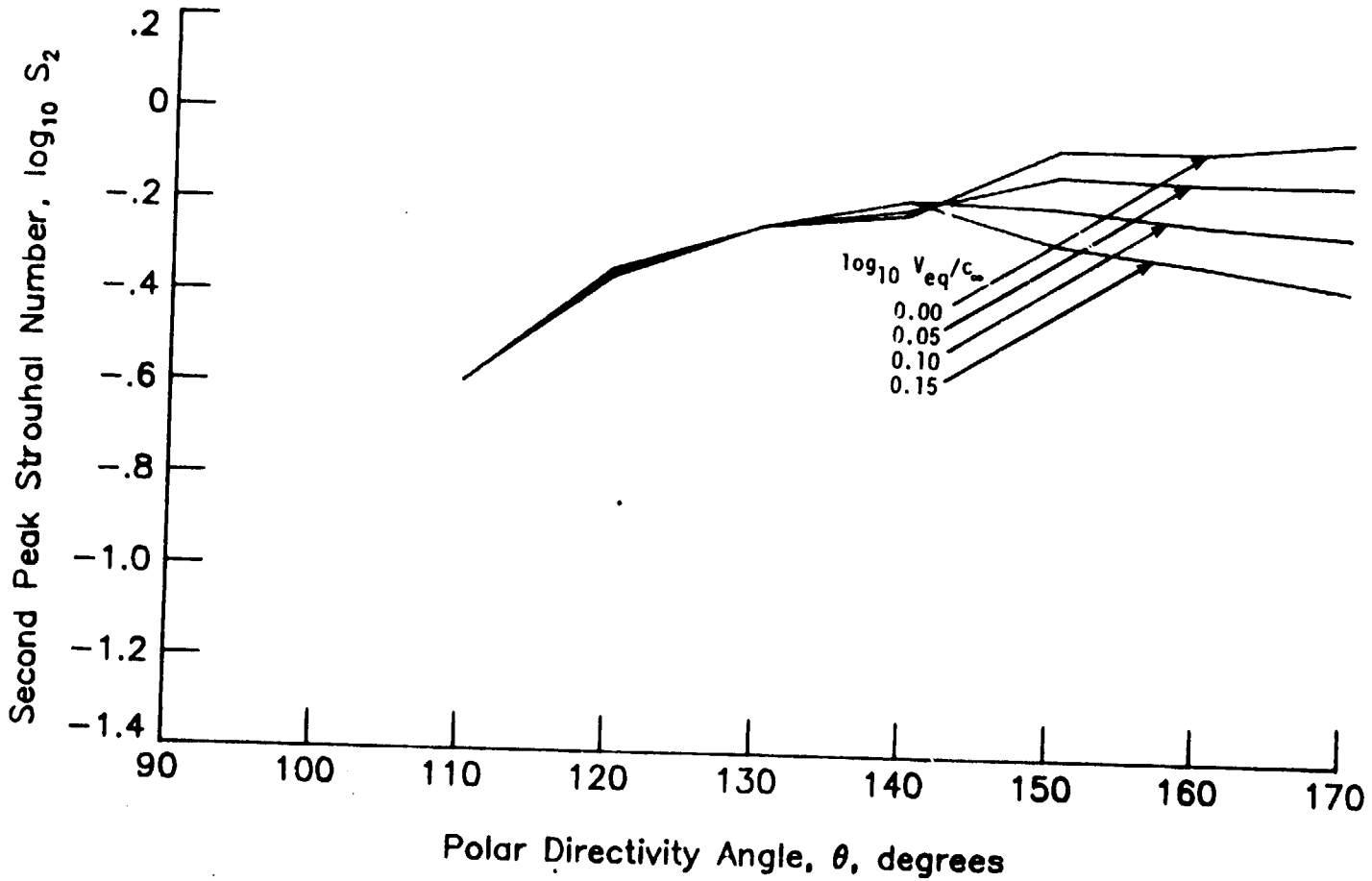

Figure 8.- Second peak Strouhal number.

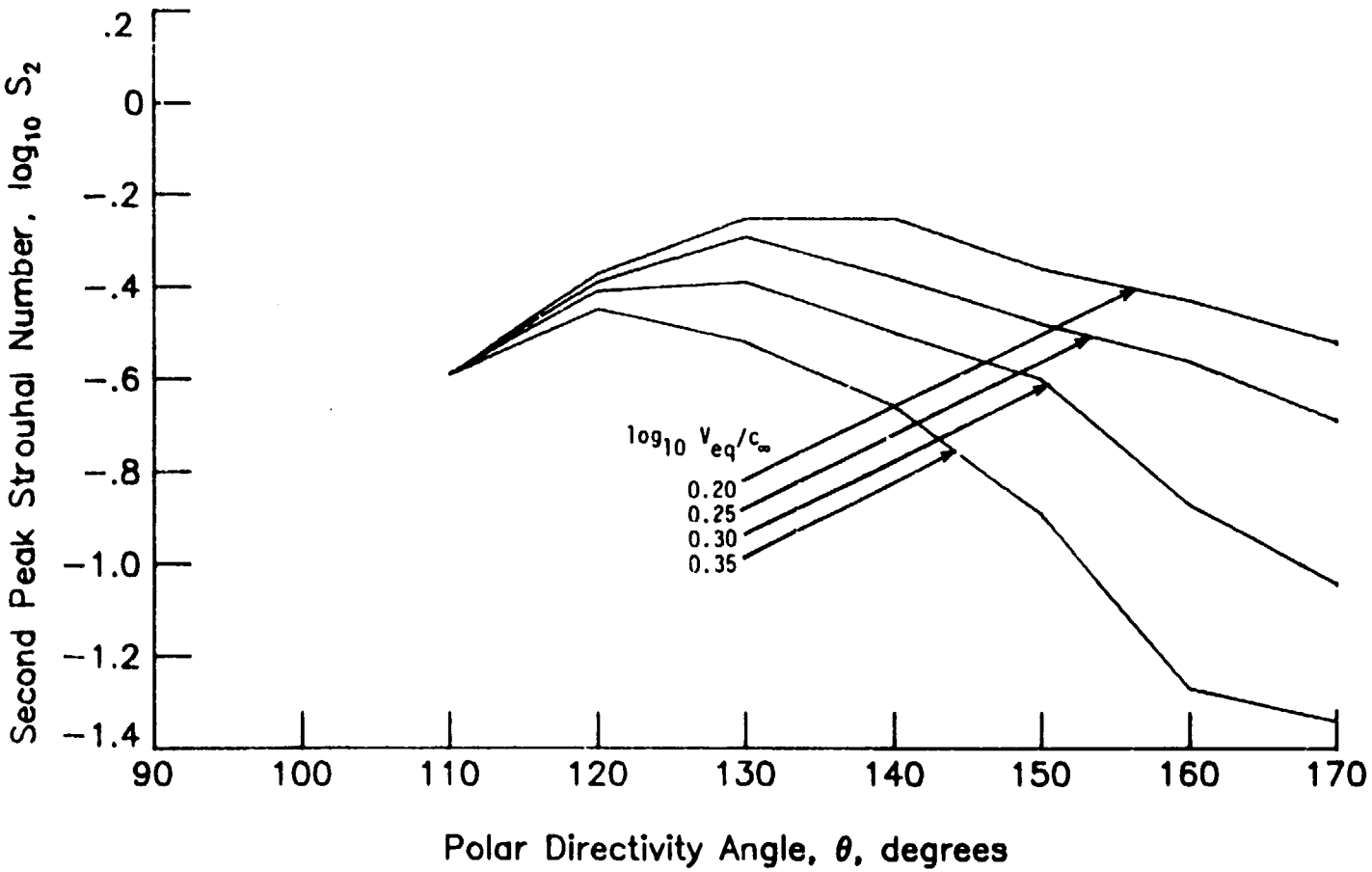

Figure 8.- Concluded.

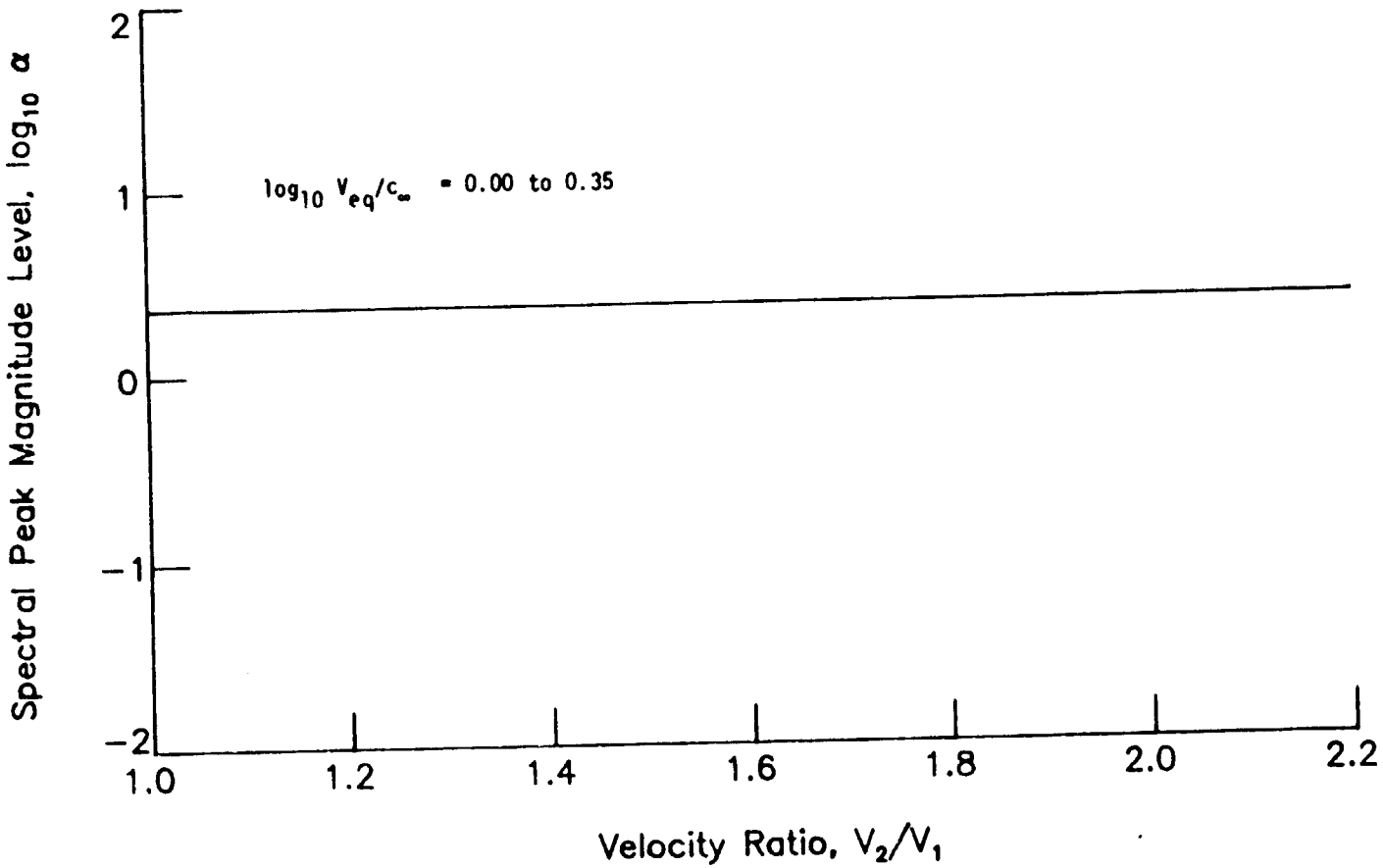

(a) $\theta = 110^{\circ}$.

Figure 9.- Spectral peak magnitude level.

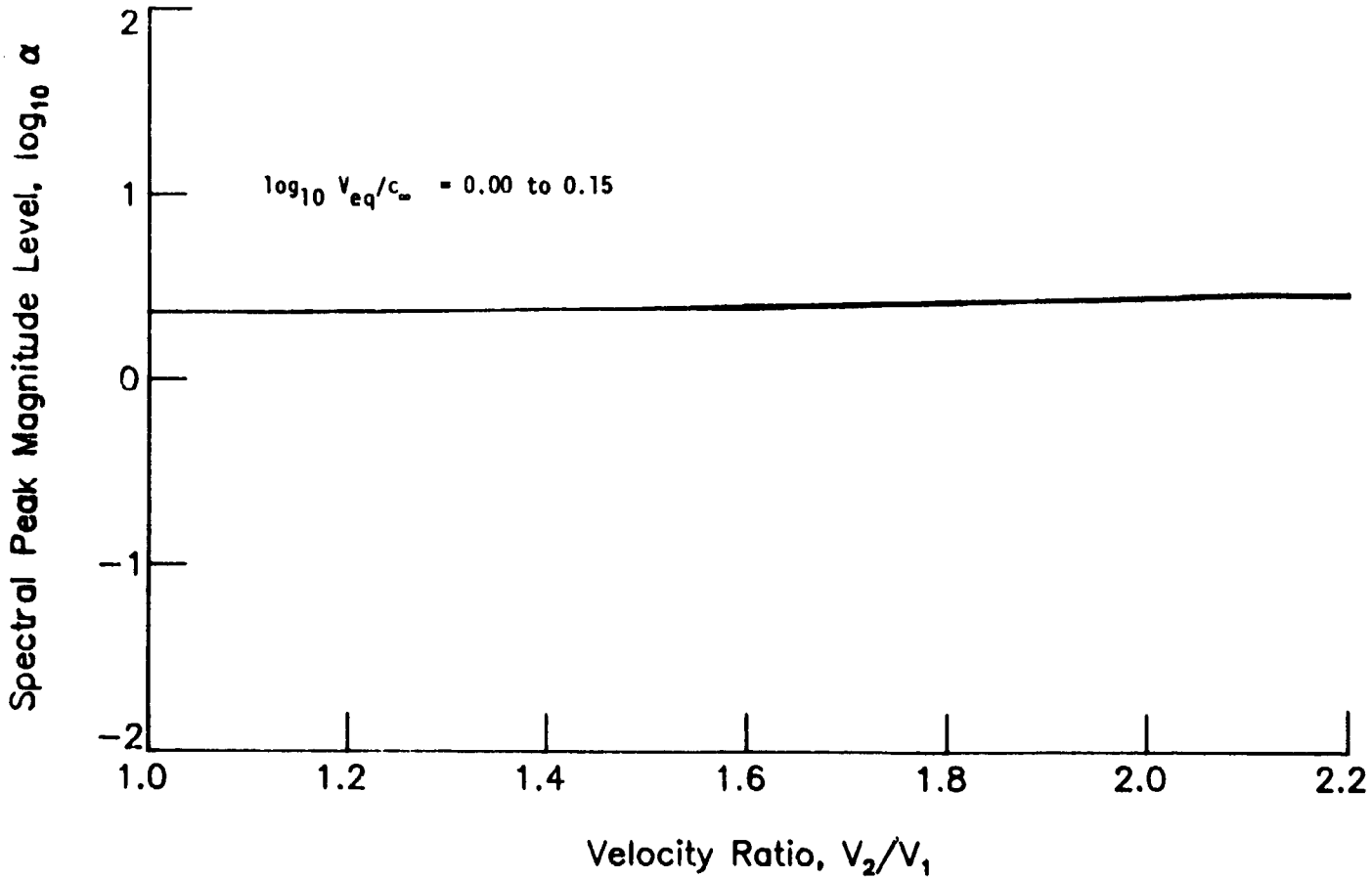

(b) $\theta = 120^{\circ}$.

Figure 9.- Continued.

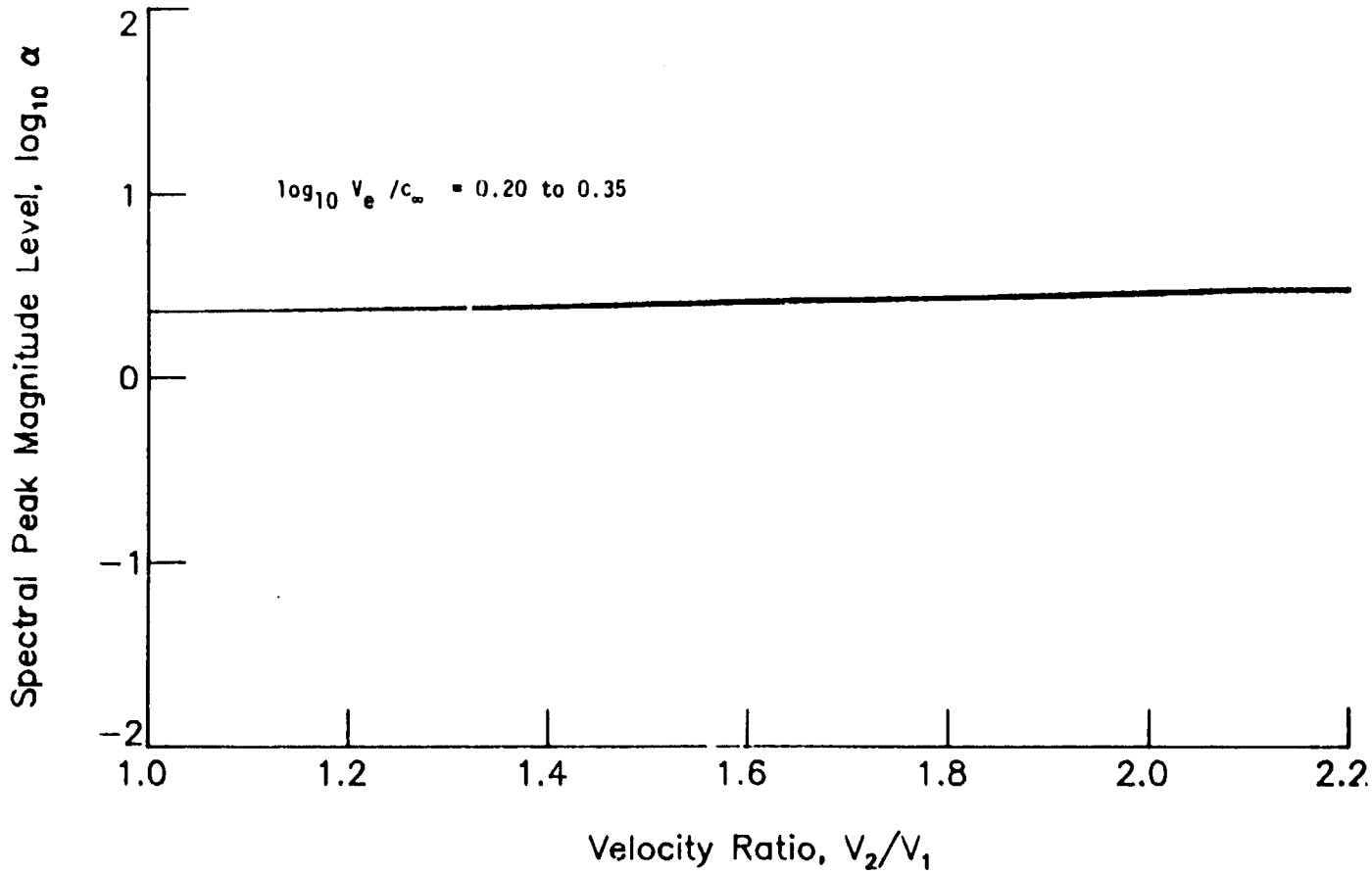

(b) $\theta = 120^\circ$ - Concluded.

Figure 9.- Continued.

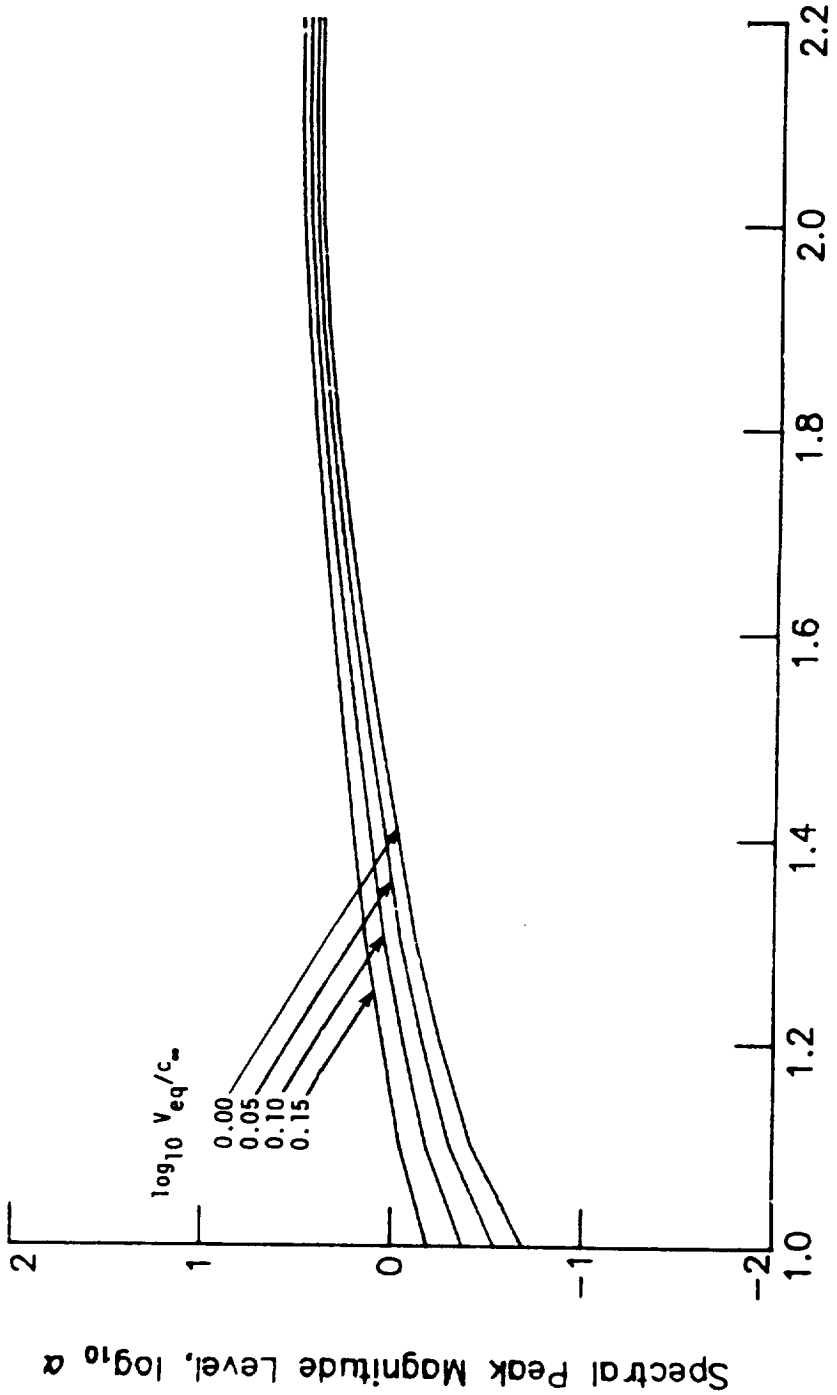

(c) $\theta = 130^{\circ}$.

Figure 9.- Continued.

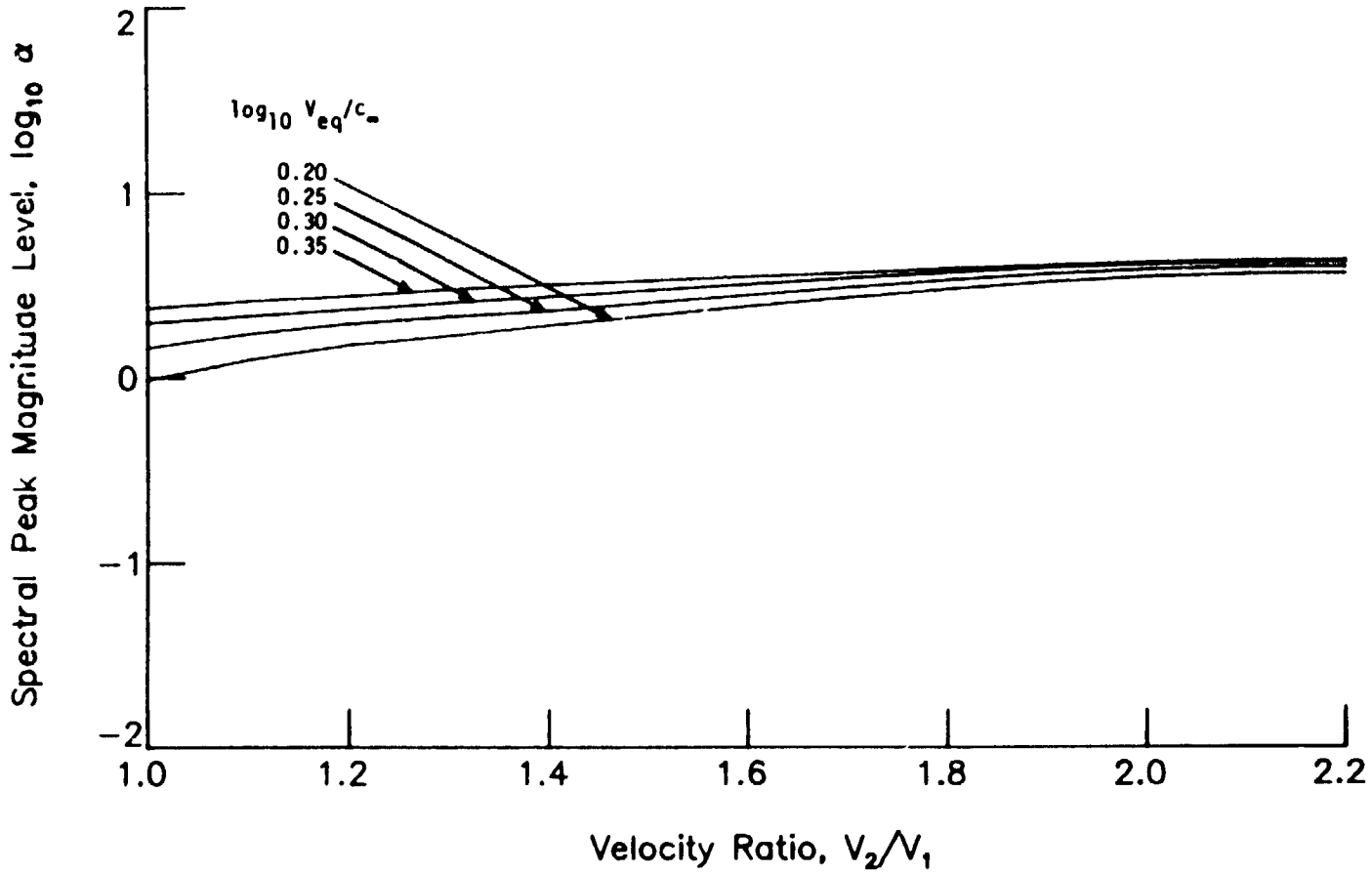

(c) $\theta = 130^\circ$ - Concluded.

Figure 9.- Continued.

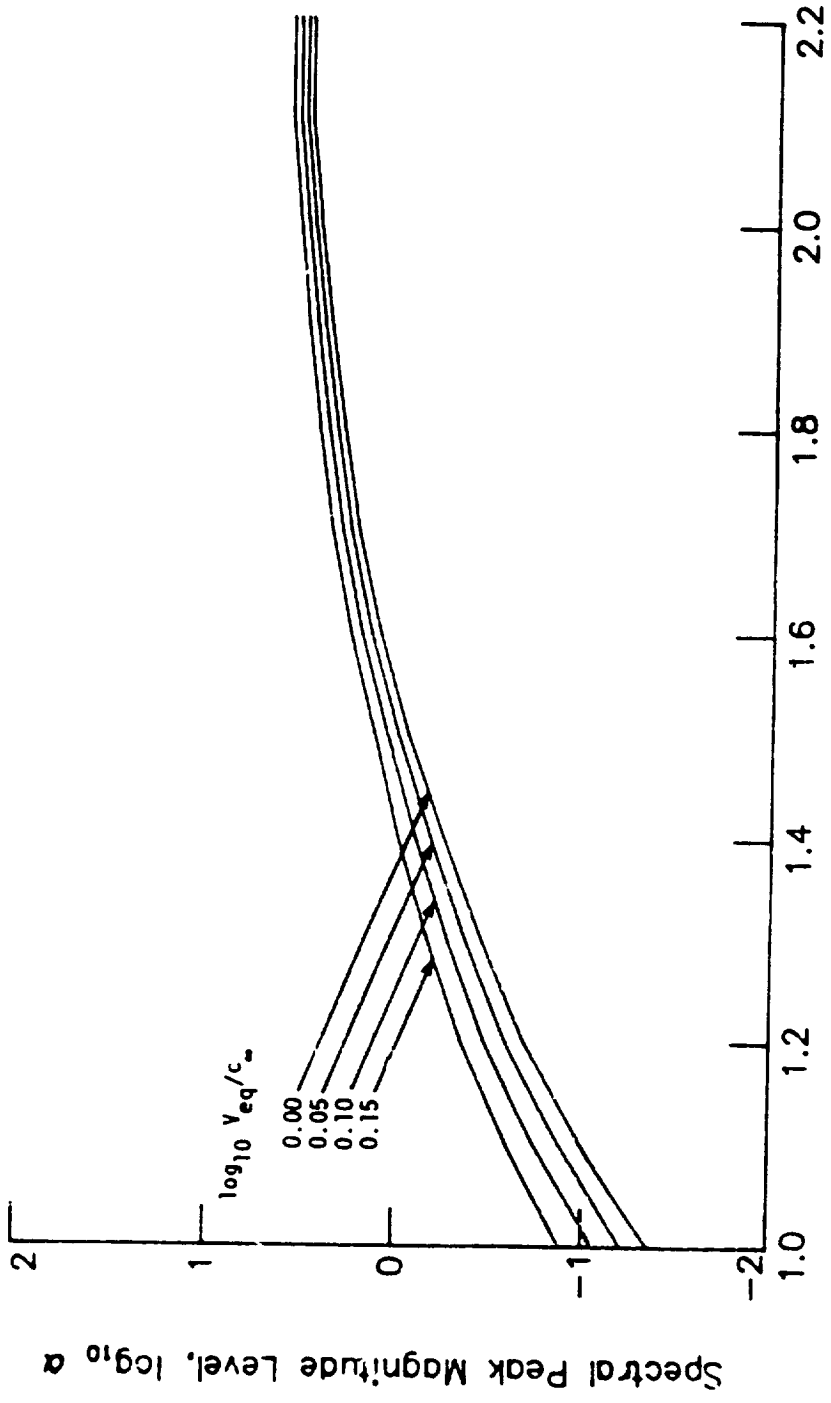

(d) $\theta = 140^\circ$.

Figure 9.- Continued.

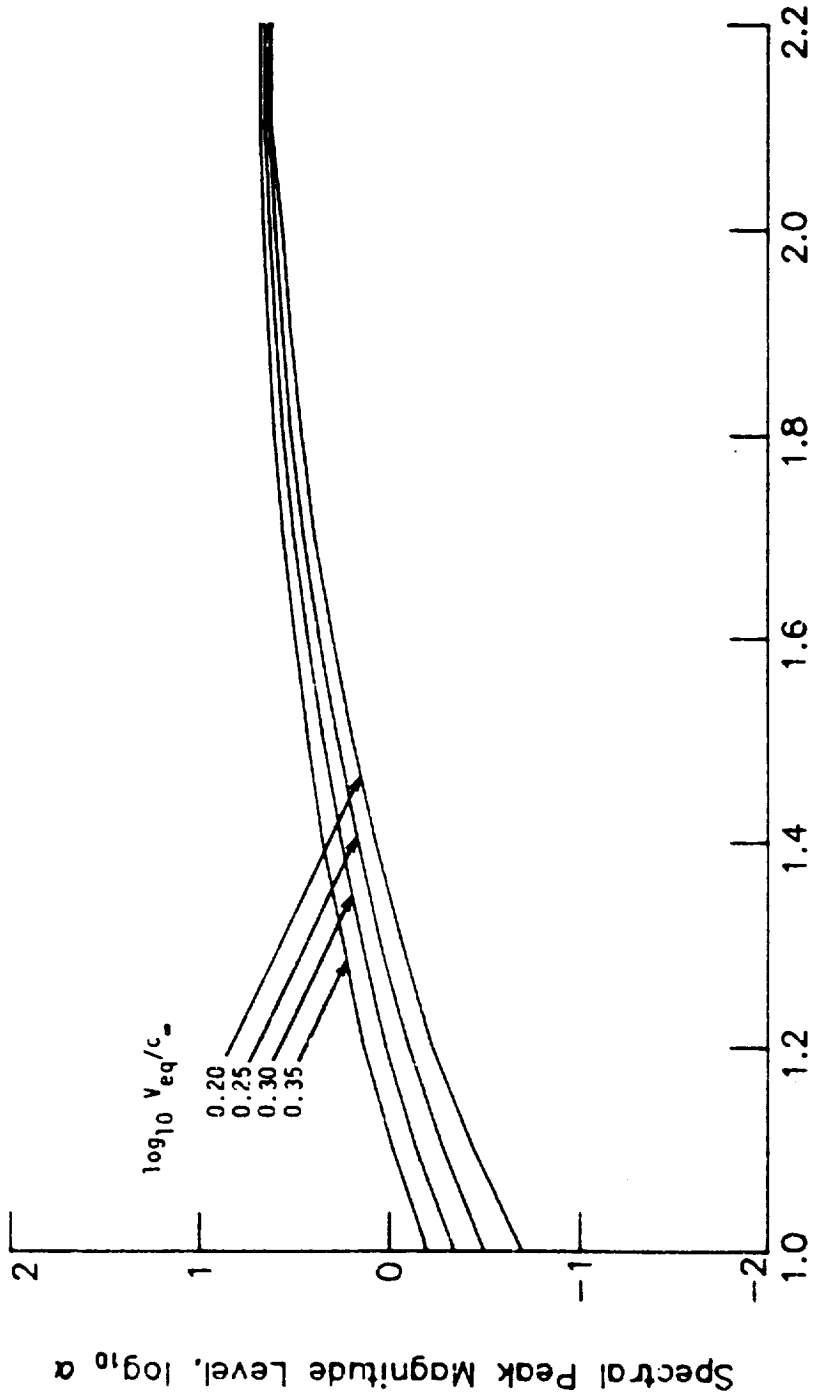

(d) $\eta = 140^\circ$ - Concluded.

Figure 9.- Continued.

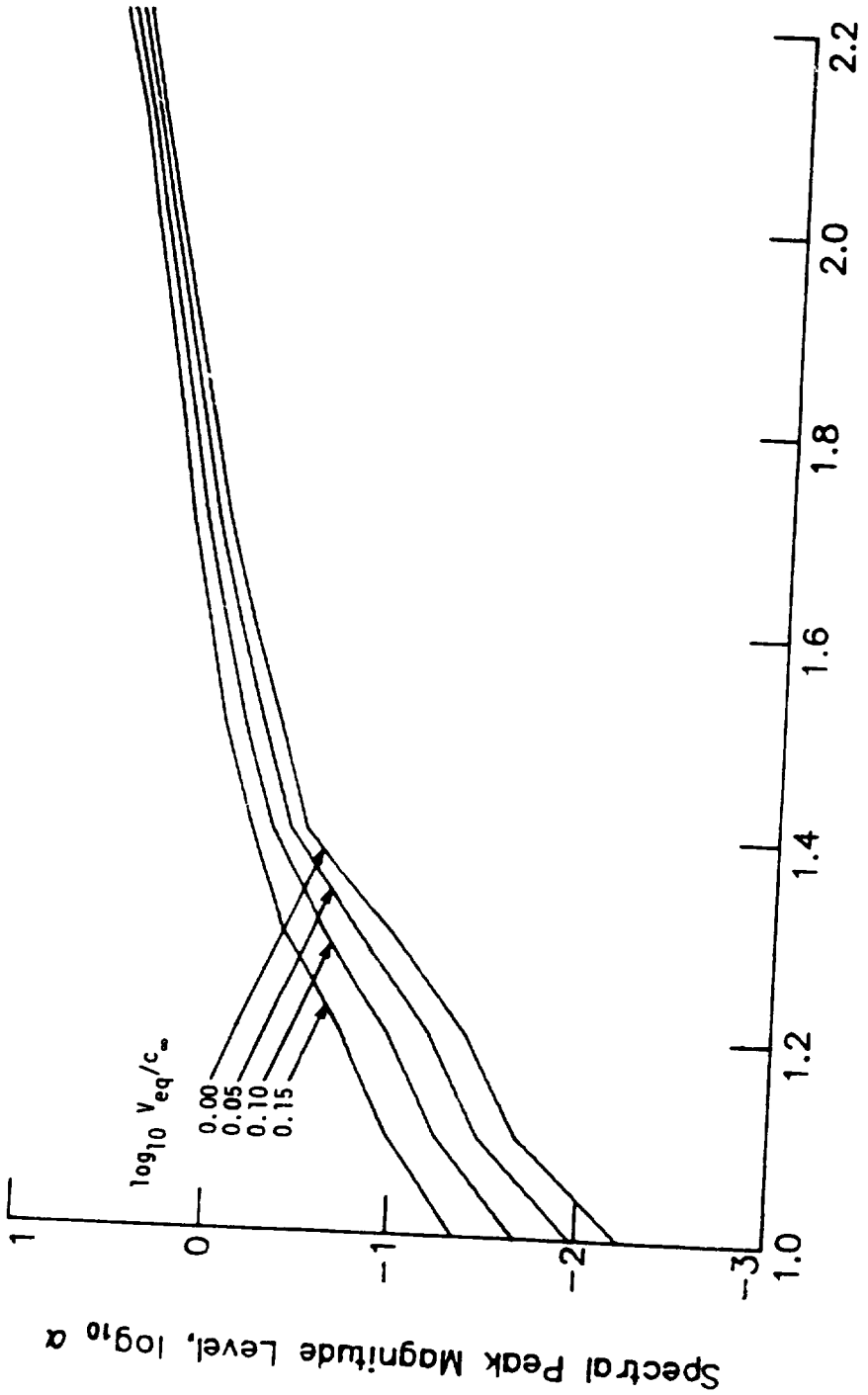

(c) $\theta = 150^\circ$.

Figure 9.- Continued.

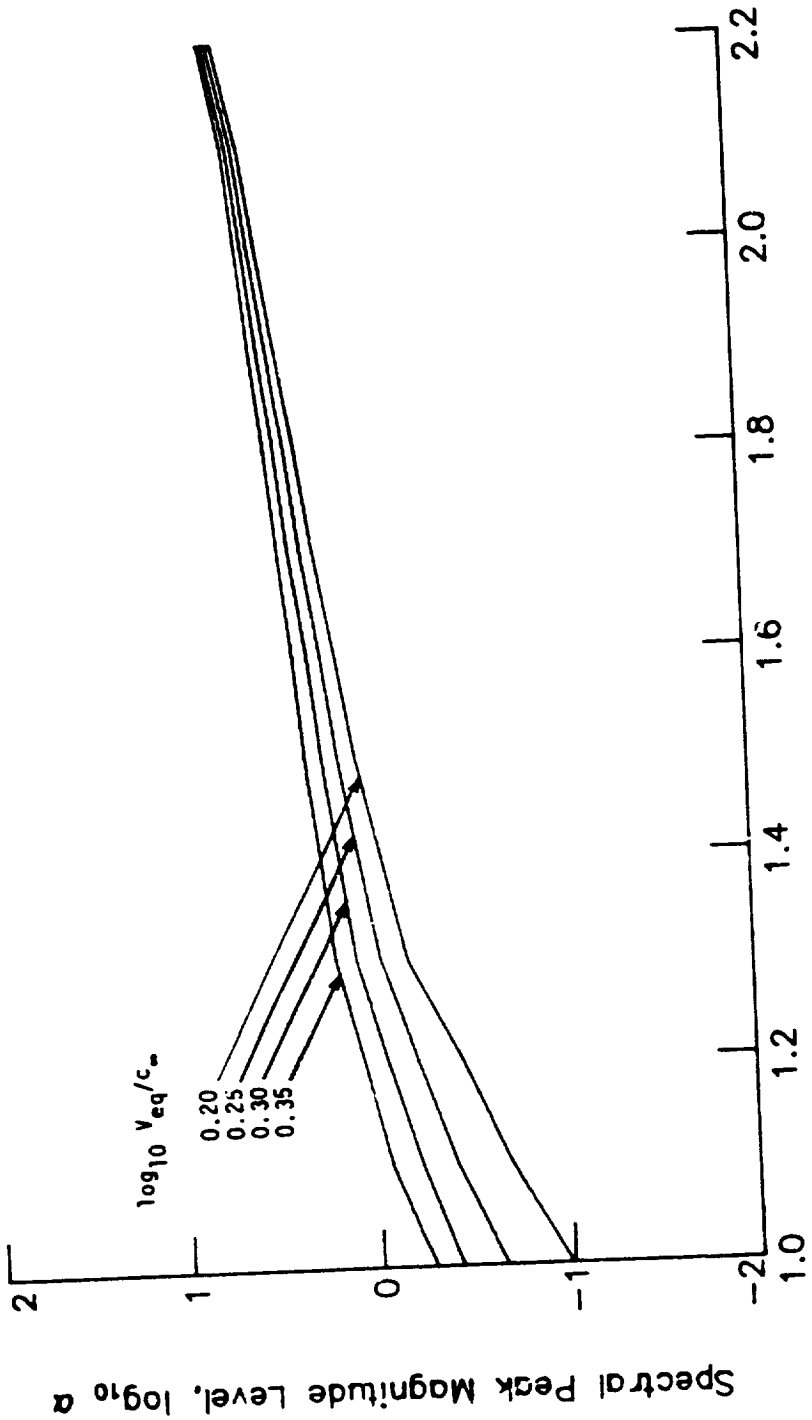

(e) $\theta = 150^\circ$ - Concluded.

Figure 9.- Continued.

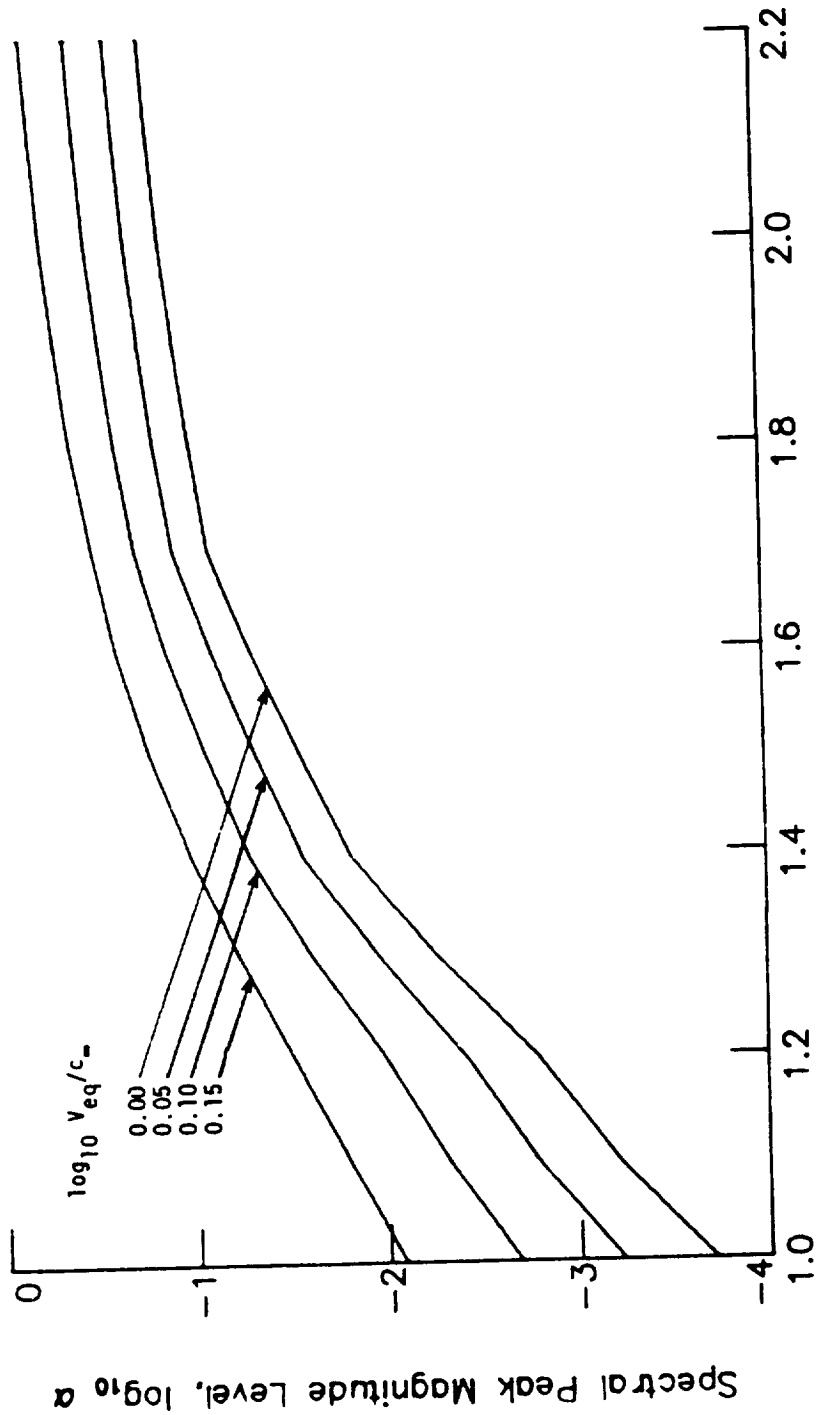

(f) $\theta = 165^\circ$.

Figure 9.- Continued.

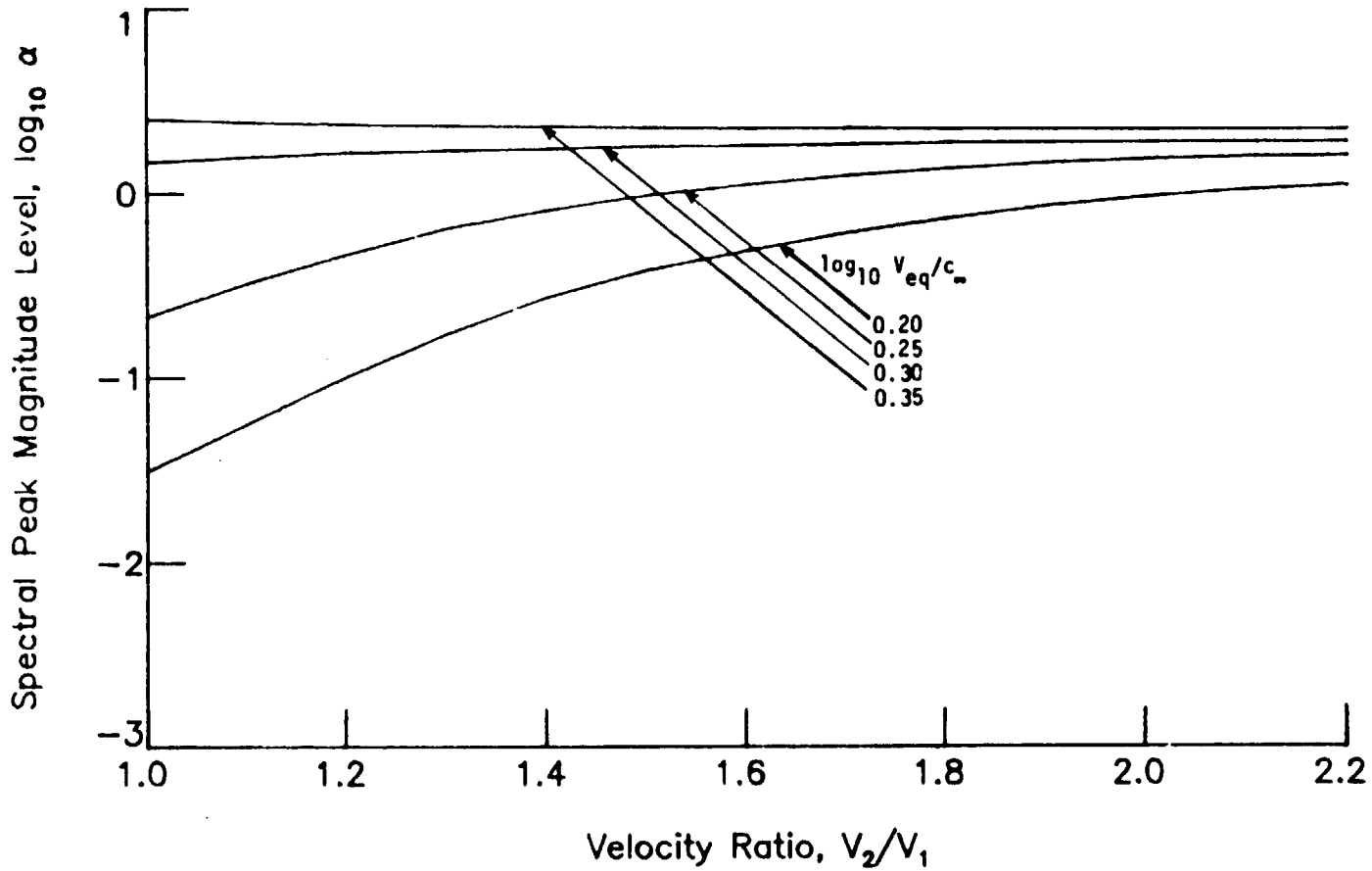

(f) $\theta = 165^\circ$ - Concluded.

Figure 9.- Concluded.

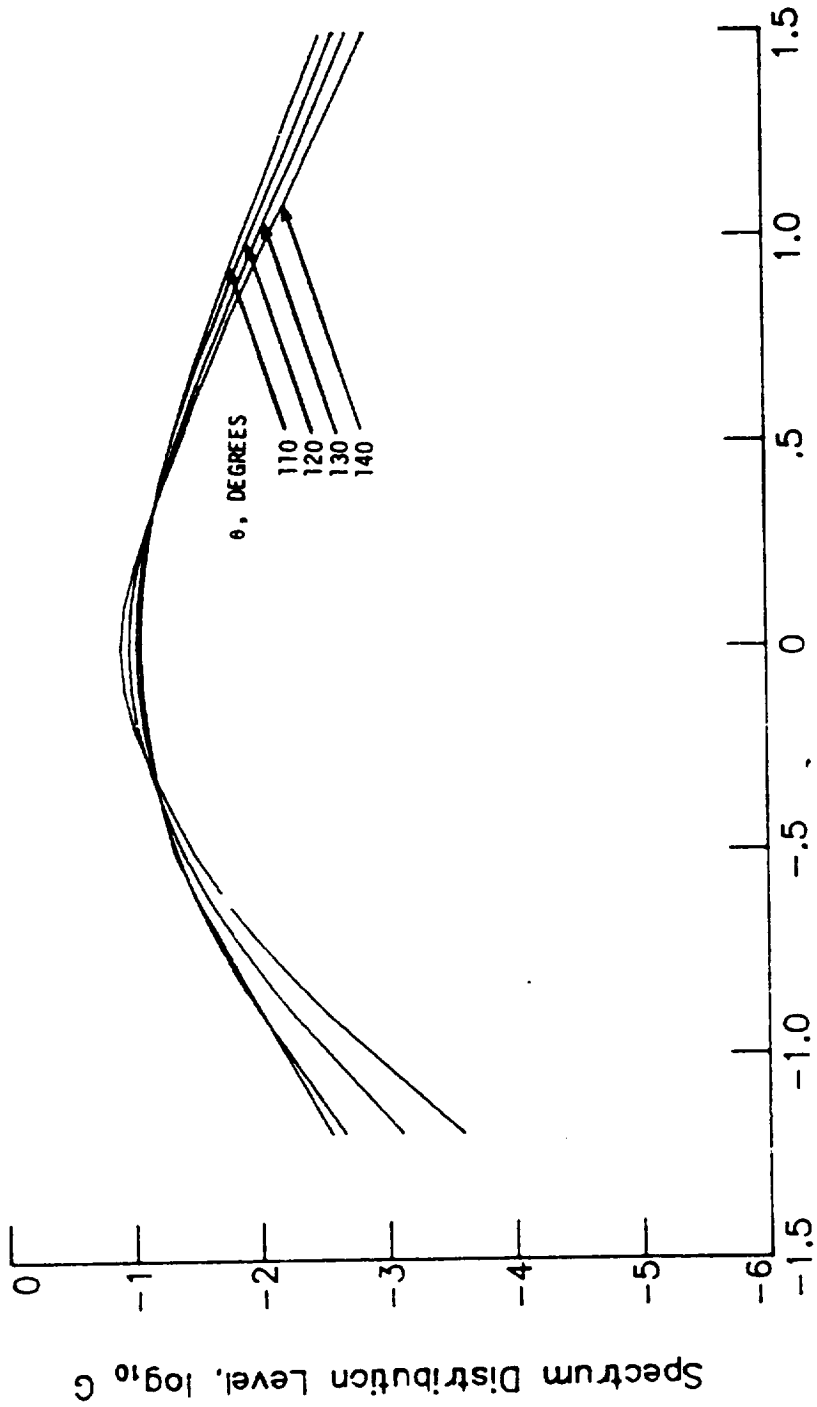

Figure 10.- Spectral distribution level.

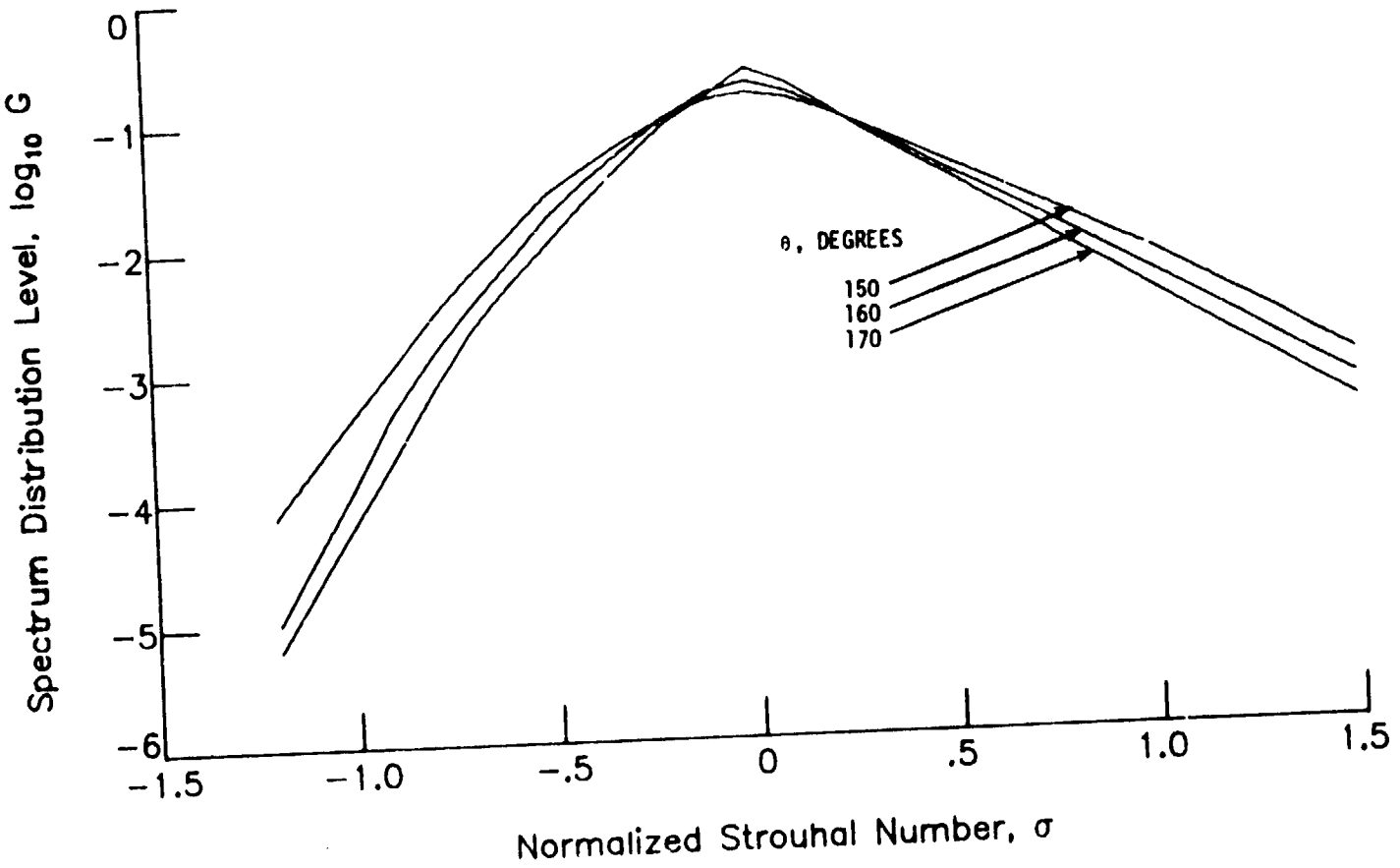

Figure 10.- Concluded.

8.8 AIRFRAME NOISE MODULE

INTRODUCTION

The Airframe Noise Module predicts the broadband noise for the dominant components of the airframe. The method is based on a method developed by Fink of the United Technologies Research Center for the Federal Aviation Administration (ref. 1). The method employs empirical and assumed functions to produce sound spectra as a function of frequency, polar directivity angle, and azimuthal directivity angle. Each spectrum is the sum of all the airframe component spectra produced by the wing, tail, landing gear, flaps, and leading-edge slats.

The method requires input of several parameters. The aircraft Mach number and control settings can be provided by the Airframe Noise Parameters Module or directly by the user. Additional user-provided parameters describe the airframe geometry. The module is executed once for each set of values of the input parameters. The output is a table of the mean-square acoustic pressure as a function of frequency, polar directivity angle, and azimuthal directivity angle.

SYMBOLS

A	area, m^2 (ft^2)
a	exponent
b	span, m (ft)
c_∞	ambient speed of sound, m/s (ft/s)
D	directivity function
d	tire diameter, m (ft)
F	spectrum function
f	frequency, Hz
G	geometry function
I_{ig}	landing-gear position
K	constant
ℓ	landing-gear strut length, m (ft)
M_∞	aircraft Mach number

N	number of landing gear
n	number of wheels per landing gear
$\langle p^2 \rangle^*$	mean-square acoustic pressure, re $\rho_\infty^2 c_\infty^4$
p_{ref}	reference pressure, 2×10^{-5} Pa (4.177×10^{-7} lb/ft^2)
r_s	distance from source to observer, m (ft)
r_s^*	dimensionless distance from source to observer, re b_w
S	Strouhal number
s	number of slats for trailing-edge flaps
δ	boundary-layer thickness, m (ft)
δ_f	flap deflection angle, deg
θ	polar directivity angle, deg
μ_∞	ambient dynamic viscosity, kg/m-s (slugs/ft-s)
Π^*	acoustic power, re $\rho_\infty c_\infty^3 b_w^2$
Π_{ref}	reference power, 1×10^{-12} W (7.376×10^{-13} ft-lb/s)
ρ_∞	ambient density, kg/m^3 (slugs/ft^3)
ϕ	azimuthal directivity angle, deg

Subscripts:

f	flap
h	horizontal tail
mg	main landing gear
ng	nose landing gear
v	vertical tail
w	wing

Superscript:

*	dimensionless quantity

INPUT

The aircraft Mach number, control settings, and ambient conditions are required from either the output of the Aircraft Noise Parameters Module or the user. The frequency, polar directivity angle, and azimuthal directivity angle arrays establish the independent variable values for the output table. Several parameters are required for the geometric description of the airframe. Finally, the distance to the pseudo-observer is required. The range and default values of the input parameters are given in table I.

Input Constant

r_s distance from source to observer, m (ft)

Airframe Geometry

A_f flap area, m^2 (ft^2)

A_h horizontal tail area, m^2 (ft^2)

A_v vertical tail area, m^2 (ft^2)

A_w wing area, m^2 (ft^2)

b_f flap span, m (ft)

b_h horizontal tail span, m (ft)

b_v vertical tail span, m (ft)

b_w wing span, m (ft)

d_{mg} tire diameter of main landing gear, m (ft)

d_{ng} tire diameter of nose landing gear, m (ft)

ℓ_{mg} main landing-gear strut length, m (ft)

ℓ_{ng} nose landing-gear strut length, m (ft)

n_{mg} number of wheels per main landing gear

n_{ng} number of wheels per nose landing gear

N_{mg} number of main landing gear

N_{ng} number of nose landing gear

s number of slots for trailing-edge flaps

Airframe Noise Parameters

I_{lg} landing-gear position

δ_f flap setting, deg

Ambient Conditions

c_∞ ambient speed of sound, m/s (ft/s)

M_∞ aircraft Mach number

ρ_∞ ambient density, kg/m^3 (slugs/ft^3)

μ_∞ ambient dynamic viscosity, kg/m-s (slugs/ft-s)

Independent Variable Array

f frequency, Hz

θ polar directivity angle, deg

ϕ azimuthal directivity angle, deg

OUTPUT

The output of this module is a table of the mean-square acoustic pressure as a function of frequency, polar directivity angle, and azimuthal directivity angle. In addition, the observer distance r_s is provided for the Propagation Module.

r_s distance from source to observer, m (ft)

Airframe Noise Table

f frequency, Hz

θ polar directivity angle, deg

ϕ azimuthal directivity angle, deg

$\langle p^2(f,\theta,\phi)\rangle^*$ mean-square acoustic pressure, re $\rho_\infty^2 c_\infty^4$

METHOD

The prediction method presented in reference 1 is used to compute the far-field noise. The airframe noise components considered in the method are shown in figure 1. The definitions of the directivity angles

are shown in figure 2. In the following discussion, the general approach for the prediction method is presented first and then the detailed method is given for each airframe component.

The equation for the far-field mean-square acoustic pressure for the airframe is

$$\langle p^2 \rangle^* = \frac{\Pi^*}{4\pi (r_s^*)^2} \frac{D(\theta,\phi)\ F(S)}{(1 - M_\infty \cos\theta)^4} \tag{1}$$

In equation (1), Π^* is the overall power, D is the directivity function, and F is the spectrum function. The source to observer distance r_s is expressed in dimensionless form as $r_s^* = r_s/b_w$. The forward velocity effect is accounted for by the Doppler factor $(1 - M_\infty \cos\theta)^4$. The Strouhal number S is defined as

$$S = \frac{fL}{M_\infty c_\infty}(1 - M_\infty \cos\theta) \tag{2}$$

where L is some length scale characteristic of the particular airframe noise source being computed.

The acoustic power for the airframe Π^* can be expressed as

$$\Pi^* = K(M_\infty)^a\ G \tag{3}$$

where K and a are constants determined from empirical data. The geometry function G is different for each airframe component and incorporates all geometry effects on the acoustic power.

As indicated by equation (1), each airframe noise source has its own directivity function D and spectrum function F. Using these functions and the acoustic power, the mean-square acoustic pressure can be computed as a function of frequency, polar directivity angle, and azimuthal directivity angle for a given set of input parameters. The empirical constants and functions used to compute the acoustic power are summarized in table II. The directivity and spectrum functions are given in table III. Each airframe noise component is described in detail below.

Trailing-Edge Noise

The primary mechanism for noise generation for clean wing and tail surfaces is the convection of the turbulent boundary layer past the trailing edge. The turbulence intensity is assumed to be independent of Reynolds number and the turbulent length scale is assumed to be the boundary-layer thickness. The directivity function is assumed to be aligned with the lift dipole, and the spectrum function is determined empirically.

The acoustic power due to trailing-edge noise of a conventionally constructed wing is

$$\Pi^* = (4.464 \times 10^{-5}) M_\infty^5 \delta_w^* \tag{4}$$

The dimensionless turbulent boundary-layer thickness δ_w^* is computed from the standard flat-plate turbulent boundary-layer model

$$\delta_w^* = 0.37 \frac{A_w}{b_w^2} \left(\frac{\rho_\infty M_\infty c_\infty A_w}{\mu_\infty b_w} \right)^{-0.2} \tag{5}$$

Similarly, the acoustic power for the horizontal tail is

$$\Pi^* = (4.464 \times 10^{-5}) M_\infty^5 \delta_h^* \left(\frac{b_h}{b_w} \right)^2 \tag{6}$$

and for the vertical tail is

$$\Pi^* = (4.464 \times 10^{-5}) M_\infty^5 \delta_v^* \left(\frac{b_v}{b_w} \right)^2 \tag{7}$$

The boundary-layer thicknesses δ_h^* and δ_v^* are computed from equation (5) using the appropriate values of A and b. If the airplane is aerodynamically clean, such as a sailplane or jet aircraft with simple trailing-edge flap mechanisms, the constants in equations (4), (6), and (7) should be reduced to 7.075×10^{-6}, an 8-dB decrease.

The directivity function D for the clean wing and horizontal tail is given by

$$D(\theta, \phi) = 4 \cos^2 \phi \cos^2 \theta/2 \tag{8}$$

and for the vertical tail

$$D(\theta, \phi) = 4 \sin^2 \phi \cos^2 \theta/2 \tag{9}$$

These directivity functions are plotted in figures 2 and 3, respectively. The spectrum function F is given by

$$F(S) = 0.613(10S)^4 \left[(10S)^{1.5} + 0.5 \right]^{-4} \tag{10}$$

for rectangular wings and

$$F(S) = 0.485(10S)^4\left[(10S)^{1.35} + 0.5\right]^{-4} \tag{11}$$

for delta wings. These spectrum functions are plotted in figure 4. The Strouhal number S is defined for this component as

$$S = \frac{f\delta^* b}{M_\infty c_\infty}(1 - M_\infty \cos\theta) \tag{12}$$

where the appropriate value of the span b and the boundary-layer thickness δ^* for the wing, vertical tail, or horizontal tail is used depending on the noise source being predicted. The mean-square acoustic pressure is then computed from equation (1).

Leading-Edge-Slat Noise

The deployment of the leading-edge slats produces increased noise by two different mechanisms. First, the slat produces an increment of wing trailing-edge noise due to its impact on the boundary layer of the wing. Second, the leading-edge slat itself produces trailing-edge noise. Both mechanisms are accounted for in this method.

The added acoustic power due to the increase in wing trailing-edge noise or the slat trailing-edge noise is assumed to be equal to the clean wing noise. Therefore, equation (4) can be used to predict the overall acoustic power for either slat noise source. The directivity function for either slat noise source is given by equation (8) and plotted in figure 2. The spectrum function for the added wing noise is given by equation (10). The spectrum function for the slat noise is

$$F(S) = 0.613(2.19S)^4\left[(2.19S)^{1.5} + 0.5\right]^{-4} \tag{13}$$

which assumes that the slat chord is 15 percent of the total wing chord. The Strouhal number S is given by equation (12). The two spectrum functions are plotted in figure 5, along with their sum, to show the combined effect of slat noise. The mean-square acoustic pressure is then computed from equation (1).

Flap Trailing-Edge Noise

Extension of the wing flaps increases the level of airframe noise. This noise is assumed to be produced by the lift fluctuations due to the incident turbulence on the flap. This noise increases as the flap extension is increased. The noise is assumed to be aligned with the lift dipole of the deflected flap.

The acoustic power due to flap noise for single or double slotted flaps is

$$\Pi^* = (2.787 \times 10^{-4}) M_\infty^6 \frac{A_f}{b_w^2} \sin^2 \delta_f \tag{14}$$

where δ_f is the flap deflection angle. For triple slotted flaps, the overall acoustic power is

$$\Pi^* = (3.509 \times 10^{-4}) M_\infty^6 \frac{A_f}{b_w^2} \sin^2 \delta_f \tag{15}$$

which increases the power by 1 dB to account for the added flap complexity.

The directivity function D for the flap noise is

$$D(\theta,\phi) = 3(\sin \delta_f \cos \theta + \cos \delta_f \sin \theta \cos \phi)^2 \tag{16}$$

which is plotted in figure 6 for $\delta_f = 30^\circ$. The spectrum functions F are

$$F(S_f) = \begin{cases} 0.0480 S_f & (S < 2) \\ 0.1406 S_f^{-0.55} & (2 \le S \le 20) \\ 216.49 S_f^{-3} & (20 < S) \end{cases} \tag{17}$$

for single and double slotted flaps and

$$F(S_f) = \begin{cases} 0.0257 S_f & (S < 2) \\ 0.0536 S_f^{-0.0625} & (2 \le S \le 75) \\ 17078 S_f^{-3} & (75 < S) \end{cases} \tag{18}$$

for triple slotted flaps. Using the flap chord as the reference length, the Strouhal number is defined as

$$S_f = \frac{f A_f}{M_\infty b_f c_\infty} (1 - M_\infty \cos \theta) \tag{19}$$

The spectrum functions given by equations (17) and (18) are plotted in figures 7 and 8, respectively. The mean-square acoustic pressure is then computed from equation (1).

Landing-Gear Noise

The mechanism for noise generation due to landing-gear extension is complex and dependent on the particular landing-gear design being considered. The process has been simplified with the assumption, based on the experimental comparisons made in reference 1, that there are only two predominant noise sources. Noise generated by the strut and wheel appears to dominate other potential sources. Separate predictions are made for the strut and wheel noise which are added together to yield the total landing-gear noise.

For a one- or two-wheel landing gear, the acoustic power due to the wheel noise is

$$\Pi^* = (4.349 \times 10^{-4}) M_\infty^6 n \left(\frac{d}{b_w}\right)^2 \tag{20}$$

and due to the strut noise is

$$\Pi^* = (2.753 \times 10^{-4}) M_\infty^6 \left(\frac{d}{b_w}\right)^2 \frac{\ell}{d} \tag{21}$$

Similarly, for a four-wheel landing gear, the acoustic power due to the wheel noise is

$$\Pi^* = (3.414 \times 10^{-4}) M_\infty^6 n \left(\frac{d}{b_w}\right)^2 \tag{22}$$

and due to the strut noise is the same as equation (21). In equations (20), (21), and (22), d is the tire diameter, ℓ is the strut length, and n is the number of wheels per landing gear.

The directivity function for the landing-gear wheel noise is

$$D(\theta,\phi) = \frac{3}{2} \sin^2 \theta \tag{23}$$

and for the strut noise

$$D(\theta,\phi) = 3 \sin^2 \theta \sin^2 \phi \tag{24}$$

These directivity functions are plotted in figures 9 and 10, respectively. For a one- or two-wheel landing gear, the spectrum function for the wheel noise is

$$F(S) = 13.59S^2(12.5 + S^2)^{-2.25} \tag{25}$$

and for the strut noise is

$$F(S) = 5.325S^2(30 + S^8)^{-1} \tag{26}$$

Similarly, for the four-wheel landing gear, the spectrum function for the wheel noise is

$$F(S) = 0.0577S^2(1 + 0.25S^2)^{-1.5} \tag{27}$$

and for the strut noise is

$$F(S) = 1.280S^3(1.06 + S^2)^{-3} \tag{28}$$

If the tire diameter is used as the reference length, the Strouhal number is defined as

$$S = \frac{fd}{M_\infty c_\infty}(1 - M_\infty \cos \theta) \tag{29}$$

The four spectrum functions are plotted in figures 11 to 14. The wheel and strut mean-square acoustic pressure are computed separately by using equation (1). They are then summed to yield the total landing-gear mean-square acoustic pressure. The noise due to the main landing gear and nose landing gear are computed separately.

Output Computation

The mean-square acoustic pressure for the airframe is the sum of all the components desired by the user. It is computed for each value of the frequency, polar directivity angle, and azimuthal directivity angle for the output table. In addition, printed output is available of the sound pressure level SPL defined as

$$SPL = 10 \log_{10} \langle p^2 \rangle^* + 20 \log_{10} \frac{\rho_\infty c_\infty^2}{p_{ref}} \tag{30}$$

and the power level PWL defined as

$$PWL = 10 \log_{10} \Pi^* + 10 \log_{10} \frac{\rho_\infty c_\infty^3 b_w^2}{\Pi_{ref}} \tag{31}$$

REFERENCE

1. Fink, Martin R.: Airframe Noise Prediction Method. FAA-RD-77-29, Mar. 1977. (Available from DTIC as AD A039 664.)

TABLE I.- RANGE AND DEFAULT VALUES OF INPUT PARAMETERS

Input parameter	Minimum	Default	Maximum
r_s, m	0.01	b_w	100
A_f, m^2	0.01	10	100
A_h, m^2	0.02	20	200
A_v, m^2	0.02	20	200
A_w, m^2	0.1	100	1000
b_f, m	0.01	5	20
b_h, m	0.02	10	20
b_v, m	0.02	10	40
b_w, m	0.1	20	100
d_{mg}, m	0.001	1	5
d_{ng}, m	0.001	1	5
ℓ_{mg}, m	0.003	3	15
ℓ_{ng}, m	0.003	3	15
n_{mg}	1	4	4
n_{ng}	1	2	4
N_{mg}	1	2	4
N_{ng}	1	1	2
s	1	3	3
$I_{\ell g}$	0	1	1
M_∞	0	0.3	0.9
δ_f, deg	0	0	45
c_∞, m/s	200	340.294	400
ρ_∞, kg/m^3	0.2	1.225	1.5
μ_∞, kg/m-s	1.5×10^{-5}	1.7894×10^{-5}	2.0×10^{-5}

TABLE II.- EMPIRICAL CONSTANTS AND FUNCTIONS FOR AIRFRAME ACOUSTIC POWER

Source	K	a	G
Clean wing and leading-edge slat (conventional construction) . . .	4.464×10^{-5}	5	δ_w^*
Horizontal tail (conventional construction) . . .	4.464×10^{-5}	5	$\delta_h^*(b_h/b_w)^2$
Vertical tail (conventional construction) . . .	4.464×10^{-5}	5	$\delta_v^*(b_v/b_w)^2$
Clean wing (aerodynamically clean)	7.075×10^{-6}	5	δ_w^*
Horizontal tail (aerodynamically clean)	7.075×10^{-6}	5	$\delta_h^*(b_h/b_w)^2$
Vertical tail (aerodynamically clean)	7.075×10^{-6}	5	$\delta_v^*(b_v/b_w)^2$
Single or double slotted trailing-edge flaps	2.787×10^{-4}	6	$\left(A_f/b_w^2\right) \sin^2 \delta_f$
Triple slotted trailing-edge flaps	3.509×10^{-4}	6	$\left(A_f/b_w^2\right) \sin^2 \delta_f$
One- or two-wheel landing-gear wheel noise	4.349×10^{-4}	6	$n(d/b_w)^2$
Four-wheel landing-gear wheel noise . .	3.414×10^{-4}	6	$n(d/b_w)^2$
Landing-gear strut noise	2.753×10^{-4}	6	$(d/b_w)^2(\ell/d)$

TABLE III.- DIRECTIVITY AND SPECTRUM FUNCTIONS FOR AIRFRAME NOISE

Source	Directivity	Strouhal number, S	Spectrum function
Clean rectangular wing	$4\cos^2\phi\cos^2\theta/2$	$\frac{f\delta_w^* b_w}{M_\infty c_\infty}(1 - M_\infty\cos\theta)$	$0.613(10S_w)^4\left[(10S_w)^{1.5} + 0.5\right]^{-4}$
Clean delta wing	$4\cos^2\phi\cos^2\theta/2$	$\frac{f\delta_w^* b_w}{M_\infty c_\infty}(1 - M_\infty\cos\theta)$	$0.485(10S_w)^4\left[(10S_w)^{1.35} + 0.5\right]^{-4}$
Clean horizontal tail	$4\cos^2\phi\cos^2\theta/2$	$\frac{f\delta_h^* b_h}{M_\infty c_\infty}(1 - M_\infty\cos\theta)$	$0.613(10S_h)^4\left[(10S_h)^{1.5} + 0.5\right]^{-4}$
Clean vertical tail	$4\sin^2\phi\cos^2\theta/2$	$\frac{f\delta_v^* b_v}{M_\infty c_\infty}(1 - M_\infty\cos\theta)$	$0.613(10S_v)^4\left[(10S_v)^{1.5} + 0.5\right]^{-4}$
Leading-edge slat	$4\cos^2\phi\cos^2\theta/2$	$\frac{f\delta_w^* b_w}{M_\infty c_\infty}(1 - M_\infty\cos\theta)$	$0.613(2.19S_w)^4\left[(2.19S_w)^{1.5} + 0.5\right]^{-4}$
Single and double slotted flaps	$2(\sin\delta_f\cos\theta + \cos\delta_f\sin\theta\cos\phi)^2$	$\frac{fA_f}{M_\infty b_f c_\infty}(1 - M_\infty\cos\theta)$	$\begin{cases} 0.0480S_f & (S_f < 2) \\ 0.1406S_f^{-0.55} & (2 \le S_f \le 20) \\ 216.49S_f^{-3} & (20 < S_f) \end{cases}$

TABLE III.- Concluded

Source	Directivity	Strouhal number, S	Spectrum function
Triple slotted flaps	$3(\sin \delta_f \cos \theta + \cos \delta_f \sin \theta \cos \phi)^2$	$\frac{fA_f}{M_\infty b_f c_\infty}(1 - M_\infty \cos \theta)$	$\begin{cases} 0.0257S_f & (S_f < 2) \\ 0.0536S_f^{-0.0625} & (2 \le S_f \le 75) \\ 17078S_f^{-3} & (75 < S_f) \end{cases}$
One- and two-wheel landing-gear wheel	$\frac{3}{2}\sin^2 \theta$	$\frac{fd}{M_\infty c_\infty}(1 - M_\infty \cos \theta)$	$13.59S^2(12.5 + S^2)^{-2.25}$
One- and two-wheel landing-gear strut	$3 \sin^2 \theta \sin^2 \phi$	$\frac{fd}{M_\infty c_\infty}(1 - M_\infty \cos \theta)$	$5.325S^2(30 + S^8)^{-1}$
Four-wheel landing-gear wheel	$\frac{3}{2}\sin^2 \theta$	$\frac{fd}{M_\infty c_\infty}(1 - M_\infty \cos \theta)$	$0.0577S^2(1 + 0.25S^2)^{-1.5}$
Four-wheel landing-gear strut	$3 \sin^2 \theta \sin^2 \phi$	$\frac{fd}{M_\infty c_\infty}(1 - M_\infty \cos \theta)$	$1.280S^3(1.06 + S^2)^{-3}$

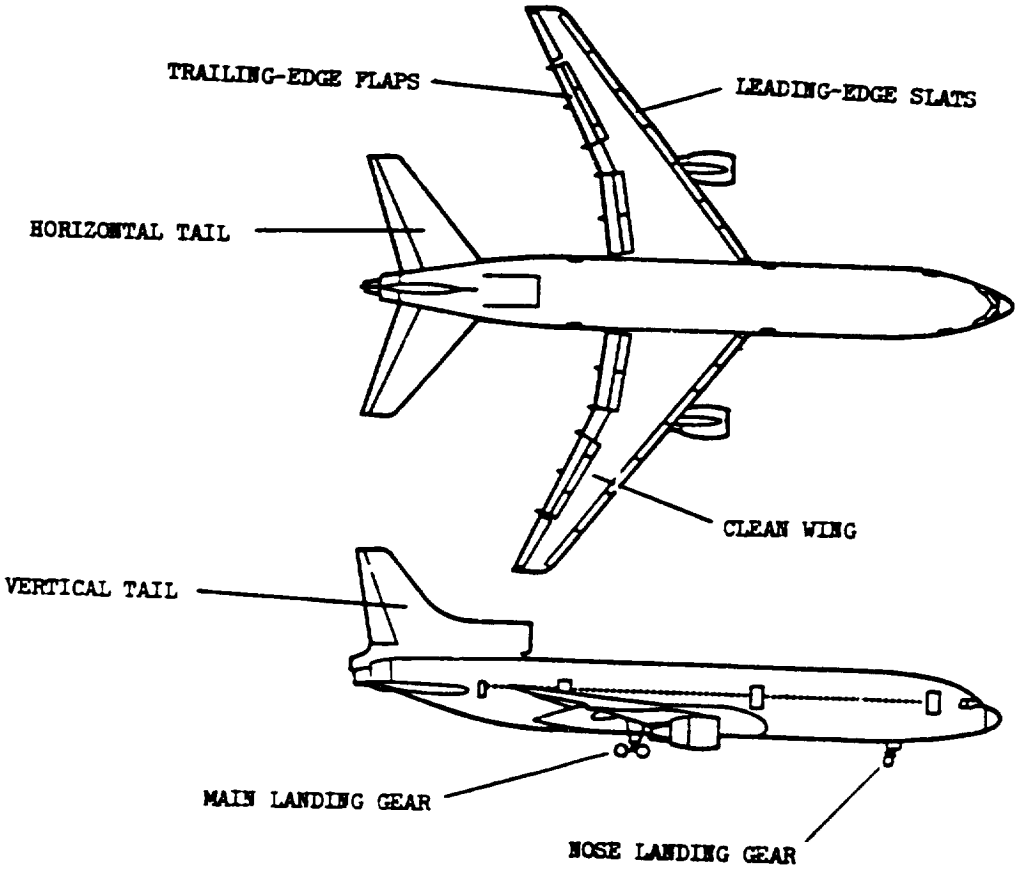

Figure 1.- Sources of airframe noise included in prediction model.

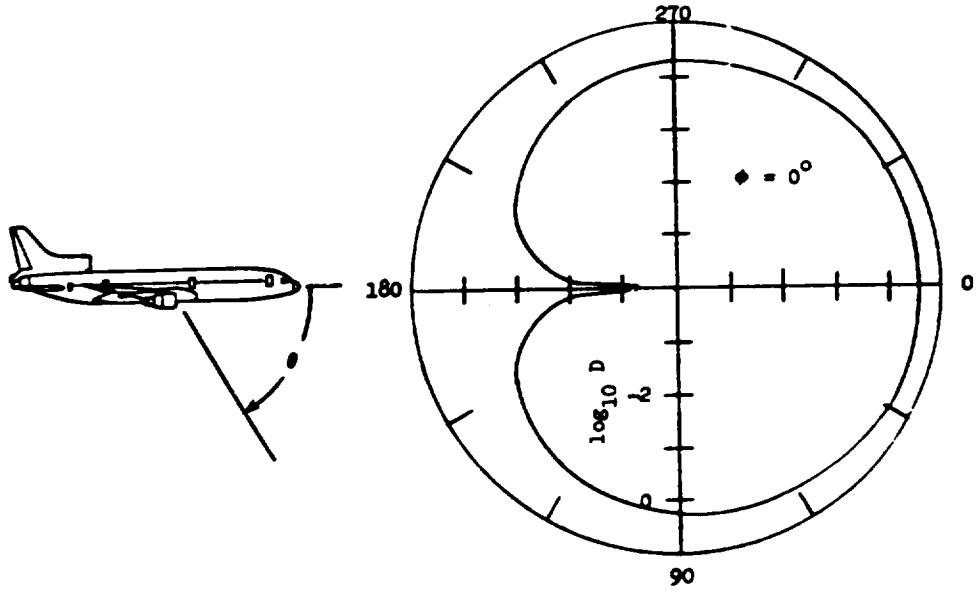

(a) Variation with polar directivity angle.

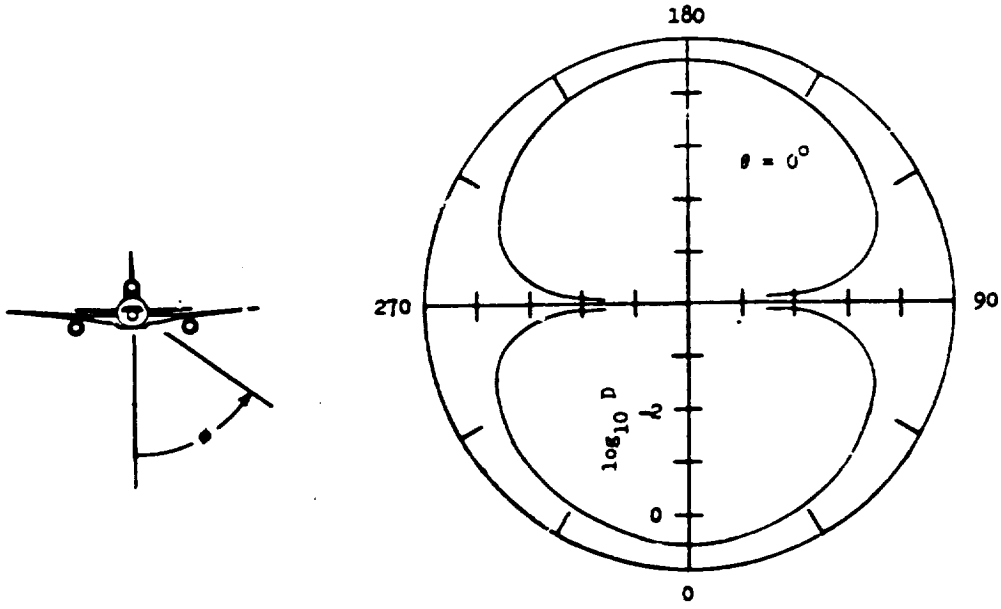

(b) Variation with azimuthal directivity angle.

Figure 2.- Directivity level for clean wing, horizontal tail, and leading-edge slat noise.

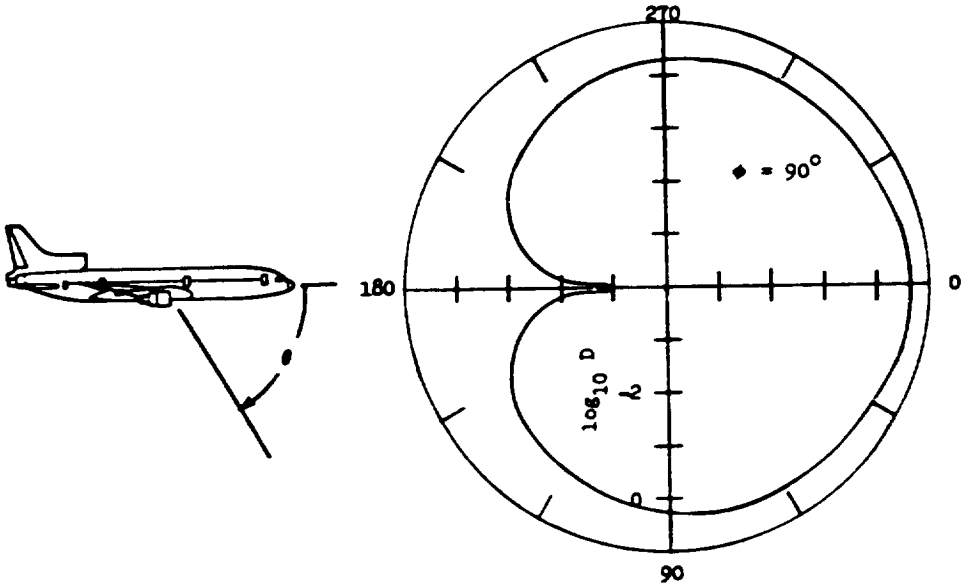

(a) Variation with polar directivity angle.

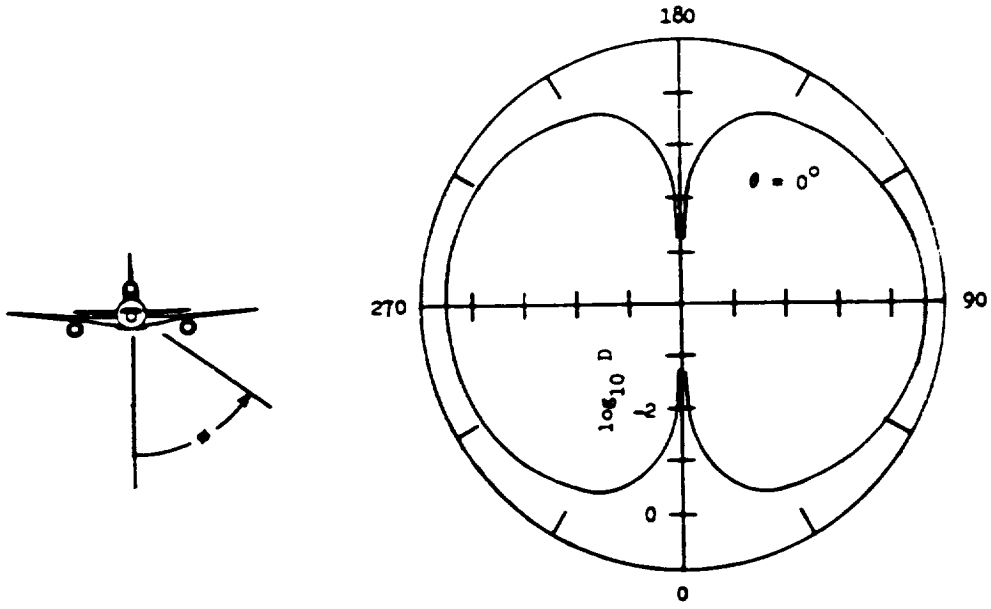

(b) Variation with azimuthal directivity angle.

Figure 3.- Directivity level for vertical-tail trailing-edge noise.

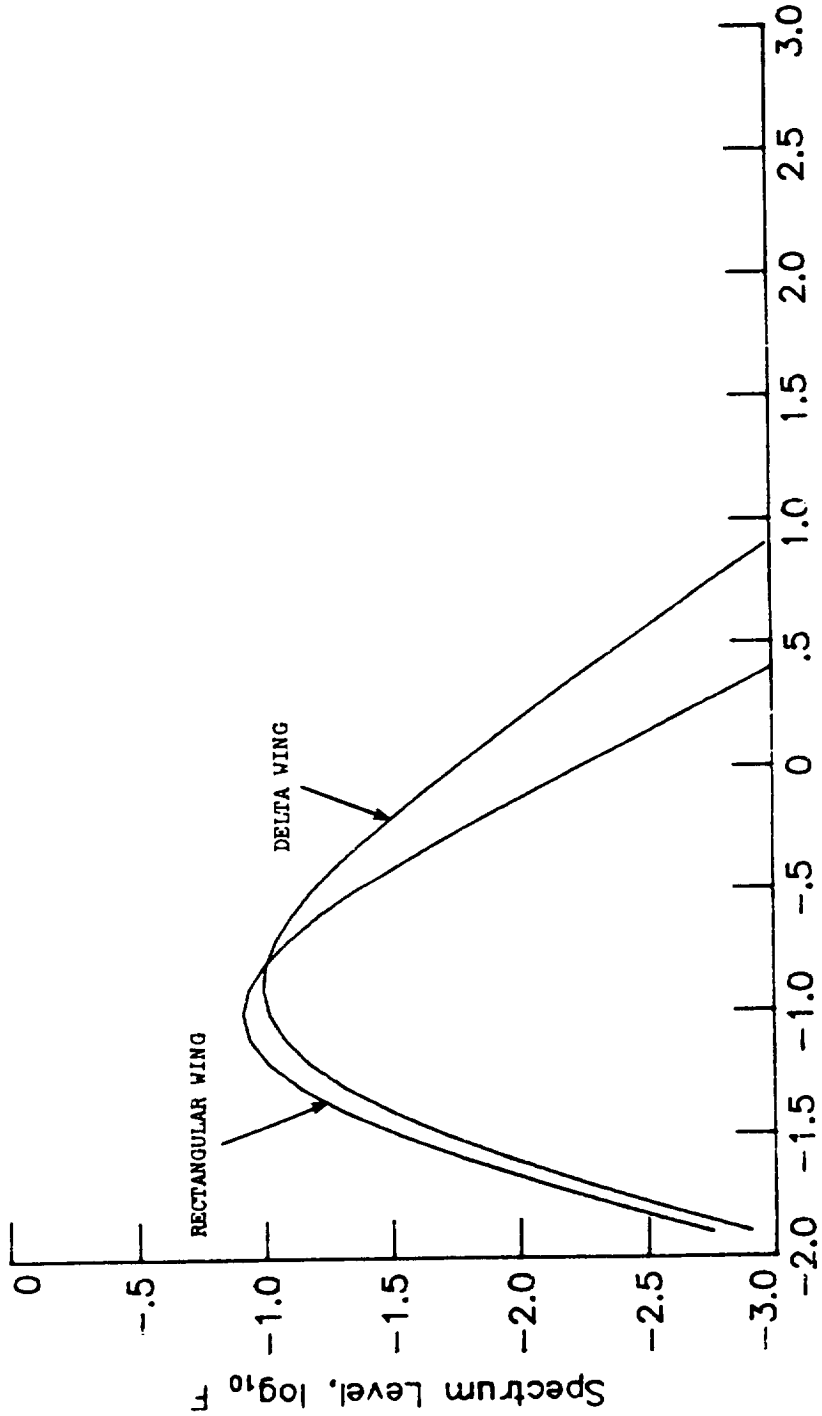

Figure 4.- Spectrum level for clean wing, horizontal tail, and vertical tail trailing-edge noise.

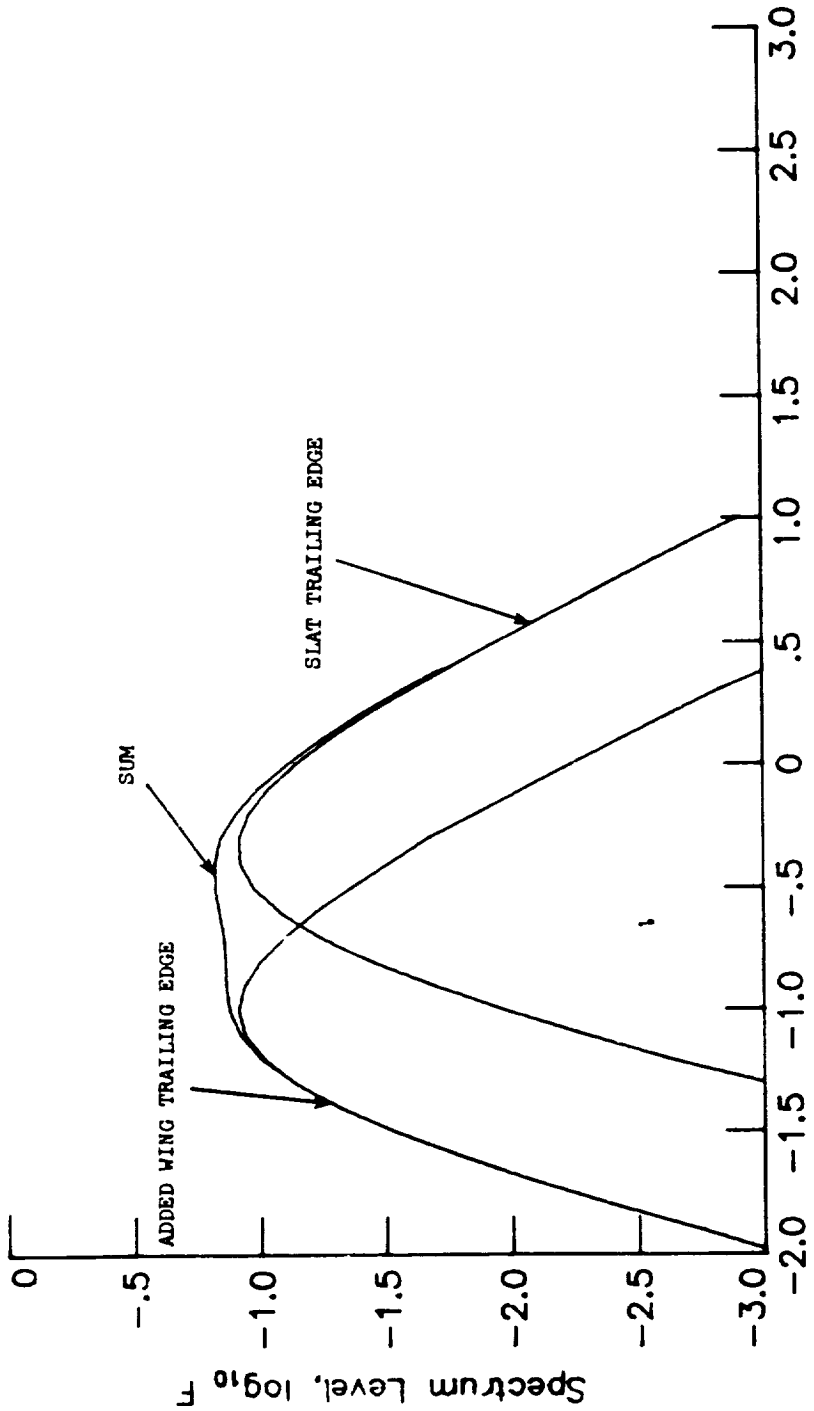

Figure 5.- Spectrum level for leading-edge slat noise.

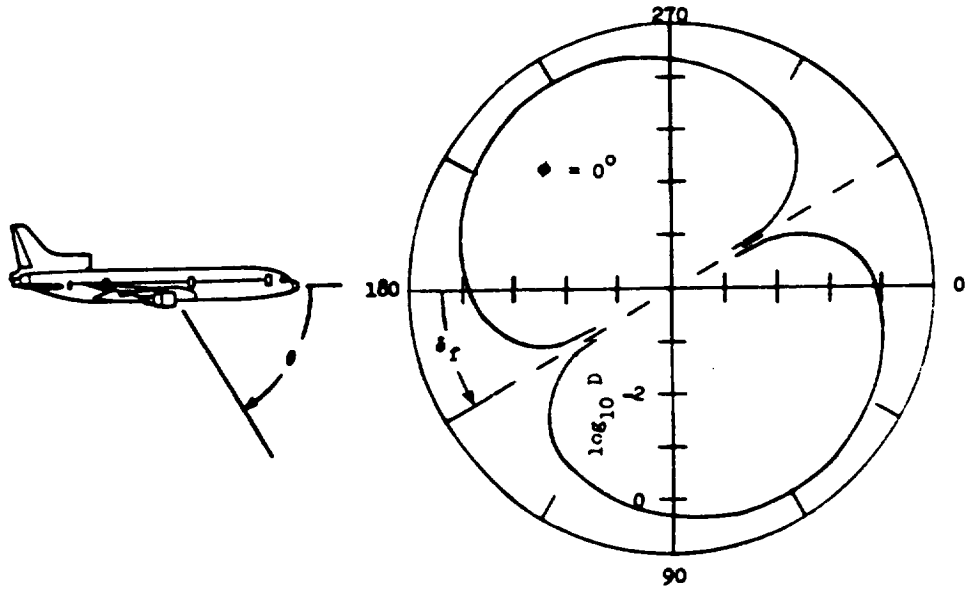

(a) Variation with polar directivity angle.

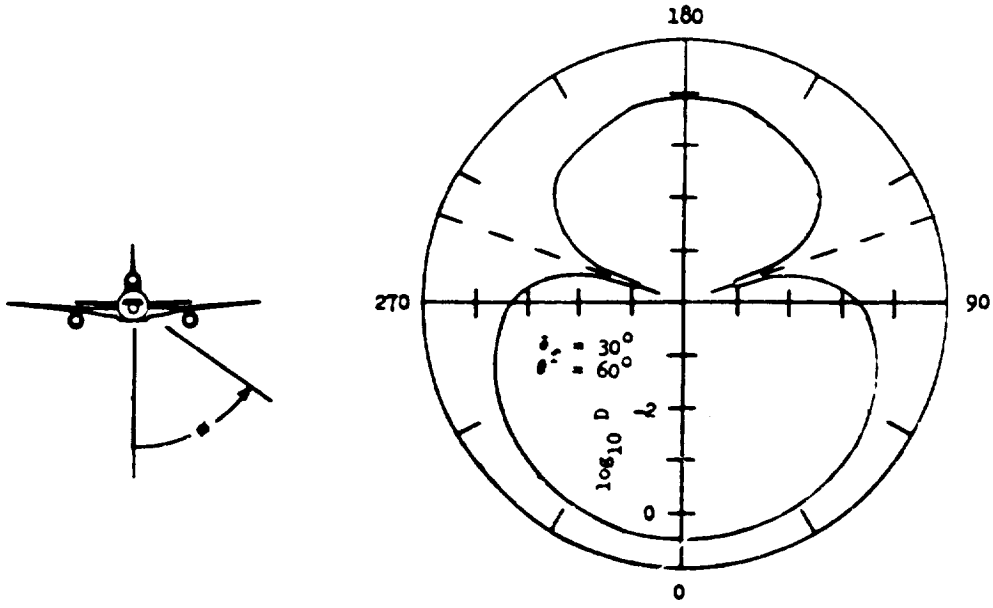

(b) Variation with azimuthal directivity angle.

Figure 6.- Directivity level for flap trailing-edge noise at a 30° flap angle.

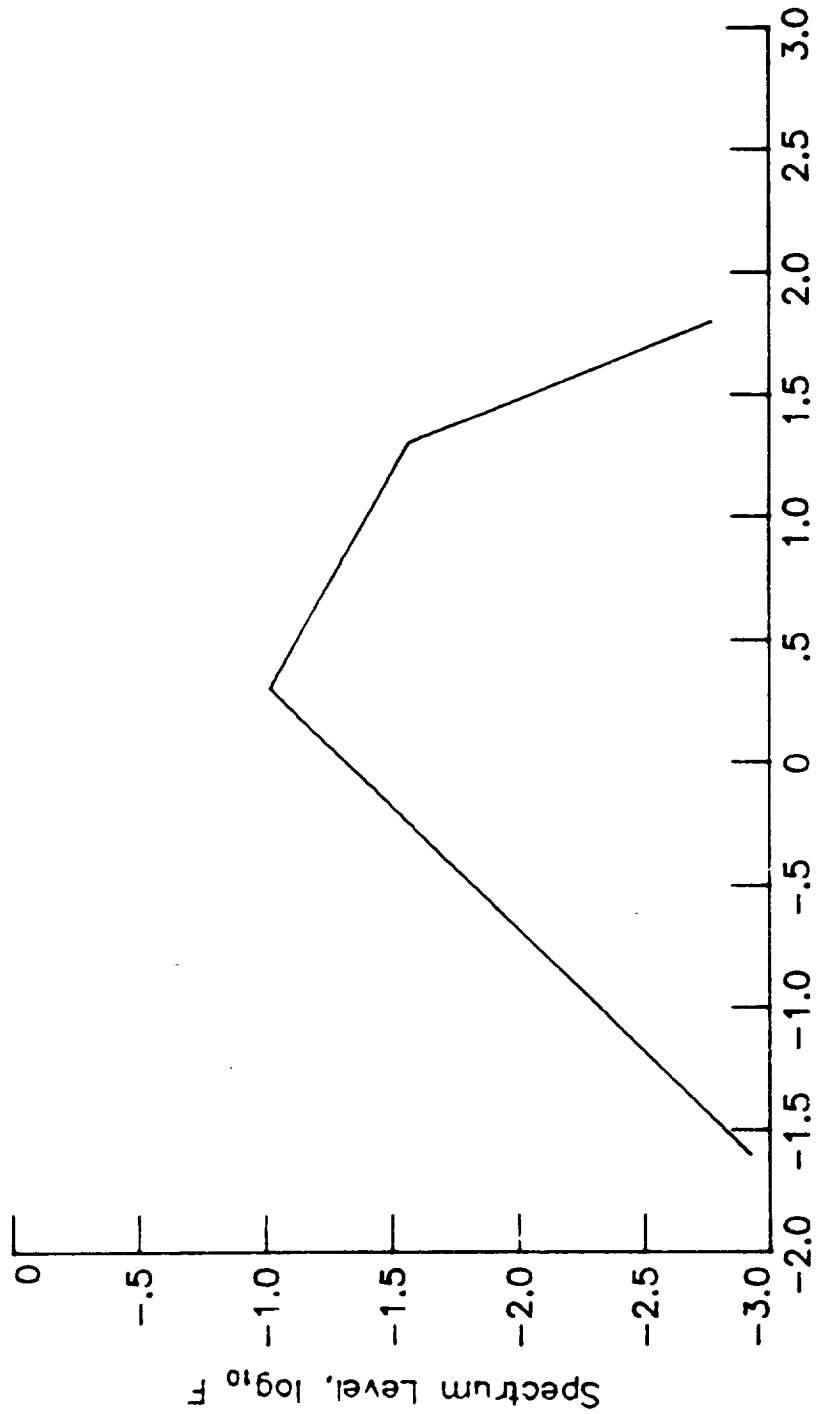

Figure 7.- Spectrum level for single and double slotted trailing-edge flap noise.

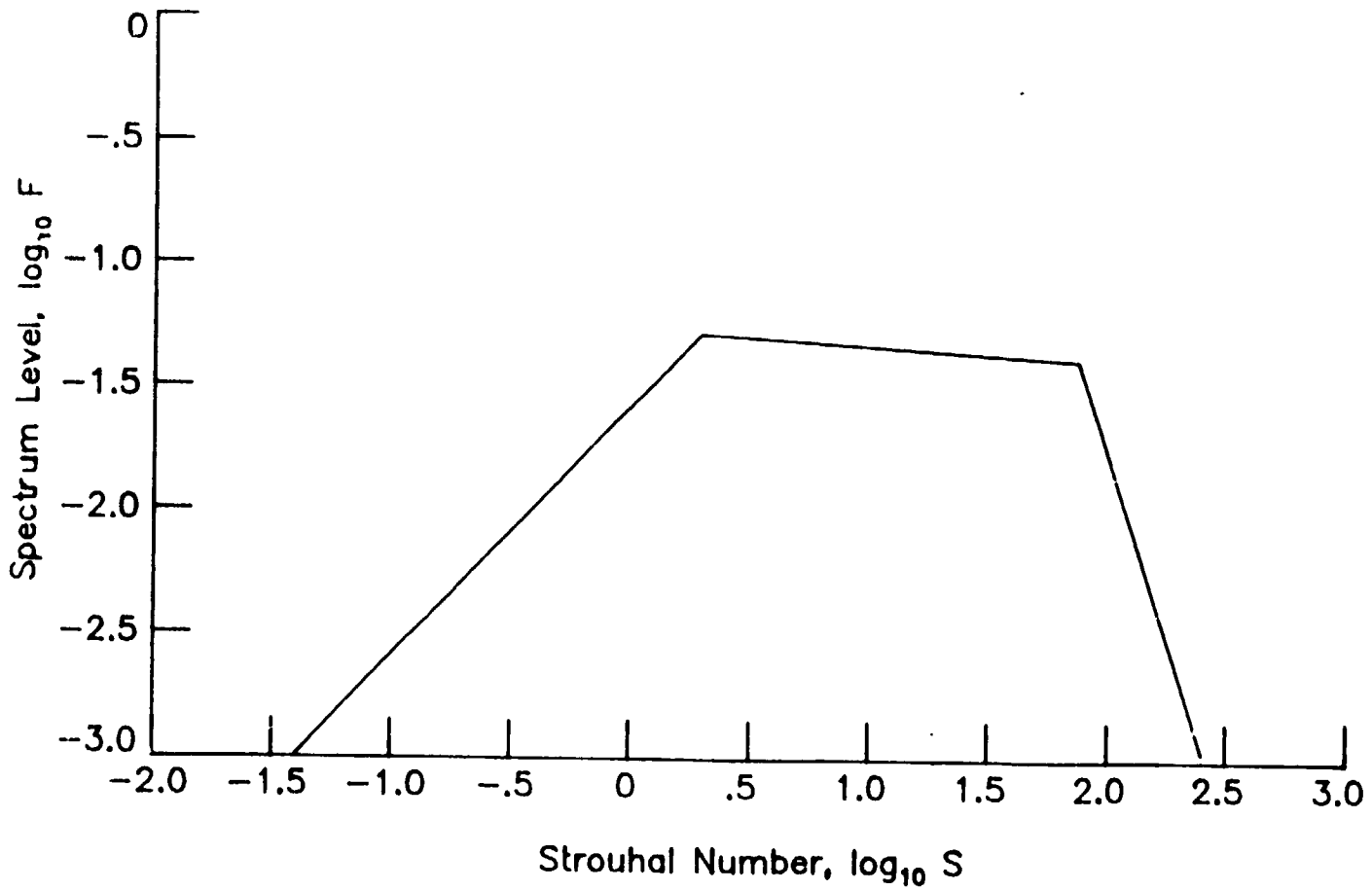

Figure 8.- Spectrum level for triple slotted trailing-edge flap noise.

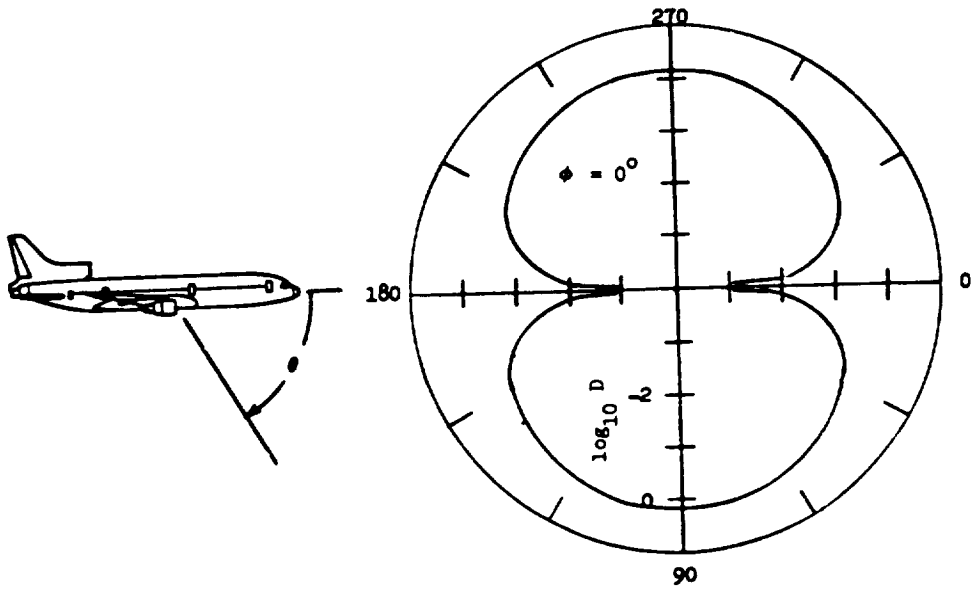

(a) Variation with polar directivity angle.

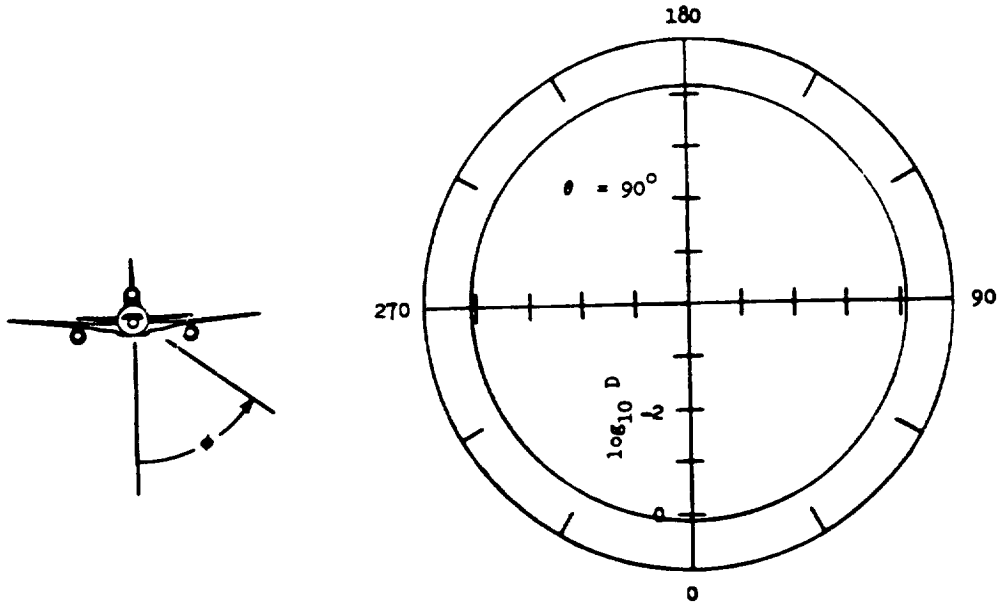

(b) Variation with azimuthal directivity angle.

Figure 9.- Directivity level for landing-gear wheel noise.

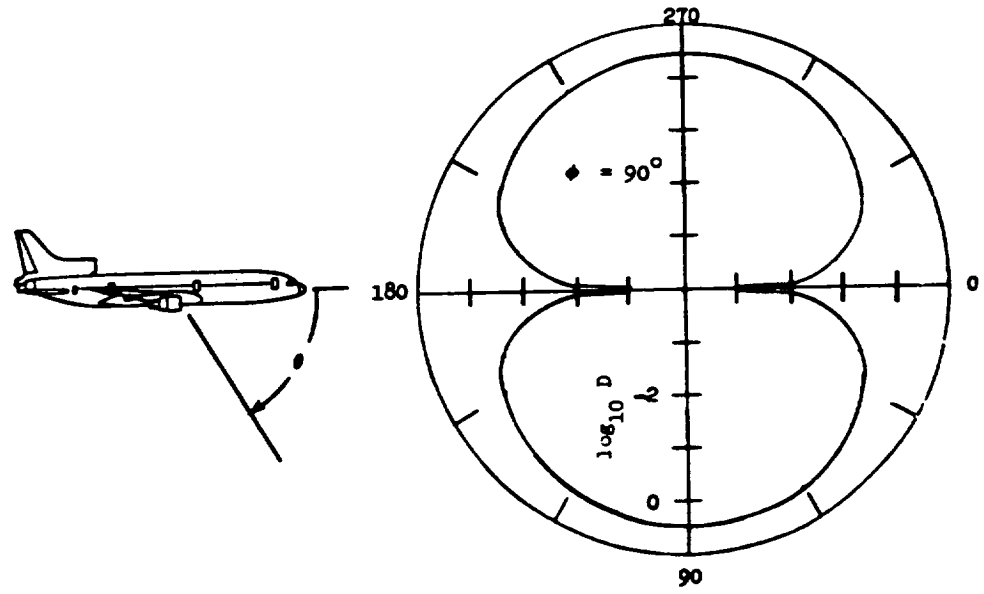

(a) Variation with polar directivity angle.

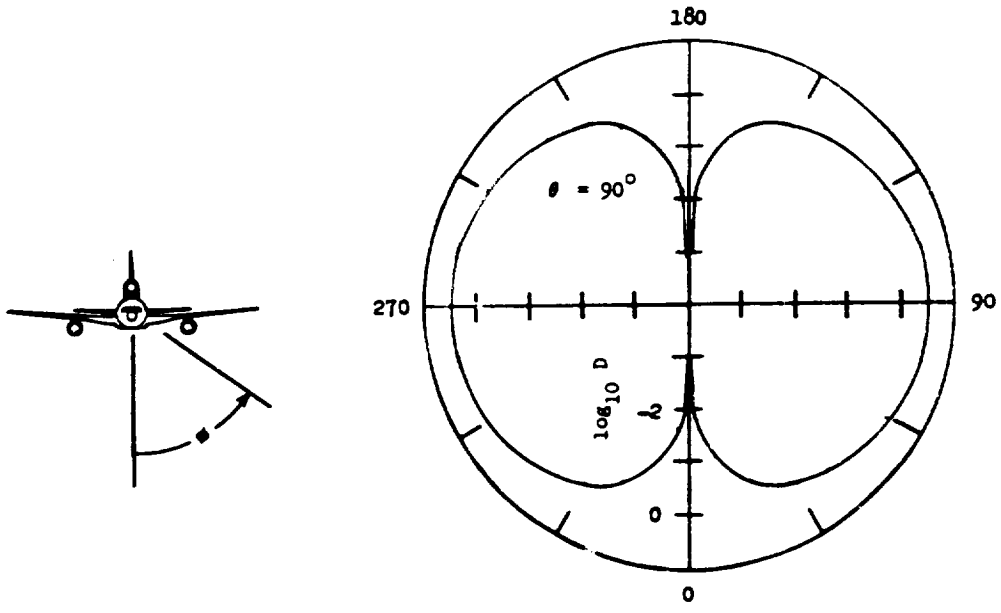

(b) Variation with azimuthal directivity angle.

Figure 10.- Directivity level for landing-gear strut noise.

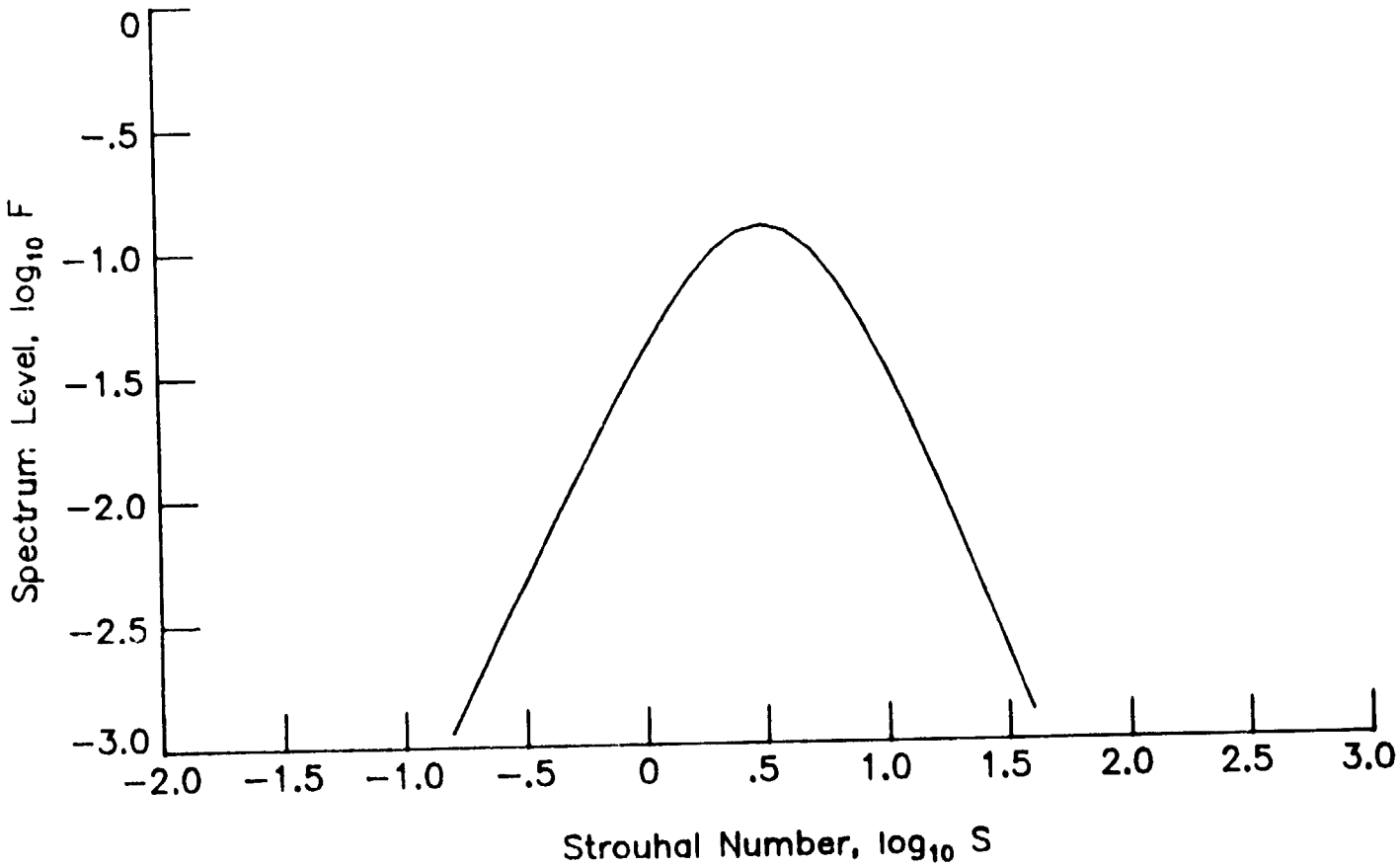

Figure 11.- Spectrum level for one- and two-wheel landing-gear wheel noise.

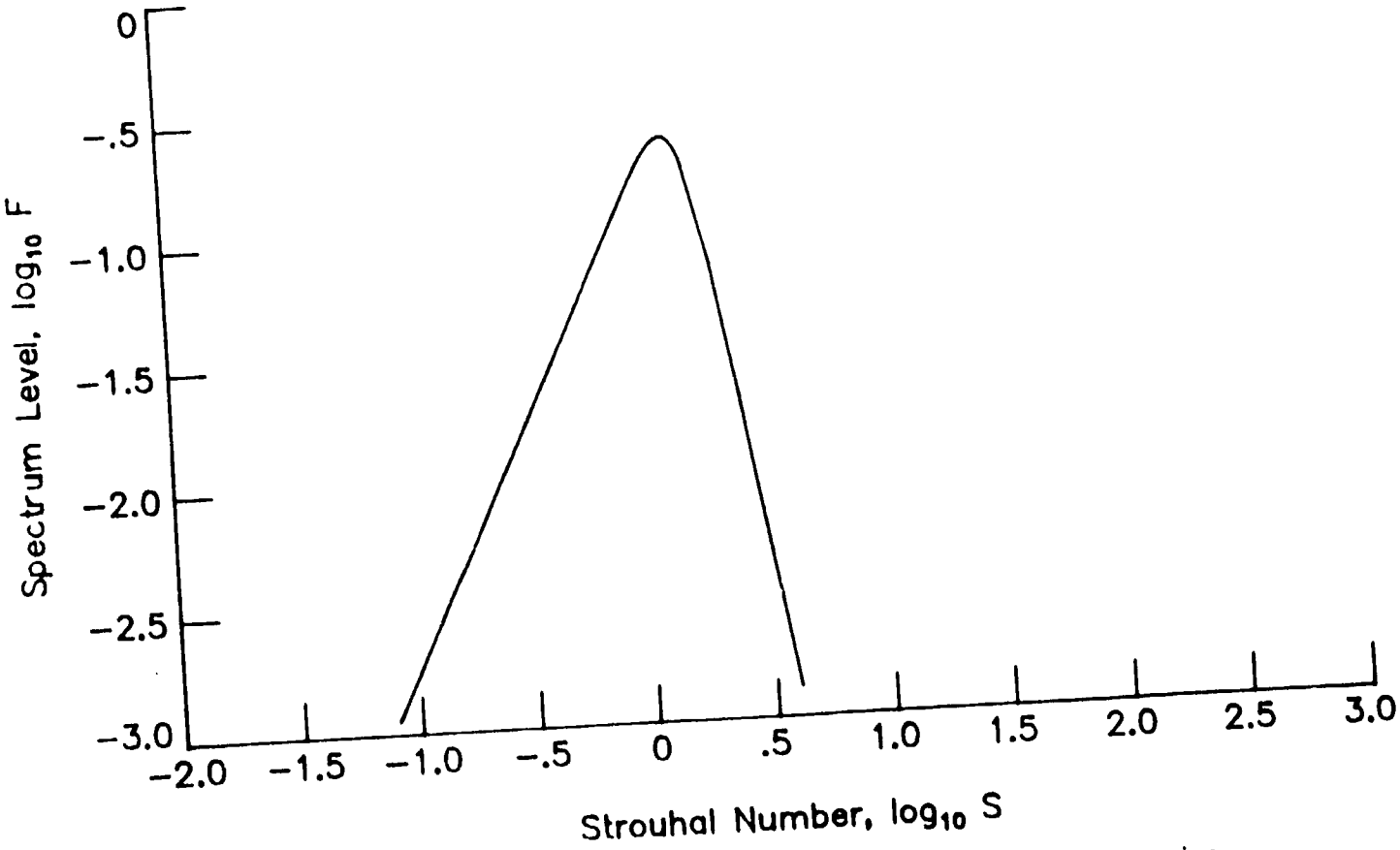

Figure 12.- Spectrum level for one- and two-wheel landing-gear strut noise.

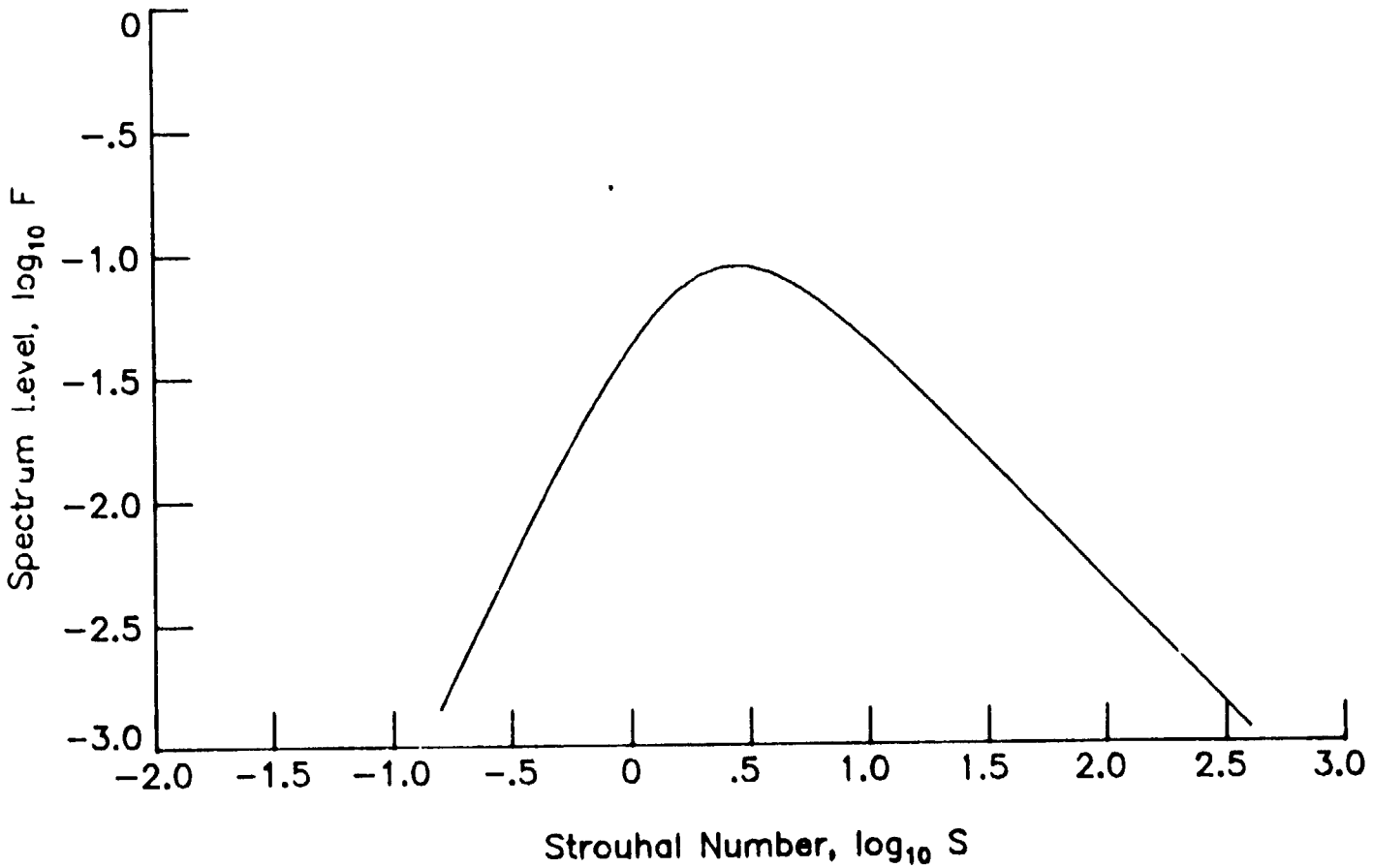

Figure 13.- Spectrum level for four-wheel landing-gear wheel noise.

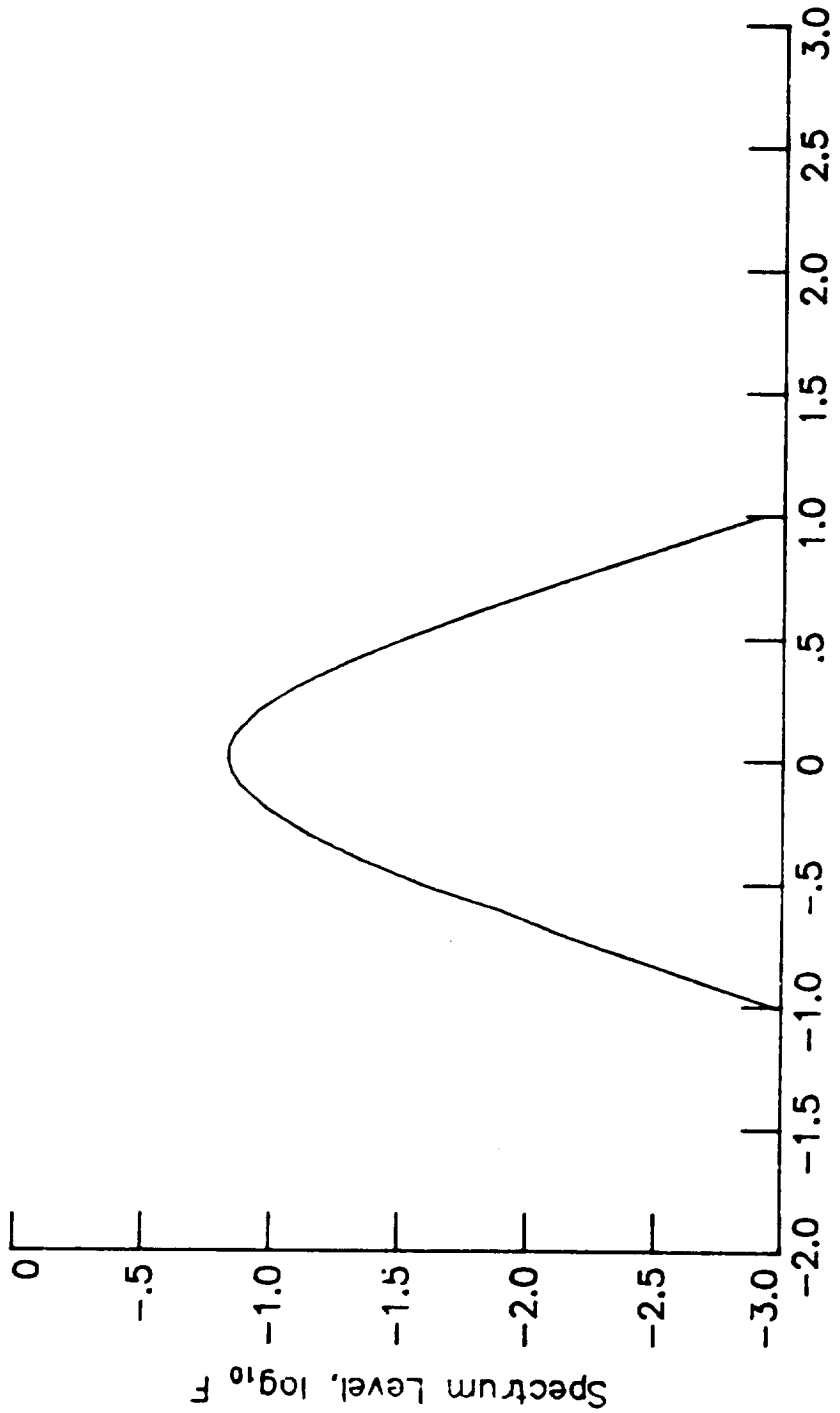

Figure 14.- Spectrum level for four-wheel landing-gear strut noise.

8.9 SMITH AND BUSHELL TURBINE NOISE MODULE

INTRODUCTION

The Smith and Bushell Turbine Noise Module predicts the broadband noise for an axial flow turbine. The prediction is based on the method developed by Smith and Bushell (ref. 1). The method employs empirical functions to produce sound spectra as a function of frequency and polar directivity angle. The method assumes that the only significant noise source is the "vortex" component, which is the broadband noise due to the interaction of the rotating blades with random velocity patterns in the flow.

The method requires input of several parameters. The turbine entrance and exit flow parameters can be provided by the Turbine Noise Parameters Module or directly by the user. Additional user-provided parameters are required. The module is executed once for each set of values of the input parameters. The output is a table of the mean-square acoustic pressure as a function of frequency, polar directivity angle, and azimuthal directivity angle. Although turbine noise is assumed not to vary with azimuthal directivity angle, it is introduced so that the output table is compatible with other noise tables.

SYMBOLS

A	turbine inlet cross-sectional area, m^2 (ft^2)
A_e	engine reference area, m^2 (ft^2)
C	rotor blade mean axial chord, m (ft)
c_∞	ambient speed of sound, m/s (ft/s)
D	directivity function
d	turbine rotor diameter, m (ft)
F	spectrum function
f	frequency, Hz
f^*	Helmholtz number, fC/c_∞
f_a	fuel-to-air ratio
h_a	absolute humidity, percent mole fraction
M_t	rotor blade tip Mach number

M_∞	aircraft Mach number
$\dot{m}$	mass flow rate, kg/s (slugs/s)
N	rotational speed, Hz
N_e	number of engines
N_s	number of turbine stages
$\langle p^2 \rangle^*$	mean-square acoustic pressure, re $\rho_\infty^2 c_\infty^4$
p_{ref}	reference pressure, 2×10^{-5} Pa (4.177×10^{-7} lb/ft^2)
R	dry air gas constant, re m^2/K-s^2 (ft^2/$^\circ$R-s^2)
$\mathcal{R}$	gas constant, m^2/K-s^2 (ft^2/$^\circ$R-s^2)
r_s	distance from source to observer, m (ft)
r_s^*	dimensionless distance from source to observer, re $\sqrt{A_e}$
T	temperature, K ($^\circ$R)
γ	ratio of specific heats
θ	polar directivity angle, deg
Π^*	acoustic power, re $\rho_\infty c_\infty^3 A$
Π_{ref}	reference power, 1×10^{-12} W (7.376×10^{-13} ft-lb/s)
ρ_∞	ambient density, kg/m^3 (slugs/ft^3)
ϕ	azimuthal directivity angle, deg

Subscripts:

i	entrance
j	exit
s	static
∞	ambient

Superscript:

*	dimensionless quantity

INPUT

The turbine parameters are required from either the output of the Turbine Noise Parameters Module or the user. Ambient conditions are required for computation of sound pressure levels. The frequency, polar directivity angle, and azimuthal directivity angle arrays establish the independent variable values for the output table. The turbine inlet cross-sectional area, rotor blade mean axial chord, and number of turbine stages are required for the geometric description of the turbine. Finally, the engine reference area, number of engines, and distance to the observer are required. The range and default values of the input parameters are given in table I.

Input Constants

A_e engine reference area, m^2 (ft^2)

N_e number of engines

r_s distance from source to observer, m (ft)

Turbine Geometry

A^* turbine inlet cross-sectional area, re A_e

C^* rotor blade mean axial chord of the last stage, re $\sqrt{A_e}$

N_s number of turbine stages

Turbine Noise Parameters

f_a fuel-to-air ratio

$\dot{m}^*$ core mass flow rate, re $\rho_\infty c_\infty A_e$

N^* rotational speed, re c_∞/d

$T^*_{s,j}$ exit static temperature, re T_∞

Ambient Conditions

c_∞ ambient speed of sound, m/s (ft/s)

h_a absolute humidity, percent mole fraction

M_∞ aircraft Mach number

ρ_∞ ambient density, kg/m^3 ($slugs/ft^3$)

Independent Variable Arrays

f	frequency, Hz
θ	polar directivity angle, deg
ϕ	azimuthal directivity angle, deg

OUTPUT

The output to this module is a table of the mean-square acoustic pressure as a function of frequency, polar directivity angle, and azimuthal directivity angle. In addition, the observer distance r_s is provided for the Propagation Module.

r_s	distance from source to observer, m (ft)

Turbine Noise Table

f	frequency, Hz
θ	polar directivity angle, deg
ϕ	azimuthal directivity angle, deg
$\langle p^2(f,\theta,\phi)\rangle^*$	mean-square acoustic pressure, re $\rho_\infty^2 c_\infty^4$

METHOD

The prediction method presented in reference 1 is used to compute the far-field noise. A schematic of a typical turbine is shown in figure 1. The Smith and Bushell method uses the coordinate system and directivity angles shown in this figure. The following prediction method gives the prediction for broadband vortex noise.

The equation for the far-field mean-square pressure for a turbine is

$$\langle p^2 \rangle^* = \frac{\Pi^* A^*}{4\pi (r_s^*)^2} \frac{D(\theta)\, F(f^*)}{(1 - M_\infty \cos\theta)^4} \tag{1}$$

In equation (1), Π^* is the overall power, D is the directivity function, and F is the spectrum function. The source to observer distance r_s is expressed in dimensionless form as

$$r_s^* = r_s / \sqrt{A_e} \tag{2}$$

The forward velocity effect is accounted for by the Doppler factor $(1 - M_\infty \cos \theta)^4$. The Helmholtz number f^* is defined as

$$f^* = \frac{fC^*\sqrt{A_e}}{c_\infty}(1 - M_\infty \cos \theta) \tag{3}$$

where C is the mean axial chord of the last stage turbine rotor blades.

The acoustic power Π^* for the turbine is

$$\Pi^* = (4.552 \times 10^{-5}) M_t^3 \dot{m}^* N_s \tag{4}$$

where N_s is the number of stages and $\dot{m}^*$ is the core mass flow rate. The blade tip Mach number M_t is defined as

$$M_t = \frac{\pi N^*}{2}\sqrt{\frac{\gamma_s R^* T^*_{s,j}}{\gamma_\infty}} \tag{5}$$

where N^* is the rotational speed and $T^*_{s,j}$ is the exit static temperature. The values of the local ratio of specific heats γ_s and the local gas constant $R^* = R/R$ are found from the input values of $T^*_{s,j}$, absolute humidity h_a, and fuel-to-air ratio f_a. The value of the ambient ratio of specific heats γ_∞ is 1.4.

The directivity function D is a function of polar directivity angle and is given in table II and plotted in figure 2. The spectrum function F is a function of Helmholtz number and is given in table III and plotted in figure 3. The mean-square acoustic pressure is then computed from equation (1). The total noise is the mean-square acoustic pressure multiplied by the number of engines N_e for the output table. In addition, printed output is available of the sound pressure level SPL defined as

$$SPL = 10 \log_{10} \langle p^2 \rangle^* + 20 \log_{10} \frac{\rho_\infty c_\infty^2}{p_{ref}} \tag{6}$$

and the power level PWL defined as

$$PWL = 10 \log_{10} \Pi^* + 10 \log_{10} \frac{\rho_\infty c_\infty^3 A^* A_e}{\Pi_{ref}} \tag{7}$$

REFERENCE

1. Smith, M. J. T.; and Bushell, K. W.: Turbine Noise - Its Significance in the Civil Aircraft Noise Problem. Paper 69-WA/GT-12, American Soc. Mech. Eng., Nov. 1969.

TABLE I.- RANGE AND DEFAULT VALUES OF INPUT PARAMETERS

Input parameter	Minimum	Default	Maximum
A_e, m^2	0.01	$\pi/4$	10
A^*	0.1	1	10
C^*	0.01	1	100
f_a	0	0	0.36767
h_a, %	0	0	4
$\dot{m}^*$	0	0.2	10
N^*	0	0.3	0.5
N_e	1	1	4
$T^*_{s,j}$	0.1	2	4
c_∞, m/s	200	340.294	400
M_∞	0	0	0.9
ρ_∞, kg/m^3	0.2	1.225	1.5
r_s, m	0.01	$\sqrt{A_e}$	100
N_s	1	1	10

TABLE II.- DIRECTIVITY FUNCTION

θ, deg	$10 \log_{10} D$
0.000	-13.400
10.000	-13.100
20.000	-12.300
30.000	-11.000
40.000	-9.100
50.000	-6.700
60.000	-3.800
70.000	-1.700
80.000	0.100
90.000	2.000
100.000	3.100
110.000	3.000
120.000	2.300
130.000	1.300
140.000	-0.700
150.000	-2.000
160.000	-2.900
170.000	-3.500
180.000	-3.700

TABLE III.- SPECTRUM FUNCTION

$\log_{10} f^*$	$10 \log_{10} F$
-1.700	-29.900
-1.600	-27.400
-1.500	-24.900
-1.400	-22.400
-1.300	-20.400
-1.200	-18.700
-1.100	-17.100
-1.000	-15.600
-0.900	-14.200
-0.800	-12.900
-0.700	-11.700
-0.600	-10.600
-0.500	-9.800
-0.400	-9.200
-0.300	-9.000
-0.200	-9.500
-0.100	-10.500
0.000	-12.200
0.100	-14.700
0.200	-17.800
0.300	-21.300
0.400	-25.100
0.500	-28.900

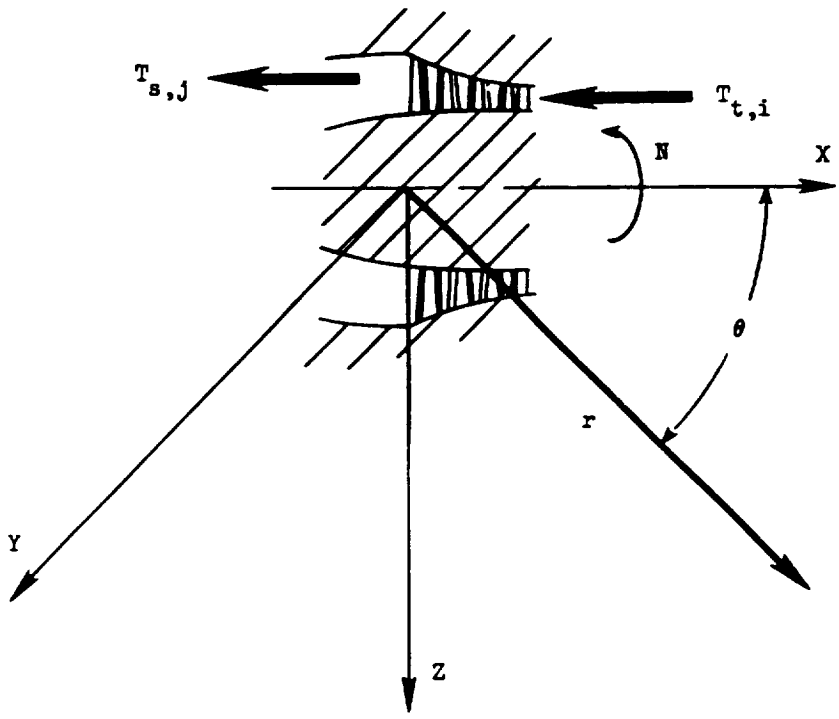

Figure 1.- Schematic diagram of typical axial-flow turbine.

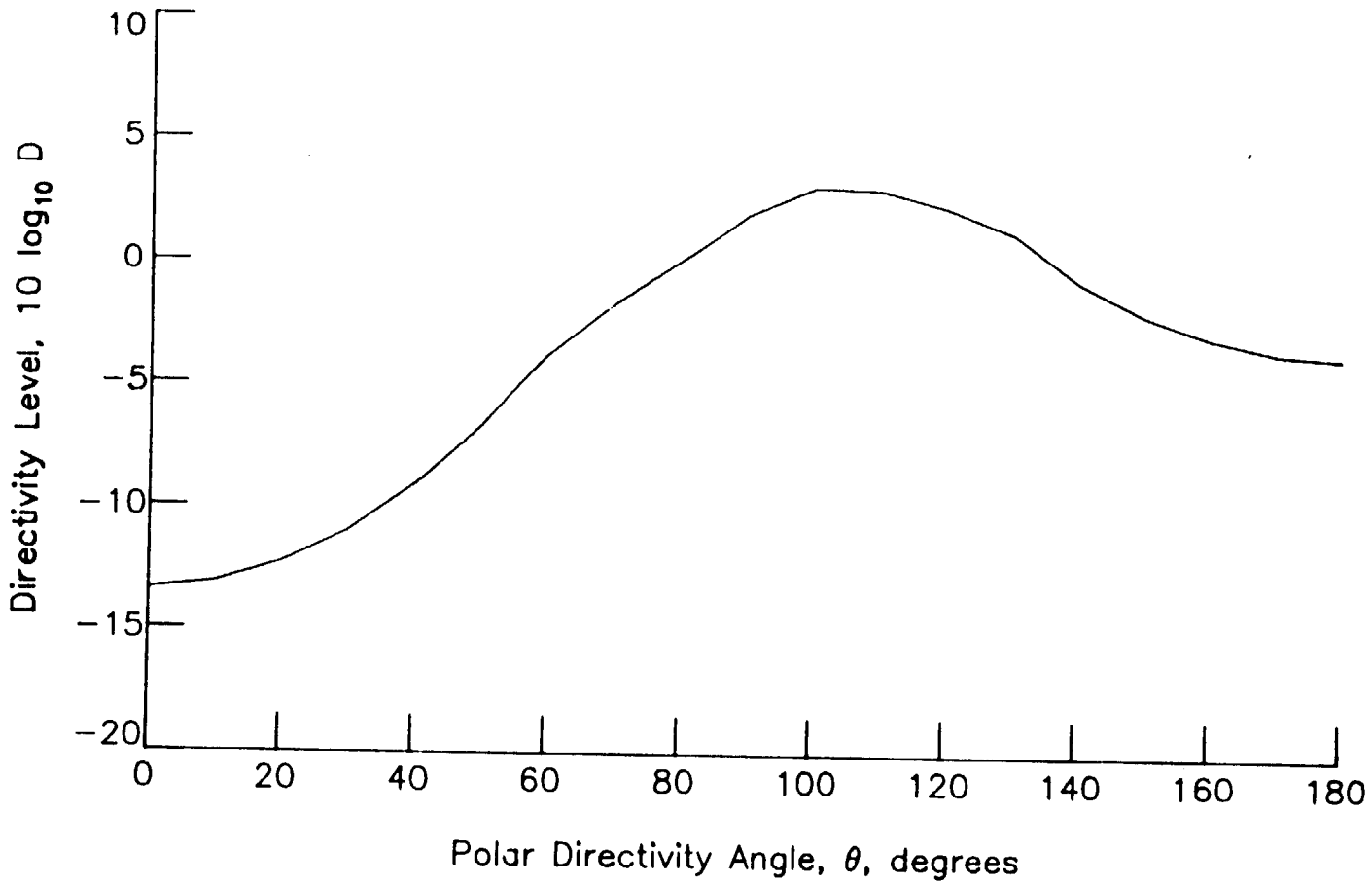

Figure 2.- Normalized directivity level for Smith and Bushell turbine noise prediction.

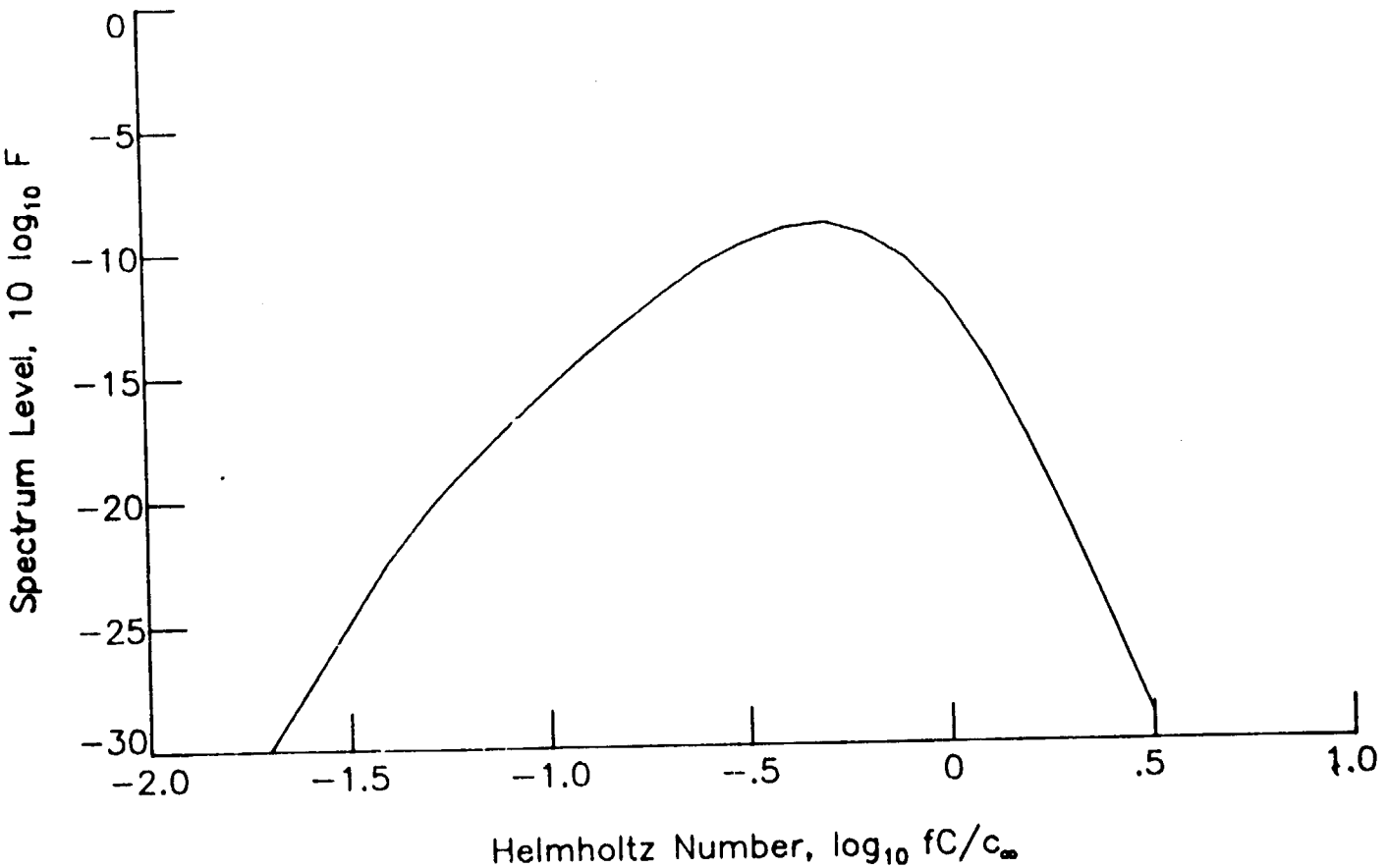

Figure 3.- Normalized spectrum level for Smith and Bushell turbine noise prediction.

9. PREDICTION PROCEDURES

9.1 ICAO REFERENCE NOISE-PREDICTION PROCEDURE (1978)

INTRODUCTION

In June of 1977, the International Civil Aviation Organization (ICAO) formed a prediction subcommittee to determine a reference noise-prediction procedure applicable to supersonic transports (SST's). The goals of the subcommittee were to:

1. Establish an agreed upon reference noise-prediction procedure

2. Assess the accuracy of the reference procedure against available measured flight-test noise levels

3. Determine, by use of the "trial engine," the differences in predicted noise level between the reference procedure and those procedures already used in parametric studies

4. Identify new noise problems associated with SST's, and to make the necessary recommendations so as to define an internationally recommended prediction procedure

Participating in the subcommittee work were NASA, British Aerospace Corporation, SNECMA, the U.S.S.R., The Boeing Company, McDonnell Douglas Corporation, Lockheed Corporation, Rolls-Royce Limited, General Electric Company, and Pratt & Whitney Aircraft Group. Each provided their predictions for a trial SST engine provided by SNECMA and for currently available measured data. Based on the results of these studies, a reference noise-prediction procedure was agreed upon. The results of the subcommittee study were presented to ICAO.

A summary of the prediction procedure used by each participant and the reference noise-prediction procedure are presented in table I. The results of the trial SST engine predictions for each method are presented in table II. It is interesting to note some of the wide variation in the component maximum perceived noise level (PNL) computations. The accuracy of the application of the reference noise-prediction procedure to various measured effective perceived noise level (EPNL) data is shown in figure 1.

All of the component methods in the ICAO reference noise-prediction procedure are included in ANOPP as separate functional modules or variants of the standard ANOPP functional modules. A discussion of each component noise-prediction method is presented subsequently.

SYMBOLS

c_r	standard sea level speed of sound, m/s (ft/s)
c_∞	ambient speed of sound, m/s (ft/s)
D	directivity function
d	fan diameter, m (ft)
F	spectral distribution function
f	frequency, Hz
f_p	peak frequency, Hz
h_a	absolute humidity, percent mole fraction
h_r	relative humidity, percent
L	acoustic liner length, m (ft)
$m(\theta)$	forward-velocity index
$\langle p^2 \rangle^*$	mean-square acoustic pressure, re $\rho_\infty^2 c_\infty^4$
p^*	ambient pressure, re p_r
p_r	standard sea level pressure, Pa (lb/ft^2)
S	suppression factor
S_c	corrected Strouhal number
T^*	ambient temperature, re T_r
T_j	jet temperature, K (^oR)
T_r	standard sea level temperature, K (^oR)
ΔT	thrust loss, percent
T_∞	ambient temperature, K (^oR)
V_j^*	jet velocity, re c_∞
X	humidity ratio
Y	vibrational absorption function
α	absorption coefficient, nepers/m (nepers/ft)

θ	polar directivity angle, deg
ρ_∞	ambient density, kg/m^3 (slugs/ft^3)

Subscripts:

cl	classical
h	high frequency
ℓ	low frequency
max	maximum
n	nitrogen
o	oxygen
ref	reference procedure
rot	rotational
sup	suppressed
vib	vibrational

JET MIXING NOISE

The method for predicting jet mixing noise is based on the method in appendix A of Society of Automotive Engineers (SAE) Aerospace Recommended Practice (ARP) 876 (ref. 1). This is presented in ANOPP as the Single Stream Circular Jet Noise Module. The method employs empirical data tabulated in terms of relevant dimensionless groups to produce sound spectra as functions of frequency and polar directivity angle.

The ICAO reference method differs from the Single Stream Circular Jet Noise Module in two ways. First, a different forward-velocity index $m(\theta)$, defined in table III and figure 2, is used. Second, additional data for the spectral distribution factor F at a value of the velocity ratio ($\log_{10} V_j^*$) of 0.3 is included. The additional spectral data are given in table IV and plotted in figure 3.

SHOCK NOISE

The method for predicting jet shock cell noise is based on proposed appendix C of SAE ARP 876 (ref. 1). This is presented in ANOPP as the Circular Jet Shock Cell Noise Module. The method uses master spectra functions and a shock-cell interference function to produce sound spectra as functions of frequency and polar directivity angle.

The ICAO reference method has an additional function not found in the Circular Jet Shock Cell Noise Module. The computed 1/3-octave-band mean-square pressure $\langle p^2 \rangle^*$ is multiplied by an additional directivity function D as follows:

$$\langle p^2 \rangle^*_{ref} = D(\theta) \langle p^2 \rangle^* \qquad (1)$$

The additional directivity function is a function of polar directivity angle θ and is given in table V and plotted in figure 4.

COMBUSTION NOISE

The method for predicting combustion noise is based on the proposed appendix C to reference 1. This is presented in ANOPP as the Combustion Noise Module. The method uses empirical data of core noise from turboshaft, turbojet, and turbofan engines to produce sound spectra as functions of frequency and polar directivity angle.

The ICAO reference method utilizes a different spectral distribution function F than the Combustion Noise Module. This spectrum function, called the "envelope spectrum," is given in table VI and plotted in figure 5.

COMPRESSOR/FAN INTAKE NOISE

The method for predicting compressor/fan intake noise is based on reference 2 by Heidman. This is presented in ANOPP as the Fan Noise Module. The method uses empirical functions to predict the sound spectra as functions of frequency and polar directivity angle.

The ICAO reference method uses the inlet broadband noise, inlet rotor-stator interaction tone, and inlet flow-distortion tone components from the Fan Noise Module. It is executed once for each of the first two stages. If performance data for the second stage are not known, then the second stage is taken to be similar to the first stage with the tone spectra shifted one 1/3-octave band higher than the first stage.

COMPRESSOR/FAN DISCHARGE-DUCT NOISE

The ICAO reference method uses the discharge broadband noise and the discharge rotor-stator interaction tone components of Heidman's method (ref. 2) as presented in the Fan Noise Module. The discharge-duct noise is only computed for bypass/fan engines. The noise is computed for a maximum of three stages, and the bypass mass flow is assumed to be the total flow. The last three stages are used if possible. If performance data are not available for a given stage, it can be assumed to be similar to the preceding stage with the tone spectra shifted one 1/3-octave band higher. Tone levels should be reduced by 5 dB if a core/bypass mixer or multielement silencer is used.

TURBINE NOISE

The method for predicting turbine noise is the vortex component of the Smith and Bushell method (ref. 3). This is presented in ANOPP as the Smith and Bushell Turbine Noise Module. The method uses empirical functions to predict sound spectra as functions of frequency and polar directivity angle. The ICAO reference method requires no changes of the Smith and Bushell Turbine Noise Module.

AIRFRAME NOISE

The method for predicting airframe noise is based on the FAA report by Fink (ref. 4). This is presented in ANOPP as the Airframe Noise Module. The method uses empirical and assumed functions to predict sound spectra as functions of frequency, polar directivity angle, and azimuthal directivity angle. The ICAO reference method requires no changes in the Airframe Noise Module.

ATMOSPHERIC ABSORPTION

The atmospheric-absorption method selected for the ICAO reference procedure is that of SAE ARP 866A (ref. 5). This method has been incorporated into the Atmospheric Absorption Module in ANOPP. The SAE absorption method is similar in procedure to the American National Standards Institute (ANSI) method contained in the module. The equations that follow directly replace the corresponding equations for the ANSI method, using the same nomenclature as the Atmospheric Absorption Module.

The sum of the absorption coefficients due to classical and molecular rotational effects is given by

$$\alpha_{cl} + \alpha_{rot} = 6.30 \times 10^{-9} \, (f/c_r) \frac{1.365 (T^*)^{3/2}}{T^* + 0.3713} \frac{f}{p^*} \tag{2}$$

where α is the absorption coefficient in nepers per unit length as defined in the Atmospheric Absorption Module. The sum of the vibrational relaxation absorption coefficients for nitrogen and oxygen is given by

$$\alpha_{vib,n} + \alpha_{vib,o} = 9.20 \times 10^{-4} \, (f/c_r) (T^*)^{1/2} \, 10^{2.43(T^*-1)} Y(X) \tag{3}$$

where the parameter X is given by

$$X = 4.05 h_r f^{-1/2} \, 10^{(T^*-1)\left\{(T^*-1)[41.9(T^*-1)-11.5]+7.62\right\}} \tag{4}$$

and $Y(X)$ is the vibrational absorption function given in table VII. In equation (4), the relative humidity h_r can be expressed in terms of the absolute humidity h_a as

$$h_r = \frac{p^*}{h_a} 10^{(8.4256-10.1995/T^*-4.922 \log_{10} T^*)} \tag{5}$$

The total absorption coefficient is the sum of equations (2) and (3). Then, the average dimensionless absorption coefficient is determined following the same procedure as the ANSI standard method.

PROPAGATION

Propagation of the sound spectra to the observer is accomplished by the Propagation Module. The tasks performed include spherical spreading, atmospheric absorption, and ground reflection and attenuation. The standard SAE atmospheric-absorption model as presented in SAE ARP 866A (ref. 5) is used. Ground reflection and attenuation is modeled by adding 2 dB to the free-field levels for a 1.2-m microphone height. The desired noise levels, including perceived noise level (PNL) and tone-corrected perceived noise level, are computed by the Noise Levels Module. Finally, the effective perceived noise level (EPNL) is computed by the Effective Noise Module.

SUPPRESSION

A variety of techniques have been developed for the suppression of aircraft engine noise, including acoustic lining, flow mixers, and silencing nozzles. The effects of noise suppression are accounted for in ANOPP by the General Suppression Module. This module takes a table of the suppression factor for a particular suppressor type as a function of frequency, polar directivity angle, and azimuthal directivity angle and multiplies each element of the appropriate noise-module output table.

The ICAO prediction subcommittee provided recommended techniques for quantifying the effects of suppression on each noise-source component. These methods are presented below for implementation by the user. Alternate techniques for estimating suppressor effects may also be used.

Jet-Noise Suppression

The ICAO Jet Suppressor Subgroup has produced a recommended technique for quantifying all types of jet-noise suppression. The suppression factor S is defined as follows:

$$\langle p^2 \rangle^*_{sup} = S \langle p^2 \rangle^* \tag{6}$$

where $\langle p^2 \rangle^*$ is the unsuppressed mean-square acoustic pressure. The expression for the jet-noise suppression factor is

$$S = 10^{0.1(1+\Delta S)S_{max}D(\theta)} \tag{7}$$

The maximum suppression S_{max} for any kind of jet-noise suppressor has been correlated with gross performance loss. The data of S_{max} as a function of gross thrust loss ΔT through use of the suppression technique are given in table VIII and plotted in figure 5. The following three curves are presented: Pre-1972 technology, latest projected technology, and a recommendation for parametric studies. A jet-velocity-suppression correction factor ΔS must be multiplied with S_{max} to incorporate the effects of the magnitude of the jet velocity. The value of ΔS as a function of the jet velocity V_j^* is given in table IX and plotted in figure 7. Finally, a directivity function $D(\theta)$, as given in table X, must be applied.

Shock-Noise Suppression

The jet-noise suppression factor is applied to the shock noise with no modifications.

Core-Noise Suppression

The core noise is assumed to be attenuated 3.3 dB/m (1.0 dB/ft) of acoustic liner ($S = 0.469^{L_\ell}$, where L_ℓ is the length of the liner in meters). The liner should be designed for low-frequency attenuation.

Turbine-Noise Suppression

Any liner designed to produce core-noise suppression will suppress turbine noise by the same amount. In addition, an acoustic lining designed to reduce high-frequency turbine noise will attenuate turbine noise by 9.8 dB/m (3.0 dB/ft). Therefore, the total suppression factor S is $(0.469)^{L_\ell}$ $(0.103)^{L_h}$, where L_ℓ and L_h are the lengths of each type of liner in meters. The total turbine-noise suppression should be limited to 20.0 dB.

Inlet-Noise Suppression

The compressor/fan intake noise is reduced 10 dB for each fan diameter of equivalent length of effective wall lining ($S = 0.100^{L/d}$). It is suggested that the overall reduction be limited to 10.0 dB.

Bypass-Duct-Noise Suppression

The compressor/fan discharge duct noise is reduced by 9.8 dB/m (3.0 dB/ft) of acoustic treatment on both inner and outer walls ($S = 0.103^{L}$). If only the outer wall is treated, reduce the noise 6.6 dB/m (2.0 dB/ft) ($S = 0.221^{L}$) and if only the inner wall is treated, reduce the noise 4.9 dB/m (1.5 dB/ft) ($S = 0.322^{L}$). The bypass-duct attenuation should be limited to 15 dB. For bypass ratios greater than 2, a maximum attenuation of 10.0 dB is suggested.

INSTALLATION EFFECTS

The interaction of the engines and airframe and the engine location affect the noise radiated from the aircraft. These deviations from the point source model are often referred to as installation effects. The ICAO prediction subcommittee recommended a 2.0-dB increase in the total engine noise levels to account for installation effects likely on a new SST.

REFERENCES

1. Gas Turbine Jet Exhaust Noise Prediction. ARP 876, Soc. Automot. Eng., Mar. 1978.

2. Heidman, M. F.: Interim Prediction Method for Fan and Compressor Source Noise. NASA TM X-71763, 1975.

3. Smith, M. J. T.; and Bushell, K. W.: Turbine Noise - Its Significance in the Civil Aircraft Noise Problem. Paper 69-WA/GT-12, American Soc. Mech. Eng., Nov. 1969.

4. Fink, Martin R.: Airframe Noise Prediction Method. FAA-RD-77-29, Mar. 1977. (Available from DTIC as AD A039 664.)

5. Standard Values of Atmosphere Absorption as a Function of Temperature and Humidity for Use in Evaluating Aircraft Flyover Noise. ARP 866A, Soc. Automot. Eng., Aug. 1964.

TABLE I.- SUMMARY OF NOISE-PREDICTION METHODS USED BY PREDICTION SUBCOMMITTEE PARTICIPANTS

Participant	Source of prediction method for -						
	Jet	Shock	Combustor	Fan, forward	Fan, aft	Turbine	Airframe
NASA-ANOPP	ARP 876 plus own modified; Hoch SAE flight exponent	SAE draft ARP 876 proposal by Tanna, Fisher, & Harper-Borne	NASA TM X-71627	NASA TM X-71763	NASA TM X-71763	No approved method	FAA RD-77-29 by M. R. Fink
SNECMA	ARP 876 plus own modified; Hoch SAE flight exponent	Own method; YKA 5982/76	SAE draft by Matta; FAA RD-74-125 with envelope spectra	NASA TM X-71763, 1st stage only	NASA TM X-71763, 1st stage only	Matta; FAA-RD-77-4	None
British Aerospace Corp.	ARP 876 (pre-publication) plus SAE Hoch Proposal	SNECMA method	SAE draft	Smith and House with Tones	None ratified	GE method (Smith and Bushell for backup)	FAA RD-77-29
The Boeing Co.	ARP 876 plus own flight exponent	Not included	Own, but similar to SAE draft	Similar to NASA CR-114649; based on JT3D and JT9D	Similar to NASA CR-114649; based on JT3D and JT9D	JT3D-JT9D data base	None

TABLE I.- Concluded

Participant	Source of prediction method for -						
	Jet	Shock	Combustor	Fan, forward	Fan, aft	Turbine	Airframe
McDonnell Douglas Corp.	Own method	Not included	Not included	Modified Smith and House with Tones	Modified Smith and House with Tones	Modified Smith and Bushell with Tones	None
Lockheed Corp.	Modified ARP 876	SAE draft	SAE draft	Own method	Own method	GE method	Own unpublished method
Pratt & Whitney Aircraft Group	ARP 876 plus near average Hoch	SAE draft	Assumed low in SST	JT3D based method and no in-flight	Proprietary on tip speed "clean-up"	Own, Matthews (modified)	None
General Electric Co.	ARP 876 plus 1 db plus Bushell flight exponent	SAE draft	SAE draft	Estimated from measured spectra	Estimated from measured spectra	Estimated from measured spectra	Not considered
Rolls-Royce Limited	ARP 876 plus modified Hoch flight exponent	SAE draft	SAE draft with modified spectra and directivity	Own method based on [illegible] bypass ratio fans	Own method based on high bypass ratio fans	Own method	PAA RD-77-29

TABLE II.- RESULTS OF TRIAL SST PREDICTIONS

[100 percent power at 305 m (1000 ft)]

Participant	EPNL, dB	Peak PNL, dB, of source for -						Comments
		Jet	Shock	Core	Fan, forward	Fan, aft	Turbine	
NASA-ANOPP	$113\frac{1}{2}$	113	$112\frac{1}{2}$	96	110	102		Tone-corrected PNL (PNLT)
British Aerospace Corp.	[a]114	111	114	95	85	[b]115	$96\frac{1}{4}$	Fan rearwards doubted
SNECMA	$112\frac{1}{2}$	111	$113\frac{1}{2}$	96	106	91	[b]$72\frac{1}{2}$	Turbine low
U.S.S.R.	110	111		101	108	$102\frac{1}{4}$	$89\frac{1}{2}$	
Boeing Co.	[a]$111\frac{1}{2}$	$111\frac{1}{4}$	[a,b]110	$96\frac{1}{2}$	$97\frac{1}{2}$	$98\frac{1}{2}$	77	Shock "assessed"
McDonnell Douglas	112	112		99	107	93	101	
Lockheed	[a]113	111	114	96	109			
General Electric	[a]$114\frac{1}{2}$	116	$113\frac{1}{4}$	$95\frac{1}{4}$	$109\frac{1}{4}$		78	Inlet guide vane fan assessed
Rolls-Royce	$113\frac{1}{2}$	109	$113\frac{1}{4}$	$101\frac{1}{2}$	100	97	$88\frac{1}{2}$	EPNL includes 1.2 m ground reflection
Pratt & Whitney	112	$112\frac{1}{4}$			$110\frac{1}{2}$	$110\frac{1}{2}$	$74\frac{1}{2}$	
Average	$113\pm1\frac{1}{2}$	112	113	$97\frac{1}{2}$	$106\frac{1}{2}$	101	86	
Reference procedure	$113\frac{1}{2}$	$115\frac{1}{2}$	$114\frac{1}{2}$	97	$107\frac{1}{2}$	102	$98\frac{1}{2}$	

[a]Assessed, not accurately predicted.
[b]Not included in total.

TABLE III.- FORWARD-VELOCITY INDEX $m(\theta)$

θ, deg	$m(\theta)$
0.000	0.000
10.000	0.000
20.000	0.000
30.000	0.000
40.000	0.000
50.000	0.000
60.000	0.000
70.000	0.000
80.000	0.000
90.000	.100
100.000	.400
110.000	.900
120.000	1.700
130.000	2.900
140.000	4.200
150.000	5.400
160.000	6.700
170.000	8.000
180.000	9.300

TABLE IV.- NORMALIZED SPECTRAL DISTRIBUTION FACTOR $-10 \log_{10} F$

(a) $T_j/T_\omega = 1.0$; $\log_{10} V_j^* = 0.3$

$\log_{10} S_c$	$-10 \log_{10} F$ for θ of -									
	90°	100°	110°	120°	130°	140°	150°	160°	170°	180°
-2.000	41.400	41.633	43.933	48.233	47.267	47.800	48.233	43.400	40.500	39.533
-1.600	32.600	32.700	34.100	36.100	35.400	34.600	34.100	30.600	28.500	27.800
-1.300	26.000	26.000	26.800	27.000	26.500	24.700	23.500	21.000	19.500	19.000
-1.150	22.900	22.500	23.200	23.400	23.100	21.100	19.400	16.900	15.400	14.900
-1.000	19.300	19.500	19.500	20.000	20.000	17.500	15.300	13.000	11.620	11.160
-.824	16.500	16.500	16.500	17.000	17.000	14.100	11.800	9.800	8.600	8.200
-.699	14.800	14.900	14.500	15.000	15.000	12.500	10.100	8.400	7.380	7.040
-.602	13.800	13.800	13.300	13.900	13.800	11.200	9.500	8.400	7.740	7.520
-.500	12.700	13.000	12.200	12.800	12.500	10.200	9.500	9.100	8.860	8.780
-.398	11.900	12.000	11.600	12.000	11.600	9.800	9.800	10.300	10.600	10.700
-.301	11.500	11.300	11.100	11.500	11.000	9.500	10.300	11.600	12.380	12.640
-.222	11.100	10.900	11.000	11.300	10.800	9.700	11.100	12.800	13.820	14.160
0.000	11.000	10.900	10.900	11.000	11.000	10.900	14.000	16.300	17.680	18.140
.477	12.900	12.900	12.900	12.900	14.000	16.500	20.500	24.000	26.100	26.800
1.000	17.500	17.500	17.500	17.500	19.000	23.300	27.800	32.500	35.820	36.260
1.600	24.700	24.400	24.000	24.000	25.300	31.000	36.500	42.000	45.300	46.400
1.700	25.900	25.550	25.083	25.083	26.350	32.283	37.950	43.583	46.963	48.090

TABLE IV.- Continued

(b) $T_j/T_\infty = 2.0$; $\log_{10} V_j^* = 0.3$

$\log_{10} S_c$	$-10 \log_{10} F$ for θ of -									
	90°	100°	110°	120°	130°	140°	150°	160°	170°	180°
-2.000	38.200	40.767	42.500	44.400	46.333	46.067	47.200	42.467	39.627	38.680
-1.600	29.800	31.300	32.500	33.600	34.200	32.600	32.800	30.200	28.640	28.120
-1.300	23.500	24.200	25.000	25.500	25.100	22.500	22.000	21.000	20.400	20.200
-1.150	20.500	21.100	21.700	22.100	21.100	18.900	18.400	18.000	17.760	17.680
-1.000	17.800	18.000	18.500	18.800	17.500	15.200	15.200	15.400	15.520	15.560
-.824	15.300	15.000	15.300	15.300	14.100	12.000	12.000	13.100	13.760	13.980
-.699	13.500	13.100	13.500	13.500	12.200	10.200	10.900	11.800	12.580	12.840
-.602	12.300	12.000	12.300	12.300	11.100	9.600	10.200	10.900	11.320	11.460
-.500	11.500	11.000	11.200	11.200	10.300	9.400	10.000	10.200	10.320	10.360
-.398	11.000	10.300	10.600	10.600	9.900	9.700	10.300	10.000	9.820	9.760
-.301	10.700	10.100	10.300	10.300	9.900	10.100	11.000	10.200	9.720	9.560
-.222	10.700	10.100	10.200	10.200	10.000	10.700	11.600	10.800	10.320	10.160
0.000	11.100	11.000	11.000	11.000	11.300	13.200	13.900	13.000	12.460	12.280
.477	14.300	14.700	14.500	15.000	17.000	20.700	19.800	19.000	18.520	18.360
1.000	19.500	20.000	20.000	21.000	24.000	29.700	26.600	25.800	24.720	24.360
1.600	26.000	26.000	26.000	28.000	32.000	40.200	34.000	33.200	32.720	32.560
1.700	27.083	27.000	27.000	29.167	33.333	41.950	35.067	34.433	34.053	33.926

TABLE IV.- Continued

(c) $T_j/T_\infty = 2.5$; $\log_{10} V_j^* = 0.3$

$\log_{10} S_c$	$-10 \log_{10} F$ for θ of -									
	90°	100°	110°	120°	130°	140°	150°	160°	170°	180°
-2.000	38.567	40.133	41.867	44.467	45.867	46.100	45.833	41.700	39.220	38.394
-1.600	29.900	30.800	32.000	33.000	33.200	32.500	31.700	28.900	27.220	26.660
-1.300	23.400	23.800	24.600	24.400	23.700	22.300	21.100	19.300	18.220	17.860
-1.150	20.400	20.800	21.400	20.900	19.800	18.400	17.800	16.900	16.360	16.180
-1.000	17.800	17.900	18.100	17.200	16.200	15.300	15.100	14.800	14.620	14.560
-.824	15.000	14.900	14.800	13.900	12.800	12.400	12.500	12.600	12.660	12.680
-.699	13.200	13.000	13.000	12.200	10.900	10.900	11.100	11.300	11.420	11.460
-.602	12.200	11.900	12.000	11.200	10.200	10.200	10.600	10.500	10.600	10.600
-.500	11.300	11.100	11.100	10.500	9.800	10.100	10.300	10.100	9.980	9.940
-.398	10.800	10.500	10.500	10.200	9.900	10.400	10.800	10.000	9.520	9.360
-.301	10.400	10.400	10.400	10.200	10.200	11.100	11.300	10.100	9.380	9.140
-.222	10.600	10.400	10.500	10.300	10.700	11.700	12.000	10.700	9.920	9.660
0.000	11.200	11.100	11.200	11.600	12.800	13.600	14.000	13.200	12.720	12.560
.477	14.700	14.800	15.400	16.500	18.000	19.000	18.400	18.900	19.200	19.300
1.000	19.800	19.800	19.800	21.800	23.400	25.000	23.500	24.900	25.740	26.020
1.600	25.300	25.300	25.300	28.000	30.100	32.000	29.200	31.600	33.040	33.520
1.700	26.217	26.217	26.217	29.033	31.217	33.162	30.150	32.717	34.257	34.771

TABLE IV.- Continued

(d) $T_j/T_\omega = 3.0$; $\log_{10} V_j^* = 0.3$

$\log_{10} S_c$	$-10 \log_{10} F$ for θ of -									
	90°	100°	110°	120°	130°	140°	150°	160°	170°	180°
-2.000	38.967	39.867	42.067	43.167	44.500	44.867	42.667	40.333	38.933	38.466
-1.600	30.300	30.800	32.600	32.500	32.500	31.600	30.000	27.000	25.200	24.600
-1.300	23.800	24.000	25.500	24.500	23.500	22.000	21.400	17.000	14.360	13.480
-1.150	20.400	21.000	21.600	21.000	19.500	18.100	18.000	14.000	11.600	10.800
-1.000	17.500	17.800	17.600	17.800	15.400	14.900	15.200	12.300	10.560	9.980
-.824	14.500	14.300	14.200	14.300	11.800	12.000	12.500	11.100	10.260	9.980
-.699	12.900	12.500	12.300	12.500	10.100	11.000	10.900	10.500	10.260	10.180
-.602	11.900	11.400	11.000	11.300	10.000	10.700	10.300	10.200	10.140	10.120
-.500	11.200	10.600	10.300	10.600	10.100	10.700	10.100	10.100	10.100	10.100
-.398	10.900	10.300	10.200	10.300	10.600	10.900	10.500	10.000	9.700	9.600
-.301	10.900	10.300	10.000	10.300	11.200	11.100	11.100	10.100	9.500	9.300
-.222	11.000	10.400	10.000	10.400	11.900	11.900	11.800	10.800	10.200	10.000
0.000	11.500	11.400	11.200	11.500	14.100	13.100	14.000	12.400	11.440	11.120
.477	15.100	15.100	15.200	16.400	18.500	17.000	19.700	16.000	13.780	13.040
1.000	19.900	20.400	20.400	22.700	23.700	21.300	25.900	20.300	16.940	15.820
1.600	25.500	24.700	25.700	29.500	29.900	26.000	33.000	25.000	20.200	18.600
1.700	25.850	25.417	26.583	30.633	30.933	26.783	34.183	25.783	20.743	19.063

TABLE IV.- Concluded

(e) $T_j/T_\infty = 3.5$; $\log_{10} V_j^* = 0.3$

$\log_{10} S_c$	$-10 \log_{10} F$ for θ of -									
	90°	100°	110°	120°	130°	140°	150°	160°	170°	180°
-2.000	38.800	39.900	42.567	43.767	45.933	45.267	44.867	38.600	34.840	33.586
-1.600	30.000	30.700	31.900	32.300	33.000	31.800	30.200	25.800	23.160	22.280
-1.300	23.400	23.800	23.900	23.700	23.300	21.700	19.200	17.400	16.320	15.960
-1.150	20.300	20.600	20.400	19.900	19.200	18.000	16.800	15.000	13.320	12.760
-1.000	17.000	17.000	17.300	16.100	15.700	14.400	14.400	13.200	12.480	12.240
-.824	14.100	14.000	14.000	12.700	12.200	11.600	12.100	11.600	11.300	11.200
-.699	12.600	12.400	12.500	11.200	10.700	10.600	10.600	10.700	10.760	10.780
-.602	11.600	11.600	11.400	10.500	10.100	10.200	10.000	10.100	10.160	10.180
-.500	11.000	11.000	10.900	10.100	10.300	10.700	10.100	10.000	9.940	9.920
-.398	10.600	10.600	10.500	10.000	11.000	11.200	10.500	10.400	10.340	10.320
-.301	10.600	10.400	10.400	10.200	11.700	12.000	11.200	11.000	10.880	10.840
-.222	10.600	10.500	10.500	10.600	12.400	13.000	12.000	11.800	11.680	11.640
0.000	11.400	11.300	11.400	12.300	15.200	15.400	14.400	14.300	14.240	14.220
.477	15.000	15.100	15.600	17.200	21.000	21.300	20.100	20.200	20.260	20.280
1.000	20.400	20.400	20.700	23.200	27.800	28.100	26.100	26.600	26.900	27.000
1.600	26.300	26.300	26.000	29.800	35.600	36.000	33.000	34.000	34.600	34.800
1.700	27.283	27.283	26.883	30.900	36.900	37.317	34.150	35.230	35.878	36.094

TABLE V.- ADDITIONAL SHOCK-CELL NOISE

DIRECTIVITY FUNCTION

θ, deg	$10 \log_{10} D$
30.000	0.000
40.000	.250
50.000	.500
60.000	1.000
70.000	1.500
80.000	2.000
90.000	2.500
100.000	3.000
110.000	3.500
120.000	4.000
130.000	5.000
140.000	6.000
150.000	7.000
160.000	8.000
170.000	8.000

TABLE VI.- ENVELOPE SPECTRUM FOR

COMBUSTION NOISE

$\log_{10} f/f_p$	$10 \log_{10} F$
-1.100	-31.500
-1.000	-28.000
-.900	-25.000
-.800	-22.000
-.700	-19.500
-.600	-17.000
-.500	-15.000
-.400	-13.500
-.300	-12.000
-.200	-11.000
-.100	-10.200
0.000	-10.000
.100	-10.200
.200	-10.500
.300	-11.000
.400	-12.000
.500	-13.000
.600	-14.000
.700	-15.000
.800	-16.000
.900	-17.500
1.000	-19.000
1.100	-20.500
1.200	-22.000
1.300	-24.000
1.400	-25.500

TABLE VII.- MOLECULAR VIBRATIONAL ABSORPTION FUNCTION

FOR SAE ATMOSPHERIC ABSORPTION METHOD

X	Y(X)
0.00	0.000
.25	.315
.50	.700
.60	.840
.70	.930
.80	.975
.90	.996
1.00	1.000
1.10	.970
1.20	.900
1.30	.840
1.50	.750
1.70	.670
2.00	.570
2.30	.495
2.50	.450
2.80	.400
3.00	.370
3.30	.330
3.60	.300
4.15	.260
4.45	.245
4.80	.230
5.25	.220
5.70	.210
6.05	.205
6.50	.200
7.00	.200
10.00	.200

TABLE VIII.- MAXIMUM JET-NOISE SUPPRESSION FACTOR

ΔT, percent	S_{max}, dB, for -		
	Demonstrated pre-1972 technology	Recommended for parametric studies	Latest technology
1.000	0.000	0.000	0.000
2.000	2.200	3.500	5.100
4.000	4.600	6.200	10.400
6.000	6.000	9.300	13.400
8.000	7.000	10.800	15.700
10.000	7.600	11.900	17.300
12.000	8.400	12.800	18.600
14.000	8.800	13.700	19.800
16.000	9.200	14.400	20.800
18.000	9.800	15.000	21.700
20.000	10.000	15.400	22.600

TABLE IX.- JET-NOISE SUPPRESSION FACTOR

VELOCITY CORRECTION

V_j^*	ΔS
0.000	-1.000
1.070	-1.000
1.250	-.800
1.430	-.600
1.610	-.400
1.790	-.200
1.970	0.000
3.000	0.000

TABLE X.- DIRECTIVITY FUNCTION FOR

JET-NOISE SUPPRESSION

θ, deg	$D(\theta)$
≤ 30	0
60	.3
80	.5
100	.7
120	1.0
>120	1.2

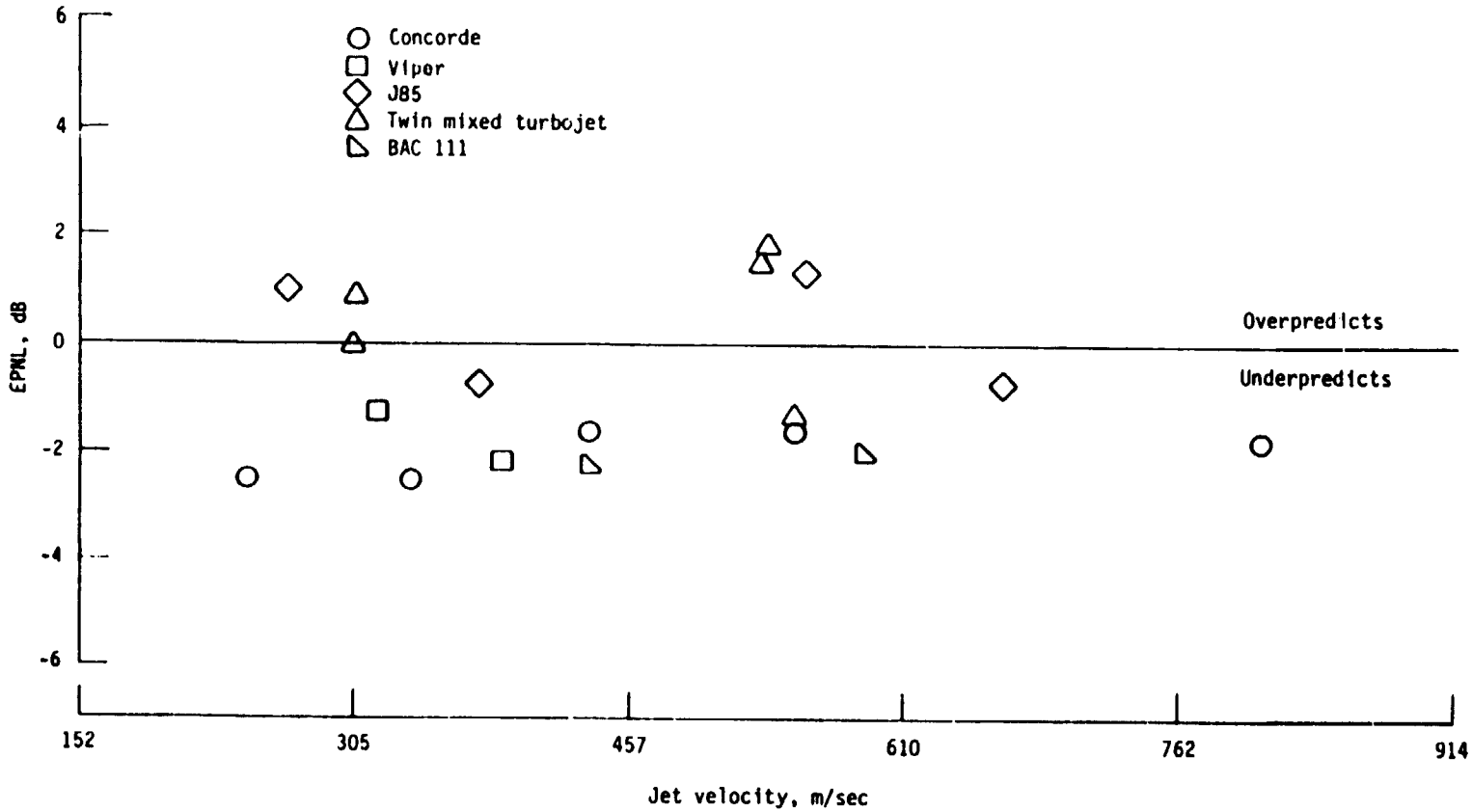

Figure 1.- Overall match of prediction by reference procedure with measurements.

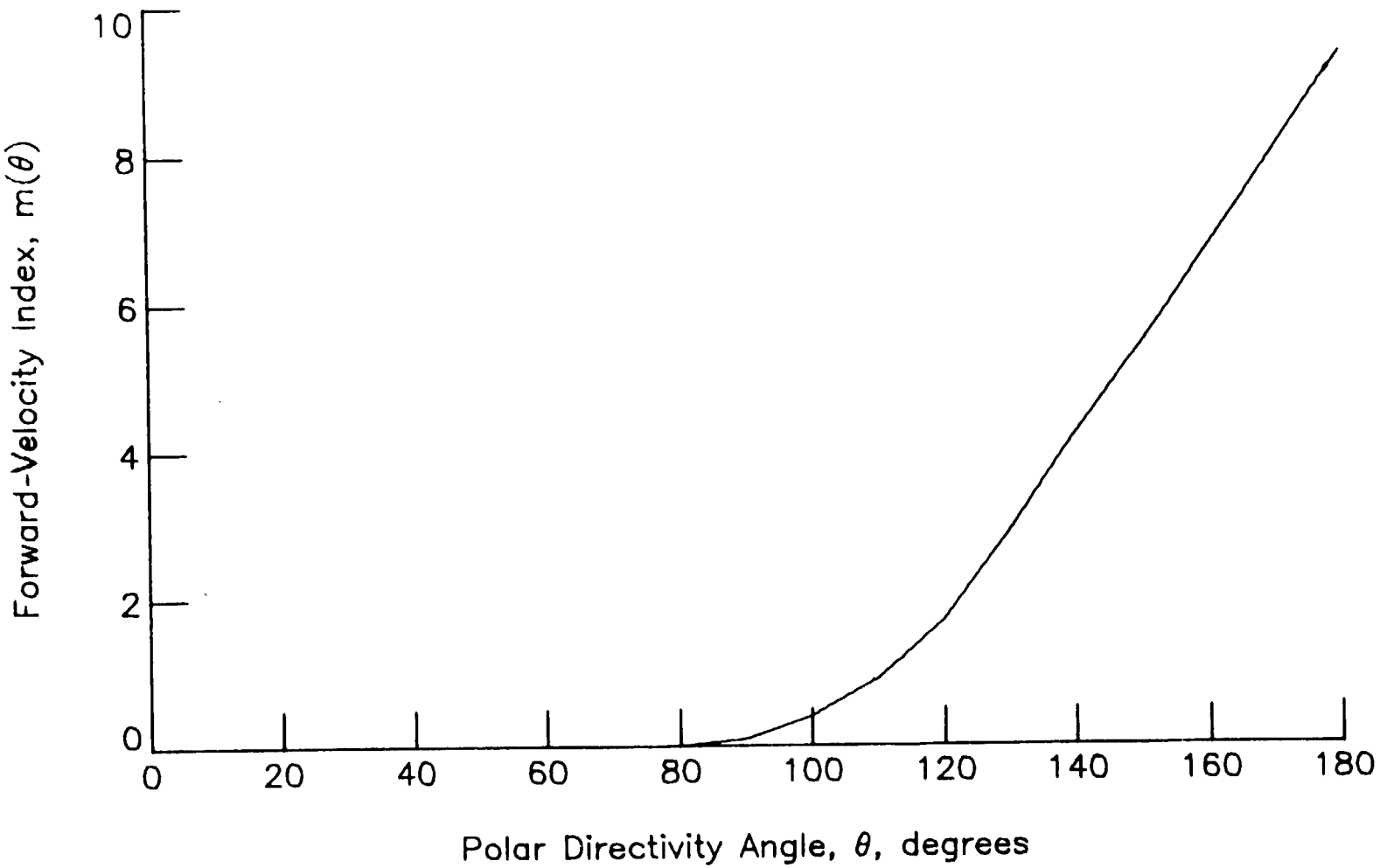

Figure 2.- Forward-velocity index.

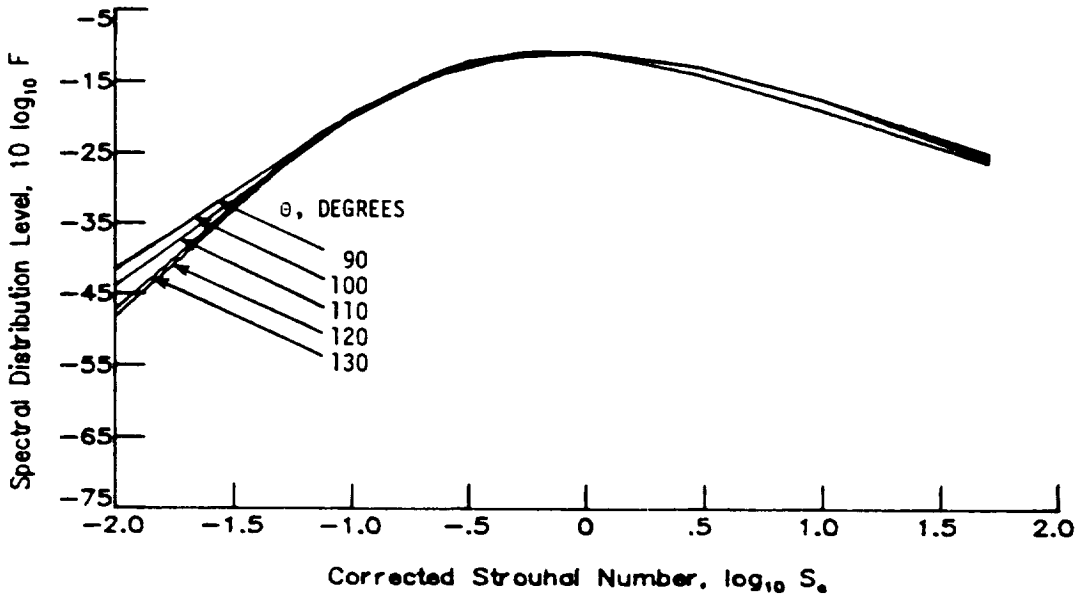

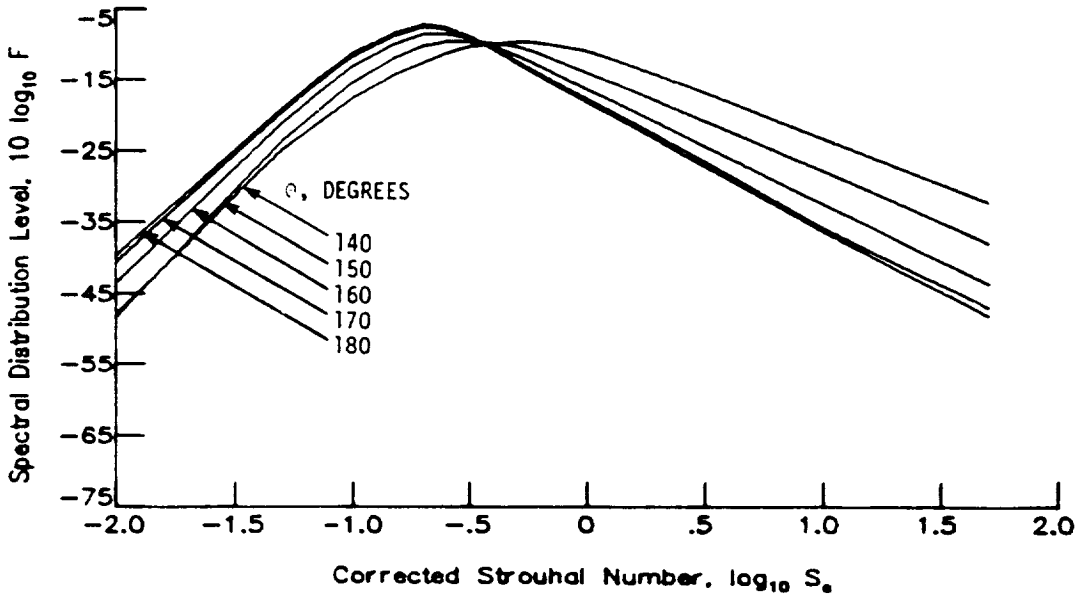

(a) $T_j/T_\infty = 1.6$; $\log_{10} V_j^* = 0.3$.

Figure 3.- Normalized spectral distribution factor.

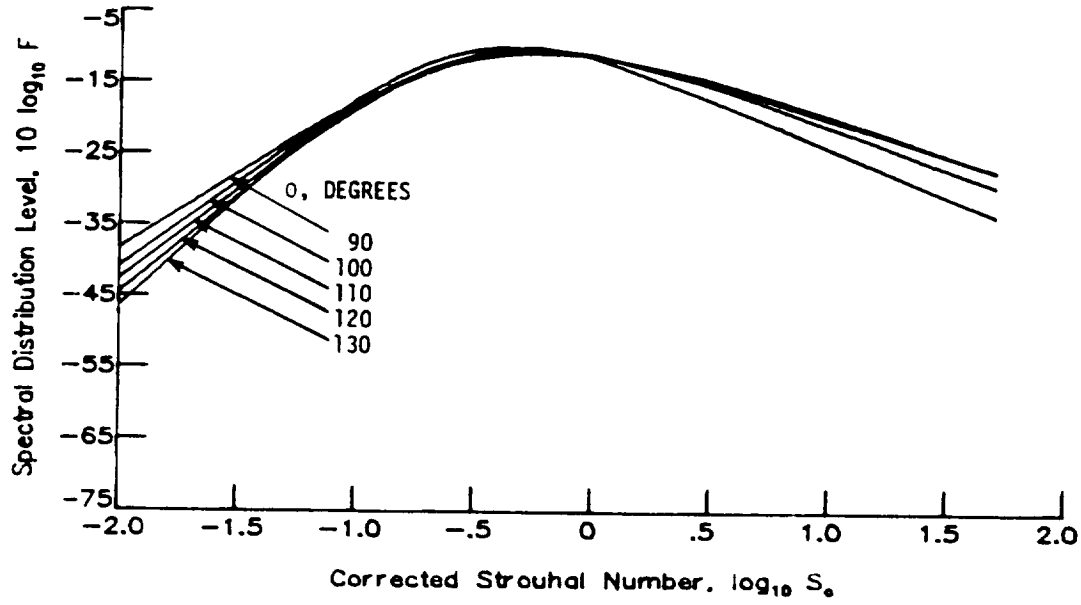

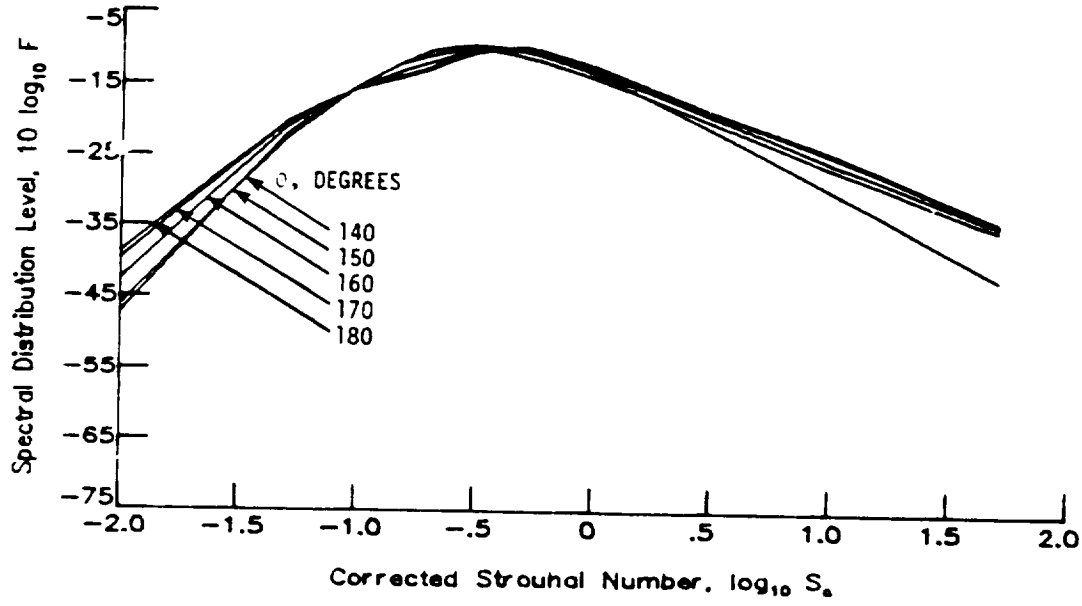

(b) $T_j/T_\infty = 2.0$; $\log_{10} V_j^* = 0.3$.

Figure 3.- Continued.

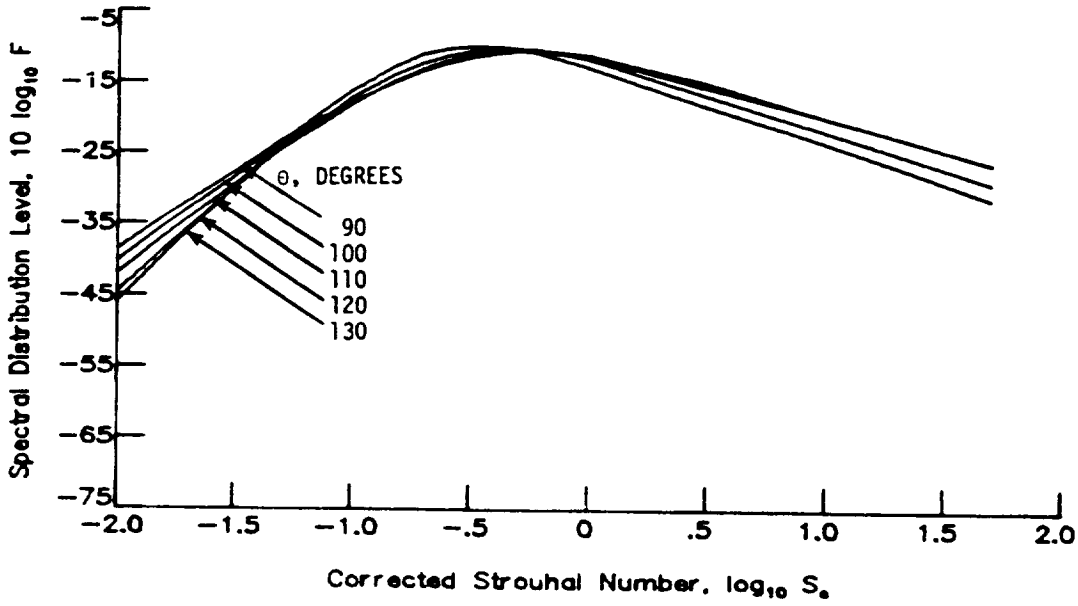

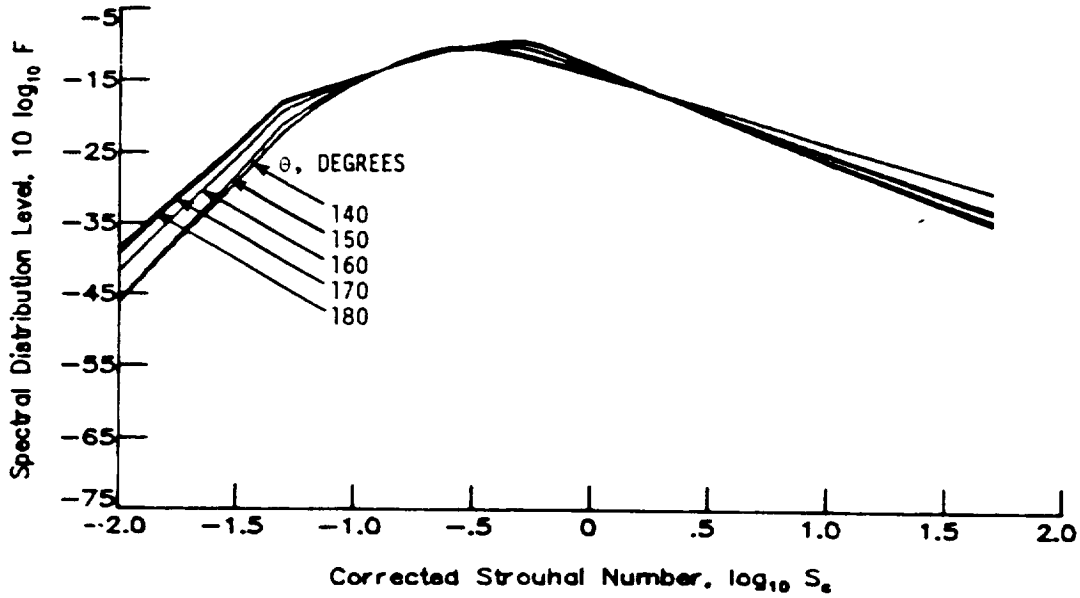

(c) $T_j/T_\infty = 2.5$; $\log_{10} V_j^* = 0.3$.

Figure 3.- Continued.

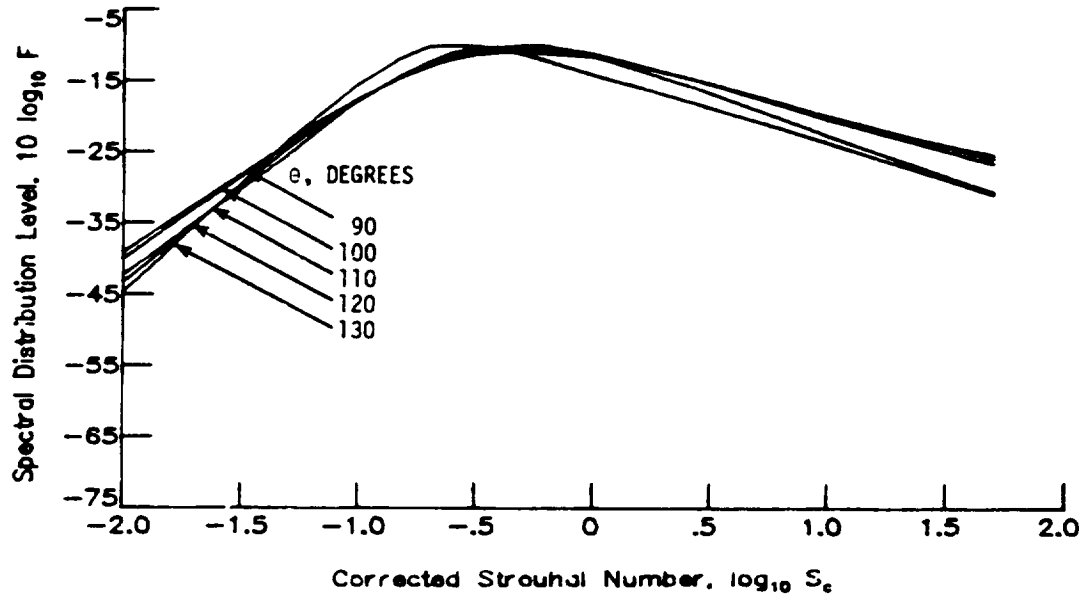

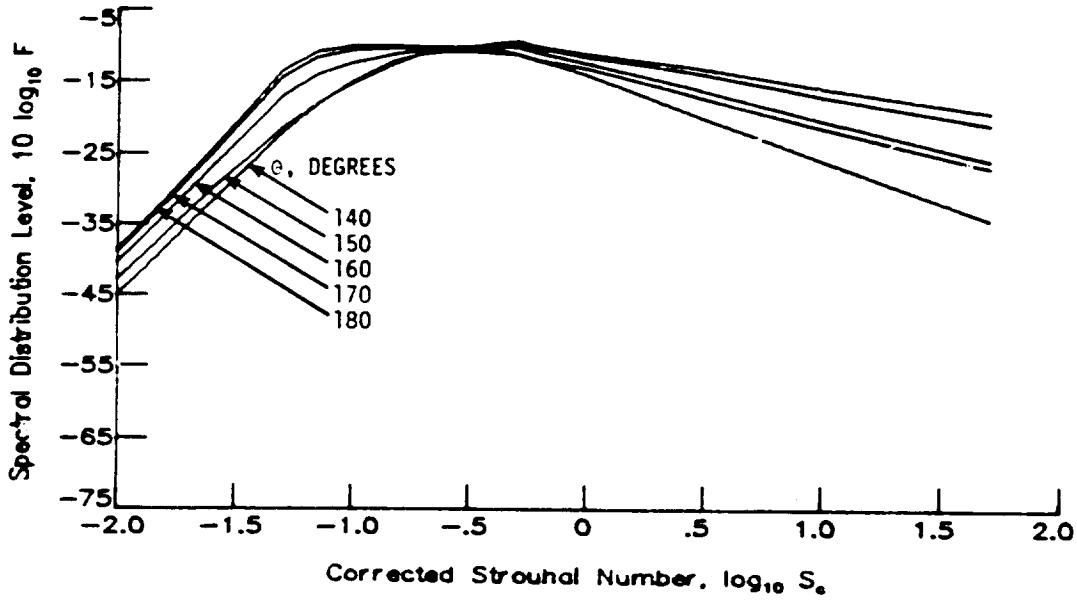

(d) $T_j/T_\infty = 3.0$; $\log_{10} V_j^* = 0.3$.

Figure 3.- Continued.

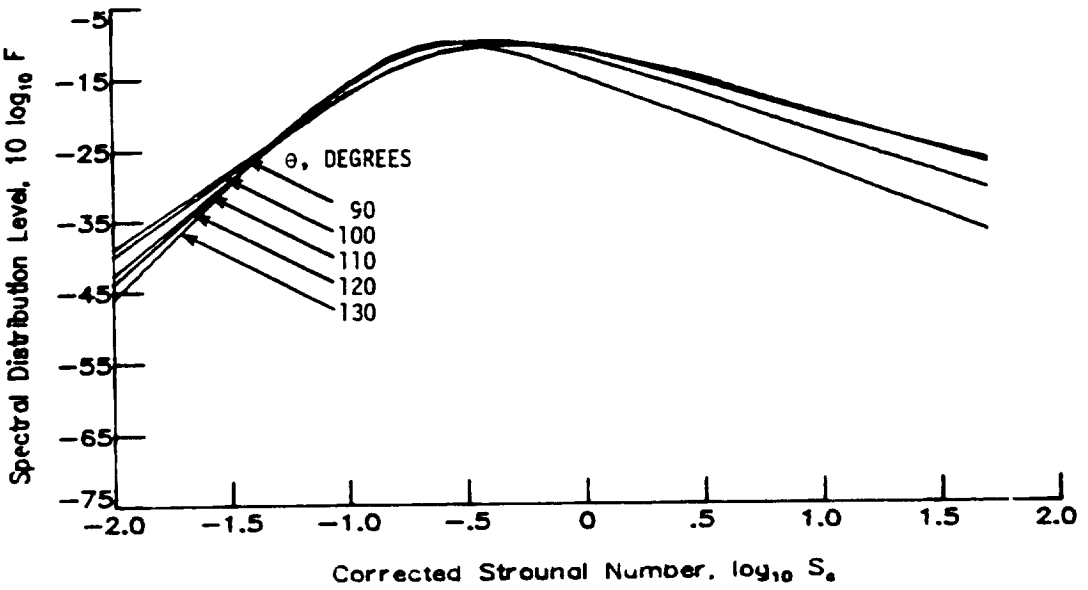

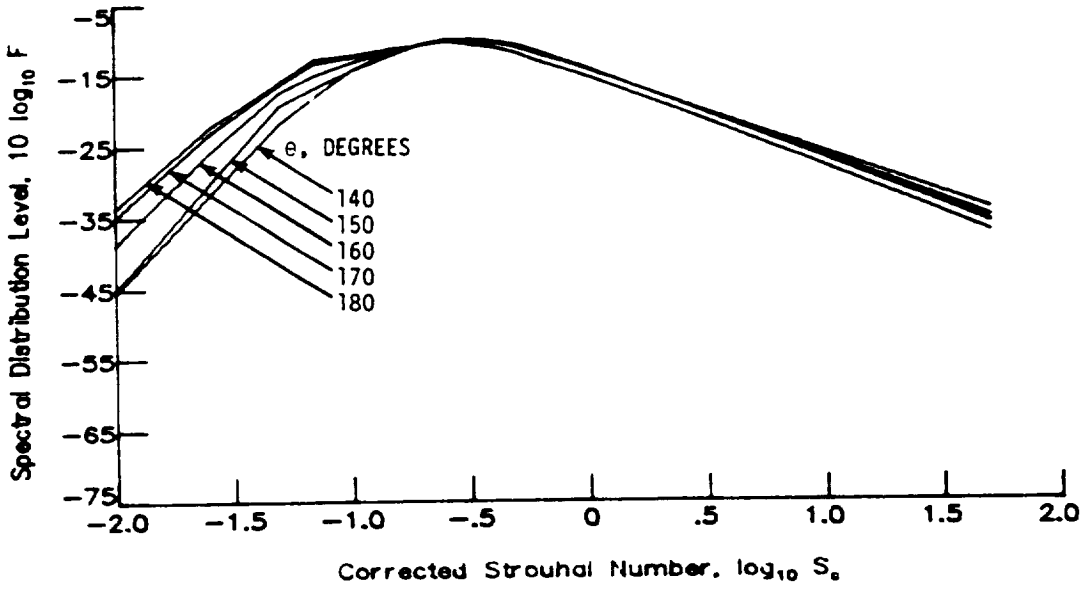

(c) $T_j/T_\infty = 3.5$; $\log_{10} V_j^* = 0.3$.

Figure 3.- Concluded.

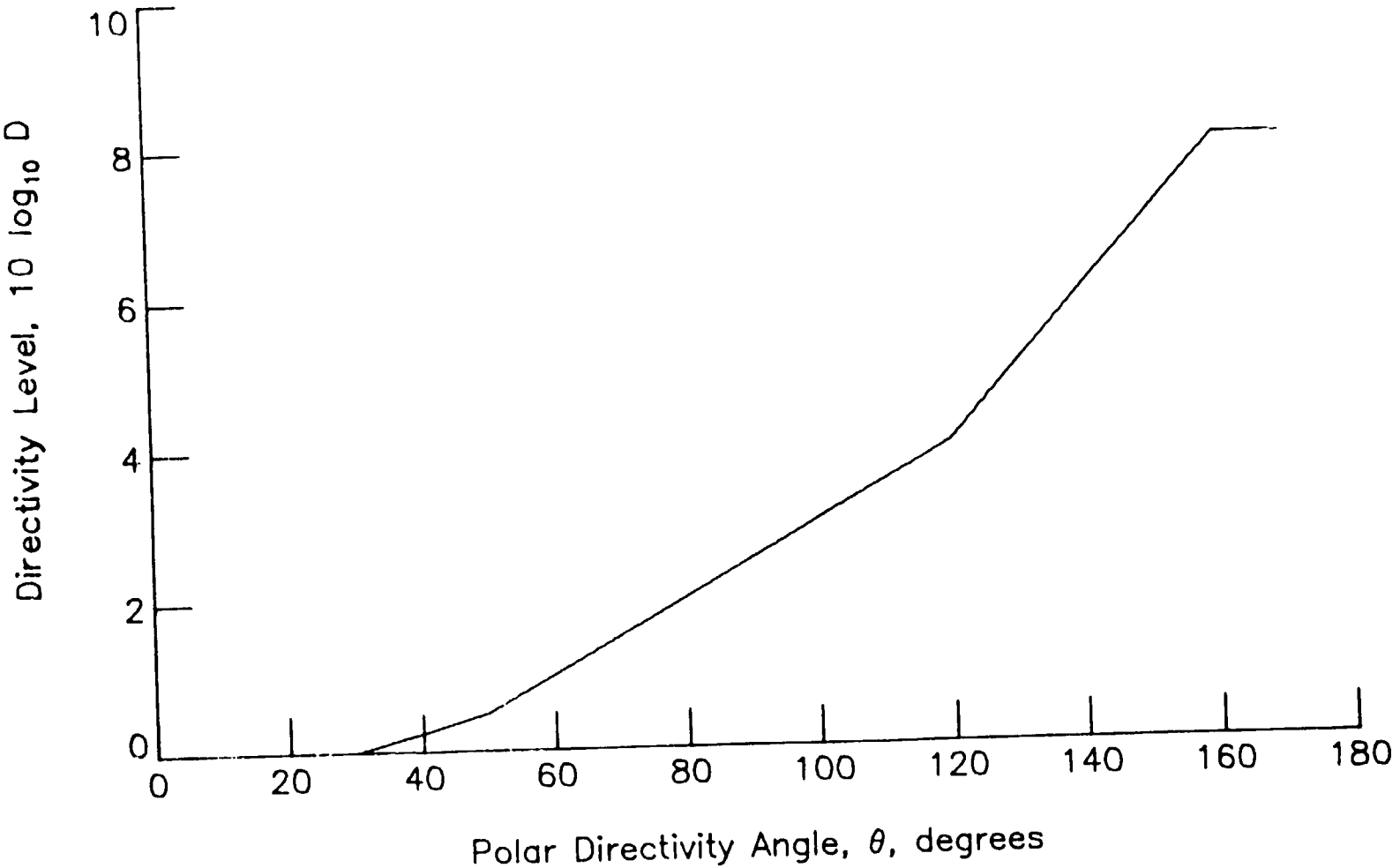

Figure 4.- Additional shock-cell noise directivity level.

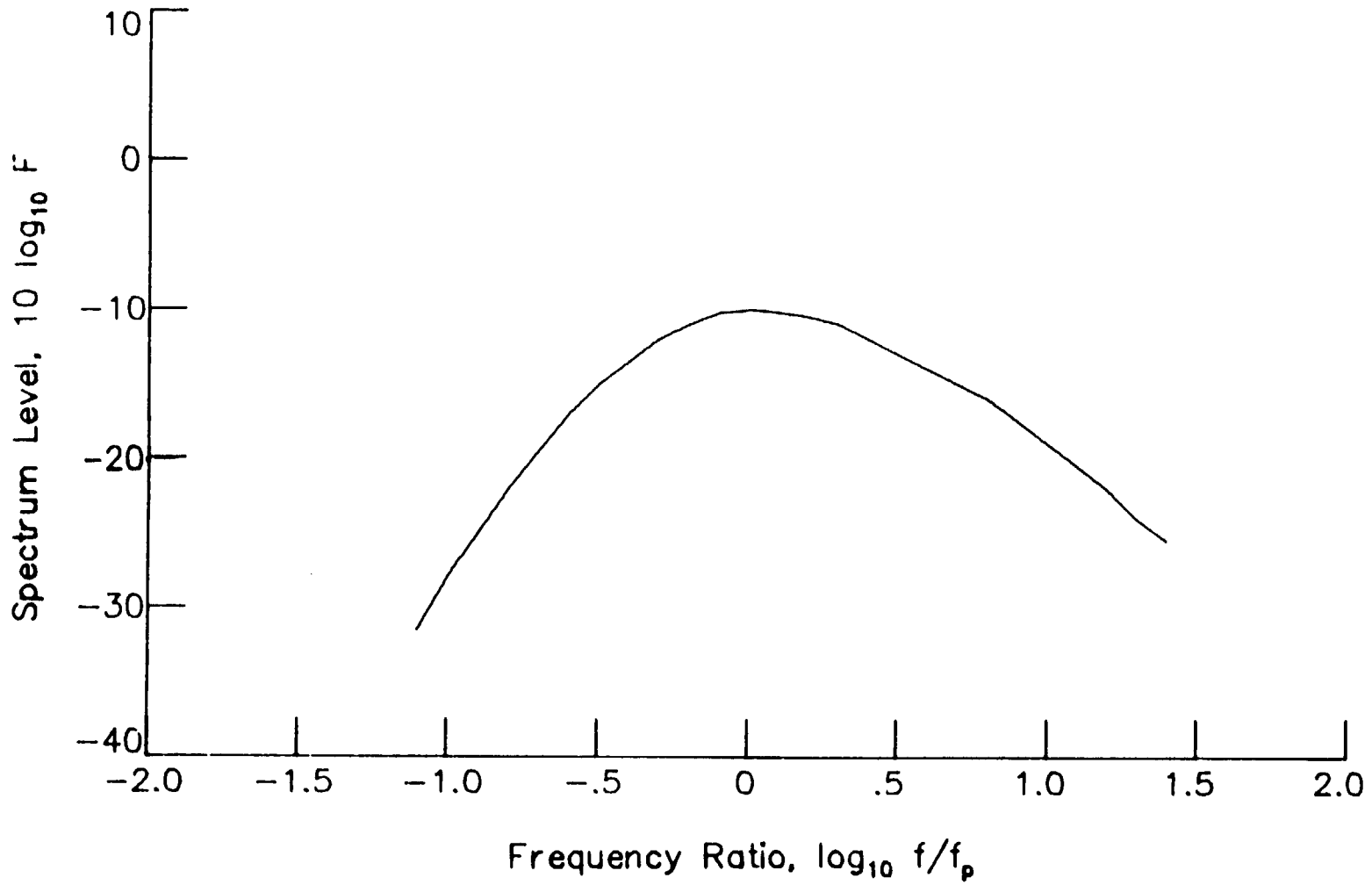

Figure 5.- Envelope spectrum for combustion noise.

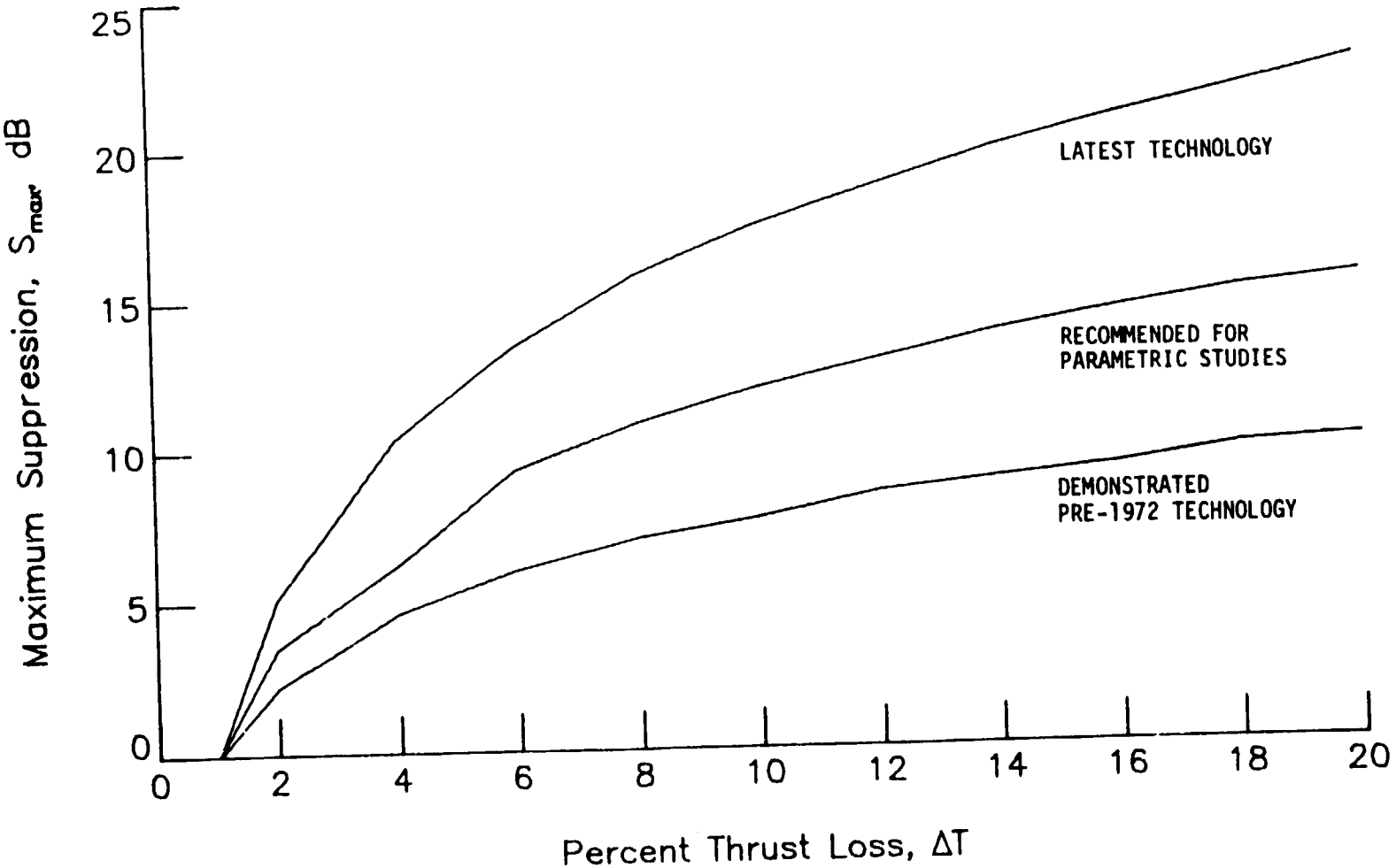

Figure 6.- The maximum jet-noise suppression.

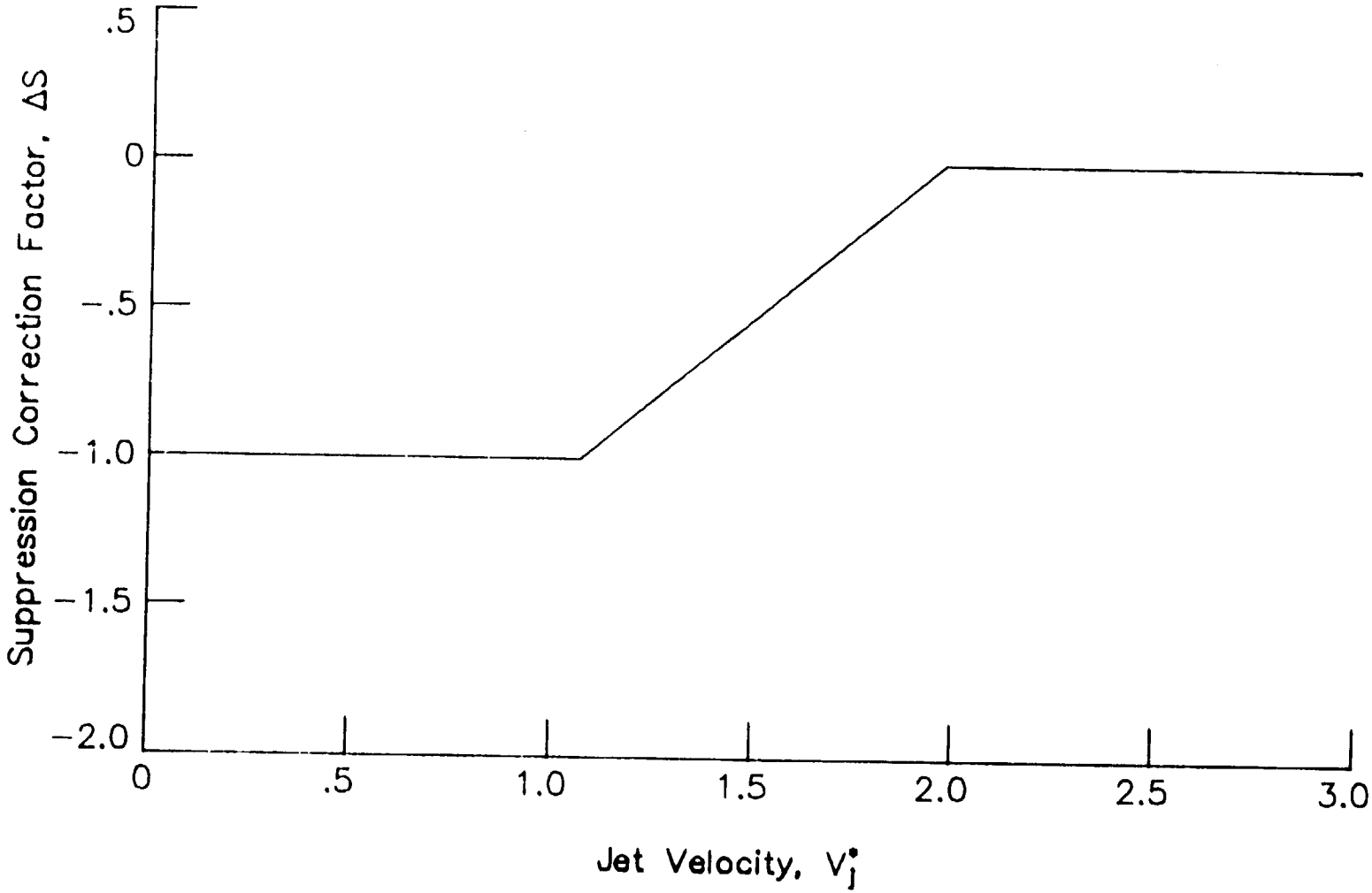

Figure 7.- The jet-velocity noise-suppression correction.